Development of hydrogels for biomedical applications

Etienne Piantanida

UNIVERSITÉ DE STRASBOURG

ÉCOLE DOCTORALE DES SCIENCES CHIMIQUES

Institut de Science et d'Ingénierie Supramoléculaires

THÈSE présentée par :

Etienne PIANTANIDA

soutenue le : **29 Octobre 2020**

pour obtenir le grade de : **Docteure de l'Université de Strasbourg**

Discipline/ Spécialité : Chimie

Development of hydrogels for biomedical applications

THÈSE dirigée par :

Mme DE COLA Luisa — Professeur, Université de Strasbourg

RAPPORTEURS :

Mme MARCHESAN Silvia — Professeur, Università di Trieste (Italie)

Mme CAUDA Valentina — Professeur, Politecnico di Torino (Italie)

AUTRES MEMBRES DU JURY :

M. LUTZ Jean François — Directeur de recherches, Université de Strasbourg

Table of Contents

Résumé de Thèse **5**

Chapter 1: General Introduction **29**

1.1. Structural properties of hydrogels 30

1.2. Structural requirements for the biomedical application of hydrogels 31

1.3. Design of hydrogels with tailored properties 34

1.3.1. The polymer selection 34

1.3.2. The cross-linking strategy 37

1.3.3. Introducing additional features in hydrogels: pending groups and nanofillers 45

1.4. Injectable hydrogels: controlling the sol-gel transition 50

1.5. Aim of the thesis 54

1.6. References 56

Chapter 2: *In situ* forming poly(amidoamine) supramolecular hydrogel for minimally-invasive gastric tumor resection **65**

2.1. Introduction 66

2.1.1. The Michael addition reaction in the synthesis of hydrogels 66

2.1.2. The use of hydrogels for the minimal invasive gastric tumor resection 69

2.1.3. Aim of the project 71

2.2. Results and Discussion 72

2.2.1. Synthesis of linear poly(amidoamine) 72

2.2.2. The interaction of linear PAA solution with gastric tissue 74

2.2.3. Mechanism of hydrogel formation investigation 80

2.2.4. Comparison of the cytocompatibility of the linear PAA and the CL_PAA 83

2.2.5. Surgical application of the linear PAA hydrogel: Endoscopic Submucosal Dissection 84

2.3. Conclusions 86

2.4. Acknowledgements 87

2.5. Experimental Section 87

2.5.1. Chemicals and Materials 87

2.5.2. Linear PAA-COOH synthesis 87

2.5.3. Linear PAA-OH solution preparation 87

2.5.4. Linear PAA-N(CH_3)$_2$ solution preparation 88

2.5.5. Molecular weight determination 88

2.5.6. CL_PAA solution synthesis for ultrasound elastography measurement 88
2.5.7. Cell lines and culture conditions 88
2.5.8. Preparation of the CL_PAA and linear PAA solutions for cytotoxicity study 88
2.5.9. Viability assay 89
2.5.10. Cytotoxicity statistical analyses 89
2.5.11. Instruments 89
2.6. References 91
Chapter 3: Injectable hydrogel for the treatment of gastrointestinal fistula 95
3.1. Introduction 96
3.1.1. Hyaluronic Acid based Hydrogels 96
3.1.2. A clinical problem: the treatment of gastrointestinal fistulas 99
3.1.3. Aim of the project 100
3.2. Results and Discussion 100
3.2.1. Design, synthesis and characterization of Hyaluronic Acid derivatives 100
3.2.2. Hydrogel preparation and characterization 104
3.2.3. The nanocomposite hydrogel: incorporation of mesoporous silica nanoparticles in the system 111
3.2.4. Enzymatic degradation of the HA based hydrogel 119
3.2.5. Evaluation of the ability of the hydrogel to adhere to the gastrointestinal tissue 120
3.2.6. *In vivo* application of the nanocomposite HA based hydrogel for the treatment of fistula 120
3.3. Conclusions 124
3.4. Acknowledgements 124
3.5. Experimental section 125
3.5.1. Chemicals and materials 125
3.5.2. HA methacrylation 125
3.5.3. Dopamine functionalization of methacrylated HA 125
3.5.4. MSN synthesis 126
3.5.5. MSN functionalization with (3-Mercaptopropyl)trimethoxysilane (MSN-SH) 126
3.5.6. MSN co-functionalization with (3-Mercaptopropyl)trimethoxysilane and (3-Aminopropyl)trimethoxysilane (MSN-NH_2-SH) 126
3.5.7. MSN functionalization with thiol-terminated PEG 126
3.5.8. Ellman's test for the quantification of thiols 127
3.5.9. Kinetic of hydrogel enzymatic degradation 127
3.5.10. *In vivo* experiment 127

3.5.11. Instruments 127
3.6. References 129
Chapter 4: Hyaluronic acid based hydrogels with biomimetic functions for cell adhesion 133
4.1. Introduction 134
4.1.1. Hydrogels for cell delivery 134
4.1.2. Aim of the project 137
4.2. Results and Discussion 138
4.2.1. Synthesis and characterization of RGD-functionalized Hyaluronic Acid 138
4.2.2 Preparation of HA based hydrogels containing RGD 141
4.2.3. Evaluation of the ability of the RGD containing hydrogel scaffolds to sustain cell adhesion 145
4.2.4. Effect of HA oligomers on the ability of hydrogel scaffolds to sustain cell adhesion 148
4.3. Conclusions 153
4.4. Acknowledgements 154
4.5. Experimental section 154
4.5.1. Chemicals and materials 154
4.5.2. RGD coupling on the carboxylic group of HA 155
4.5.3. Quantification of the coupled RGD 155
4.5.4. Thiol-Michael addition of the GCGY*RGD*SPG peptide on the methacrylate group of HA 155
4.5.5. Quantification of the GCGY*RGD*SPG peptide linked to HA 155
4.5.6. MSN functionalization with RGD groups (MSN-RGD) 156
4.5.7. MSN functionalization with PEG-RGD (MSN-PEG-RGD) 156
4.5.8. Quantification of the RGD grafted on MSN 156
4.5.9. Hydrogel preparation 156
4.5.10. Evaluation of the mechanical properties of the HA hydrogel functionalized with GCGY*RGD*SPG 157
4.5.11. HeLa cell adhesion tests 157
4.5.12. Kinetic of hydrogel enzymatic degradation 158
4.5.13. Instruments 158
4.6. References 159
Chapter 5: Hybrid scaffolds for peripheral nerve regeneration 163
5.1. Introduction 164
5.1.1 Porous silicon nanotechnology 164

5.1.2 Peripheral nerve regeneration 168
5.1.3. Aim of the project 169
5.2. Results and discussion 169
5.2.1 Synthesis and Characterization of porous silicon nano- and micro-particles 169
5.2.2. Protein loading in the pSiNP and pSiMP 171
5.2.3. Protein release from pSi particles 172
5.2.4. pSiP functionalization 174
5.2.5. Printing of the hybrid pSi particles/PEG-hydrogel scaffold 175
5.2.6. Protein release from the hybrid pSiP/PEG hydrogel scaffold 176
5.3. Conclusions 177
5.4. Experimental section 178
5.4.1. Chemicals and materials 178
5.4.2. Anisotropic and Isotropic particle dissolution: mathematical model 178
5.4.3. Synthesis of porous silicon nanoparticles 179
5.4.4. Synthesis of porous silicon micro-particles 179
5.4.5. Lysozyme loading in pSiNP and pSiMP 180
5.4.6. pSi particle functionalization 180
5.4.7. Lysozyme quantification 181
5.4.8. Printing of the hybrid pSi particles/PEG-hydrogel scaffold 181
5.4.9. Instruments 181
5.5. References 183
General Summary and Perspectives 187
Acknowledgments 191
Curriculum Vitae 193

Résumé de Thèse

Les hydrogels sont des structures polymériques hydrophiles tridimensionnelles qui peuvent absorber l'eau et gonfler sans se dissoudre (Figure 1). Ils sont considérés comme le matériau artificiel qui ressemble le plus à la matrice extracellulaire (MEC) des tissus mous, tant du point de vue structurel que mécanique. C'est pourquoi les hydrogels présentent un intérêt particulier en médecine régénérative où ils peuvent être utilisés comme vecteur de biomolécules[1] et de cellules[2] et comme support pour la greffe, la prolifération et la différenciation cellulaires *in vivo*.[3–5] La prolifération des cellules dans les hydrogels requièrent toutefois une microarchitecture,[6] des propriétés mécaniques et une composition chimique appropriés.[7–9]

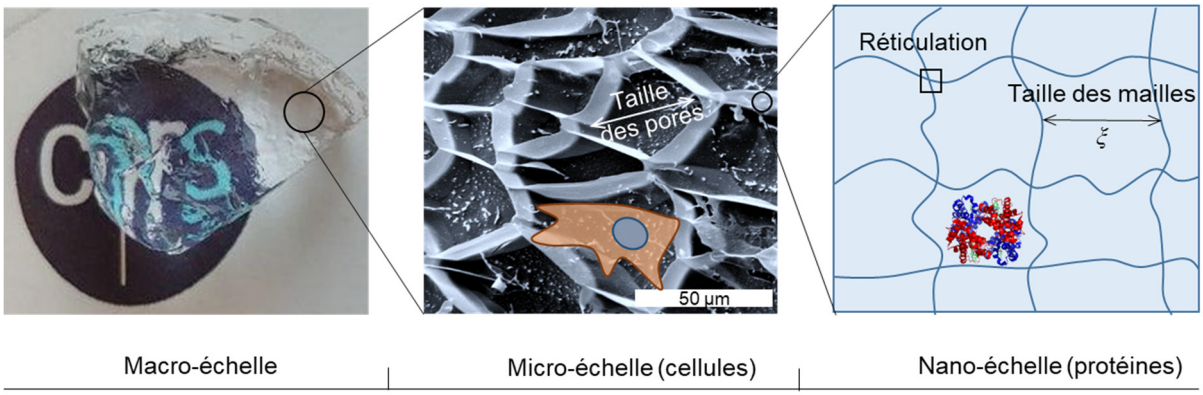

Figure 1 : Structure hiérarchique d'un hydrogel : macro, micro et nano-échelle.

Les hydrogels avec des propriétés adaptées sont obtenus par la sélection du polymère constitutif, le mécanisme de réticulation, l'introduction de groupements fonctionnels suspendus et l'incorporation d'une nano- ou micro-filler dans le matériau.[10] Le réseau d'hydrogel peut être constitué de polymères naturels ou synthétiques, le premier ayant l'avantage général de la biocompatibilité et le second étant associé à une conception plus précise et ajustable. Le processus de réticulation consiste en la génération d'interactions intermoléculaires responsables de la transition sol-gel. Ces interactions peuvent être covalentes, associée à la formation d'un hydrogel irréversible, ou bien supramoléculaires, permettant la création d'un système dynamique et donc réversible. Les principaux avantages des hydrogels supramoléculaires sont l'absence de réactifs chimiques qui pourraient donner une cytotoxicité en cas de réaction de réticulation incomplète, le comportement sensible aux stimuli et la propriété d'auto-guérison. D'autre part, les systèmes covalents ont comme points forts des propriétés mécaniques et une stabilité accrues dans des conditions physiologiques.[11] La sélection précise de la stratégie de réticulation permet de régler, entre autres, les propriétés mécaniques en fonction de l'application

souhaitée du matériau final. En général, une rigidité plus élevée peut être obtenue en augmentant le degré de réticulation, ou en utilisant des molécules réactives ramifiées, bien que cela puisse également conduire à la formation d'un matériau fragile.[12] Pour surmonter cette contrainte et générer des matériaux auto-guérissant et éventuellement hautement étirables, une combinaison de réticulation supramoléculaire et covalente est généralement utilisée.[13]

Des caractéristiques supplémentaires peuvent être introduites dans les hydrogels avec la greffe au réseau polymérique de groupes fonctionnels suspendu tels que les catéchols, connus pour conférer une adhésion tissulaire,[14,15] ou la séquence tripeptidique RGD qui joue un rôle crucial dans l'interaction cellule-matériau.[16] Une autre stratégie pour obtenir des hydrogels aux propriétés émergentes est l'incorporation d'un nanofiller dans la matrice pour générer des systèmes nanocomposites. Par exemple, l'élasticité,[17] la capacité d'étirer[18] et l'adhésivité[19] ont été obtenues avec l'introduction de nanofillers qui interagissent de manière supramoléculaire avec le réseau polymérique. L'effet antimicrobien peut être facilement et efficacement obtenu en combinant des particules de métal ou d'oxyde métallique avec les hydrogels.[20] La conductivité thermique et électrique est conférée aux matériaux par l'introduction de nanotubes de carbone[21] ou d'oxyde de graphène.[22] Des hydrogels aux propriétés anisotropes, capables d'imiter la structure ordonnée des tissus vivants, peuvent être obtenus avec l'introduction de substances de remplissage ordonnées dans l'espace.[23] L'incorporation de nanoparticules dans des matrices d'hydrogel peut être exploitée davantage pour la préparation de systèmes avancés de relargage de biomolécules qui permettent de contrôler la libération de la charge.[24–26] Parmi les systèmes développés, les hydrogels injectables présentent l'avantage de pouvoir être implantés dans la zone souhaitée par des techniques peu invasives et de pouvoir remplir intégralement la cavité en assurant la continuité avec le tissu natif. Le développement des hydrogels injectables par rapport aux échafaudages apporte cependant de nouveaux défis. En effet, si dans la préparation des échafaudages le contrôle de la cinétique de gélification n'est pas crucial et qu'il est possible de purifier le matériau avant l'implantation, la formation *in situ* d'hydrogels nécessite un contrôle précis de la transition sol-gel et l'absence de sous-produits toxiques. Différentes approches ont été mises en œuvre pour contrôler le processus de gélification. L'environnement *in vivo* (c'est-à-dire le pH, la température) peut par exemple être utilisé pour déclencher la gélification d'hydrogels supramoléculaires.[27] Une autre approche consiste à utiliser des hydrogels covalents qui peuvent être synthétisés *in situ* à l'aide d'une seringue à double chambre pour délivrer les réactifs.[28] Une approche différente consiste à utiliser des hydrogels à amincissement par cisaillement qui sont des matériaux injectables

idéaux puisqu'ils peuvent se comporter comme des gels élastiques au repos, grâce à l'établissement de liaisons par des interactions dynamiques, tandis qu'ils peuvent s'écouler comme des fluides visqueux lorsqu'une force est appliquée.[29]

L'objectif de cette thèse est le développement et la caractérisation d'hydrogels aux propriétés adaptées à différentes applications biomédicales. L'accent est mis en particulier sur les matériaux injectables qui peuvent être implantés par des procédures mini-invasives. La possibilité d'introduire des nanoparticules poreuses ayant la fonction de système de livraison de biomolécules est également explorée. Enfin, l'incorporation de biomolécules spécifiques pour induire l'adhésion cellulaire aux hydrogels est présentée.

Les poly(amidoamines) (PAA) sont une classe de polymères préparés par réaction d'aza-Michael dans l'eau à température modérée, sans besoin de catalyseur et sans libération de sous-produits. Combinés à la grande polyvalence structurelle et à leur biocompatibilité, les PAA présentent un intérêt particulier pour les applications biomédicales.[30–32] Notre groupe a démontré que les hydrogels injectables à base de PAA constituaient un matériau de levage optimal pour faciliter la résection moins invasive des tumeurs gastriques.[26] Le succès du matériau tient à sa capacité à former immédiatement, lorsqu'il est injecté dans la couche sous-muqueuse gastrique, un solide mou adhérant aux tissus qui donne un levage durable. Le mécanisme sous-jacent qui convertit la solution d'oligomère de PAA injectée en hydrogel reste cependant inconnu et soulève des inquiétudes quant à la sécurité du matériau qui contient un grand nombre de groupes terminaux réactifs lorsqu'il est administré. L'objectif du Chapitre 2 de la thèse est d'étudier la possibilité de changer la stratégie de réticulation en passant d'un système covalent à un système supramoléculaire qui ne nécessite aucune réaction chimique pour se produire *in vivo*.

Des PAA linéaires ont été préparés en faisant réagir le *N,N'*-Méthylenbisacrylamide (MBA) avec des molécules de monoamines primaires dans un rapport stœchiométrique (Schéma 1).

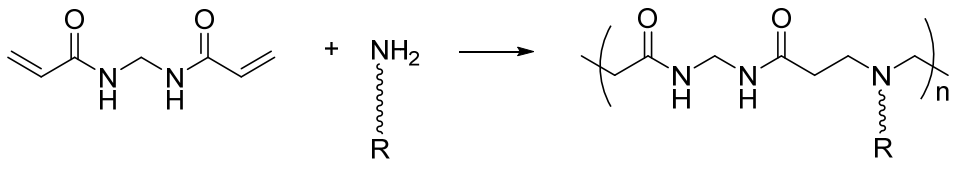

R= -COOH, -OH, -$N(CH_3)_2$

Schéma 1 : Synthèse du PAA linéaire.

Les solutions aqueuses de PAA préparées sont caractérisées par une faible viscosité qui les rend facilement injectables même avec une aiguille endoscopique (23 G, 1,5 m de long) (Figure 2).

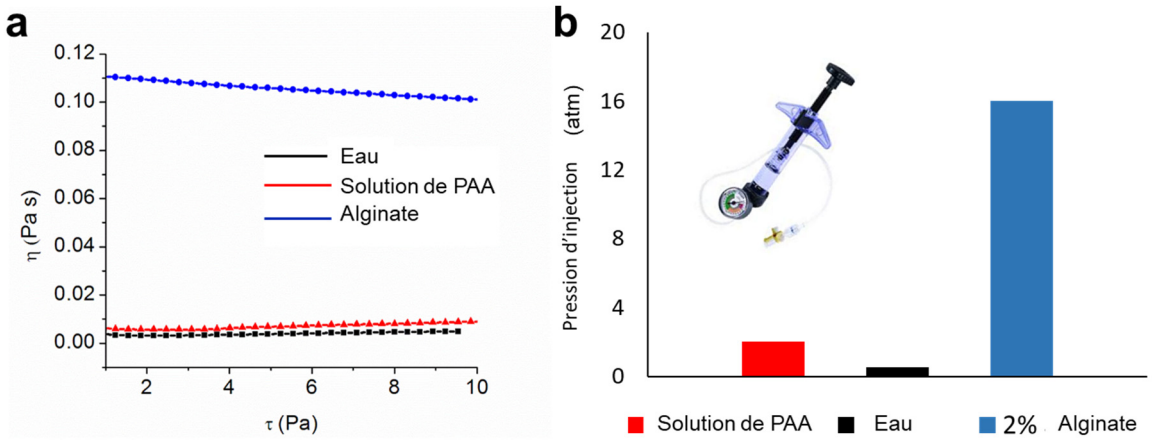

Figure 2 : Caractérisation rhéologique de la solution aqueuse de PAA. a) Mesure de la viscosité de l'eau (noir), de la solution de PAA (rouge) et de la solution d'alginate à 2% (bleu) ; 37 °C, géométrie : cylindre coaxial 25 mm. b) Pression nécessaire pour faire passer les différentes solutions à travers une aiguille endoscopique (23 G, 1,5 m) ; les mesures sont effectuées à l'aide d'une seringue équipée d'un manomètre (insert). Eau (noire), solution de PAA (rouge), solution d'alginate à 2% (bleue).

Lorsque la solution de PAA est injectée dans la couche sous-muqueuse du tissu gastrique, elle subit la transition sol-gel en quelques secondes pour former un hydrogel fortement adhérent au tissu (Figure 3). Après injection, l'hydrogel formé reste stable pendant au moins une heure, tandis que si le tissu est réséqué, le matériau revient à l'état de sol en 30 minutes environ. Ces observations suggèrent que l'hydrogel est formé par des interactions supramoléculaires réversibles qui sont induites par le tissu.

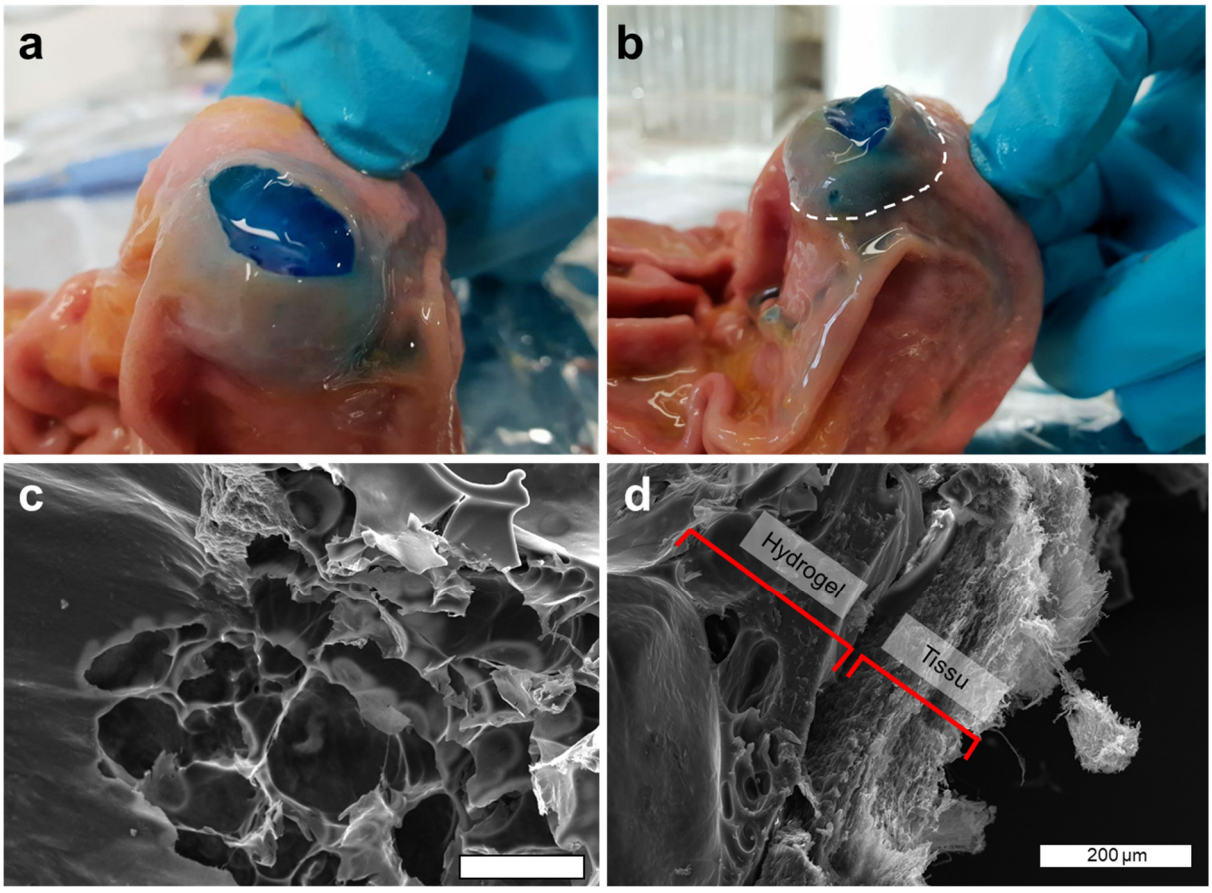

Figure 3 : Formation d'hydrogel dans le tissu gastrique après injection d'une solution linéaire de PAA. Du bleu de méthylène a été ajouté à la solution pour une meilleure visualisation. a) Vue de dessus de l'hydrogel dans le tissu gastrique, b) Vue latérale de l'hydrogel dans le tissu gastrique, la ligne en pointillés met en évidence le soulèvement du tissu obtenu avec l'injection d'hydrogel. c) Image SEM de l'hydrogel ; d) Image SEM d'une partie du tissu avec l'hydrogel adhérent. Barre d'échelle 200µm.

La transition sol-gel pourrait être attribuée à différents stimuli présents dans le tissu tels que le pH, les ions ou la présence de biomolécules, entre autres. Pour tenter de reproduire la formation d'hydrogel dans des flacons, différents tests ont été réalisés, notamment l'ajustement du pH, l'ajout d'ions ou de morceaux de tissu gastrique à la solution de PAA. Dans tous les cas, la transition sol-gel en flacon ne s'est pas produite. L'hypothèse est que la gélification observée lorsque la solution de PAA est injectée dans le tissu est induite par le confinement du matériau qui est exposé à des forces de compression qui déclenchent la formation d'interactions supramoléculaires intermoléculaires. Après la résection du tissu, les forces de compression sont supprimées, les interactions supramoléculaires sont affaiblies et le matériau revient à l'état de sol (Figure 4).

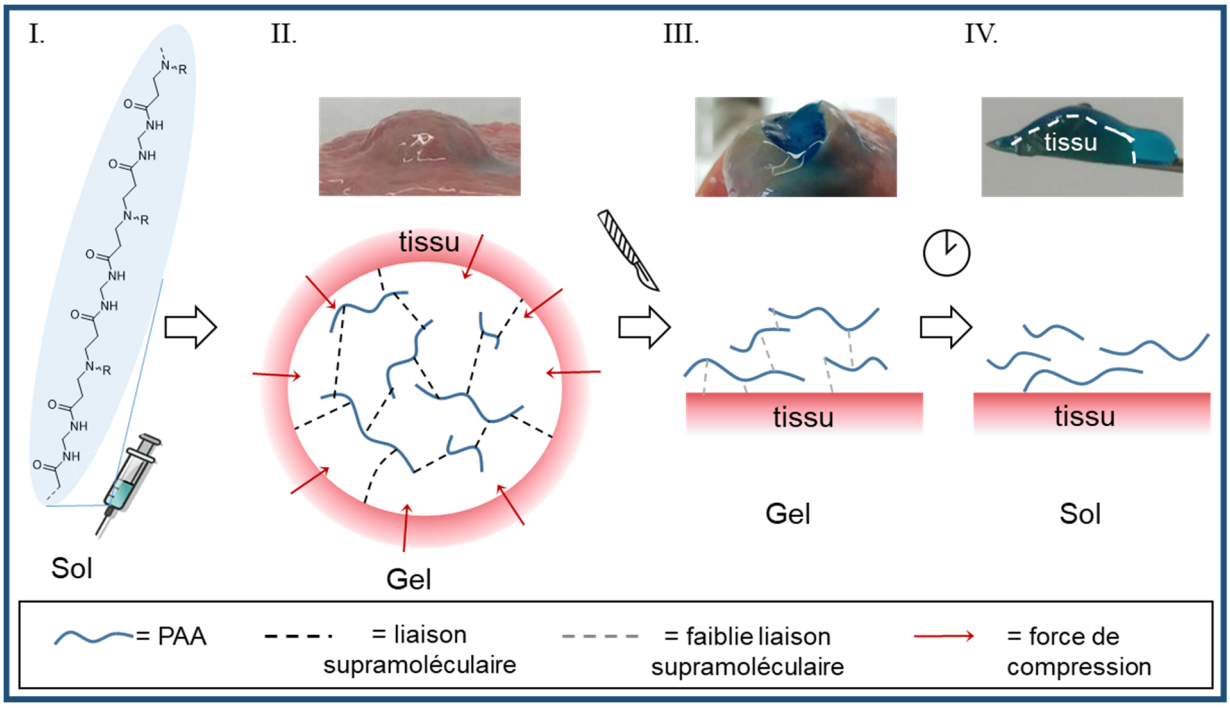

Figure 4 : La solution de PAA à l'état de sol (I.) est injectée dans le tissu gastrique où elle forme un gel (II.). Lors de la résection du tissu, les forces de compression sont supprimées et la liaison supramoléculaire est affaiblie (III.) jusqu'à la rupture du réseau tridimensionnel et au passage à l'état sol (IV.).

L'hydrogel PAA supramoléculaire a été testé *in vivo* sur un modèle de cochon comme matériau de soulèvement pour la dissection sous-muqueuse endoscopique des tumeurs du côlon (Figure 5a). La solution de PAA décrite était facilement injectable avec l'aiguille endoscopique et formait immédiatement un hydrogel supramoléculaire adhérent au tissu qui permettait un soulèvement élevé et stable de la couche sous-muqueuse. Par rapport à la solution saline qui est la solution actuellement utilisée dans les cliniques, l'hydrogel a facilité l'intervention. La durée de l'intervention a été réduite de moitié en moyenne (Figure 5b) et la fréquence des perforations a été réduite à un tiers (Figure 5c).

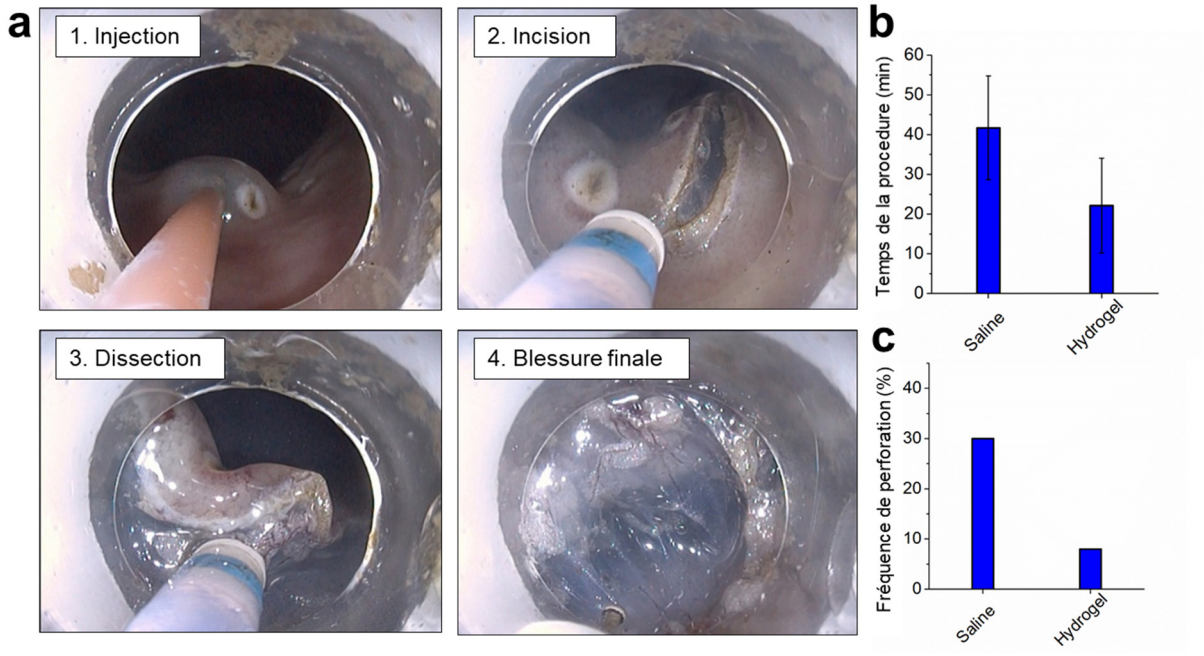

Figure 5: a) Dissection sous-muqueuse endoscopique dans le côlon. 1. Injection : la solution de PAA linéaire est facilement injectée et forme immédiatement un hydrogel solide et mou. 2. Incision : l'hydrogel réduit le risque de perforation. 3. Dissection : l'hydrogel facilite la résection en bloc de la lésion. 4. Plaie finale. b) Réduction du temps de l'intervention. c) Diminution de la fréquence des perforations.

La réaction de thiol-Michael, comparée à la réaction d'aza-Michael, est généralement plus rapide et peut être réalisée à un pH physiologique.[33,34] Au Chapitre 3, la réaction de thiol-Michael est exploitée pour la préparation d'un hydrogel injectable à base d'acide hyaluronique (HA) avec application comme matériau de remplissage pour la guérison stimulée de la fistule. Le HA est un polymère naturel et, en solution, il présente un fort comportement d'amincissement par cisaillement qui le rend optimal pour la préparation d'hydrogels injectables. En outre, le HA présente différents groupes latéraux qui peuvent être utilisés pour introduire des fonctionnalités dans le réseau polymérique afin d'obtenir des matériaux polyvalents.[35,36] L'hydrogel à base de HA est préparé en faisant réagir le dithiothréitol (DTT) et l'acide hyaluronique méthacrylate (Me_HA) (Figure 6a). L'imagerie Cryo-SEM a montré une microarchitecture très poreuse du matériau avec des pores dans la gamme de 10 à 50 µm (Figure 6b). La présence de pores plus grands que la taille des cellules est d'une importance fondamentale pour permettre la prolifération des cellules dans le matériau.

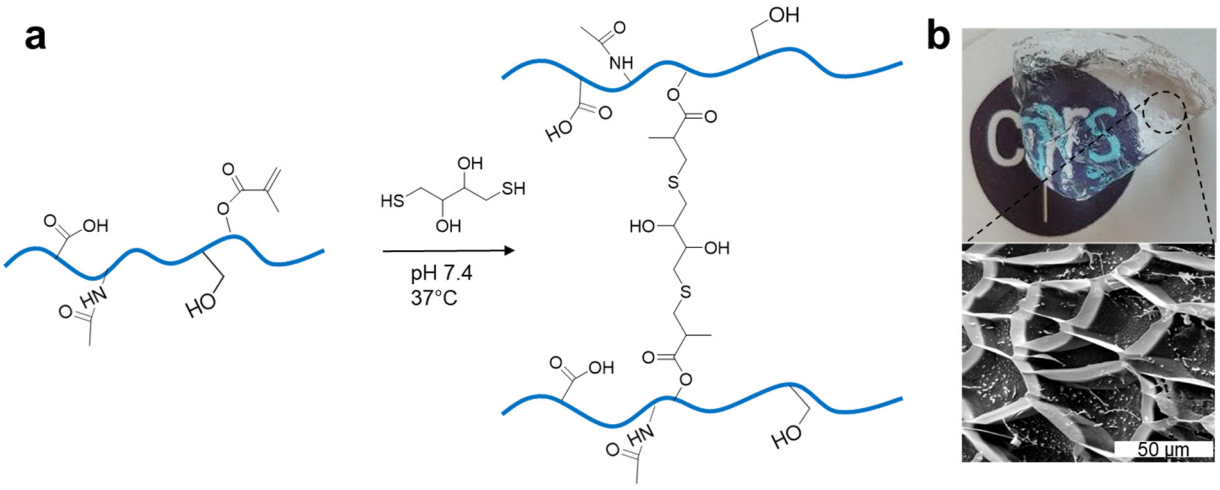

Figure 6 : a) Synthèse de l'hydrogel à base de HA par addition de thiol-Michael. b) L'hydrogel obtenu et l'image SEM cryogénique montrant la structure poreuse.

La cinétique de formation d'hydrogel et les propriétés mécaniques finales du matériau ont été optimisées en fonction du poids moléculaire (MW) et de la concentration en HA (Figure 7). L'augmentation de la concentration a eu pour effet, dans tous les échantillons, de réduire le temps de formation du gel et d'augmenter le module G' à la fois de la solution de départ et de l'hydrogel final (Figure 7a-c). L'effet du MW sur le module G' et sur le temps de gélification, au contraire, n'est pas triviale (Figure 7b, c).

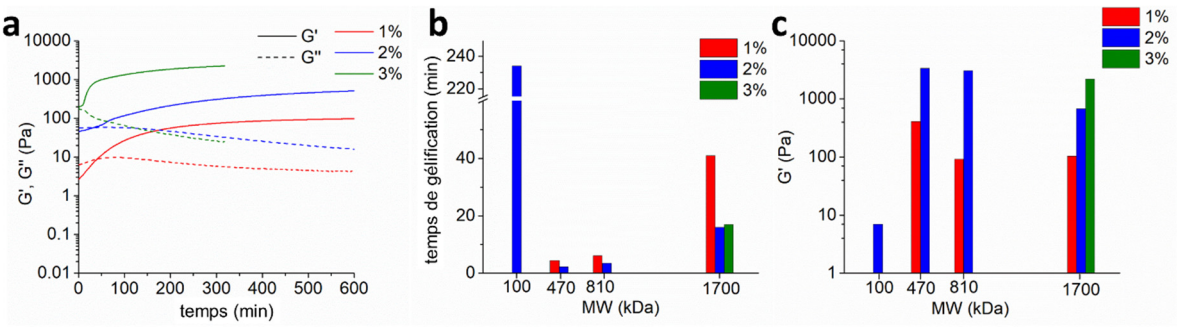

Figure 7 : a) Cinétique de la formation d'hydrogel de HA de 1700 kDa à 37 °C. Ligne continue : G', ligne pointillée : G", ligne rouge : concentration 1%, ligne bleue : concentration 2%, ligne verte : concentration 3%. b) effet du MW et de la concentration sur le temps de gel ; c) effet du MW et de la concentration sur le module élastique.

Le MW du polymère détermine la viscosité de la solution de pré-gel et le nombre de réactions de réticulation efficaces nécessaires à la formation d'un réseau tridimensionnel et d'un hydrogel

solide. Les polymères de faible MW génèrent une solution de viscosité moindre dans laquelle la mobilité moléculaire est plus élevée et les réactions de réticulation sont plus rapides. D'autre part, les polymères de faible masse moléculaire nécessitent un plus grand nombre de réactions de réticulation pour obtenir un hydrogel, tandis que pour les polymères de forte masse moléculaire, un plus petit nombre de réactions de réticulation suffit pour la formation du réseau percolé.

L'hydrogel préparé à partir de 1700 kDa HA et d'une concentration de 3% en masse est formé en 16 min, un temps compatible avec la procédure chirurgicale, et il a un module G' final de 2,2 kPa (Figure 7a), adapté à la prolifération des cellules épithéliales. Ce matériau a donc été choisi comme le candidat optimal pour le traitement des fistules. Les nanoparticules de silice mésoporeuse (MSN) sont caractérisées par une surface élevée et ont été utilisées pour la livraison de cargaisons allant de petites molécules jusqu'aux protéines.[37,38] Les MSN sont introduites dans l'hydrogel de HA avec la fonction de système de livraison de biomolécules. Les MSN de 50 nm sont préparés selon un procédé Stöber modifié (Figure 8a, b).

La possibilité de relier le MSN au réseau polymérique, soit par la formation d'une liaison covalente, soit par une interaction supramoléculaire a été étudiée. Les particules sont fonctionnalisées sur la surface extérieure avec des groupes thiol pour évaluer la formation de liaisons covalentes avec le HA méthacrylate. Les groupes amine sont plutôt été greffés pour introduire des charges positives sur la surface des MSN afin d'obtenir une interaction supramoléculaire avec le HA chargé négativement. Une quantification colorimétrique des thiols (test d'Ellman) à la surface du MSN a été effectuée avant et après le mélange des particules avec le Me_HA ; les expériences ont montré que la réaction entre les groupes thiols et les groupes méthacryliques ne se produit pas, probablement en raison d'un obstacle stérique. D'autre part, lorsque des MSN chargées positivement sont mélangées avec de l'acide hyaluronique, elles interagissent électrostatiquement, comme le montrent le changement de ζ-potentiel en valeurs négatives et l'augmentation du diamètre hydrodynamique mesuré par la diffusion dynamique de la lumière (Figure 8c, d, e). Les MSN chargés positivement ont été introduits dans le réseau d'hydrogel dans le but d’obtenir un système nanocomposite (Figure 8f).

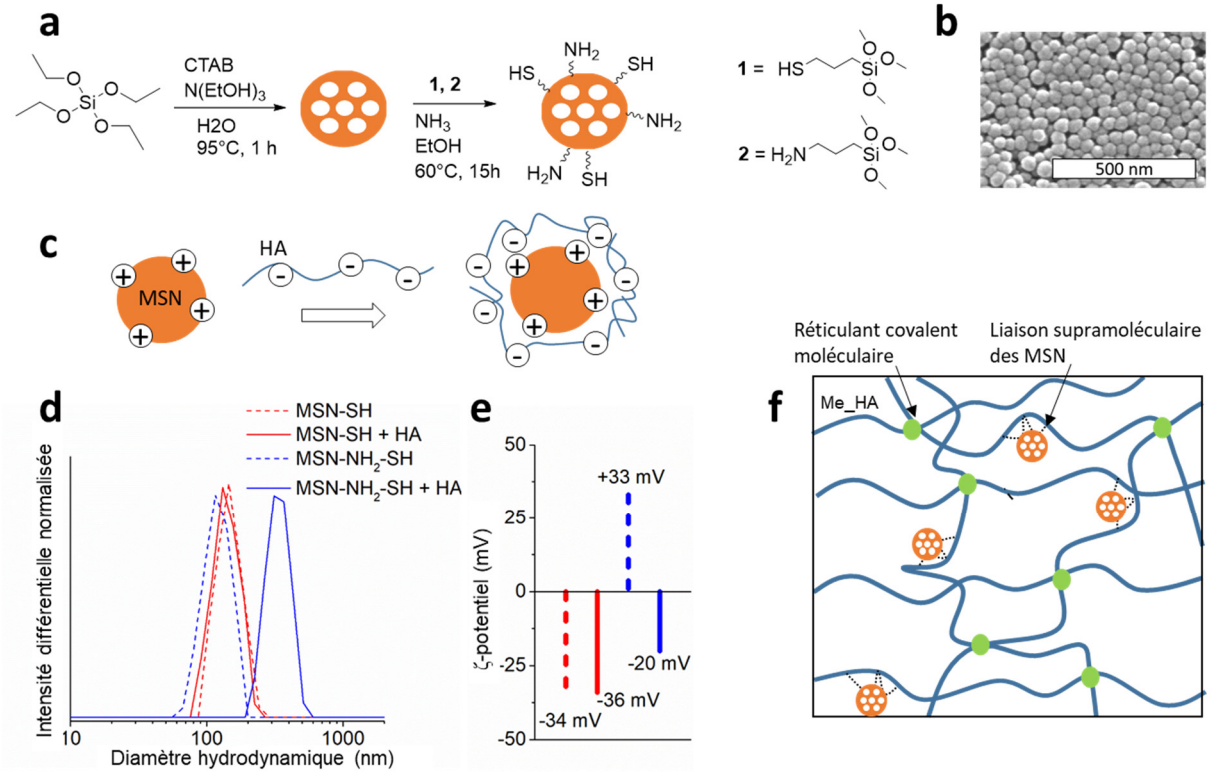

Figure 8 : a) Synthèse et fonctionnalisation du MSN avec des groupes thiol et amine. b) Image SEM du MSN. c) Interaction supramoléculaire entre le MSN chargé positivement et le HA chargé négativement. d) Mesure de la diffusion dynamique de la lumière montrant l'augmentation du diamètre hydrodynamique des particules chargées positivement (ligne bleue) après l'interaction avec le HA (MSN : ligne pointillée, MSN interagissant avec le HA : ligne pleine). e) ζ-potentiel des particules avant l'interaction avec HA (lignes pointillées) et après (lignes pleines). f) Dessin montrant la structure de l'hydrogel de HA nanocomposite contenant à la fois un réticulant covalent moléculaire et MSN interagissant électrostatiquement avec le polymère.

Les propriétés mécaniques de l'hydrogel n'ont pas été affectées par l'introduction de MSN à la concentration de 1 mg/mL. L'hydrogel nanocomposite développé a été testé *in vivo* sur un modèle de cochon clinique pertinent pour le traitement des fistules œsophagiennes. Deux fistules œsophagiennes ont été créées chez chaque animal selon une procédure bibliographique.[39] Le groupe témoin (CG) n'a pas été traité, tandis que dans le groupe hydrogel (HG), une valeur moyenne de 6,7 (3,2) ml de gel a été injectée dans l'orifice fistuleux interne au moyen d'une approche endoscopique. Après 15 jours, dans le groupe CG, l'orifice de la fistule externe était encore persistant avec une inflammation locale concomitante (Figure 9a). À l'inverse, dans la HG, tous les orifices de fistules externes étaient correctement fermés dans 5 cas sur 5 (Figure 9b). L'analyse histopathologique a montré qu'une réponse inflammatoire chronique spécifique était documentée dans la CG (Figure 9c) tandis que dans la HG, une forte

concentration d'éléments gigantocellulaires a été observée, suggérant un processus de cicatrisation approprié (Figure 9d). L'amélioration de la cicatrisation obtenue avec l'hydrogel est attribuée au rôle naturel de l'acide hyaluronique dans la stimulation du processus de cicatrisation.[40,41] De plus, la structure poreuse de l'hydrogel (Figure 6b) et les propriétés mécaniques du matériau (Figure 7a) joueraient un rôle crucial dans l'induction de la prolifération des cellules épithéliales dans la matrice.

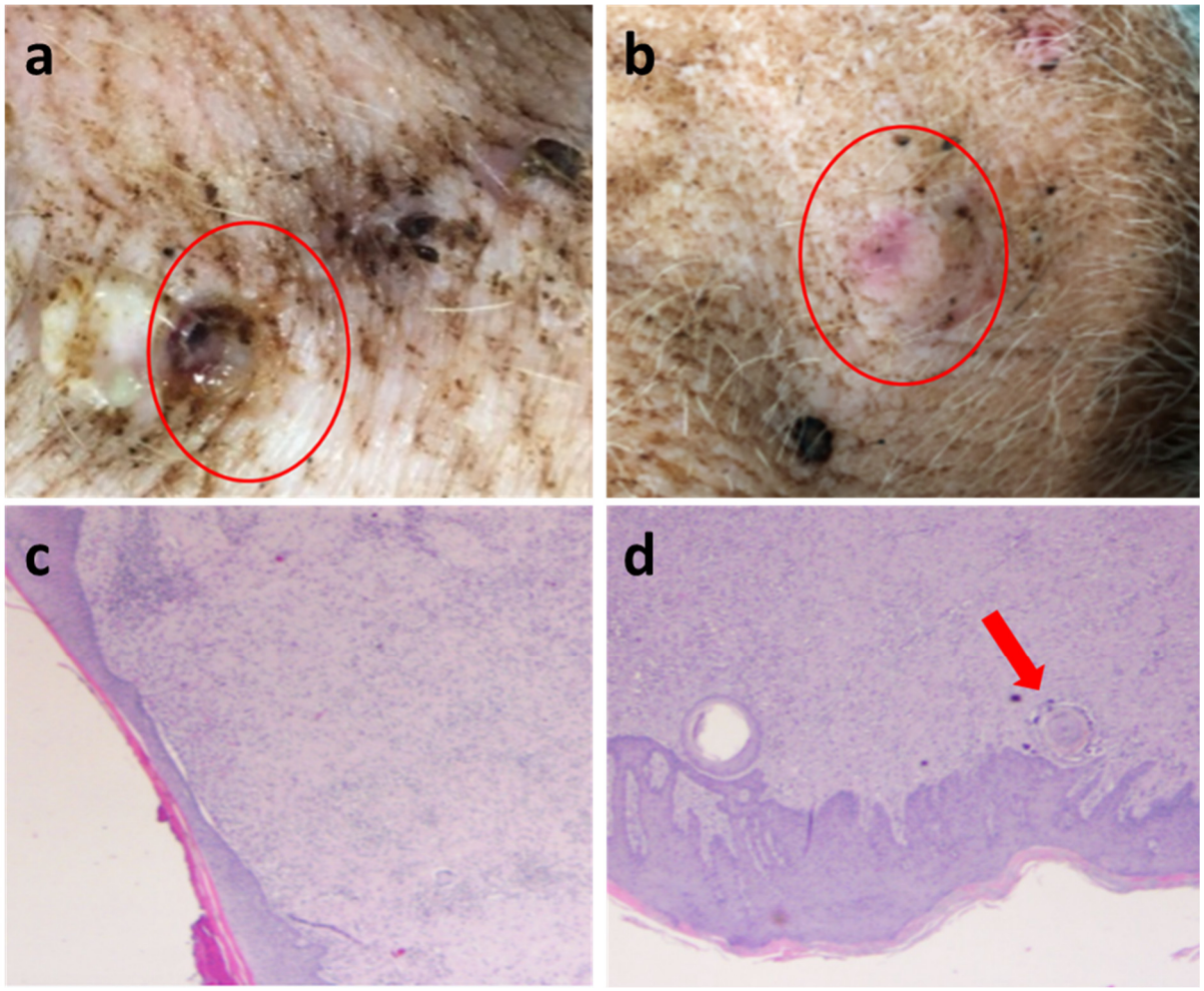

Figure 9 : Aspect macroscopique de l'orifice externe des fistules (cercles rouges) après 15 jours à partir des traitement : persistance et inflammation locale dans la CG (a), fermeture appropriée dans la HG (b). Aspect hystopathologique de l'orifice externe (cutané) (c-d) après 15 jours à partir du traitement : réponse inflammatoire chronique aspécifique sans éléments gigantocellulaires dans la CG (c) ; réponse inflammatoire avec une forte concentration d'éléments gigantocellulaires dans la HG (d).

Le HA de haut poids moléculaire (MW) utilisé dans la préparation de l'hydrogel injectable est connu pour ne pas favoriser l'adhésion cellulaire médié par le récepteur transmembranaire CD44 en raison de sa fonction de remplissage de l'espace dans la matrice extracellulaire qui empêche la signalisation intercellulaire.[40] La possibilité d'introduire des modifications appropriées dans le matériau pour induire l'adhésion cellulaire et éventuellement la différenciation est étudiée au Chapitre 4 dans le but d'ouvrir de nouvelles applications possibles du matériau dans le domaine de la médecine régénérative. Les stratégies étudiées comprennent l'incorporation de biomolécules se liant aux intégrines et l'introduction d'oligomères de HA qui, au contraire de le HA de haut poids moléculaire, interagissent avec le récepteur CD44 d'une manière monovalente permettant la liaison de plusieurs fragments et stimulant les cascades de signalisation cellulaire.[40,41]

L'une des stratégies couramment utilisées pour obtenir l'adhésion cellulaire est l'introduction dans le réseau du tripeptide RGD (arginine-glycine-acide aspartique) qui se lie aux intégrines.[42] L'effet de l'introduction du peptide RGD dans les hydrogels fabriqués avec de l'HA de différents MW (470 kDa et 1700 kDa) été évalué. La séquence peptidique GCGY*RGD*SPG a été liée de manière covalente au groupe méthacrylate du Me_HA par le groupe latéral thiol de l'unité cystéine. La présence d'acides aminés adjacents à la séquence RGD a un effet synergique sur la liaison peptide-intégrité. Les solutions de 1700 kDa et 470 kDa de Me_HA fonctionnalisées avec la séquence GCGY*RGD*SPG ont été utilisées directement pour la préparation d'hydrogels par l'ajout direct du réticulant dithiothréitol. La concentration finale de RGD lié par covalence est de 0,9 mM. Après la préparation de l'hydrogel, les cellules HeLa ont été répandues sur le matériau et leur adhérence a été évaluée par microscopie (Figure 10).

Dans l'hydrogel de pure HA, les cellules sont partiellement fixées au matériau mais elles ont tendance à former des agrégats et à ne pas s'étaler (Figure 10a). Au contraire, une adhésion cellulaire homogène a été observée lorsque la séquence peptidique GCGY*RGD*SPG a été liée soit au Me_HA de 1700 kDa (Figure 10b) soit au Me_HA de 470 kDa (Figures 10c), nonobstant les deux échafaudages aient des propriétés mécaniques sensiblement différentes ($G'_{HA1700\text{-}RGD}$: 95 Pa, $G'_{HA470\text{-}RGD}$: 800 Pa).

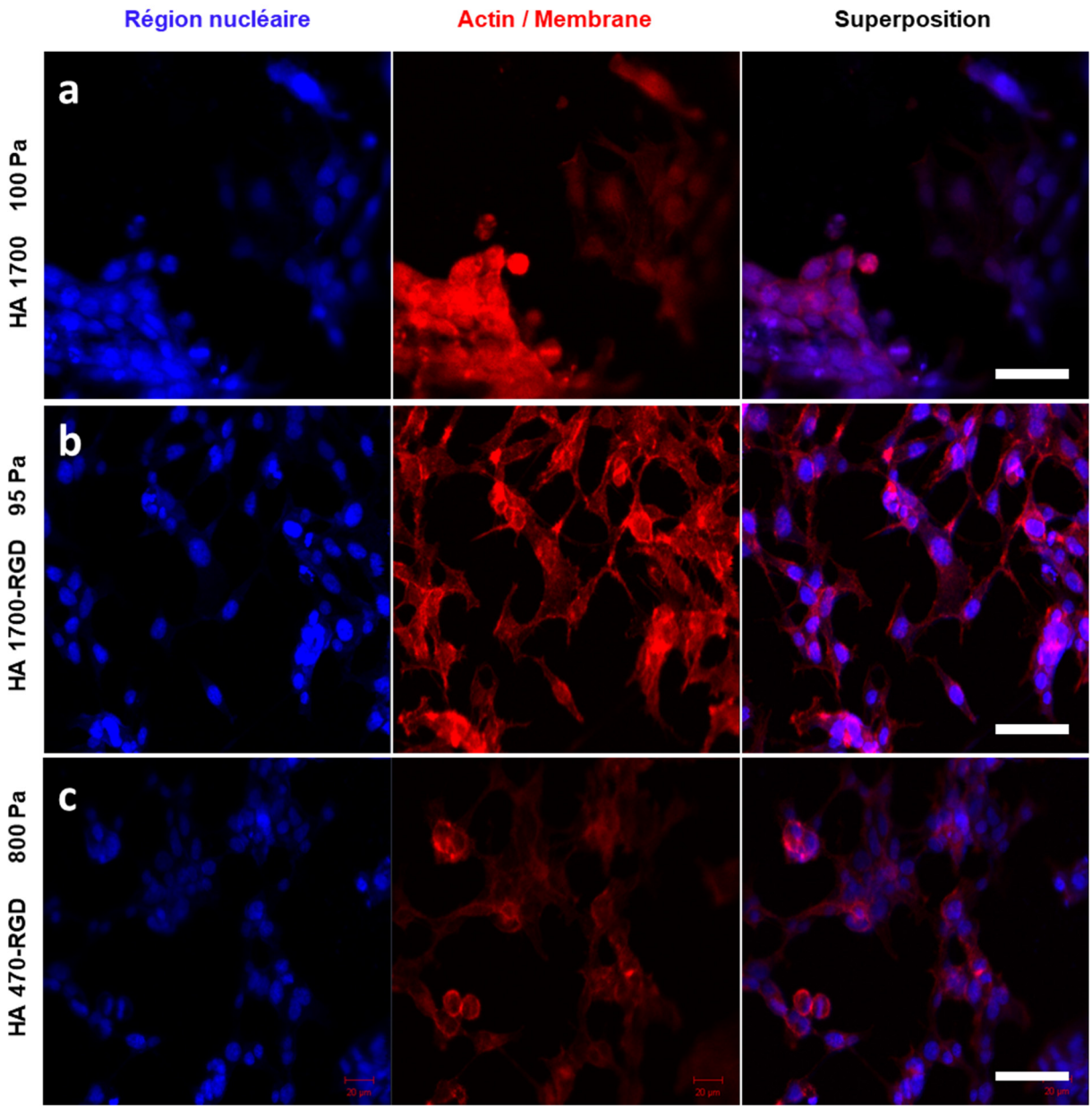

Figure 10 : Évaluation de l'adhésion des cellules HeLa dans des hydrogels de a) HA pure (1700 kDa, 1%), b) HA (1700 kDa, 1%) fonctionnalisé avec le RGD et c) HA (470 kDa, 1%) fonctionnalisé avec le RGD. Régions nucléaires bleu, actine/membrane rouge. Barres d'échelle : 50 µm.

Une autre approche testée pour obtenir l'adhésion cellulaire consistait à incorporer dans le matériau des oligomères de HA méthacrylate (Figure 11). L'introduction d'oligomères à 5% et 10% (Figures 11a, b) dans le matériau a induit une bonne adhésion cellulaire HeLa, tandis qu'une nouvelle augmentation de la concentration en oligomères (15%) a donné l'effet inverse, les cellules étant de forme ronde, probablement en raison d'une diminution du module élastique de l'hydrogel (Figure 11c).

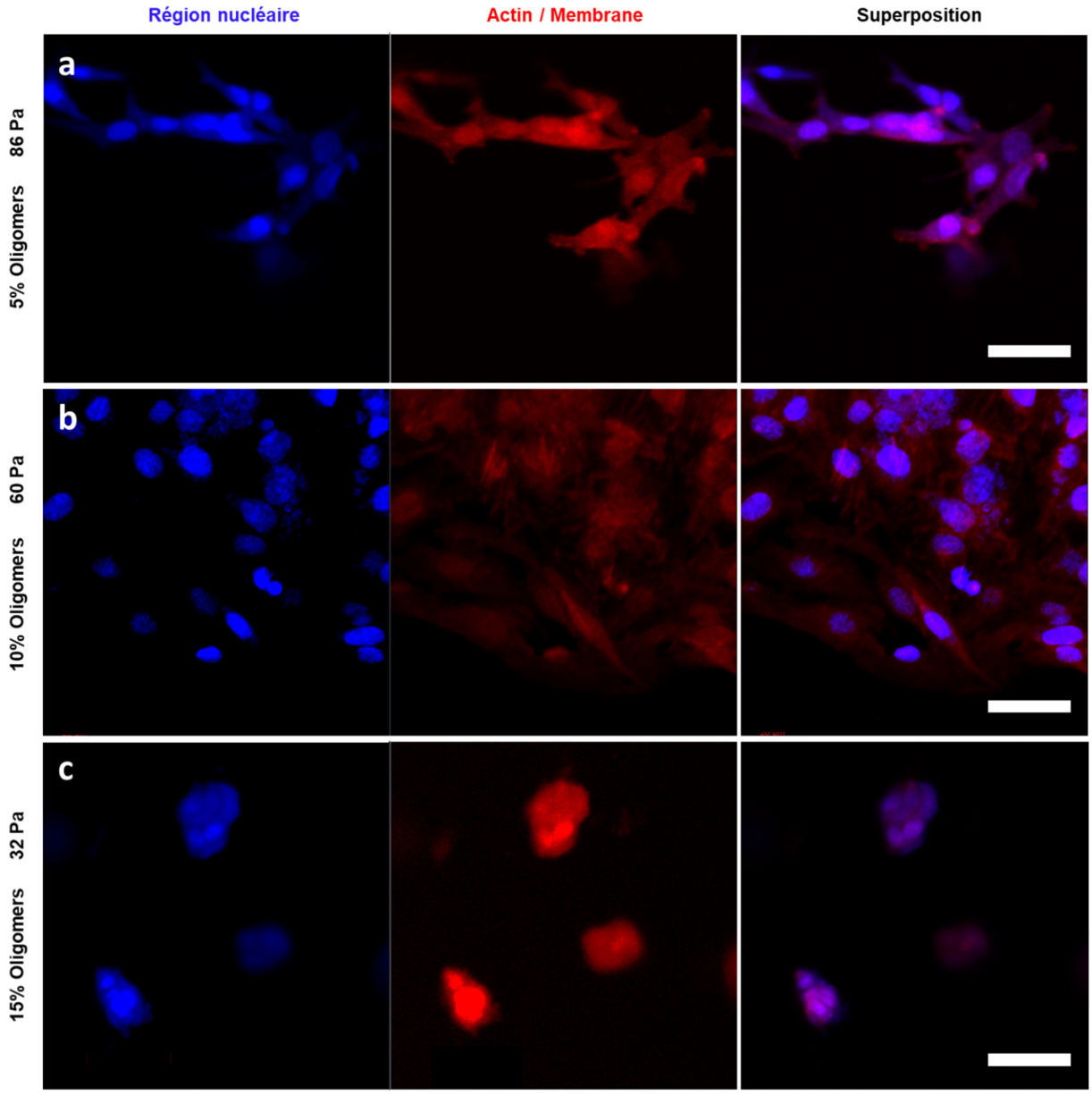

Figure 11 : Effet de l'introduction d'oligomères de HA sur la capacité des cellules HeLa à adhérer à l'hydrogel. a) 5% oligomères, b) 10% oligomères et c) 15% oligomères. Régions nucléaires bleu, actine/membrane rouge. Barres d'échelle : 50 µm

La capacité des oligomères à induire l'adhésion des cellules à la matrice d'HA est particulièrement intéressante car elle suggère que l'application *in vivo* du matériau peut ne nécessiter aucune modification puisque l'enzyme hyaluronidase (Hhase) naturellement présente peut partiellement dégrader l'hydrogel générant les oligomères. La possibilité de reproduire *in vitro* la dégradation de le HA par la Hhase pour donner des oligomères capables de favoriser l'adhésion cellulaire a été étudiée. Des échantillons d'hydrogel constitués de HA (1700 kDa, 1%) ont été traités avec de l'Hhase à différentes concentrations dans la fourchette des conditions

physiologiques (0,0059 U/mL dans le plasma humain à 38,5 U/mL dans les ovaires humains)[40] et incubés à 37 °C, 5% CO_2 pendant 8 h ou 24 h avant l'ensemencement des cellules HeLa. Les hydrogels d'HA traités à l'Hhase ont subi une réduction de masse significative confirmant l'efficacité de la dégradation dans les conditions testées (Figure 12a). Les propriétés mécaniques des matériaux traités par voie enzymatique sont restées inchangées (Figure 12b). Toutes les conditions de concentration enzymatique et de temps d'incubation n'ont pas induit d'adhésion cellulaire (Figure 13). Il est possible que l'activité de la Hhase n'ait pas généré d'oligomères en concentration et en poids moléculaire appropriés pour favoriser l'adhésion cellulaire.

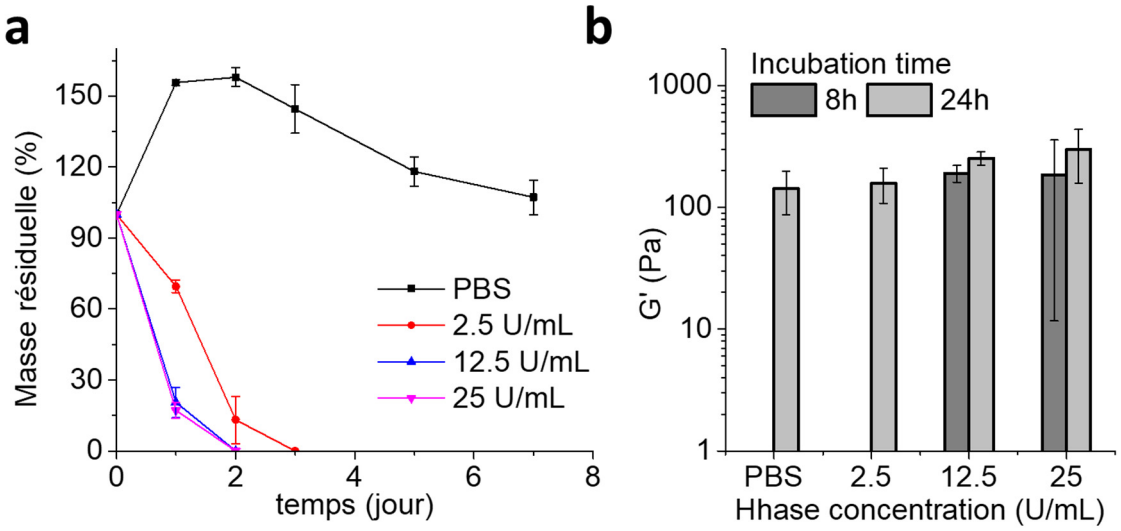

Figure 12 : Traitement de l'hydrogel de HA par la hyaluronidase. a) Cinétique de la perte de masse ; b) effet sur les propriétés mécaniques du matériau.

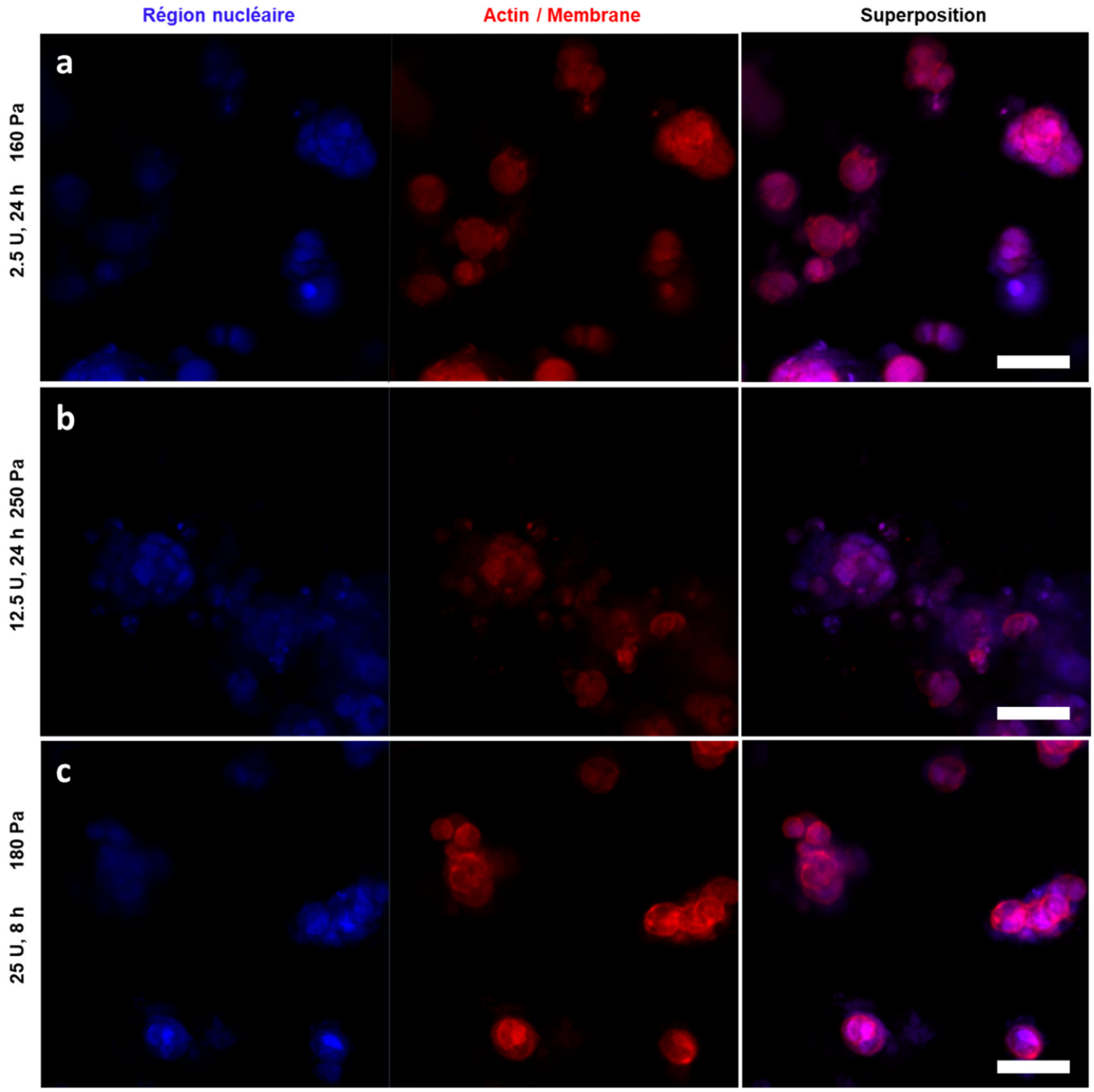

Figure 13 : Effet de la dégradation enzymatique de HA sur la capacité des cellules HeLa à adhérer à l'hydrogel. Incubation a) avec 2.5 U/mL pour 24 h, b) 12.5 U/mL pour 24 h et c) 25 U/mL pour 8 h. Régions nucléaires bleu, actine/membrane rouge. Barres d'échelle : 50 µm

En médecine régénérative, un rôle clé est joué par les facteurs de croissance (GF) qui permettent d'activer la migration des cellules résidentes et la réparation des tissus.[45] Il a été démontré que leur incorporation dans les hydrogels utilisés en médecine régénérative favorise la migration des cellules souches autologues vers le site de l'inflammation[31] et induit la formation de néo-cartilage par les cellules souches mésenchymateuses.[2] La charge de GF dans un nano-porteur lié de manière covalente aux réseaux d'hydrogels permet de protéger la biomolécule pendant la préparation du matériau et de contrôler sa libération. Les nanoparticules de silicium poreux

(pSiNP) sont apparues comme un système de libération de biomolécules intéressant et prometteur grâce à leur facilité intrinsèque d'élimination du corps, leur luminescence et leur dissolution anisotrope.[46] Au Chapitre 5, des nanoparticules et microparticules de silicium poreux (pSiP) de différentes tailles (allant de 250 nm à 20 µm) et tailles de pores sont préparées par gravure électrochimique et fracturées par ultrasons dans le but d'évaluer la capacité du pSiP à soutenir la libération d'une protéine modèle (Figure 14).

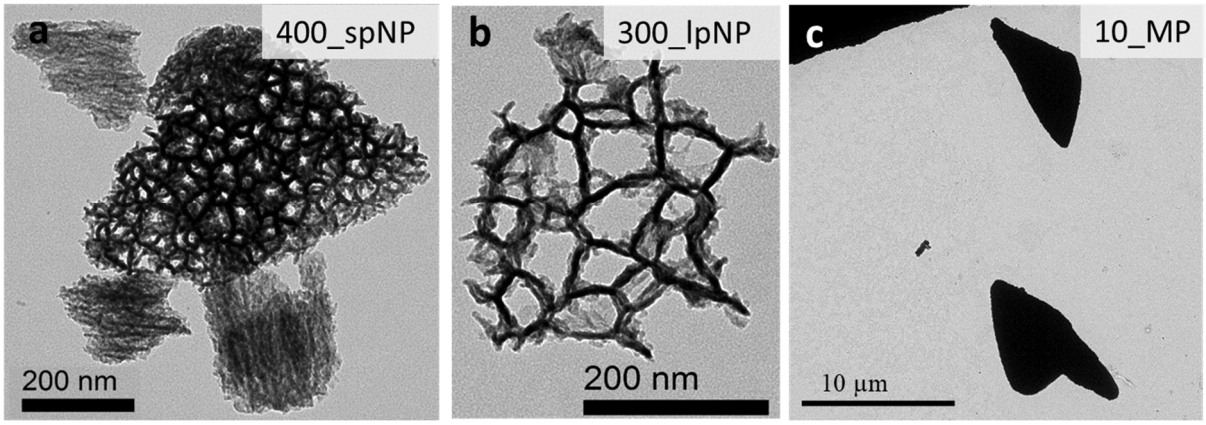

Figure 14: Images TEM des a) nanoparticules de 400 nm, b) nanoparticules de 300 nm avec grands pores et c) microparticules de silicium poreux.

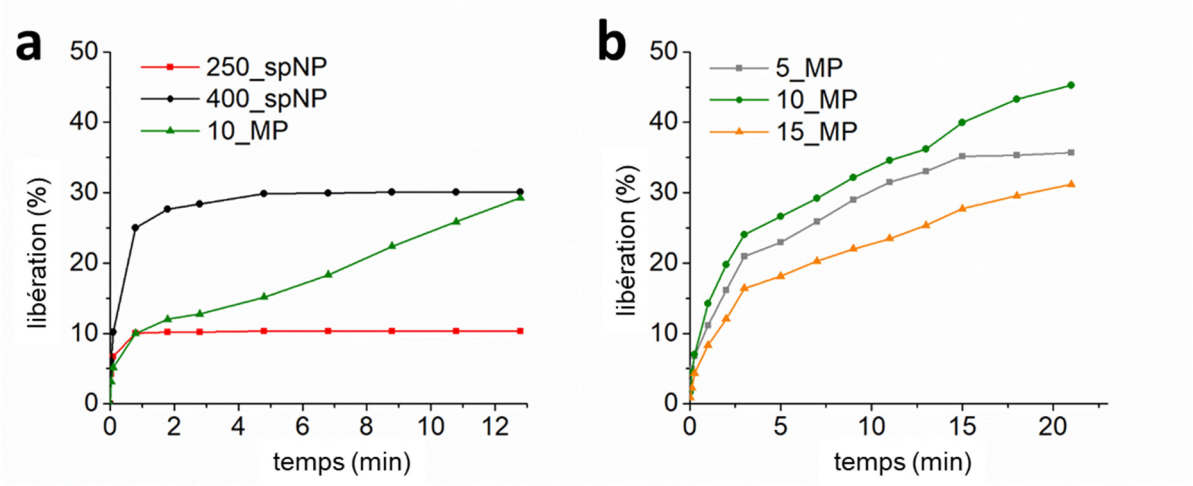

Figure 15 : Lysozyme actif libéré par a) le pSi nano et b) les microparticules.

Le lysozyme a été utilisé comme protéine modèle pour remplacer le, plus coûteux, facteur neurotrophique dérivé du cerveau. La charge est effectuée dans une solution saline tris-tamponnée (Tris) pour obtenir du pSiNP partiellement oxydé. Les expériences de libération réalisées dans le PBS ont montré un fort effet de la taille des particules, les microparticules

donnant une libération nettement plus prolongée que les nanoparticules (Figure 15). La libération constante et prolongée de la protéine est attribuée à la dégradation plus lente prévue pour les plus grosses particules.

Afin de relier par liaison covalente les particules au réseau 3D de l'hydrogel, les particules chargées ont été fonctionnalisées avec du PEG-acrylate. L'hydrogel a été préparé par photopolymérisation UV du PEG-diacrylate en présence du pSiNP acrylés. La stéréolithographie a été utilisée pour imprimer des échafaudages 3D multi-lumières avec une résolution micrométrique (Figure 16).

La libération de protéines de la matrice nanocomposite a été étudiée dans le PBS (Figure 17). La charge directe de lysozyme dans l'hydrogel a induit la perte d'activité de la protéine, ce qui montre l'importance de l'utilisation du pSiP pour protéger la charge pendant le processus d'impression 3D. L'augmentation de la taille des particules a eu pour effet de ralentir la cinétique de libération, mais elle a également réduit la quantité totale de lysozyme libéré. La libération totale de protéines plus faible a été attribuée à une teneur totale en charge mineure dans l'hydrogel plutôt qu'à un effet de taille direct. En effet, lors du processus d'impression 3D, les grosses particules sont plus susceptibles de sédimenter dans la solution de précurseur, ce qui entrave leur incorporation, et par conséquent celle du lysozyme, dans l'échafaudage. Une possibilité de surmonter le problème et d'obtenir une libération élevée et prolongée de protéines à partir des échafaudages pourrait être la combinaison de particules de taille différente.

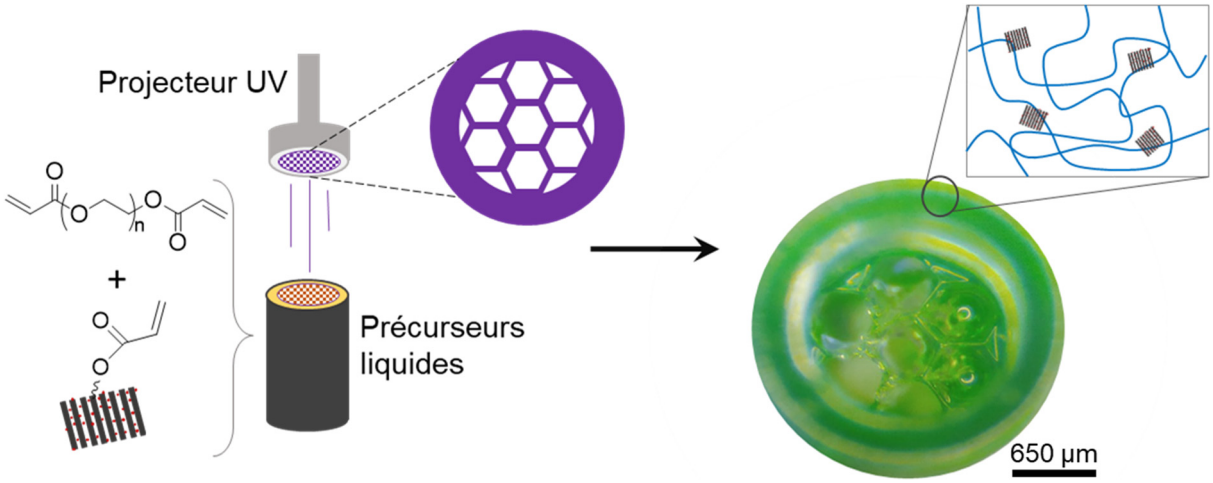

Figure 16 : Impression 3D de l'hydrogel nanocomposite par stéréolithographie.

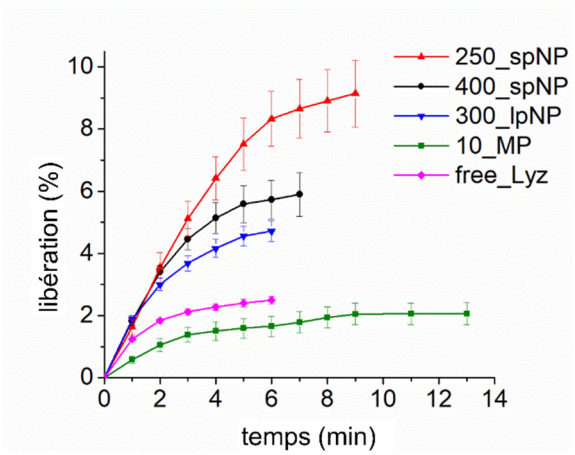

Figure 17 : Libération cumulée de lysozyme à partir d'échafaudages d'hydrogel contenant des particules de différentes tailles.

En conclusion, cette thèse a montré qu'à partir de la sélection du polymère approprié et de la stratégie de réticulation, il est possible de contrôler et de régler la cinétique de la formation d'hydrogel et ses propriétés mécaniques finales. De plus, avec l'introduction dans le réseau de groupements fonctionnels suspendus spécifiques (par exemple la séquence peptidique RGD), il est possible de conférer au matériau des caractéristiques émergentes telles que l'adhésion cellulaire. En outre, l'introduction dans les hydrogels de nanoparticules a été présentée comme une approche intéressante pour contrôler et prolonger la livraison de biomolécules. Les propriétés structurelles, mécaniques et chimiques des matériaux décrits ont été adaptées à des applications biomédicales spécifiques ; les expériences *in vivo* ont montré que les hydrogels étaient capables de faciliter les procédures chirurgicales et d'améliorer les processus de régénération des tissus.

Nous pensons que d'autres études donneront la possibilité d'utiliser les hydrogels comme vecteur de livraison de cellules souches, ce qui ouvrira la voie à différentes applications innovantes en médecine régénérative.

Références

1. Li, J. & Mooney, D. J. Designing hydrogels for controlled drug delivery. *Nature Reviews Materials* 1, 16071 (2016).

2. Bian, L., Zhai, D. Y., Tous, E., Rai, R., Mauck, R. L., *et al.* Enhanced MSC chondrogenesis following delivery of TGF-β3 from alginate microspheres within hyaluronic acid hydrogels in vitro and in vivo. *Biomaterials* 32, 6425–6434 (2011).

3. Daly, A. C., Riley, L., Segura, T. & Burdick, J. A. Hydrogel microparticles for biomedical applications. *Nature Reviews Materials* 5, 20–43 (2020).

4. Xavier, J. R., Thakur, T., Desai, P., Jaiswal, M. K., Sears, N., *et al.* Bioactive Nanoengineered Hydrogels for Bone Tissue Engineering: A Growth-Factor-Free Approach. *ACS Nano* 9, 3109–3118 (2015).

5. Li, F., Truong, V. X., Fisch, P., Levinson, C., Glattauer, V., *et al.* Cartilage tissue formation through assembly of microgels containing mesenchymal stem cells. *Acta Biomaterialia* 77, 48–62 (2018).

6. Loh, Q. L. & Choong, C. Three-Dimensional Scaffolds for Tissue Engineering Applications: Role of Porosity and Pore Size. *Tissue Engineering Part B: Reviews* 19, 485–502 (2013).

7. Lou, J., Stowers, R., Nam, S., Xia, Y. & Chaudhuri, O. Stress relaxing hyaluronic acid-collagen hydrogels promote cell spreading, fiber remodeling, and focal adhesion formation in 3D cell culture. *Biomaterials* 154, 213–222 (2018).

8. Gerecht, S., Burdick, J. A., Ferreira, L. S., Townsend, S. A., Langer, R., *et al.* Hyaluronic acid hydrogel for controlled self-renewal and differentiation of human embryonic stem cells. *Proceedings of the National Academy of Sciences* 104, 11298–11303 (2007).

9. Lou, J., Stowers, R., Nam, S., Xia, Y. & Chaudhuri, O. Stress relaxing hyaluronic acid-collagen hydrogels promote cell spreading, fiber remodeling, and focal adhesion formation in 3D cell culture. *Biomaterials* 154, 213–222 (2018).

10. Spicer, C. D. Hydrogel scaffolds for tissue engineering: the importance of polymer choice. *Polym. Chem.* 11, 184–219 (2020).

11. Hu, W., Wang, Z., Xiao, Y., Zhang, S. & Wang, J. Advances in crosslinking strategies of biomedical hydrogels. *Biomater. Sci.* 7, 843–855 (2019).

12. Piantanida, E., Alonci, G., Bertucci, A. & De Cola, L. Design of Nanocomposite Injectable Hydrogels for Minimally Invasive Surgery. *Acc. Chem. Res.* 52, 2101–2112 (2019).

13. Dutta, A., Maity, S. & Das, R. K. A Highly Stretchable, Tough, Self-Healing, and Thermoprocessable Polyacrylamide–Chitosan Supramolecular Hydrogel. *Macromolecular Materials and Engineering* 303, 1800322 (2018).

14. Han, L., Wang, M., Li, P., Gan, D., Yan, L., *et al.* Mussel-Inspired Tissue-Adhesive Hydrogel Based on the Polydopamine–Chondroitin Sulfate Complex for Growth-Factor-Free Cartilage Regeneration. *ACS Applied Materials & Interfaces* 10, 28015–28026 (2018).

15. Peng, B., Lai, X., Chen, L., Lin, X., Sun, C., *et al.* Scarless Wound Closure by a Mussel-Inspired Poly(amidoamine) Tissue Adhesive with Tunable Degradability. *ACS Omega* 2, 6053–6062 (2017).

16. Xu, Q., Zhang, Z., Xiao, C., He, C. & Chen, X. Injectable Polypeptide Hydrogel as Biomimetic Scaffolds with Tunable Bioactivity and Controllable Cell Adhesion. *Biomacromolecules* 18, 1411–1418 (2017).

17. Eslahi, N., Simchi, A., Mehrjoo, M., Shokrgozar, M. A. & Bonakdar, S. Hybrid cross-linked hydrogels based on fibrous protein/block copolymers and layered silicate nanoparticles: tunable thermosensitivity, biodegradability and mechanical durability. *RSC Advances* 6, 62944–62957 (2016).

18. Liu, R., Liang, S., Tang, X.-Z., Yan, D., Li, X., *et al.* Tough and highly stretchable graphene oxide/polyacrylamide nanocomposite hydrogels. *Journal of Materials Chemistry* 22, 14160 (2012).

19. Rose, S., Prevoteau, A., Elzière, P., Hourdet, D., Marcellan, A., *et al.* Nanoparticle solutions as adhesives for gels and biological tissues. *Nature* 505, 382–385 (2014).

20. Wahid, F., Zhong, C., Wang, H.-S., Hu, X.-H., Chu, L.-Q., *et al.* Recent Advances in Antimicrobial Hydrogels Containing Metal Ions and Metals/Metal Oxide Nanoparticles. *Polymers* 9, 636 (2017).

21. Mehrali, M., Thakur, A., Pennisi, C. P., Talebian, S., Arpanaei, A., *et al.* Nanoreinforced Hydrogels for Tissue Engineering: Biomaterials that are Compatible with Load-Bearing and Electroactive Tissues. *Advanced Materials* 29, 1603612 (2017).

22. Zhou, J., Yang, X., Liu, W., Wang, C., Shen, Y., *et al.* Injectable OPF/graphene oxide hydrogels provide mechanical support and enhance cell electrical signaling after implantation into myocardial infarct. *Theranostics* 8, 3317–3330 (2018).

23. Liu, M., Ishida, Y., Ebina, Y., Sasaki, T., Hikima, T., *et al.* An anisotropic hydrogel with electrostatic repulsion between cofacially aligned nanosheets. *Nature* 517, 68–72 (2015).

24. Thoniyot, P., Tan, M. J., Karim, A. A., Young, D. J. & Loh, X. J. Nanoparticle–Hydrogel Composites: Concept, Design, and Applications of These Promising, Multi-Functional Materials. *Advanced Science* 2, 1400010 (2015).

25. Zhang, H., Patel, A., Gaharwar, A. K., Mihaila, S. M., Iviglia, G., *et al.* Hyperbranched Polyester Hydrogels with Controlled Drug Release and Cell Adhesion Properties. *Biomacromolecules* 14, 1299–1310 (2013).

26. Alonci, G., Fiorini, F., Riva, P., Monroy, F., López-Montero, I., *et al.* Injectable Hybrid Hydrogels, with Cell-Responsive Degradation, for Tumor Resection. *ACS Appl. Bio Mater.* 1, 1301–1310 (2018).

27. Sang, L., Liu, Y., Hua, W., Xu, K., Wang, G., *et al.* Thermally sensitive conductive hydrogel using amphiphilic crosslinker self-assembled carbon nanotube to enhance neurite outgrowth and promote spinal cord regeneration. *RSC Adv.* 6, 26341–26351 (2016).

28. Park, S. H., Seo, J. Y., Park, J. Y., Ji, Y. B., Kim, K., *et al.* An injectable, click-crosslinked, cytomodulin-modified hyaluronic acid hydrogel for cartilage tissue engineering. *NPG Asia Materials* 11, 1–16 (2019).

29. Yesilyurt, V., Webber, M. J., Appel, E. A., Godwin, C., Langer, R., *et al.* Injectable Self-Healing Glucose-Responsive Hydrogels with pH-Regulated Mechanical Properties. *Advanced Materials* 28, 86–91 (2016).

30. Ferruti, P. Poly(amidoamine)s: Past, present, and perspectives. *Journal of Polymer Science Part A: Polymer Chemistry* 51, 2319–2353 (2013).

31. Fiorini, F., Prasetyanto, E. A., Taraballi, F., Pandolfi, L., Monroy, F., *et al.* Nanocomposite Hydrogels as Platform for Cells Growth, Proliferation, and Chemotaxis. *Small* 12, 4881–4893 (2016).

32. Giménez, M. E., Davrieux, C. F., Serra, E., Palermo, M., Houghton, E. J., *et al.* Application of a novel material in the inguinal region using a totally percutaneous approach in an animal model: a new potential technique? *Hernia* 23, 1175–1185 (2019).

33. Nair, D. P., Podgórski, M., Chatani, S., Gong, T., Xi, W., *et al.* The Thiol-Michael Addition Click Reaction: A Powerful and Widely Used Tool in Materials Chemistry. *Chem. Mater.* 26, 724–744 (2014).

34. Liu, Z. Q., Wei, Z., Zhu, X. L., Huang, G. Y., Xu, F., *et al.* Dextran-based hydrogel formed by thiol-Michael addition reaction for 3D cell encapsulation. *Colloids and Surfaces B: Biointerfaces* 128, 140–148 (2015).

35. Burdick, J. A. & Prestwich, G. D. Hyaluronic Acid Hydrogels for Biomedical Applications. *Advanced Materials* 23, H41–H56 (2011).

36. Prestwich, G. D. Hyaluronic Acid-Based Clinical Biomaterials Derived for Cell and Molecule Delivery in Regenerative Medicine. *J Control Release* 155, 193–199 (2011).

37. Gao, Y., Chen, Y., Ji, X., He, X., Yin, Q., *et al.* Controlled Intracellular Release of Doxorubicin in Multidrug-Resistant Cancer Cells by Tuning the Shell-Pore Sizes of Mesoporous Silica Nanoparticles. *ACS Nano* 5, 9788–9798 (2011).

38. Slowing, I. I., Trewyn, B. G. & Lin, V. S.-Y. Mesoporous Silica Nanoparticles for Intracellular Delivery of Membrane-Impermeable Proteins. *Journal of the American Chemical Society* 129, 8845–8849 (2007).

39. Rahmi, G., Perretta, S., Pidial, L., Vanbiervliet, G., Halvax, P., *et al.* A Newly Designed Enterocutaneous Esophageal Fistula Model in the Pig. *Surgical Innovation* 23, 221–228 (2016).

40. Stern, R. Hyaluronan catabolism: a new metabolic pathway. *European Journal of Cell Biology* 83, 317–325 (2004).

41. Ibrahim, S., Kang, Q. K. & Ramamurthi, A. The Impact of HA Oligomer Content on Physical, Mechanical, and Biologic Properties of Divinyl Sulfone-Crosslinked HA Hydrogels. *J Biomed Mater Res A* 94, 355–370 (2010).

42. Tarus, D., Hamard, L., Caraguel, F., Wion, D., Szarpak-Jankowska, A., *et al.* Design of Hyaluronic Acid Hydrogels to Promote Neurite Outgrowth in Three Dimensions. *ACS Appl. Mater. Interfaces* 8, 25051–25059 (2016).

43. Xu, Q., Zhang, Z., Xiao, C., He, C. & Chen, X. Injectable Polypeptide Hydrogel as Biomimetic Scaffolds with Tunable Bioactivity and Controllable Cell Adhesion. *Biomacromolecules* 18, 1411–1418 (2017).

44. Domingues, R. M. A., Silva, M., Gershovich, P., Betta, S., Babo, P., *et al.* Development of Injectable Hyaluronic Acid/Cellulose Nanocrystals Bionanocomposite Hydrogels for Tissue Engineering Applications. *Bioconjugate Chem.* 26, 1571–1581 (2015).

45. Shi, Y., Wang, Y., Li, Q., Liu, K., Hou, J., *et al.* Immunoregulatory mechanisms of mesenchymal stem and stromal cells in inflammatory diseases. *Nature Reviews Nephrology* 14, 493–507 (2018).

46. Park, J.-H., Gu, L., von Maltzahn, G., Ruoslahti, E., Bhatia, S. N., *et al.* Biodegradable luminescent porous silicon nanoparticles for *in vivo* applications. *Nature Materials* 8, 331–336 (2009).

Chapter 1: General Introduction

Abstract

Hydrogels are three-dimensional hydrophilic polymeric structures that can absorb water and swell without getting solubilized. They are considered the artificial materials that better resemble the extracellular matrix of soft tissues from both a structural and a mechanical point of view. This chapter presents first the structural requirements, including microarchitecture, mechanical properties and bio-signaling, to obtain a suitable hydrogel for biomedical applications. Then it is discussed how to design hydrogels with the desired properties by i) the selection of the polymeric back-bone, ii) the choice of the cross-linking strategy and iii) the introduction of additional features such as pending groups and nanoparticles. Specifically, the introduction of nanoparticles has emerged as a strategy to generate nanocomposite systems with advanced properties, such as elasticity and anisotropy, beside the possibility to exploit them for the controlled delivery of biomolecules. Finally, this chapter describes the advantages and the challenges associated with the preparation of *in situ* forming injectable hydrogels for minimally invasive medicine. In particular the possible techniques to obtain an accurate control over the sol-gel transition are discussed.

Part of this chapter has been published:

E. Piantanida, G. Alonci, A. Bertucci, L. De Cola ”Design of Nanocomposite Injectable Hydrogels for Minimally Invasive Surgery” *Acc. Chem. Res.* 52, 2101, 2019.

1.1. Structural properties of hydrogels

Hydrogels such as gelatin, egg-white and agarose have been part of the daily human life for centuries, and starting from the 1940s they have been subjects of scientific studies.[1] Pioneering publications include the work of Flory about the sol-gel transition,[2,3] the thermodynamic description of the cross-linking process by Eldridge and Ferry[4,5] and the recognition of the structure similarity between hydrogels and biological tissues by Wichterle and Lim.[6] Hydrogels are defined as three dimensional hydrophilic polymeric structures that can absorb water and swell without dissolution. The hydrogel formation process consists in the generation of intermolecular linking extended throughout the space up to the creation of a polymeric system with infinite molecular weight (percolated network).[7] The critical phenomenon of gelation has been described by Stauffer *et al*. on the basis of the percolation model (Figure 1.1).[8]

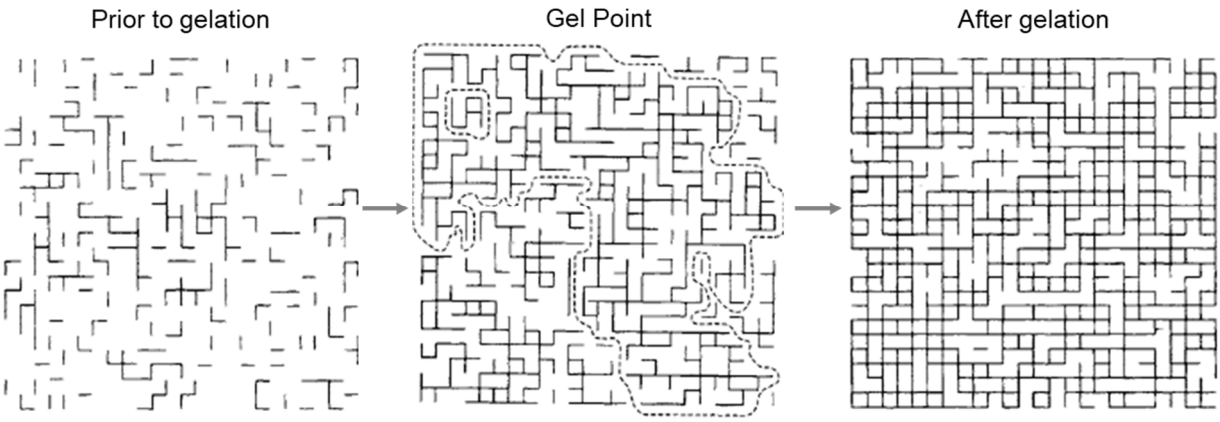

Figure 1.1: Schematic representation of percolation. Prior to gelation the clusters are sparse, randomly distributed and the interactions are scarce. At the gel point the inter-cluster interactions are enough to form a lattice that reaches the edges of the system (cluster surrounded by the dashed lines); randomly distributed clusters are still present. After the gelation the system is constituted of a single cluster. Adapted from *Gels Handbook* by Kajiwara, K. Copyright 2001 Elsevier Inc.

The parameters used to describe the hydrogel network structure on the nanoscale are the polymer volume fraction in the swollen state, that is a measure of the amount of water entrapped in the material, the molecular weight of the polymer chain between two consecutive cross-linking points, that represents the degree of cross-linking, and the mesh size, that describes the linear space between the polymeric chains and it is crucial for biomolecule diffusion (Figure 1.2).

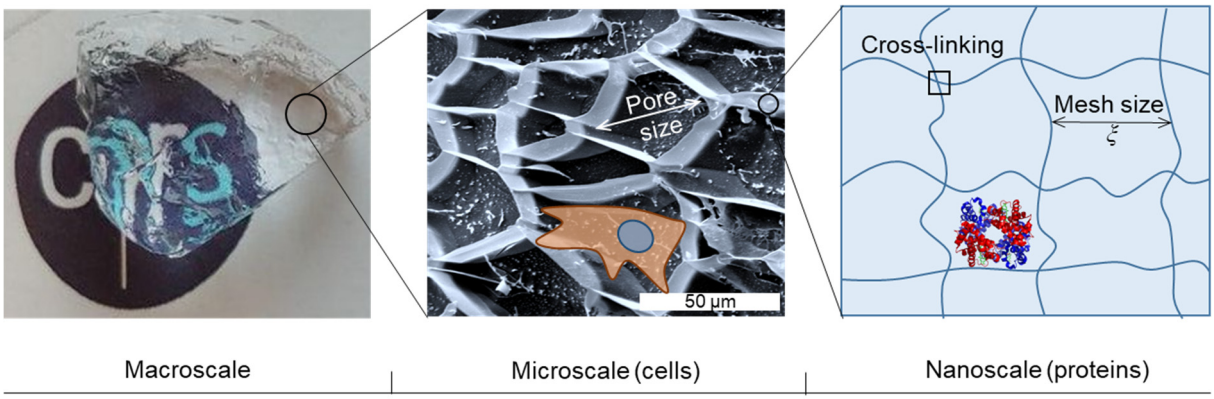

Figure 1.2: Hierarchical structure of a hydrogel: macro, micro and nanoscale.

The structure of hydrogels is described by the equilibrium-swelling theory that relates the structure to the swelling, the rubber-elasticity theory that relates the structure to the stiffness and the mesh size theory that relates the structure to the solute diffusivity.[9,10] Hydrogels can be considered as a solid from a mechanical point of view and thermodynamically as solutions.[11] The polymeric networks are solutes that act both as semipermeable membranes and as pressure actuators to increase the chemical potential of the solvent by elastic force.[11] The swelling equilibrium is the thermodynamic equilibrium determined by the balance between the entropy of mixing and the retractive force of the polymer chains.[12] From a mechanical point of view, the equilibrium is achieved when the osmotic pressure arising from the difference in solute concentration equals the osmotic pressure from the elasticity of the network on the surface of the gel.[11] The water entrapped in the network plasticizes the material and induces a reduction in the polymer glass transition temperature to well below the operating temperature of 37 °C establishing the transition of the polymer from the glassy state to the rubbery-elastic regime.[12] The rubber elasticity originates from the micro-Brownian motion of the polymeric chains ruled by entropy.[7]

1.2. Structural requirements for the biomedical application of hydrogels

The extracellular matrix (ECM) is composed of biological molecules, secreted by cells, that act as a scaffold responsible for the bioactive signaling of cells and for the mechanical integrity of tissues and organs. The ECM is a dynamic hydrated network tailored to the micro-environmental needs of the inhabiting cells.[13] Hydrogels are considered the artificial materials that better resemble the ECM of soft tissues from both a structural and a mechanical point of

view. Different hydrogels are already being used in clinical applications with soft contact lenses being the most abundant, followed by materials used as dressing to facilitate the wound healing or as tissue substitute.[14] A listing of the most significant hydrogels present on the market is reported in the work recently published by Cascone and Lamberti.[15] Hydrogels are of particular interest in regenerative medicine where they can be used as delivery vehicle for biomolecules[16] and cells.[17] Also, they serve as scaffolds for the *in vivo* cellular engraftment, proliferation and differentiation.[18–20] The implanted hydrogel plays an active role in the regeneration of the tissue providing mechanical functions and bio-factors.[21] The proliferation of cells in hydrogels requires, however, suitable microarchitecture[22] and mechanical properties besides chemical composition.[23–25] The porosity of hydrogels, in the typical size range of 1-100 μm, can be tuned by manipulating the cross-linking density and the polymer concentration or it can be designed by exploiting suitable techniques including 3D-printing, freeze-drying, and salt-leaching.[16] Of particular interest is the possibility to reproduce the anisotropic structure of biological systems with the orientation of the polymeric structure along a preferential direction or with the introduction of aligned fillers or void channels.[26] The size distribution and the shape of pores significantly influence both the physical and biological properties of the material. The rise in porosity increases the network deformability and promotes the water flow by capillarity and convection instead of by diffusion only.[16,27,28] Hollister performed a computational study about the effect of porosity and pore shape on the mechanical properties and permeability of hydrogel scaffolds (Figure 1.3). He observed that an increase of porosity is associated, as expected, with a decrease in the elastic modulus and with an increase in permeability. Furthermore the study showed that, for a given porosity, the pore shape and the 3D pore arrangement impact both the mechanical properties and the permeability with cylindrical pores giving lower elastic modulus and higher permeability compared with spherical pores.[21] The mean diameter and the shape of the pores determine also the transport rate of oxygen and nutrients, and the possibility for cells to move and proliferate. For example, pores of 5-15 μm are reported to be suitable for fibroblast proliferation, while bigger pores, in the range of 20-125 μm, are required for mature mammalian cells.[29] The mechanical properties of the scaffold also have a tremendous impact on its ability to interact with cells, through a mechanism known as mechanotransduction, which is how the mechanical properties of the environment are translated into biochemical signals.[30,31] Each cell type is specifically tuned to the specific tissue in which they reside and consequently their growth and differentiation are promoted by defined mechanical properties (Figure 1.4).[32]

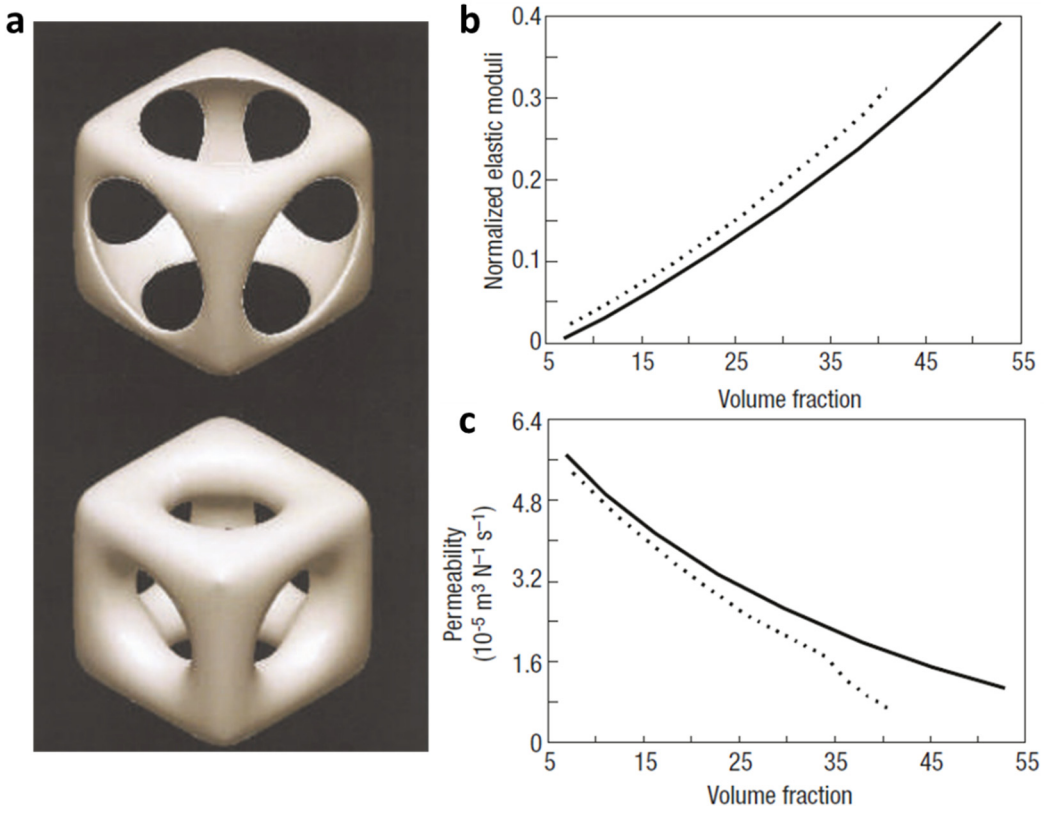

Figure 1.3. a) Spherical pore (top) and cylindrical pore (bottom) microstructure models. b) Effect of volume fraction and pore shape on the b) elastic modulus and c) permeability of the material. Dashed line: spherical pore; solid line: cylindrical pore. Reprinted with permission from *Nat. Mater.* **2005**, 4, 518. Copyright 2005, Springer Nature.

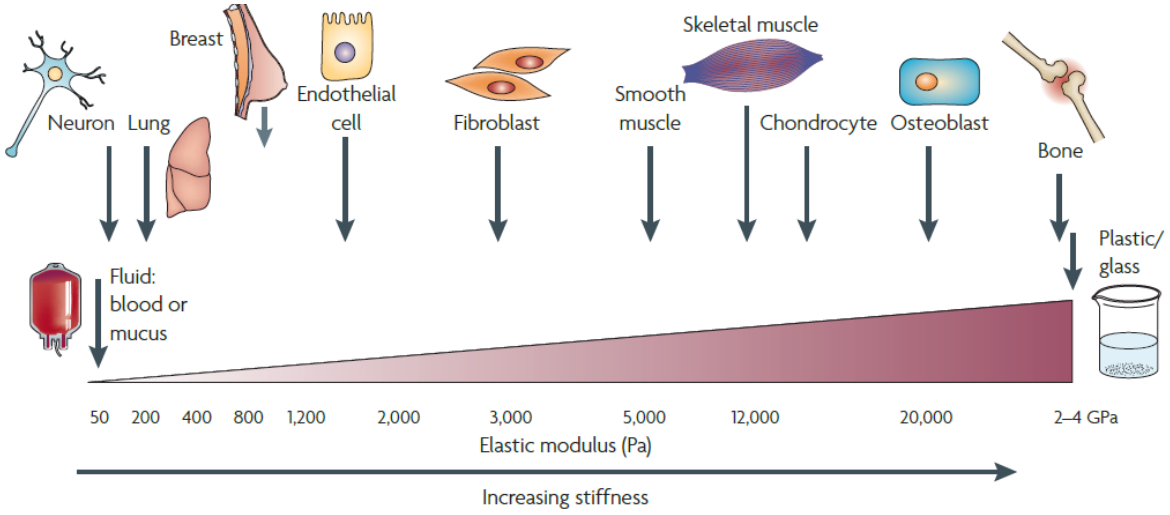

Figure 1.4: Cells are exposed to isometric forces generated locally by cell-cell and cell-extracellular matrix interactions. Reprinted with permission from *Nature Rev. Cancer*, **2009**, 9, 108. Copyright 2009, Springer Nature.

1.3. Design of hydrogels with tailored properties

Hydrogels with tailored properties are obtained from the selection of the constituent polymer, the cross-linking mechanism, the introduction of specific pending groups and the incorporation of a nano- or micro-filler in the material (Figure 1.5).

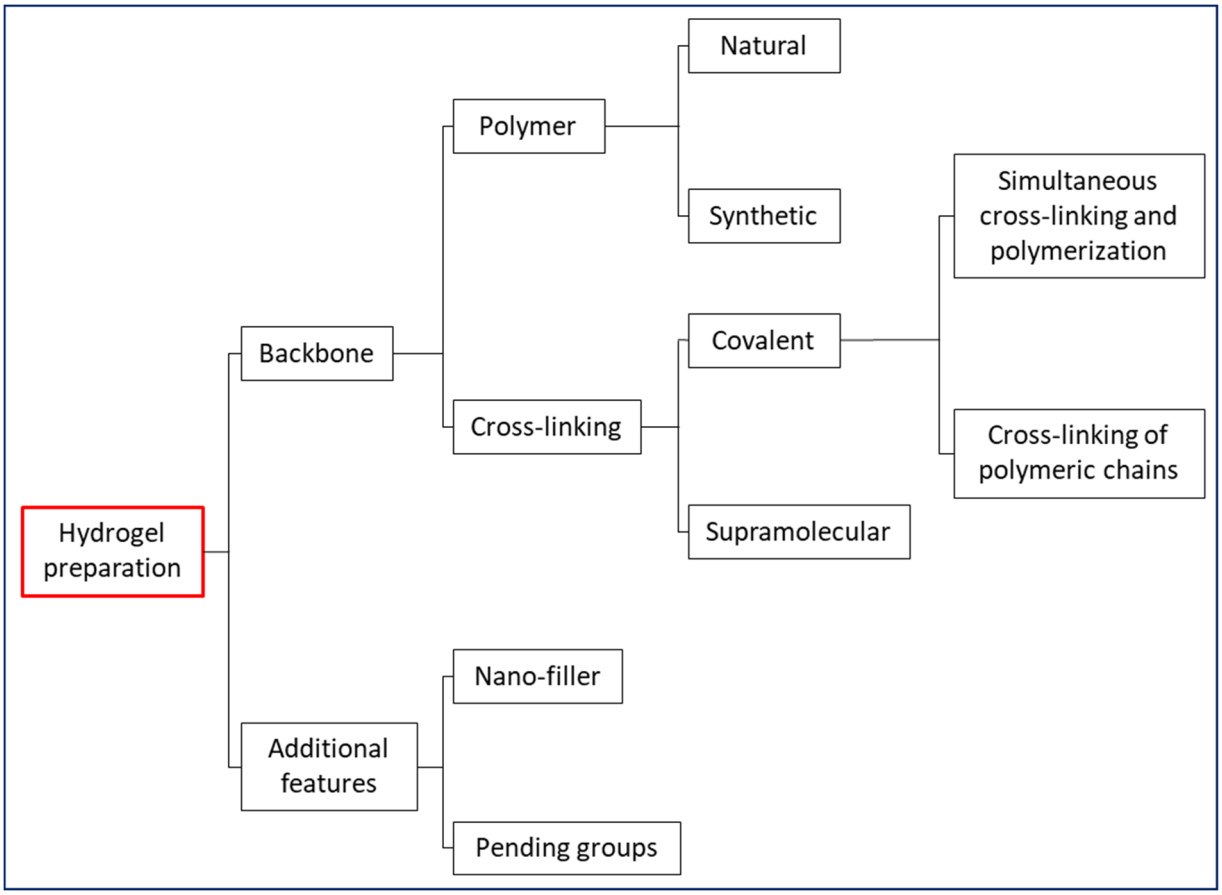

Figure 1.5: Parameters in hydrogel preparation.

1.3.1. The polymer selection

The hydrogel network may be constituted either of natural or synthetic polymers with the former having the general advantage of biocompatibility and the latter being associated with a more precise and tunable design. Selected representative examples of synthetic polymers employed in the preparation of hydrogels are polyethylene glycol (PEG), polyvinyl alcohol (PVA) and polyesters (Figure 1.6). PEG is the most used synthetic polymer in the preparation of hydrogels due to its chemical and biological inertness combined with the large number of commercially available architectures.[33] It has been used as a blank slate for the preparation of cell growth scaffolds with tunable degradation time[34] and stress relaxation kinetics ranging from seconds to months.[35] Despite the general bio-inertness attributed to PEG, it has been

recently demonstrated that certain patients develop anti-PEG antibodies suggesting that genetics might play a role in PEG immunogenicity.[36] PVA is a synthetic polymer widely used in the preparation of hydrogels due to its high elasticity and biocompatibility even though it does not induce cell adhesion.[33] The lack in cell adhesion of PVA has been exploited to restrict stem cell differentiation in the preparation of scaffolds for the packaging and storage of cells.[37] Thanks to its ability to sustain mechanical loads PVA has been used as lubricant in cartilage tissue engineering.[38] Synthetic cartilage implants made of PVA and produced by Cartiva™ have been approved by FDA, the satisfaction of the patients treated with this material remains however variable and neutral on average.[39] Among synthetic polymers, polyesters, are attractive thanks to their biodegradability. Due to their hydrophobic character they are generally combined with PEG to form block-copolymers in the preparation of supramolecular thermoresponsive hydrogels. The optimization of the amphiphilic ratio and the block composition in the preparation of polyester based hydrogels allows to tune the kinetic of the material degradation in a time span ranging from days up to years.[40] A drawback of the use of polyesters in biomedical applications is the release, during degradation, of monomers bearing carboxylic acids that can impact the local pH and induce tissue damage.[41]

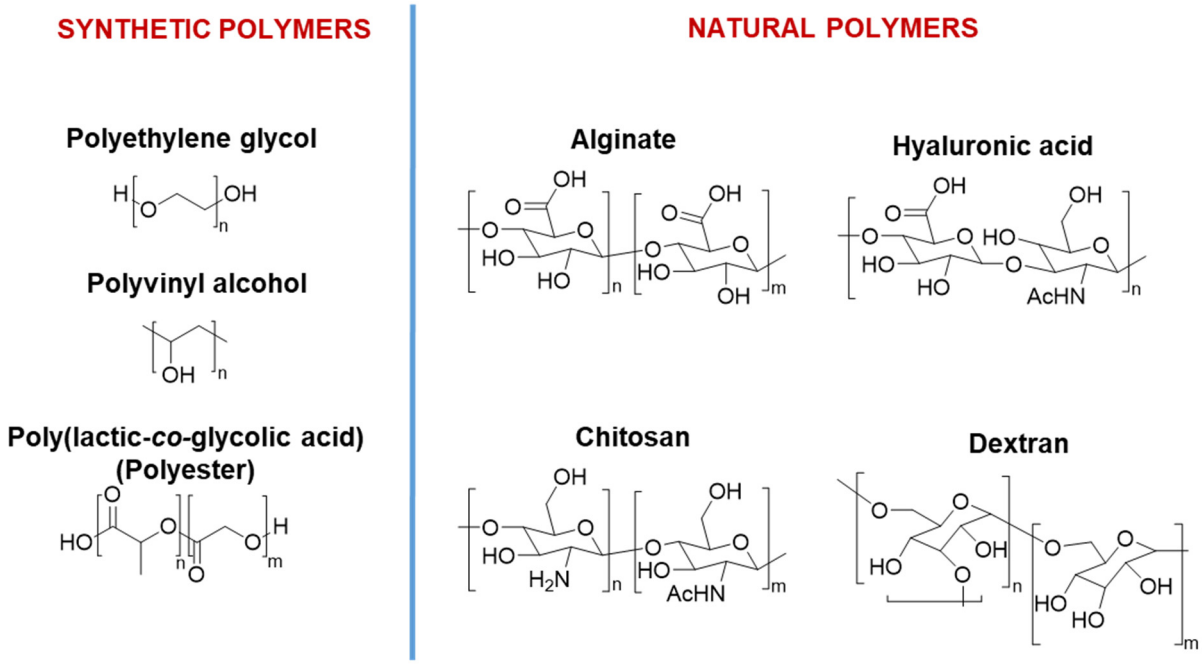

Figure 1.6: Synthetic and natural polymers commonly employed in the preparation of hydrogels.

The natural polymers employed in the preparation of hydrogels are either peptide-based such as collagen, silk and elastin or polysaccharides such as alginate, chitosan, hyaluronic acid and dextran (Figure 1.6). Peptide-based material are generally able to mediate cell signaling and adhesion and they can be modulated by cells. The weak point of protein-derived substrates is the difficulty to obtain contamination-free and homogeneous polymers from natural sources and this may lead to immunogenicity.[33] Collagen based hydrogels are formed *via* the non-covalent hierarchical assembly of the protein triple helix. The risk of immunogenicity and the problem of heterogeneity associated to the *in vivo* use of this protein has been recently overcome with the use of recombinant human collagen that allows furthermore to introduce in the polymeric chains the desired adhesive, signaling and degradable motifs.[42] The chemical modification of collagen is hindered by the sensitivity of the hierarchical assembly and therefore the possibility of functionalization and the introduction of covalent cross-linking sites are limited. A better tolerance to chemical modification is found in gelatin - partially hydrolyzed collagen - that is commonly functionalized on the lysine residues to introduce for example methacrylate groups.[43] Gelatin retains the bioactive sites of collagen while missing the triple helix structure. Polysaccharides, compared with protein-based materials, give significantly lower immunogenicity, are more hydrophilic and present abundant chemical modification sites. The main limit of polysaccharides is the high batch-to-batch variability.[44] Alginate can be easily cross-linked with divalent cations to form hydrogels that are able to relax after strain thanks to the supramolecular nature of the material. Alginate does not give cell adhesion and it is not biodegradable but the hydrogels prepared using this polysaccharide are dissolved by cation exchange. The fast ionic gelation has been exploited for the preparation of printable biomaterials.[45] Among the polysaccharides, chitosan is of particular interest because it promotes cell adhesion while having antimicrobial activity.[46] Its use in the preparation of hydrogels is however limited by its low solubility at physiological pH.[33] Hyaluronic acid (HA) is widely used in the preparation of injectable hydrogels thanks to its strong shear-thinning behavior. Hydrogels based on HA have a high swelling degree due to the presence of carboxylic groups which provide high density of negative charges at neutral pH and they undergo fast *in vivo* degradation by hyaluronidase enzymes. From the combination of protein-derivatives and polysaccharides it is possible to obtain hydrogels that combine desirable properties. Mao and coworkers for example combined silk, that has hemostatic properties, and cellulose with the function of improving the mechanical properties of the system through the formation of H-bonding.[47]

1.3.2. The cross-linking strategy

The cross-linking process consists in the generation of inter-molecular interactions that bring to the sol-gel transition. Such interactions might be covalent or supramolecular with the former associated to the formation of an irreversible hydrogel and the latter to a dynamic system. The main advantages of supramolecular hydrogels are the absence of chemical reagents that could give cytotoxicity in case of incomplete cross-linking reaction, the stimuli-responsive behavior and the self-healing property. On the other side, covalent systems have enhanced mechanical properties and stability at physiological conditions as strong points.[48,49] Physically cross-linked hydrogels can be formed thanks to the generation of self-assemblies controlled by H-bonding, crystallization or hydrophobic interactions or thanks to the presence of other inter-chain linking mechanisms such as metal coordination, ionic/electrostatic, or host-gust interactions (Figures 1.7 and 1.8). Hydrogen-bonding is one of the most important non-covalent interactions. For example, the formation of both weak H-bonds and strong multiple H-bonds in a hierarchical fashion has been used to impart to hydrogels unique properties such as tunable Young's modulus, high stretchability and toughness (Figure 1.7a).[50] Hydrophobic interactions are at the base of the gelation process of thermoresponsive systems. These materials are constituted by amphiphilic blocks which contain segments of hydrophilic and hydrophobic nature that can self-assemble into an organized structure (e.g. micelle). The hydrophobic parts are constrained in the same micellar core with the hydrophilic groups forming loops. With a thermal stimuli, hydrophobic interactions generate bridges between micelles inducing a phase transition and eventually the formation of a hydrogel.[48] Pluronic® is an example of commercially available polymer that can be used for the preparation of thermoresponsive hydrogels (Figure 1.7b).[51] The ability of polymers to generate crystalline domains can also bring to the formation of supramolecular hydrogels, a classic example is polyvinyl alcohol that, in water solution, forms over time a soft hydrogel. The material properties can be tailored applying freeze-thawing cycles (Figure 1.7c).

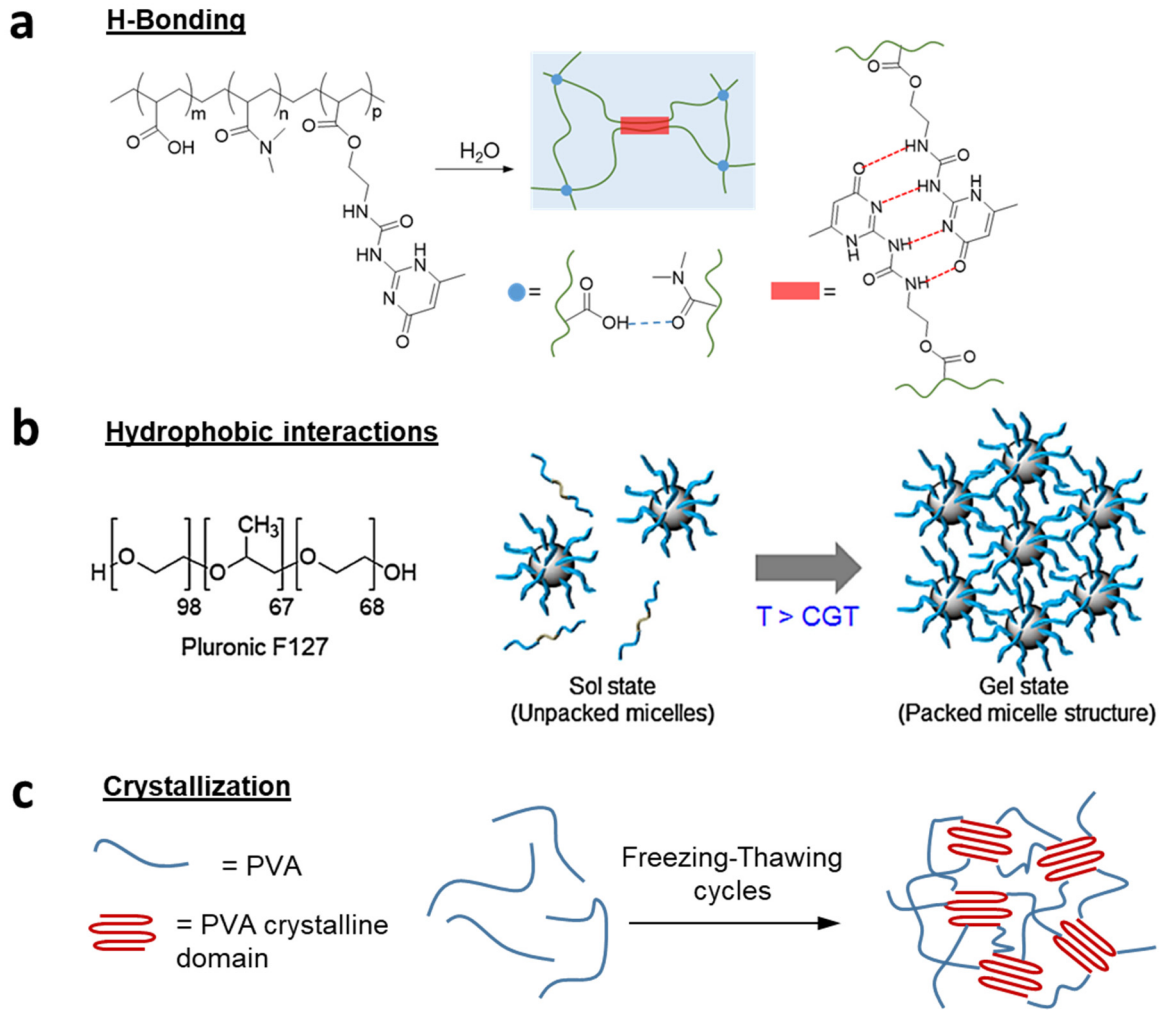

Figure 1.7: a) Hierarchical hydrogen bonds in a hydrogel: weak H-bonds in blue and strong multiple H-bonds in red. Adapted with permission from *Sci. report* **2020,** 10, 11727. Copyright 2020, Springer Nature. b) Packing of bridged micelles driven by hydrophobic interactions in a Pluronic® based hydrogel. (CGT: critical gel temperature). Adapted with permission from *Carbohydrate Polymers* **2017**, 156, 403. Copyright 2016, Elsevier Ltd. c) Freezing-thawing cycles of a PVA solution generate the crystalline domains that are responsible of the sol-gel transition.

Ionic interactions are the basis of the formation of the widely employed alginate-calcium hydrogel (Figure 1.8a) and they can be used to cross-link the commercial polymer Nafion®.[52] Another strategy for the formation of supramolecular hydrogels is the coordination of metal ions to functional groups in polymer chains. This kind of interaction is exploited, for example, in the preparation of mussel inspired catechol-ferric ions systems. The complex structures and therefore the hydrogels based on these interactions are pH dependent (Figure 1.8b). Highly selective physical cross-linking can be obtained employing host-guest interactions in which a large cavity molecule (host) binds with complementary guest (Figure 1.8c).[53] The host-guest

inclusion is promoted by H-bonding, electrostatics, van der Waals and hydrophobic interactions.[48]

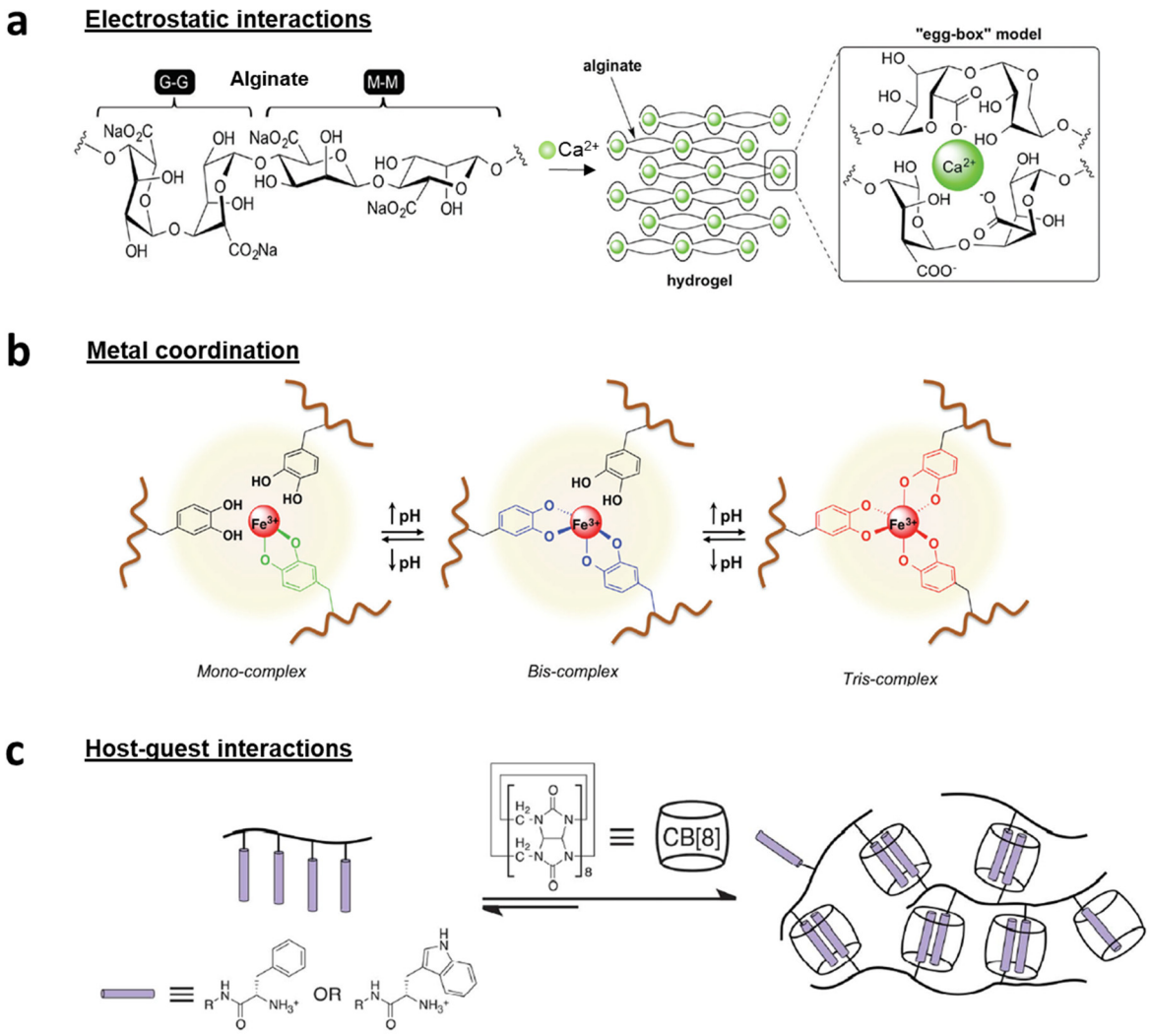

Figure 1.8: a) Hydrogel formation mediated by electrostatic interactions. Reproduced with permission from *New J.Chem.* **2016**, 40, 8493. Copyright 2016, The Royal Society of Chemistry. b) Cross-linking of hydrogel driven by metal-ligand interactions. The sol-gel transition is influenced by the pH. Reproduced with permission from *New J.Chem.* **2016**, 40, 8493. Copyright 2016, The Royal Society of Chemistry. c) Formation of a supramolecular hydrogel by host-guest interactions. Reprinted with permission from *J. Mater. Chem. B* **2013**, 1, 2904. Copyright 2013, The Royal Society of Chemistry.

Common chemical cross-linking strategies employed in the preparation of hydrogels for biomedical applications include photo-polymerization,[54,55] enzyme-induced linking[56,57] and click chemistry comprising Diels-Alder,[58,59] Michael addition[60,61] and Schiff base formation[62,63] reactions. The parameters that must be taken into account in the selection of the cross-linking

reaction are the reaction conditions (i.e. time, pH, temperature, catalyst, photo-radiation) and the need of purification in case by-products are formed or if the process is not quantitative. The use of photo-polymerization in hydrogel preparation has the advantages of rapid formation and wide tunability of the mechanical properties.[64] Furthermore, the fact that the cross-linking takes place only in the area irradiated by the light, allows to have a precise control over the geometry of the obtained material and it makes this cross-linking strategy an optimal method for the 3D bio-printing of tissues with micrometric resolution (Figure 1.9a).[65] This hydrogel preparation strategy will be presented in Chapter 5 in relation to the development of a multi-channel scaffold for peripheral nerve regeneration. Irgacure 2959 is considered the most promising UV photoinitiator thanks to its high cytocompatibility.[66,67] The UV light itself, however, arises concerns about possible DNA and tissue damage. This issue can be overcome with the use of visible light initiators such as camphorquinone,[68] eosin Y[69] and vitamin B_{12}[70] with the further advantage of deeper tissue penetration compared with UV light.[71] GelrinC™ from Regentis Biomaterials is a an example of photopolymerized material in clinical study for the treatment of damaged articular cartilage. GelrinC™ is made of diacrylate-PEG and fibrinogen, it can be injected in the target site and cured *in situ* where it promotes the body's own stem cell migration.[72] Enzyme mediated cross-linking is endowed with biocompatible fast gelation at physiological conditions.[48] For example, transglutaminase is used to cross-link protein derivatives such as gelatin, elastin and fibrin, via the formation of amide bonds in presence of calcium ions.[74] Additionally, polymers functionalized with aniline, tyramine or tyrosine can be cross-linked via oxidative coupling initiated by horseradish peroxidase (HRP) in presence of H_2O_2 (Figure 1.9b).[75,76]

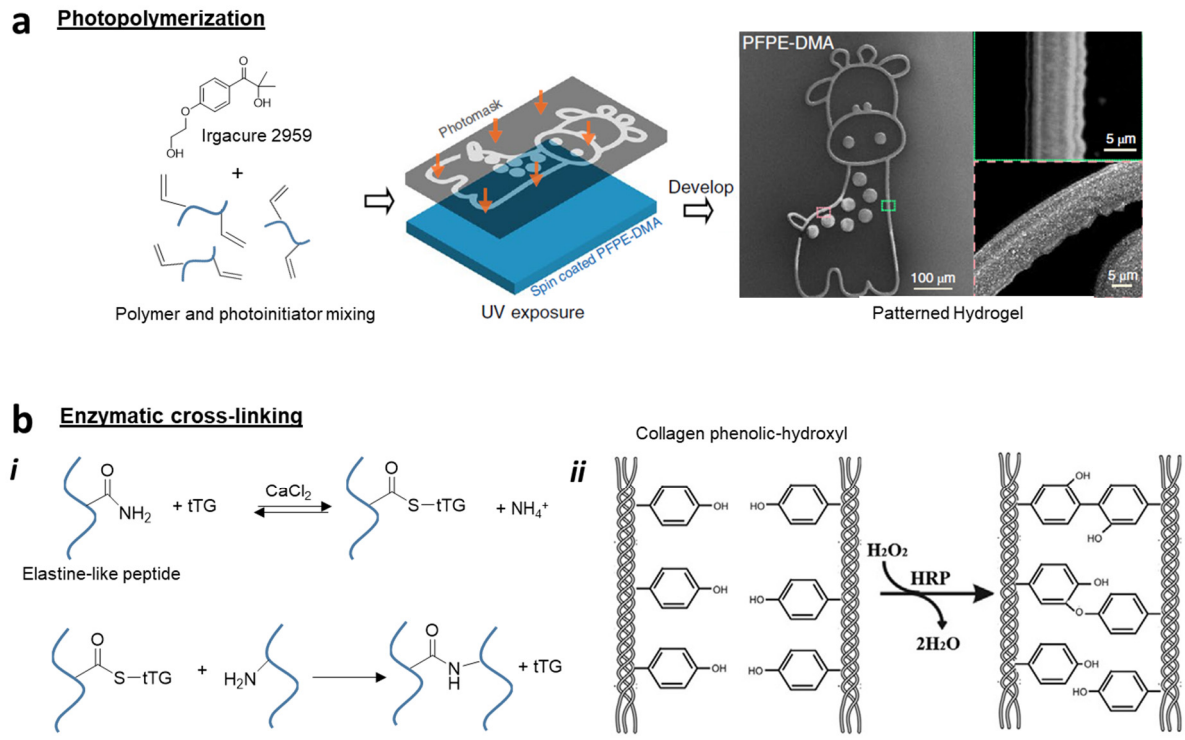

Figure 1.9: a) Use of photopolymerization for the preparation of a micropatterned hydrogel by photo-lithography.; The application of a photomask while irradiating the polymer mixed with the photoinitiator allows to impart the desired pattern to the final material. Adapted with permission from *Nat. Biomed Eng.* **2019**, 3, 58. Copyright 2019, Springer Nature. b) Enzyme mediated cross-linking. *i)* Elastine-like cross-linking mediated by transglutaminase (tTG) in presence of calcium iones. *ii)* Collagen functionalized with phenolic-hydroxyl groups and cross-linked by horseradish peroxidase (HRP) in presence of H_2O_2. Adapted with permission from *Acta Biomater.* **2015**, 27, 151. Copyright 2015, Elsevier Ltd.

Click chemistry reactions, such as Diels-Alder, Schiff-base formation and Michael addition, offer the possibility to prepare covalent hydrogels at physiological conditions, without the need of an external initiator, with high selectivity and few by-products. The highly selective Diels-Alder reaction between methylfuran and maleimide has been exploited for the cross-linking of a hyaluronic acid-PEG hydrogel at pH 7.4 allowing the encapsulation of viable cells (Figure 1.10a).[77] While, the Schiff base formation between amino and aldehyde groups constitutes a dynamic bond and it can be utilized to impart self-healing capability to hydrogels (Figure 1.10b).[78] However, the presence of free aldehyde groups, that could react with amino groups in the native tissue, arises biocompatibility concerns.[51] Besides, the Michael addition reaction is thermodynamically favored at physiological conditions and it is used to cross-link a nucleophile (generally amines and thiols) to an unsaturated carboxylic group (typically acrylates and acrylamides) (Figure 1.10c). When amines are used, alkaline pH is necessary to activate the

reaction hindering the application of this synthetic route for *in situ* forming systems; this limit is usually overcome substituting amines with thiols.[51] The preparation of hydrogels based on the Michael addition reaction will be presented in Chapter 2 (aza-Michael) and Chapter 3 (thiol-Michael).

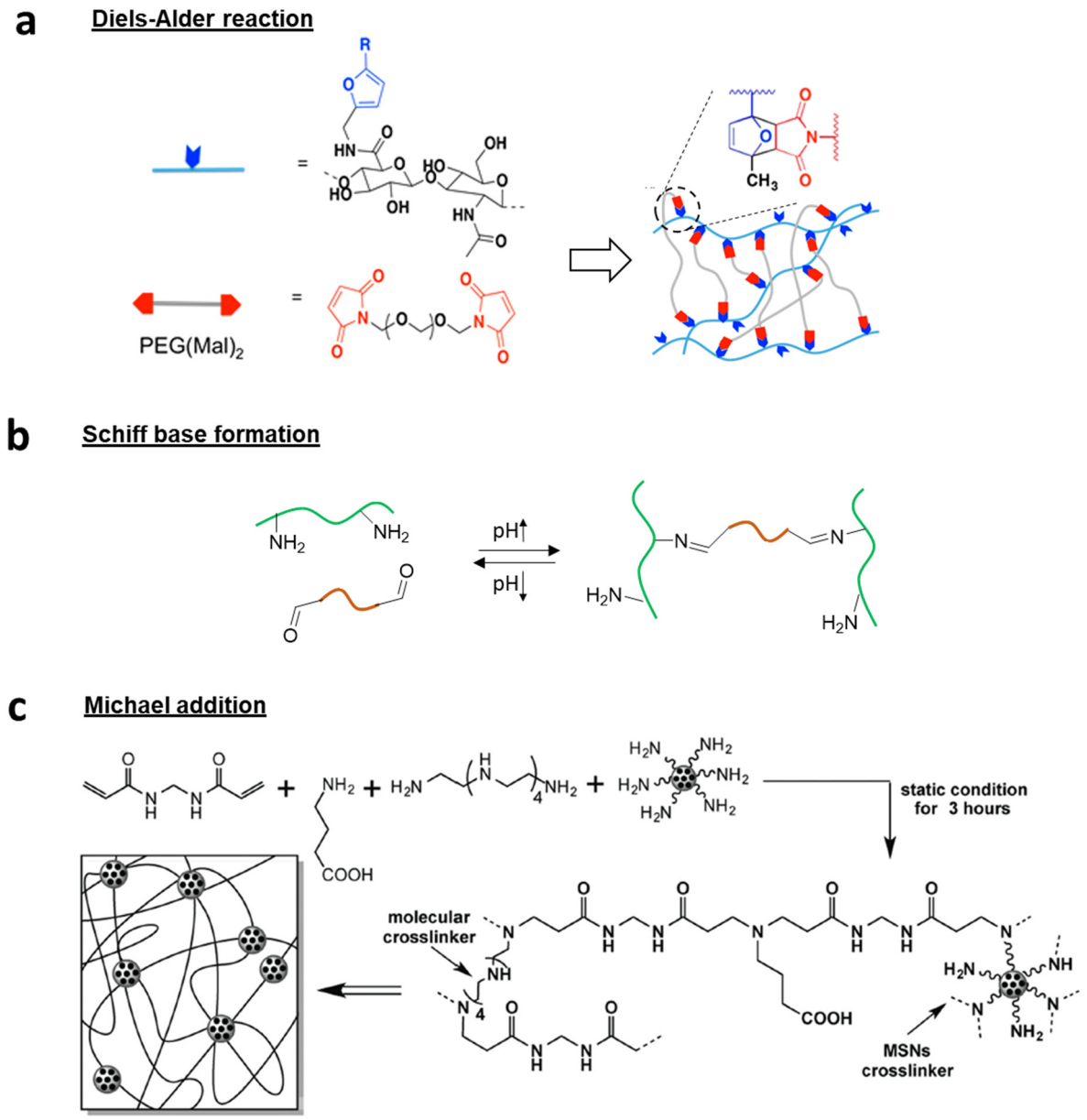

Figure 1.10: Click chemistry reactions commonly employed in the preparation of hydrogels. a) Diels-Alder reaction between methylfuran and maleimide groups. Adapted with permission from *Biomacromol.* **2018**, 19, 926. Copyright 2018, American Chemical Society. b) The Schiff base formation gives a dynamic, pH-dependent cross-linking. c) Use of aza-Michael reaction for the formation of a poly(amidoamine) hydrogel containing covalently linked nanoparticles. Reproduced with permission from *Small,* **2016**, 35, 4881. Copyright 2016, Wiley.

Covalent hydrogels can be obtained by simultaneous cross-linking and polymerization or cross-linking polymer chains after polymerization (Figure 1.11).

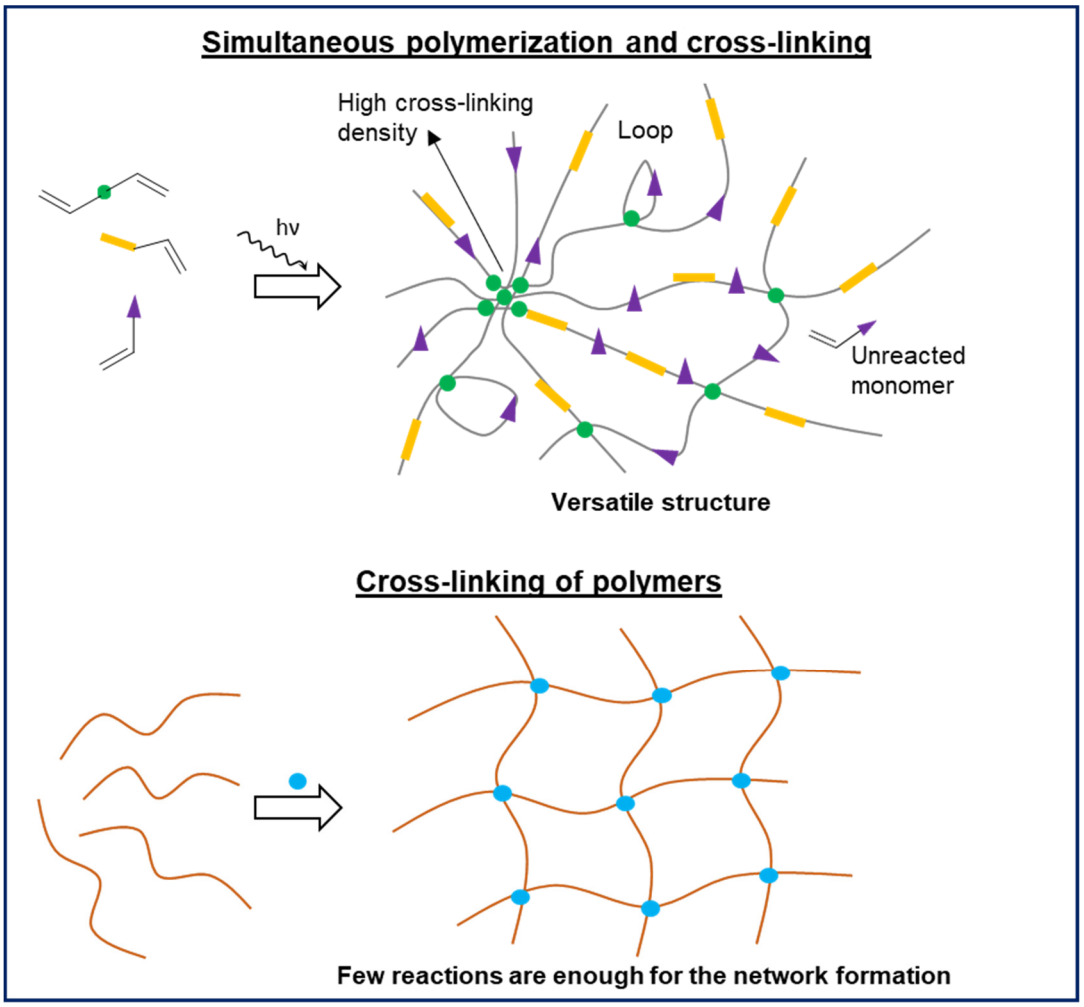

Figure 1.11: Different approaches in the preparation of covalently linked hydrogels. The simultaneous polymerization and cross-linking of the systems allows to obtain a versatile material but at the same time the obtained network is heterogeneous with the presence of loops and different spatial cross-linking density distribution. Unreacted monomers are generally present. The preparation of hydrogels by the cross-linking of polymers has the advantages of generating a homogeneous network and of requiring a limited number of reactions for the formation of the percolated system.

The first approach, commonly used for the preparation of hydrogels by photopolymerization, has the main advantage of giving the possibility to use a wide variety of monomers to introduce the desired chemical structures in the material. However, this method is limited by the possible formation of an heterogeneous network due to the different reactivity of monomers and cross-linker and by the need of material purification before use due to the presence of unreacted monomers.[33,79,80] To overcome these limitations, the commonly employed strategy is the

preparation of hydrogels by the cross-linking of pre-formed polymeric chains. The use of polymers with a narrow molecular weight distribution in particular, allows to accurately control the sol-gel transition and to obtain homogeneous materials.[33] The advantage of this cross-linking approach is the reduction to a minimum of the monomer concentration and the chemical reactions necessary to obtain the percolated network with clear biocompatibility benefits in the *in situ* preparation of injectable hydrogels.

The accurate selection of the cross-linking strategy allows to tune, among others, the mechanical properties according to the desired application of the final material. In general, higher stiffness can be obtained increasing the cross-linking degree, or using branched reactive molecules, although this could also lead to the formation of a brittle material. To overcome this constraint and generate self-healing and eventually highly-stretchable materials, a combination of supramolecular and covalent cross-linking is generally used.[81–84] Sun et al. developed a hydrogel able to stretch over 20 times its original length based on the combination of ionically cross-linked alginate and covalently cross-linked polyacrylamide.[85] Using a clever supramolecular strategy, Scherman and coworkers reported the use of cucurbit-mediated host-guest interactions in combination with covalent cross-linking to obtain robust and elastic materials.[86] In order to extend the functional life of materials that are expected to undergo significant stress, the hydrogels need to be self-healable. A self-healing behavior is obtained when the constituting network is based on dynamic linkers that are able to autonomously, rapidly, and repeatedly regenerate. Besides the use of supramolecular cross-linking, dynamic covalent cross-linking can be obtained using Shiff's base, imine, or disulfide groups.[87]

The chemical nature of the backbone together with the mesh size influence the kinetics of covalent bond cleavage and the consequent hydrogel degradation rate.[88] The degradation of the material should proceed in parallel with the population of the matrix by cells and eventually with the growth of the new native tissue. Hydrogel degradation starts with a scission of the polymeric network, followed by a decrease in compactness and a shift in the thermodynamic equilibrium between swelling and elastic retractile forces, which causes an increase in the water influx and the solvation of the polymer chains.[89] The majority of hydrogels are designed to degrade hydrolytically, yet there are examples of materials that are biodegraded by enzymatic activity, or cleaved in presence of external stimuli such as pH, temperature, light or redox reactions.[89] For example, recently, light has been exploited for the *in vivo* degradation of hydrogels with gastrointestinal applications. The developed light-degradable material offers

noncontact on-demand degradation with high spatial and temporal resolution and it may be considered as a new clinical tool for the design of dynamic implantable devices.[73] Synchronizing the degradation of the hydrogel with the growth of the tissue is a major goal. Madl *et al*. used a standard peptide engineering approach to design an elastin-like gel that can enzymatically degrade between 12 hours and 9 days with tunable cleavage rate by changing the cross-linker functionality.[90]

1.3.3. Introducing additional features in hydrogels: pending groups and nanofillers

Besides controlling the properties of hydrogels by the selection of the suitable backbone (i.e. polymer and cross-linking system), it is possible to impart additional characteristics to the material with the introduction of pending functional groups or nanofillers. For example urethane linkages[91] and catechol groups[92,93] are used to obtain tissue-adhesive hydrogels that ensures continuity between the living tissue and the implanted material and to avoid unwanted displacement outside the intended area. Chen *et al.* functionalized alginate with dopamine obtaining a hydrogel with an adhesive strength with skin of 6.5 kPa.[63] The choice of catechol groups is inspired by mussels that, thanks to the abundant presence of this functional group in their foot, can strongly adhere to a wide range of foreign surfaces (Figure 1.12a). The adhesion mechanism is attributed to multiple interactions including H-bonding, coordination bond, cation-π interaction, π-π interaction and covalent linking (Figure 1.12b).[94–96] The adhesion of cells to synthetic materials is dependent on the presence of cell binding motifs such as the RGD peptide sequence that can be introduced in hydrogels as a pending group.[97] Segura and co-workers have shown that controlling the clustering of RGD covalently linked to a hyaluronic acid backbone, it is possible to control the spreading of mesenchymal stem cells and their expression of integrin.[98]

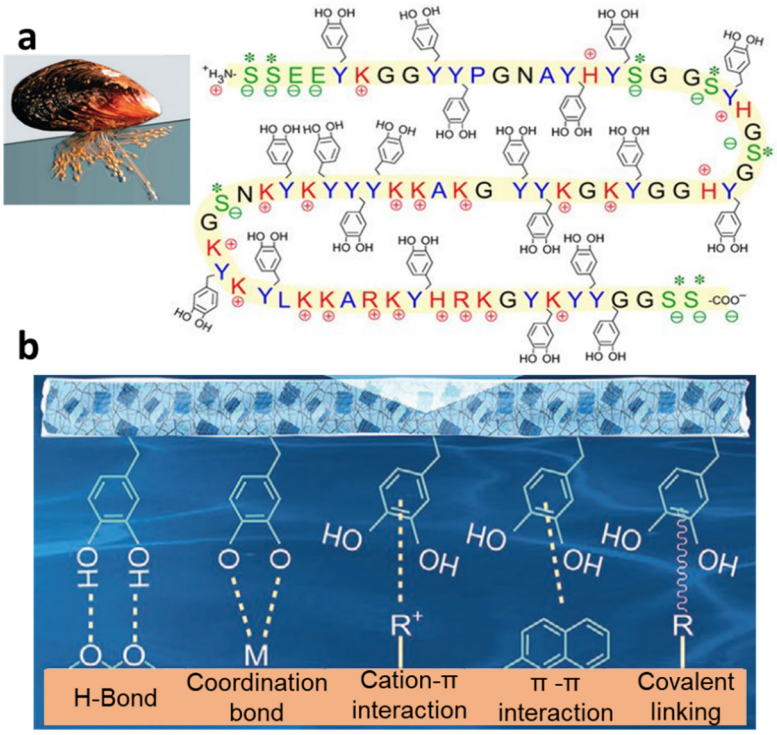

Figure 1.12: Catechol mediated adhesion. a) Sequence of a mussel foot protein showing the prominence of catechol groups. Adapted with permission from *J. of Exp. Biology,* **2017**, 220, 517. Copyright 2017, The company of Biologists Ltd. b) Different possible interactions of a catechol-modified hydrogel with the substrate. Adapted with permission from *Adv. Funct. Mater,* **2020**, 30, 1909954. Copyright 2020, Wiley.

The use of micro and nanofillers has emerged as a strategy for generating hydrogel systems equipped with sets of advanced properties.[99,100] It should be noted that the integration of nanomaterials into the structural network not only provides the hydrogel with properties typical of the fillers, but it also contributes to determining the bulk mechanical and biological behavior. For instance, mechanical reinforcement of hydrogels, measured as the increase of the elastic modulus, can be obtained following this strategy.[101] Eslahi *et al.* reported a 6-fold G' increase achieved with the introduction of nanoclay in their hydrogel network, such increment was explained by the formation of physical cross-linking between the polymer and the filler.[102] Another interesting example is the purely supramolecular yet stiff hydrogel prepared combining a dendritic macromolecule with clay nanosheets reported by Aida and co-workers.[103] The stretchability of hydrogels can also be significantly improved using nanoparticles as filling elements. Liu *et al.* prepared a tough and highly stretchable hydrogel able to elongate over 3000% by introducing graphene oxide (GO) in the network (Figure 1.13a).[104] The mechanical properties of the material were eventually dictated by its microstructure, characterized by non-

covalent interactions between the polymeric chains and the GO, which allowed dynamic behavior of the system. Self-healing properties have been obtained with the incorporation of oxidized carbon nanotubes (CNT) in a tripeptide supramolecular hydrogel. Interestingly, the authors showed that the shape of the CNT is a key parameter in defining the mechanical properties of the nanocomposite hydrogel with the filler acting as nucleation site for the peptide reassembly.[105] Hydrogels with anisotropic properties, able to mimic the ordered structure of living tissues, can be obtained with the introduction of spatially ordered nano or microfillers.[106] For example, negatively charged unilamellar Ti nanosheets were aligned coaxially at uniform face-to-face distance in a hydrogel and, because of the electrostatically repulsion between the nanosheets, the resulting material exhibited remarkable optical and mechanical anisotropy (Figure 1.13b).[54] Adhesive properties can also be tuned in soft materials by incorporating nanoparticles (e.g., silica nanoparticles) of nanometric size.[107] The adhesiveness results from the ability of the polymer chains to adsorb on the nanoparticles with designed surface chemistry acting as connectors (Figure 1.13c).[96] Antimicrobial effect can be easily and effectively obtained combining metal or metal oxide particles with polymeric hydrogels. Different mechanisms had been proposed to explain the antimicrobial activity of metal/metal oxide particles: (1) release of ions from the NP that can be internalized in bacteria cells and inhibit DNA replication and (2) generation of ROS on the surface of NP that induces oxidative lesions. The antibacterial properties of metal and metal oxide NP is enhanced by their positive-charged surface that facilitates their binding with negatively-charged bacterial cells.[108] The use of metal and metal-oxide nanoparticles also provides the material thermal and electric conductivity,[109] which are fundamental attributes for cardiac and nerve regeneration applications. Such systems have however limited applications due to their high surface energy that promotes aggregation.[109] Conductive alternatives to metal NP are carbon derivatives such as GO and carbon nanotubes.

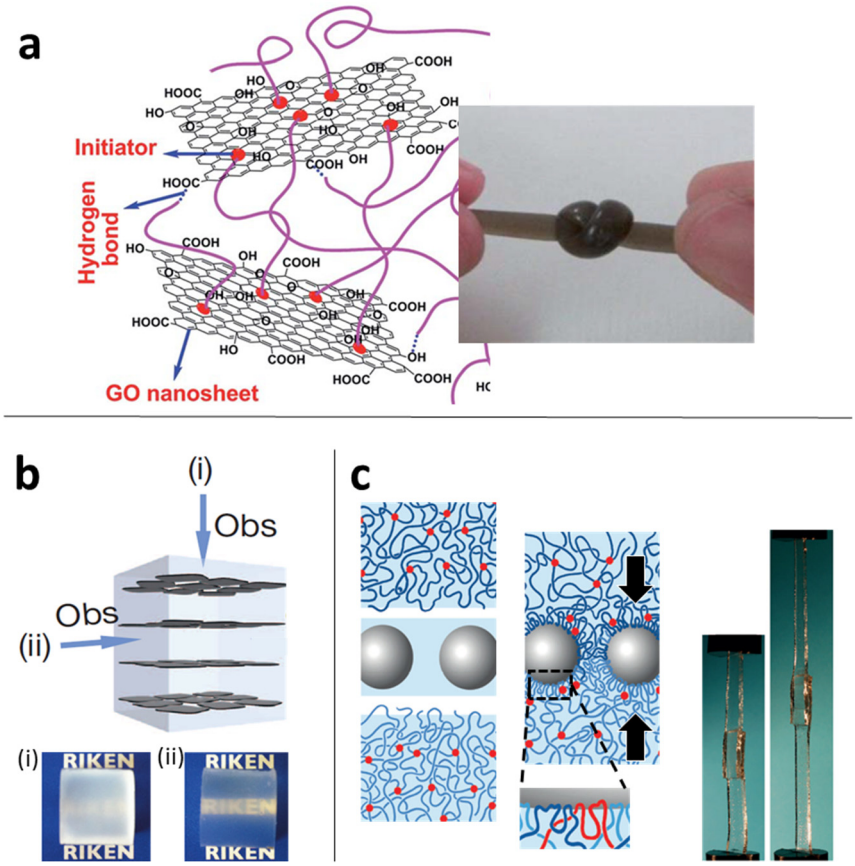

Figure 1.13: Emerging properties from the incorporation of nanofillers in hydrogels. a) The non-covalent interactions between the polymeric chain and the GO impart stretchability to the material. Adapted with permission from *J. Mater. Chem*. **2012** 22, 14160. Copyright 2012, The Royal Society of Chemistry b) Co-facially oriented Ti nanosheets in a hydrogel prepared in presence of a 10 T magnetic field. Optical features of the material viewed along the orthogonal (i) and parallel (ii) direction to the aligned Ti nanosheets. Adapted with permission from *Nature,* **2015**, 517, 68. Copyright 2014, Springer Nature. c) Hydrogel adhesiveness given by the adsorption of polymeric chains on nanoparticles. Glued hydrogels can sustain large deformation. Adapted with permission from *Nature* **2014**, 505, 382. Copyright 2013, Springer Nature.

The incorporation of nanoparticles in hydrogel matrices can be further exploited for the preparation of advanced biomolecule-delivery systems that allow to control the payload release. Two strategies are generally employed for the controlled release. I) Incorporation in thermo-responsive hydrogels of photo-thermal particles that, upon exposure to a stimulus (e.g. light irradiation, magnetic field), induce a localized temperature change and the consequent network modification that promotes/hinders the biomolecule release.[106,110,111] For example the irradiation of Au-nanorods with a near-IR laser has been used to control the swelling and shrinking of a *N*-isopropylacrylamide hydrogel with high spatial resolution.[112] A similar approach was used by Satarkar *et al.* that, with the introduction of Fe_3O_4 NP in a thermo-

responsive hydrogel, were able to control the on-demand pulsatile release of a drug with the exposure of the material to an alternating magnetic field (Figure 1.14a).[113] II) Loading of the payload inside porous nanoparticles incorporated in the hydrogel. This method allows to obtain high loading, it ensures the protection of labile biomolecule during the hydrogel synthesis and it permits to control the release if degradable particles are used. For example Zhang *et al.* exploited the globe-like structure of a hyperbranched polyester to encapsulate bioactive hydrophobic agents and to sustain their release.[114] Our group has covalently linked to a poly(amidoamine) hydrogel network redox responsive mesoporous silica nanocapsules loaded with a protein. The nanocapsules protected the payload during the hydrogel synthesis and in presence of a reductant they released the protein (Figure 1.14b).[115]

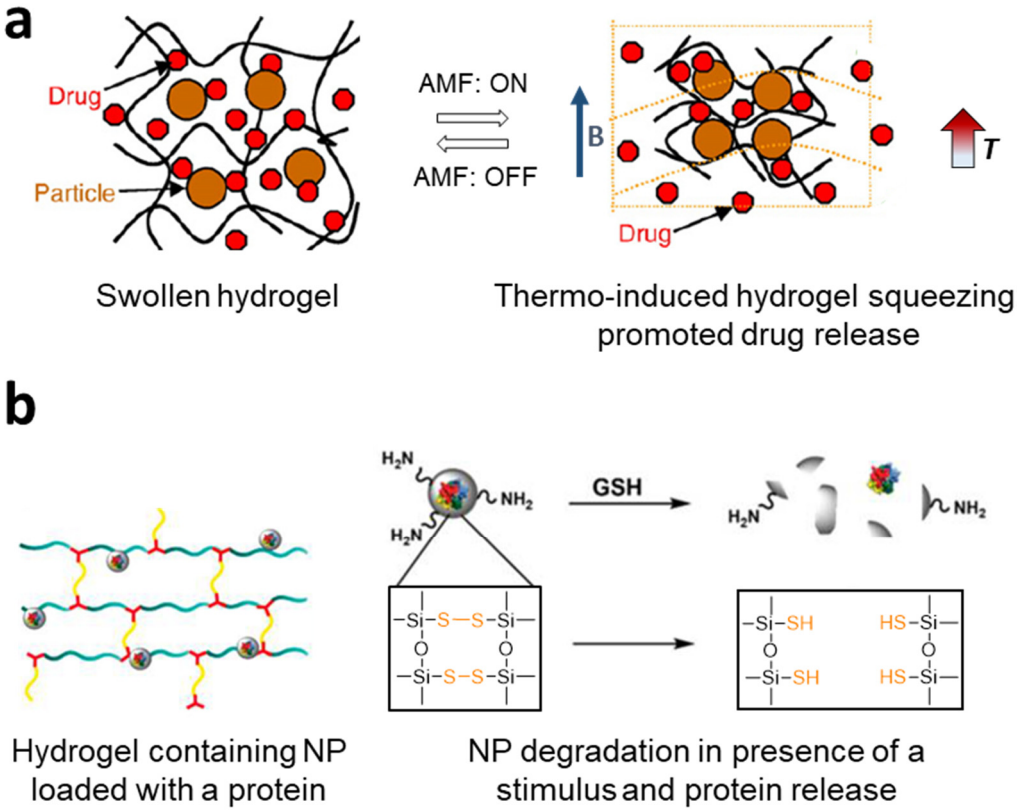

Figure 1.14: Incorporation of nanoparticles in hydrogels for controlled payload release. a) Thermo-responsive hydrogel containing magnetic nanoparticles. In presence of an alternated magnetic field (AMF) the temperature of the system increases causing the squeezing of the polymeric network and promoting the drug release. The reversibility of the system allows to have an on-demand pulsatile release. Adapted with permission from *J. of Controlled Rel.* **2008**, 130, 246. Copyright 2008, Elsevier B.V. b) Porous NP loaded with a protein and covalently linked to a poly(amidoamine) hydrogel. The NP protect the payload during the synthesis of the material and in presence of a stimulus they release the protein. Adapted with permission from *ACS Appl. Bio Mater*. **2018**, 1, 1301. Copyright 2018, American Chemical Society.

1.4. Injectable hydrogels: controlling the sol-gel transition

Injectable hydrogels have the advantages that they can be implanted in the desired area through minimal invasive techniques and that they can completely fill the cavity ensuring continuity with the native tissue. However, the development of injectable hydrogels, compared with scaffolds, brings new challenges. In fact, if in the preparation of scaffolds the control over the kinetic of gelation is not crucial and it is possible to purify the material prior to implantation, *in situ* forming hydrogels require a precise control over the sol-gel transition and the absence of toxic by-products.

The most reliable technique to study the gelation kinetic is oscillatory rheology as described for the first time by Tung and Dynes.[116] This method evaluates the evolution of the elastic (G') and the viscous (G'') moduli over time and it allows to clearly identify the gel-point as the time at which G'=G''. Following the process of hydrogel formation with a rheometer allows to visualize not only the final mechanical properties of the material but all the kinetic profile that covers a crucial role in injectable hydrogels. An injectable material with biomedical application, must be characterized by low viscosity during injection, be able to sustain its own weight after injection to avoid percolation outside the injection site and the cross-linking process must occur in a time scale compatible with the surgery. If the gelation occurs too fast (e.g. < 5 min) there is the risk of needle clogging, if the gelation is too long (e.g. >1 h) the material may spread and its clinical application will not be possible also for practical reasons. Another commonly used method to identify the formation of a hydrogel is the "inverted vial test" that consists in tilting a vial containing the hydrogel and in attributing the sol-gel transition to the moment at which the material sustains its own weight without percolating along the walls of the vial. This test has the advantages of being easy and not requiring any equipment nevertheless, it is only indicative and it could give false results especially if the pre-gel solution is viscous and can stick to the bottom of the vial. Shibayama and Norisuye developed a different approach to evaluate the gelation time based on time resolved Dynamic Light Scattering measurement that also allows to obtain information about the gelation mechanism and the architecture of the gelling clusters.[1]

Three different main approaches can be implemented to control the gelation process (Figure 1.15): I) The use of supramolecular materials whose gelation is triggered by the *in vivo* environment (i.e. pH, temperature). For example, Sang *et al.* prepared an amphiphilic poly(amidoamine) containing both PEG and aliphatic chains and they exploited the difference

between room and body temperature to control the gelation. They exploited the thermo-sensitivity of the system to obtain an injectable material with application in spinal cord regeneration.[117] In an interesting work, Khademhosseini and coworkers developed an injectable and conductive bioelectronics whose temperature-triggered gelation rely on the formation of micellar structures, π-π stacking and hydrophobic interactions.[118] However, thermo-responsive hydrogels are suitable for applications that use a rather short needle, but they result inadequate in endoscopic applications where the long pathway, needed in this type of surgery, may result in needle clogging.

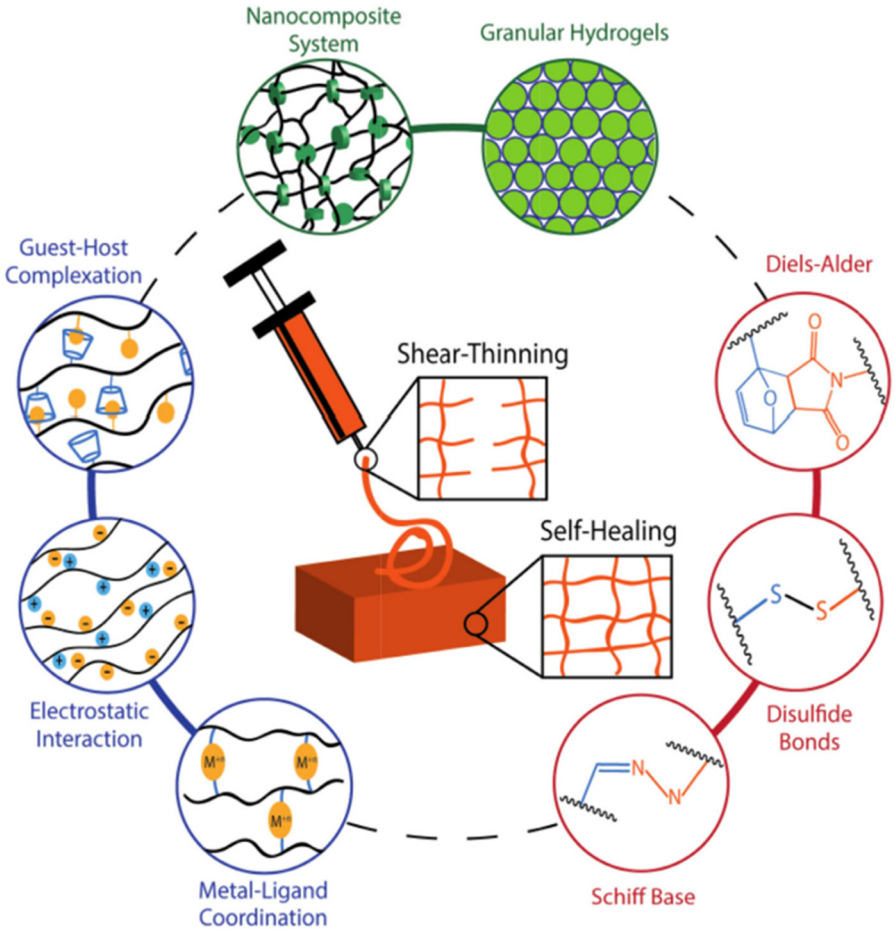

Figure 1.15: Dynamic and reversible interactions at the basis of shear-thinning and self-healable hydrogels. Reprinted with permission from *J. Appl. Polym. Sci,* **2020**,137, 48668. Copyright 2019, Wiley.

II) The use of dual chamber syringe to mix *in situ* two reactive solutions. For example hyaluronic acid modified with cyclo-octene or tetrazine have been loaded in two different barrels of the same syringe to obtain the hydrogel formation in the target site via click chemistry in less than three seconds.[119] It is important to underline that this approach might raise

biocompatibility concerns and that the prediction of the gelation time could be complicated by the presence in the *in vivo* environment of variants such as confinement, biomolecules and pH. III) Shear-thinning hydrogels are ideal injectable materials because they can behave as elastic gels at rest, owing to the establishment of bonds through dynamic interactions, but they can flow as viscous fluids when a force is applied.[120] The sear-response of the material is dictated by the kinetic of bond formation compared with the polymer relaxation time.[121] The most common interactions at the basis of fast dynamic systems are physical associations such as host-guest complexation, electrostatic interactions and metal-ligand coordination (Figure 1.15).[122] Burdick and co-workers for example, exploited the rapid bonding kinetic of host-guest interactions to improve the retention of a hydrogel injected in the myocardial tissue compared with a covalent cross-linked system.[123] In another interesting work, the interactions between cyclodextrine and the aromatic groups of gelatin have been used to impart shear thinning behavior to a hydrogel containing an aligned nanomesh. These dynamic host-guest interactions allowed to implant the material in the spinal cord of a rat model with a 22-gauge needle maintaining the anisotropy of the system (Figure 1.16).[124]

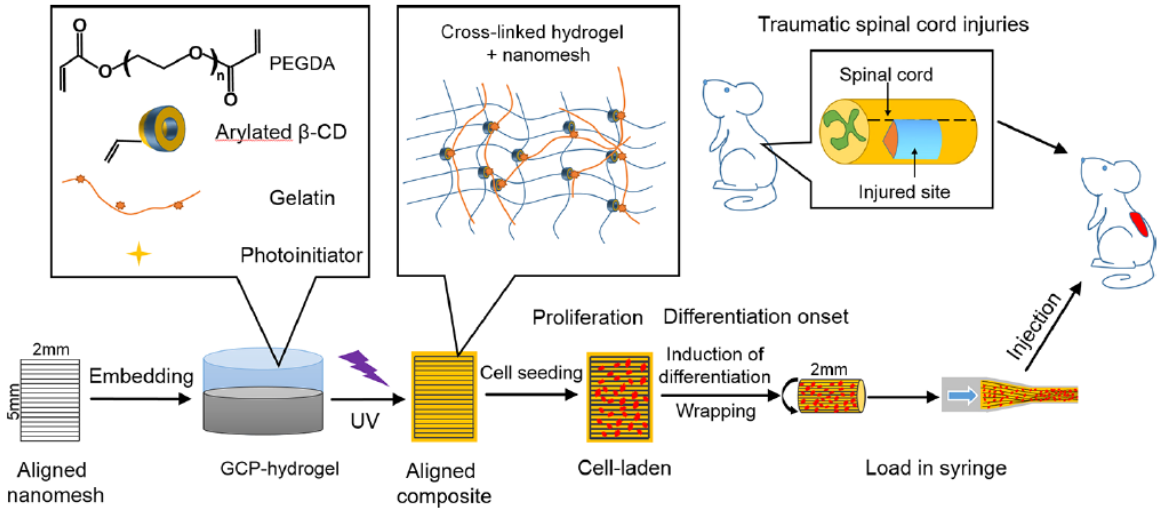

Figure 1.16: Injectable hydrogel containing a shape memory aligned nanomesh. The covalent cross-linking is triggered by UV irradiation. Stem cells are loaded in the material before injection. The host-guest interactions between cyclodextrin and gelatin give the shear thinning behavior. The shape memory aligned nanomesh imparts anisotropy to the implanted material. Reprinted with permission from *ACS Appl. Mater. Interfaces*, **2018**, 10, 29299. Copyright 2018, American Chemical Society.

Supramolecular systems, in general, lack mechanical strength; this limit can be overcome with the combination of supramolecular and covalent cross-linking in a dual-network hydrogel.[125] Dynamic covalent bonds are generally static at ambient conditions but their reversible equilibrium can be activated upon stimuli (e.g. light, pH, chemical agent) and it can be exploited for the preparation of shear-thinning yet stiff materials.[126] Examples of dynamic covalent bonds are imides, disulfide bonds and Diels-Alder products (Figure 1.15). Disulfide cross-linking is formed in the presence of a mild oxidizing agent such as the environmental oxygen and it can be used to prepare injectable self-healing hydrogels whose dynamic properties can be modulated by a change in pH.[127] A different approach to prepare shear thinning materials consists in the design of hydrogels containing non-covalently linked nanoparticles. For example, Avery *et al.* have developed an injectable hydrogel containing gelatin and silicate nanoplatelets able to flow in a catheter 1.5 m long and to immediately form an occlusive solid with application in endovascular embolization.[128] Another interesting material design characterized by shear-thinning properties are granular hydrogels (GH).[18] GH can be considered as hydrogel scaffolds scaled-down to the micrometric scale. The inter-granules physical interactions make this class of hydrogels undergo a reversible transition between a cohesive elastic state at rest and a fluid state under shear stress.[129] This approach offers the advantages of allowing the purification of the material before implantation and of not requiring a strict control over the kinetics of hydrogel formation. It has been shown that the single hydrogel granules can be loaded with cells maintaining high viability and that the GH can act as a perfect matrix for the growth of cells thanks to the presence of voids between granules that facilitate the permeation of nutrients and oxygen and that provide a porous deformable architecture.[20,130] These characteristics make GH an interesting solution for the development of injectable materials for the delivery of cells (Figure 1.17).

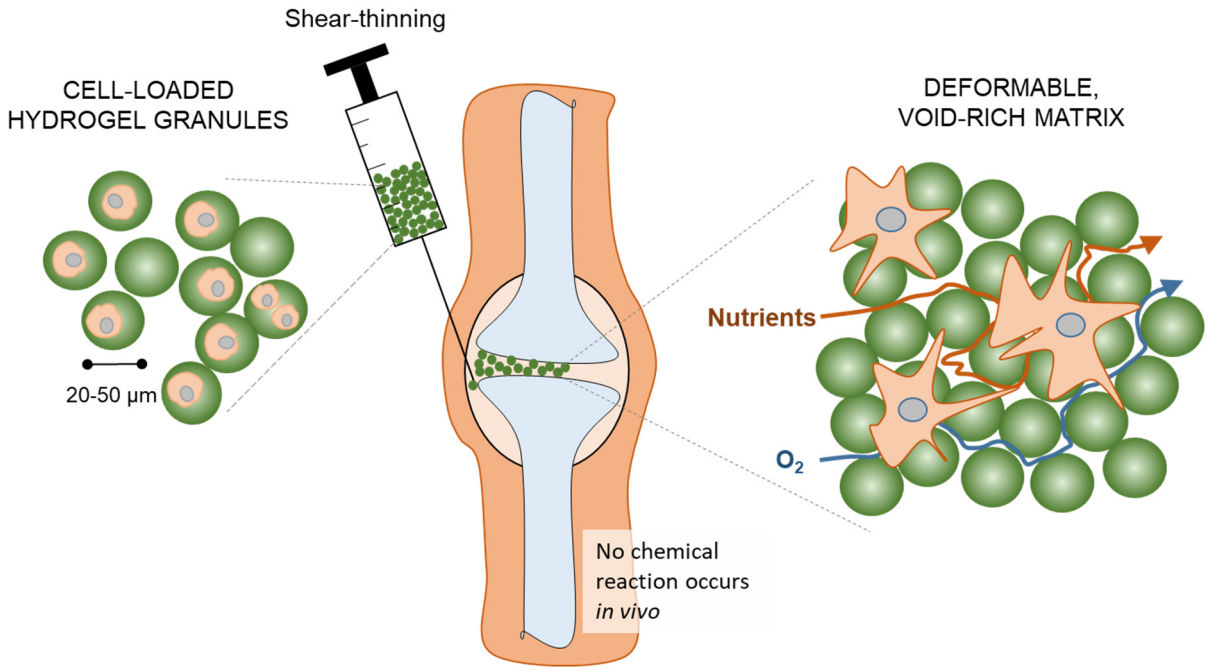

Figure 1.17: Granular hydrogel for the delivery of cells. Cells are loaded in the hydrogel granules and the material is injected in the target site thanks to the shear-thinning behavior. The implanted material behaves as a cohesive elastic soft solid and it does not require any chemical process to occur *in vivo*. The Granular hydrogel constitutes a void-rich matrix where nutrients and oxygen can penetrate and that offers a porous deformable architecture for the proliferation of cells.

1.5. Aim of the thesis

The aim of this thesis is the development and characterization of hydrogels with tailored properties for different biomedical applications. In particular, focusing on injectable materials that can be implanted through minimally-invasive procedures. The possibility to introduce porous nanoparticles with the function of biomolecule delivery systems is furthermore explored. In summary, Chapter 2 presents the preparation and characterization of an injectable poly(amidoamine) based hydrogel formed through supramolecular interactions. The gelation of the material occurs selectively in the gastric tissue and the described hydrogel is exploited as a tool for the facilitate and minimally invasive resection of gastric tumors. Next, Chapter 3 discusses the development of a hyaluronic acid (HA) based shear-thinning hydrogel cross-linked *in situ* via thiol-Michael reaction. The optimization of the material to achieve the desired kinetic of gelation and final mechanical properties is presented. Furthermore, the effect of the introduction of mesoporous silica nanoparticles in the network as biomolecule-delivery system is investigated. This nanocomposite hydrogel has been tested *in vivo* as a filling material for the treatment of fistula. Different modifications of the developed HA based hydrogel are then

presented in Chapter 4 with the aim of introducing in the material fundamental bio-signals to induce cellular growth and eventually differentiation in the matrix. Finally, Chapter 5 discusses the preparation of a PEG based hydrogel containing porous silicon nanoparticles designed to sustain the prolonged release of a biomolecule. This nanocomposite hydrogel is 3D printed by stereolitography to form multi-channel scaffolds with micrometric resolution with potential application as implantable materials for peripheral nerve regeneration.

1.6. References

1. Shibayama, M. & Norisuye, T. Gel Formation Analyses by Dynamic Light Scattering. *Bull. Chem. Soc. Jpn.* 75, 641–659 (2002).

2. Flory, P. J. Molecular Size Distribution in Three Dimensional Polymers. I. Gelation1. *J. Am. Chem. Soc.* 63, 3083–3090 (1941).

3. Flory, P. J. Fundamental Principles of Condensation Polymerization. *Chem. Rev.* 39, 137–197 (1946).

4. Eldridge, J. E. & Ferry, J. D. Studies of the Cross-linking Process in Gelatin Gels. III. Dependence of Melting Point on Concentration and Molecular Weight. *J. Phys. Chem.* 58, 992–995 (1954).

5. Ferry, I. J. D. & Eldridge, J. E. Studies of the Cross-Linking Process in Gelatin Gels. *J. Phys. Colloid Chem.* 53, 184–196 (1949).

6. Wichterle, O. & Lím, D. Hydrophilic Gels for Biological Use. *Nature* 185, 117–118 (1960).

7. Kajiwara, K. Section 1 - Structure of gels. in *Gels Handbook* 122–171 (Academic Press, 2001).

8. Stauffer, D., Aharony, A. & Aharony, A. *Introduction to Percolation Theory : Second Edition*. (Taylor & Francis, 2018).

9. Peppas, N. A., Hilt, J. Z., Khademhosseini, A. & Langer, R. Hydrogels in Biology and Medicine: From Molecular Principles to Bionanotechnology. *Adv. Mater.* 18, 1345–1360 (2006).

10. Richbourg, N. R. & Peppas, N. A. The swollen polymer network hypothesis: Quantitative models of hydrogel swelling, stiffness, and solute transport. *Prog. Polym. Sci.* 105, 101243 (2020).

11. Hirotsu, T. Section 3 - Theory of swelling. in *Gels Handbook* 65–97 (Academic Press, 2001).

12. Slaughter, B. V., Khurshid, S. S., Fisher, O. Z., Khademhosseini, A. & Peppas, N. A. Hydrogels in Regenerative Medicine. *Adv. Mater.* 21, 3307–3329 (2009).

13. Su, J., Satchell, S. C., Wertheim, J. A. & Shah, R. N. Poly(ethylene glycol)-crosslinked gelatin hydrogel substrates with conjugated bioactive peptides influence endothelial cell behavior. *Biomaterials* 201, 99–112 (2019).

14. Mandal, A., Clegg, J. R., Anselmo, A. C. & Mitragotri, S. Hydrogels in the clinic. *Bioeng. Transl. Med.* 5, 1 (2020).

15. Cascone, S. & Lamberti, G. Hydrogel-based commercial products for biomedical applications: A review. *Int. J. Pharm.* 573, 118803 (2020).

16. Li, J. & Mooney, D. J. Designing hydrogels for controlled drug delivery. *Nat. Rev. Mater.* 1, 16071 (2016).

17. Bian, L., Zhai, D. Y., Tous, E., Rai, R., Mauck, R. L., *et al.* Enhanced MSC chondrogenesis following delivery of TGF-β3 from alginate microspheres within hyaluronic acid hydrogels in vitro and in vivo. *Biomaterials* 32, 6425–6434 (2011).

18. Daly, A. C., Riley, L., Segura, T. & Burdick, J. A. Hydrogel microparticles for biomedical applications. *Nat. Rev. Mater.* 5, 20–43 (2020).

19. Xavier, J. R., Thakur, T., Desai, P., Jaiswal, M. K., Sears, N., *et al.* Bioactive Nanoengineered Hydrogels for Bone Tissue Engineering: A Growth-Factor-Free Approach. *ACS Nano* 9, 3109–3118 (2015).

20. Li, F., Truong, V. X., Fisch, P., Levinson, C., Glattauer, V., *et al.* Cartilage tissue formation through assembly of microgels containing mesenchymal stem cells. *Acta Biomater.* 77, 48–62 (2018).

21. Hollister, S. J. Porous scaffold design for tissue engineering. *Nat. Mater.* 4, 518–524 (2005).

22. Loh, Q. L. & Choong, C. Three-Dimensional Scaffolds for Tissue Engineering Applications: Role of Porosity and Pore Size. *Tissue Eng. Part B Rev.* 19, 485–502 (2013).

23. Lou, J., Stowers, R., Nam, S., Xia, Y. & Chaudhuri, O. Stress relaxing hyaluronic acid-collagen hydrogels promote cell spreading, fiber remodeling, and focal adhesion formation in 3D cell culture. *Biomaterials* 154, 213–222 (2018).

24. Gerecht, S., Burdick, J. A., Ferreira, L. S., Townsend, S. A., Langer, R., *et al.* Hyaluronic acid hydrogel for controlled self-renewal and differentiation of human embryonic stem cells. *Proc. Natl. Acad. Sci.* 104, 11298–11303 (2007).

25. Lou, J., Stowers, R., Nam, S., Xia, Y. & Chaudhuri, O. Stress relaxing hyaluronic acid-collagen hydrogels promote cell spreading, fiber remodeling, and focal adhesion formation in 3D cell culture. *Biomaterials* 154, 213–222 (2018).

26. Sano, K., Ishida, Y. & Aida, T. Synthesis of Anisotropic Hydrogels and Their Applications. *Angew. Chem. Int. Ed.* 57, 2532–2543 (2018).

27. Gemeinhart, R. A., Park, H. & Park, K. Pore structure of superporous hydrogels. *Polym. Adv. Technol.* 11, 617–625 (2000).

28. Salerno, A., Borzacchiello, R. & Netti, P. A. Pore structure and swelling behavior of porous hydrogels prepared via a thermal reverse-casting technique. *J. Appl. Polym. Sci.* 122, 3651–3660 (2011).

29. Staruch, R. M. T., Glass, G. E., Rickard, R., Hettiaratchy, S. P. & Butler, P. E. M. Injectable Pore-Forming Hydrogel Scaffolds for Complex Wound Tissue Engineering: Designing and Controlling Their Porosity and Mechanical Properties. *Tissue Eng. Part B Rev.* 23, 183–198 (2017).

30. Das, R. K., Gocheva, V., Hammink, R., Zouani, O. F. & Rowan, A. E. Stress-stiffening-mediated stem-cell commitment switch in soft responsive hydrogels. *Nat. Mater.* 15, 318–325 (2016).

31. Tanaka, M., Nakahata, M., Linke, P. & Kaufmann, S. Stimuli-responsive hydrogels as a model of the dynamic cellular microenvironment. *Polym. J.* 52, 861–870 (2020).

32. Butcher, D. T., Alliston, T. & Weaver, V. M. A tense situation: forcing tumour progression. *Nat. Rev. Cancer* 9, 108–122 (2009).

33. Spicer, C. D. Hydrogel scaffolds for tissue engineering: the importance of polymer choice. *Polym. Chem.* 11, 184–219 (2020).

34. Boehnke, N., Cam, C., Bat, E., Segura, T. & Maynard, H. D. Imine Hydrogels with Tunable Degradability for Tissue Engineering. *Biomacromolecules* 16, 2101–2108 (2015).

35. Richardson, B. M., Wilcox, D. G., Randolph, M. A. & Anseth, K. S. Hydrazone covalent adaptable networks modulate extracellular matrix deposition for cartilage tissue engineering. *Acta Biomater.* 83, 71–82 (2019).

36. Chang, C.-J., Chen, C.-H., Chen, B.-M., Su, Y.-C., Chen, Y.-T., *et al.* A genome-wide association study identifies a novel susceptibility locus for the immunogenicity of polyethylene glycol. *Nat. Commun.* 8, 1–7 (2017).

37. Oda, H., Konno, T. & Ishihara, K. Efficient differentiation of stem cells encapsulated in a cytocompatible phospholipid polymer hydrogel with tunable physical properties. *Biomaterials* 56, 86–91 (2015).

38. Miao, T., Miller, E. J., McKenzie, C. & Oldinski, R. A. Physically crosslinked polyvinyl alcohol and gelatin interpenetrating polymer network theta-gels for cartilage regeneration. *J. Mater. Chem. B* 3, 9242–9249 (2015).

39. Cassinelli, S. J., Chen, S., Charlton, T. P. & Thordarson, D. B. Early Outcomes and Complications of Synthetic Cartilage Implant for Treatment of Hallux Rigidus in the United States. *Foot Ankle Int.* 40, 1140–1148 (2019).

40. Kang, Y. M., Lee, S. H., Lee, J. Y., Son, J. S., Kim, B. S., *et al.* A biodegradable, injectable, gel system based on MPEG-b-(PCL-ran-PLLA) diblock copolymers with an adjustable therapeutic window. *Biomaterials* 31, 2453–2460 (2010).

41. Kim, M. S., Ahn, H. H., Shin, Y. N., Cho, M. H., Khang, G., *et al.* An in vivo study of the host tissue response to subcutaneous implantation of PLGA- and/or porcine small intestinal submucosa-based scaffolds. *Biomaterials* 28, 5137–5143 (2007).

42. Parmar, P. A., Skaalure, S. C., Chow, L. W., St-Pierre, J.-P., Stoichevska, V., *et al.* Temporally degradable collagen–mimetic hydrogels tuned to chondrogenesis of human mesenchymal stem cells. *Biomaterials* 99, 56–71 (2016).

43. Sun, Y., Deng, R., Ren, X., Zhang, K. & Li, J. 2D Gelatin Methacrylate Hydrogels with Tunable Stiffness for Investigating Cell Behaviors. *ACS Appl. Bio Mater.* 2, 570–576 (2019).

44. Majcher, M. J. Hydrogel Synthesis and Design. in *Functional Biopolymers* 1–41 (Springer International Publishing, 2018).

45. Freeman, F. E. & Kelly, D. J. Tuning Alginate Bioink Stiffness and Composition for Controlled Growth Factor Delivery and to Spatially Direct MSC Fate within Bioprinted Tissues. *Sci. Rep.* 7, 1–12 (2017).

46. Yang, K., Han, Q., Chen, B., Zheng, Y., Zhang, K., *et al.* Antimicrobial hydrogels: promising materials for medical application. *Int. J. Nanomedicine* 13, 2217–2263 (2018).

47. Wang, Z., Hu, W., Du, Y., Xiao, Y., Wang, X., *et al.* Green Gas-Mediated Cross-Linking Generates Biomolecular Hydrogels with Enhanced Strength and Excellent Hemostasis for Wound Healing. *ACS Appl. Mater. Interfaces* 12, 13622–13633 (2020).

48. Hu, W., Wang, Z., Xiao, Y., Zhang, S. & Wang, J. Advances in crosslinking strategies of biomedical hydrogels. *Biomater. Sci.* 7, 843–855 (2019).

49. GhavamiNejad, A., Ashammakhi, N., Wu, X. Y. & Khademhosseini, A. Crosslinking Strategies for 3D Bioprinting of Polymeric Hydrogels. *Small* 16, 2002931 (2020).

50. You, Y., Yang, J., Zheng, Q., Wu, N., Lv, Z., *et al.* Ultra-stretchable hydrogels with hierarchical hydrogen bonds. *Sci. Rep.* 10, 11727 (2020).

51. Sivashanmugam, A., Arun Kumar, R., Vishnu Priya, M., Nair, S. V. & Jayakumar, R. An overview of injectable polymeric hydrogels for tissue engineering. *Eur. Polym. J.* 72, 543–565 (2015).

52. Garner, J. & Park, K. Types and Chemistry of Synthetic Hydrogels. in *Gels Handbook* 17–44 (2016).

53. Tabet, A., Gebhart, T., Wu, G., Readman, C., Smela, M. P., *et al.* Applying support-vector machine learning algorithms toward predicting host–guest interactions with cucurbit[7]uril. *Phys. Chem. Chem. Phys.* 22, 14976–14982 (2020).

54. Liu, M., Ishida, Y., Ebina, Y., Sasaki, T., Hikima, T., *et al.* An anisotropic hydrogel with electrostatic repulsion between cofacially aligned nanosheets. *Nature* 517, 68–72 (2015).

55. Qi, C., Liu, J., Jin, Y., Xu, L., Wang, G., *et al.* Photo-crosslinkable, injectable sericin hydrogel as 3D biomimetic extracellular matrix for minimally invasive repairing cartilage. *Biomaterials* 163, 89–104 (2018).

56. Kobayashi, S., Uyama, H. & Kimura, S. Enzymatic Polymerization. *Chem. Rev.* 101, 3793–3818 (2001).

57. Lee, F., Bae, K. H. & Kurisawa, M. Injectable hydrogel systems crosslinked by horseradish peroxidase. *Biomed. Mater. Bristol Engl.* 11, 014101 (2015).

58. Yu, F., Cao, X., Li, Y., Zeng, L., Yuan, B., *et al.* An injectable hyaluronic acid/PEG hydrogel for cartilage tissue engineering formed by integrating enzymatic crosslinking and Diels–Alder "click chemistry". *Polym. Chem.* 5, 1082–1090 (2013).

59. Kirchhof, S., Brandl, F. P., Hammer, N. & Goepferich, A. M. Investigation of the Diels–Alder reaction as a cross-linking mechanism for degradable poly(ethylene glycol) based hydrogels. *J. Mater. Chem. B* 1, 4855–4864 (2013).

60. Nair, D. P., Podgórski, M., Chatani, S., Gong, T., Xi, W., *et al.* The Thiol-Michael Addition Click Reaction: A Powerful and Widely Used Tool in Materials Chemistry. *Chem. Mater.* 26, 724–744 (2014).

61. Ferruti, P. Poly(amidoamine)s: Past, present, and perspectives. *J. Polym. Sci. Part Polym. Chem.* 51, 2319–2353 (2013).

62. Jia, Y. & Li, J. Molecular Assembly of Schiff Base Interactions: Construction and Application. *Chem. Rev.* 115, 1597–1621 (2015).

63. Chen, T., Chen, Y., Rehman, H. U., Chen, Z., Yang, Z., *et al.* Ultratough, Self-Healing, and Tissue-Adhesive Hydrogel for Wound Dressing. *ACS Appl. Mater. Interfaces* 10, 33523–33531 (2018).

64. Fenn, S. L. & Oldinski, R. A. Visible light crosslinking of methacrylated hyaluronan hydrogels for injectable tissue repair. *J. Biomed. Mater. Res. B Appl. Biomater.* 104, 1229–1236 (2016).

65. Cha, C., Piraino, F. & Khademhosseini, A. Microfabrication Technology in Tissue Engineering. in *Tissue Engineering (Second Edition)* 283–310 (Academic Press, 2014).

66. Williams, C. G., Malik, A. N., Kim, T. K., Manson, P. N. & Elisseeff, J. H. Variable cytocompatibility of six cell lines with photoinitiators used for polymerizing hydrogels and cell encapsulation. *Biomaterials* 26, 1211–1218 (2005).

67. Bryant, S. J., Nuttelman, C. R. & Anseth, K. S. Cytocompatibility of UV and visible light photoinitiating systems on cultured NIH/3T3 fibroblasts in vitro. *J. Biomater. Sci. Polym. Ed.* 11, 439–457 (2000).

68. Hu, J., Hou, Y., Park, H., Choi, B., Hou, S., *et al.* Visible light crosslinkable chitosan hydrogels for tissue engineering. *Acta Biomater.* 8, 1730–1738 (2012).

69. Park, Y. D., Tirelli, N. & Hubbell, J. A. Photopolymerized hyaluronic acid-based hydrogels and interpenetrating networks. *Biomaterials* 24, 893–900 (2003).

70. Rodgers, Z. L., Hughes, R. M., Doherty, L. M., Shell, J. R., Molesky, B. P., *et al.* B12-Mediated, Long Wavelength Photopolymerization of Hydrogels. *J. Am. Chem. Soc.* 137, 3372–3378 (2015).

71. Ash, C., Dubec, M., Donne, K. & Bashford, T. Effect of wavelength and beam width on penetration in light-tissue interaction using computational methods. *Lasers Med. Sci.* 32, 1909–1918 (2017).

72. Regentis Biomaterials. *Pivotal Study to Evaluate the Safety and Efficacy of GelrinC for Treatment of Cartilage Defects (SAGE)*. https://clinicaltrials.gov/ct2/show/NCT03262909 (2020).

73. Raman, R., Hua, T., Gwynne, D., Collins, J., Tamang, S., *et al.* Light-degradable hydrogels as dynamic triggers for gastrointestinal applications. *Sci. Adv.* 6, eaay0065 (2020).

74. McHale, M. K., Setton, L. A. & Chilkoti, A. Synthesis and in Vitro Evaluation of Enzymatically Cross-Linked Elastin-Like Polypeptide Gels for Cartilaginous Tissue Repair. *Tissue Eng.* 11, 1768–1779 (2005).

75. Jeznach, O., Kołbuk, D. & Sajkiewicz, P. Injectable hydrogels and nanocomposite hydrogels for cartilage regeneration. *J. Biomed. Mater. Res. A* 106, 2762–2776 (2018).

76. Hasturk, O., Jordan, K. E., Choi, J. & Kaplan, D. L. Enzymatically crosslinked silk and silk-gelatin hydrogels with tunable gelation kinetics, mechanical properties and bioactivity for cell culture and encapsulation. *Biomaterials* 232, 119720 (2020).

77. Smith, L. J., Taimoory, S. M., Tam, R. Y., Baker, A. E. G., Binth Mohammad, N., *et al.* Diels–Alder Click-Cross-Linked Hydrogels with Increased Reactivity Enable 3D Cell Encapsulation. *Biomacromolecules* 19, 926–935 (2018).

78. Ding, F., Wu, S., Wang, S., Xiong, Y., Li, Y., *et al.* A dynamic and self-crosslinked polysaccharide hydrogel with autonomous self-healing ability. *Soft Matter* 11, 3971–3976 (2015).

79. Vats, K., Marsh, G., Harding, K., Zampetakis, I., Waugh, R. E., *et al.* Nanoscale physicochemical properties of chain- and step-growth polymerized PEG hydrogels affect cell-material interactions. *J. Biomed. Mater. Res. A* 105, 1112–1122 (2017).

80. Metters, A. & Hubbell, J. Network Formation and Degradation Behavior of Hydrogels Formed by Michael-Type Addition Reactions. *Biomacromolecules* 6, 290–301 (2005).

81. Dutta, A., Maity, S. & Das, R. K. A Highly Stretchable, Tough, Self-Healing, and Thermoprocessable Polyacrylamide–Chitosan Supramolecular Hydrogel. *Macromol. Mater. Eng.* 303, 1800322 (2018).

82. Wang, Z., Ren, Y., Zhu, Y., Hao, L., Chen, Y., *et al.* A Rapidly Self-Healing Host–Guest Supramolecular Hydrogel with High Mechanical Strength and Excellent Biocompatibility. *Angew. Chem. Int. Ed.* 57, 9008–9012 (2018).

83. Wang, Z., An, G., Zhu, Y., Liu, X., Chen, Y., *et al.* 3D-printable self-healing and mechanically reinforced hydrogels with host–guest non-covalent interactions integrated into covalently linked networks. *Mater. Horiz.* 6, 733–742 (2019).

84. Tavafoghi, M., Sheikhi, A., Tutar, R., Jahangiry, J., Baidya, A., *et al.* Engineering Tough, Injectable, Naturally Derived, Bioadhesive Composite Hydrogels. *Adv. Healthc. Mater.* 9, 1901722 (2020).

85. Sun, J.-Y., Zhao, X., Illeperuma, W. R. K., Chaudhuri, O., Oh, K. H., *et al.* Highly stretchable and tough hydrogels. *Nature* 489, 133 (2012).

86. Liu, J., Tan, C. S. Y., Yu, Z., Lan, Y., Abell, C., *et al.* Biomimetic Supramolecular Polymer Networks Exhibiting both Toughness and Self-Recovery. *Adv. Mater.* 29, 1604951 (2017).

87. Saunders, L. & Ma, P. X. Self-Healing Supramolecular Hydrogels for Tissue Engineering Applications. *Macromol. Biosci.* 19, 1800313 (2019).

88. Kharkar, P. M., Kiick, K. L. & Kloxin, A. M. Designing degradable hydrogels for orthogonal control of cell microenvironments. *Chem. Soc. Rev.* 42, 7335–7372 (2013).

89. Sivak, W. N., Minteer, D. M., Lannau, B. & Marra, K. G. Controlling Hydrogel Biodegradability. in *Gels Handbook* 131–173 (2016).

90. Madl, C. M., Katz, L. M. & Heilshorn, S. C. Tuning Bulk Hydrogel Degradation by Simultaneous Control of Proteolytic Cleavage Kinetics and Hydrogel Network Architecture. *ACS Macro Lett.* 7, 1302–1307 (2018).

91. Le, T. M. D., Duong, H. T. T., Thambi, T., Giang Phan, V. H., Jeong, J. H., *et al.* Bioinspired pH- and Temperature-Responsive Injectable Adhesive Hydrogels with Polyplexes Promotes Skin Wound Healing. *Biomacromolecules* 19, 3536–3548 (2018).

92. Han, L., Wang, M., Li, P., Gan, D., Yan, L., *et al.* Mussel-Inspired Tissue-Adhesive Hydrogel Based on the Polydopamine–Chondroitin Sulfate Complex for Growth-Factor-Free Cartilage Regeneration. *ACS Appl. Mater. Interfaces* 10, 28015–28026 (2018).

93. Peng, B., Lai, X., Chen, L., Lin, X., Sun, C., *et al.* Scarless Wound Closure by a Mussel-Inspired Poly(amidoamine) Tissue Adhesive with Tunable Degradability. *ACS Omega* 2, 6053–6062 (2017).

94. Xie, C., Wang, X., He, H., Ding, Y. & Lu, X. Mussel-Inspired Hydrogels for Self-Adhesive Bioelectronics. *Adv. Funct. Mater.* 30, 1909954 (2020).

95. Hofman, A. H., van Hees, I. A., Yang, J. & Kamperman, M. Bioinspired Underwater Adhesives by Using the Supramolecular Toolbox. *Adv. Mater.* 30, 1704640 (2018).

96. Yang, J., Bai, R., Chen, B. & Suo, Z. Hydrogel Adhesion: A Supramolecular Synergy of Chemistry, Topology, and Mechanics. *Adv. Funct. Mater.* 30, 1901693 (2020).

97. Xu, Q., Zhang, Z., Xiao, C., He, C. & Chen, X. Injectable Polypeptide Hydrogel as Biomimetic Scaffolds with Tunable Bioactivity and Controllable Cell Adhesion. *Biomacromolecules* 18, 1411–1418 (2017).

98. Lam, J. & Segura, T. The modulation of MSC integrin expression by RGD presentation. *Biomaterials* 34, 3938–3947 (2013).

99. Gaharwar, A. K., Peppas, N. A. & Khademhosseini, A. Nanocomposite hydrogels for biomedical applications. *Biotechnol. Bioeng.* 111, 441–453 (2014).

100. Zhao, H., Liu, M., Zhang, Y., Yin, J. & Pei, R. Nanocomposite hydrogels for tissue engineering applications. *Nanoscale* 12, 14976–14995 (2020).

101. Boyer, C., Figueiredo, L., Pace, R., Lesoeur, J., Rouillon, T., *et al.* Laponite nanoparticle-associated silated hydroxypropylmethyl cellulose as an injectable reinforced interpenetrating network hydrogel for cartilage tissue engineering. *Acta Biomater.* 65, 112–122 (2018).

102. Eslahi, N., Simchi, A., Mehrjoo, M., Shokrgozar, M. A. & Bonakdar, S. Hybrid cross-linked hydrogels based on fibrous protein/block copolymers and layered silicate nanoparticles: tunable thermosensitivity, biodegradability and mechanical durability. *RSC Adv.* 6, 62944–62957 (2016).

103. Wang, Q., Mynar, J. L., Yoshida, M., Lee, E., Lee, M., *et al.* High-water-content mouldable hydrogels by mixing clay and a dendritic molecular binder. *Nature* 463, 339–343 (2010).

104. Liu, R., Liang, S., Tang, X.-Z., Yan, D., Li, X., *et al.* Tough and highly stretchable graphene oxide/polyacrylamide nanocomposite hydrogels. *J. Mater. Chem.* 22, 14160 (2012).

105. Iglesias, D., Melle-Franco, M., Kurbasic, M., Melchionna, M., Abrami, M., *et al.* Oxidized Nanocarbons-Tripeptide Supramolecular Hydrogels: Shape Matters! *ACS Nano* 12, 5530–5538 (2018).

106. Shi, W., Huang, J., Fang, R. & Liu, M. Imparting Functionality to the Hydrogel by Magnetic-Field-Induced Nano-assembly and Macro-response. *ACS Appl. Mater. Interfaces* 12, 5177–5194 (2020).

107. Rose, S., Prevoteau, A., Elzière, P., Hourdet, D., Marcellan, A., *et al.* Nanoparticle solutions as adhesives for gels and biological tissues. *Nature* 505, 382–385 (2014).

108. Wahid, F., Zhong, C., Wang, H.-S., Hu, X.-H., Chu, L.-Q., *et al.* Recent Advances in Antimicrobial Hydrogels Containing Metal Ions and Metals/Metal Oxide Nanoparticles. *Polymers* 9, 636 (2017).

109. Chen, T., Hou, K., Ren, Q., Chen, G., Wei, P., *et al.* Nanoparticle-Polymer Synergies in Nanocomposite Hydrogels: From Design to Application. *Macromol. Rapid Commun.* 39, 1800337 (2018).

110. Thoniyot, P., Tan, M. J., Karim, A. A., Young, D. J. & Loh, X. J. Nanoparticle–Hydrogel Composites: Concept, Design, and Applications of These Promising, Multi-Functional Materials. *Adv. Sci.* 2, 1400010 (2015).

111. Sun, Z., Song, C., Wang, C., Hu, Y. & Wu, J. Hydrogel-Based Controlled Drug Delivery for Cancer Treatment: A Review. *Mol. Pharm.* 17, 373–391 (2020).

112. Shiotani, A., Mori, T., Niidome, T., Niidome, Y. & Katayama, Y. Stable Incorporation of Gold Nanorods into N-Isopropylacrylamide Hydrogels and Their Rapid Shrinkage Induced by Near-Infrared Laser Irradiation. *Langmuir* 23, 4012–4018 (2007).

113. Satarkar, N. S. & Hilt, J. Z. Magnetic hydrogel nanocomposites for remote controlled pulsatile drug release. *J. Controlled Release* 130, 246–251 (2008).

114. Zhang, H., Patel, A., Gaharwar, A. K., Mihaila, S. M., Iviglia, G., *et al.* Hyperbranched Polyester Hydrogels with Controlled Drug Release and Cell Adhesion Properties. *Biomacromolecules* 14, 1299–1310 (2013).

115. Alonci, G., Fiorini, F., Riva, P., Monroy, F., López-Montero, I., *et al.* Injectable Hybrid Hydrogels, with Cell-Responsive Degradation, for Tumor Resection. *ACS Appl. Bio Mater.* 1, 1301–1310 (2018).

116. Tung, C.-Y. M. & Dynes, P. J. Relationship between viscoelastic properties and gelation in thermosetting systems. *J. Appl. Polym. Sci.* 27, 569–574 (1982).

117. Sang, L., Liu, Y., Hua, W., Xu, K., Wang, G., *et al.* Thermally sensitive conductive hydrogel using amphiphilic crosslinker self-assembled carbon nanotube to enhance neurite outgrowth and promote spinal cord regeneration. *RSC Adv.* 6, 26341–26351 (2016).

118. Zhang, S., Chen, Y., Liu, H., Wang, Z., Ling, H., *et al.* Room-Temperature-Formed PEDOT:PSS Hydrogels Enable Injectable, Soft, and Healable Organic Bioelectronics. *Adv. Mater.* 32, 1904752 (2020).

119. Park, S. H., Seo, J. Y., Park, J. Y., Ji, Y. B., Kim, K., *et al.* An injectable, click-crosslinked, cytomodulin-modified hyaluronic acid hydrogel for cartilage tissue engineering. *NPG Asia Mater.* 11, 1–16 (2019).

120. Yesilyurt, V., Webber, M. J., Appel, E. A., Godwin, C., Langer, R., *et al.* Injectable Self-Healing Glucose-Responsive Hydrogels with pH-Regulated Mechanical Properties. *Adv. Mater.* 28, 86–91 (2016).

121. Xu, D., Liu, C.-Y. & Craig, S. L. Divergent Shear Thinning and Shear Thickening Behavior of Supramolecular Polymer Networks in Semidilute Entangled Polymer Solutions. *Macromolecules* 44, 2343–2353 (2011).

122. Uman, S., Dhand, A. & Burdick, J. A. Recent advances in shear-thinning and self-healing hydrogels for biomedical applications. *J. Appl. Polym. Sci.* 137, 48668 (2020).

123. Rodell, C. B., MacArthur, J. W., Dorsey, S. M., Wade, R. J., Wang, L. L., *et al.* Shear-Thinning Supramolecular Hydrogels with Secondary Autonomous Covalent Crosslinking to Modulate Viscoelastic Properties In Vivo. *Adv. Funct. Mater.* 25, 636–644 (2015).

124. Wang, C., Yue, H., Feng, Q., Xu, B., Bian, L., *et al.* Injectable Nanoreinforced Shape-Memory Hydrogel System for Regenerating Spinal Cord Tissue from Traumatic Injury. *ACS Appl. Mater. Interfaces* 10, 29299–29307 (2018).

125. Rodell, C. B., Dusaj, N. N., Highley, C. B. & Burdick, J. A. Injectable and Cytocompatible Tough Double-Network Hydrogels through Tandem Supramolecular and Covalent Crosslinking. *Adv. Mater.* 28, 8419–8424 (2016).

126. Chakma, P. & Konkolewicz, D. Dynamic Covalent Bonds in Polymeric Materials. *Angew. Chem. Int. Ed.* 58, 9682–9695 (2019).

127. Barcan, G. A., Zhang, X. & Waymouth, R. M. Structurally Dynamic Hydrogels Derived from 1,2-Dithiolanes. *J. Am. Chem. Soc.* 137, 5650–5653 (2015).

128. Avery, R. K., Albadawi, H., Akbari, M., Zhang, Y. S., Duggan, M. J., *et al.* An injectable shear-thinning biomaterial for endovascular embolization. *Sci. Transl. Med.* 8, 365ra156-365ra156 (2016).

129. Highley, C. B., Song, K. H., Daly, A. C. & Burdick, J. A. Jammed Microgel Inks for 3D Printing Applications. *Adv. Sci.* 6, 1801076 (2019).

130. Nichol, J. W., Koshy, S. T., Bae, H., Hwang, C. M., Yamanlar, S., *et al.* Cell-laden microengineered gelatin methacrylate hydrogels. *Biomaterials* 31, 5536–5544 (2010).

Chapter 2: *In situ* forming poly(amidoamine) supramolecular hydrogel for minimally-invasive gastric tumor resection

Abstract

Poly(amidoamine) (PAA) are a class of synthetic polymers characterized by wide structural variability and good biocompatibility that make them an interesting material for the preparation of hydrogels for biomedical applications. Herein we present the preparation and characterization of a linear PAA with application in the minimal invasive resection of gastric tumors. When the linear PAA solution is injected in the gastric tissue, it immediately forms a supramolecular tissue-adhesive hydrogel. The gelation process is reversible with the gel to sol transition observed after the resection of the material from the organ. The experiments done to investigate the mechanism of the sol-gel-sol process suggest that the hydrogel formation is related to the presence of compressive forces exerted by the tissue which trigger the generation of supramolecular bindings between the tissue and the PAA and among polymer chains leading to the hydrogel formation (Figure 2.1). The linear PAA solution was used *in vivo* for the endoscopic tumor dissection, compared with saline solution, it halved the time necessary for the procedure and it reduced to one third the occurrence of perforation.

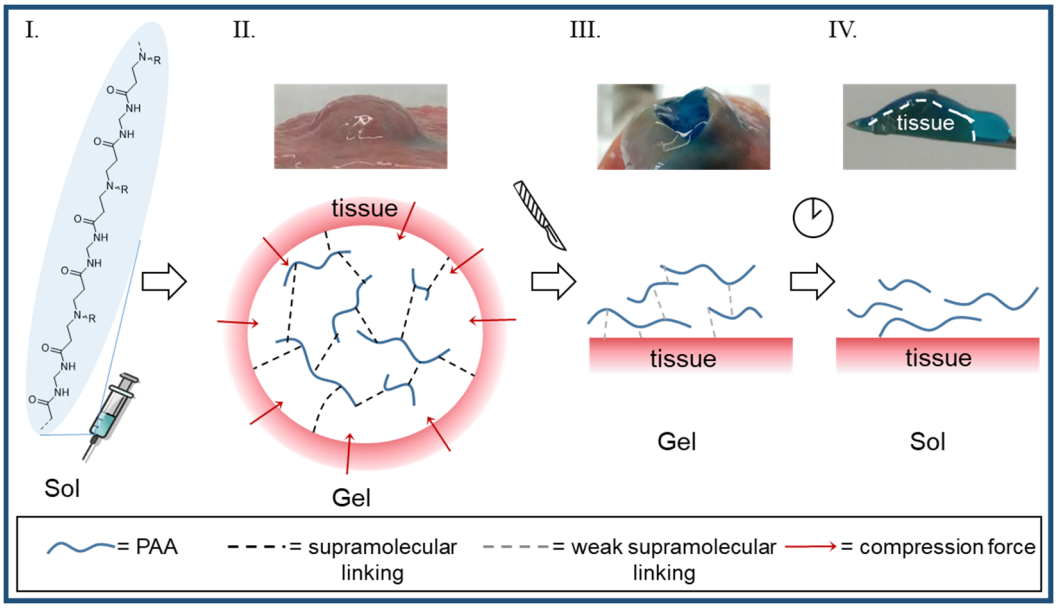

Figure 2.1: The PAA solution in the sol state (I.) is injected in the gastric tissue where it forms a gel (II.) thanks to the presence of compression forces that promote the formation of supramolecular bonding between the tissue and the PAA chains and among the polymeric chains. If the tissue is resected, the compression forces are removed, and the supramolecular bonding is weakened (III.) up to the disruption of the three-dimensional network and to the transition to the sol state (IV.).

2.1. Introduction

2.1.1. The Michael addition reaction in the synthesis of hydrogels

In Chapter 1, the possible cross-linking reactions to obtain hydrogels have been introduced. The Michael addition reaction is widely used thanks to its versatility, the absence of by-products and to the possibility to conduct it at physiological temperature, in water and in presence of oxygen. In the preparation of hydrogels, amines (aza-Michael reaction) or thiols (thiol-Michael reaction) are commonly selected to act as nucleophiles to *α,β*-unsatured carbonyls such as acrylates, acrylamides, malemides or vinyl sulfones (Scheme 2.1).[1]

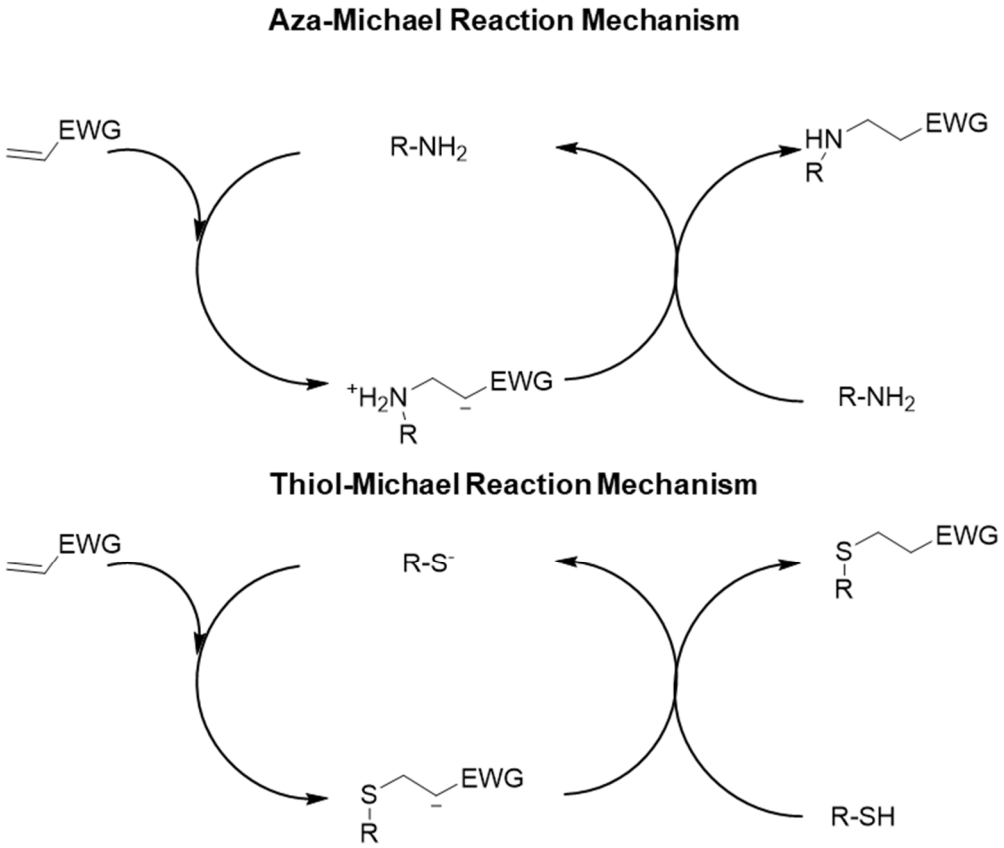

Scheme 2.1: Reaction Mechanism of the aza- and thiol-Michael addition. EWG represents an electron withdrawing group.

The stepwise aza-Michael poly-addition of monoamines or diamines to bisacrylamides (Scheme 2.2) is at the basis of the preparation of poly(amidoamine)s. It is necessary to point out that the term *poly(amidoamine)* may refer either to hyper-branched, not cross-linked dendrimer-like polymers or to single chain amine-polymers.[2] In this chapter the focus is on the latter, initialed PAAs and reported for the first time in an international journal by Danusso and Ferruti in 1970.[3]

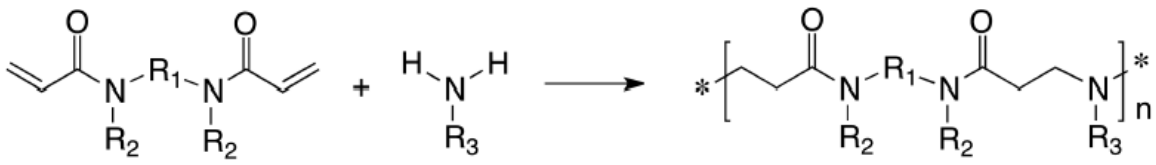

Scheme 2.2: General synthesis of PAAs. Reprinted with permission from *J. Pol. Sci. A Pol. Chem.* **2013**, 51, 2319. Copyright 2013, Wiley.

The polymerization degree depends on the solvent, the monomer concentration, the presence of steric hindrance, the temperature and the time of reaction.[2] Warming the solution allows to speed up the process but at the same it increases the rate of side reactions (retro-Michael and amide hydrolysis) reducing the molecular weight of the product.[2,3] LiOH has been reported to have optimal catalytic activity for the aza-Michael reaction owing to the ability of lithium to coordinate with the electron withdrawing group of the conjugated alkene and to consequently increase its electrophilicity.[4,5] The use of $CaCl_2$ has been proposed as a more mild and biocompatible alternative.[6] By employing primary diamines, that act as tetra-functional monomers in the synthesis of PAA, it is possible to obtain cross-linked PAA which, in appropriate conditions, form hydrogels entrapping the water used as solvent.[7] PAA hydrogels with an extremely versatile range of side-substituents and cross-linking chains can be easily obtained by employing selected monomers bearing the desired functional groups. For example, the use of γ-aminobutyric acid introduces in the network carboxylic pending groups that increase the hydrophilicity and the amphoteric character of the PAA hydrogel improving its biocompatibility.[8] Our group demonstrated that amino functionalized silica nanoparticles can also act as an efficient covalent cross-linkers in PAA hydrogels where they are introduced with the primary function of biomolecule delivery system.[9] In another study, the combination of two different cross-linking molecules bearing secondary amines or ether groups along the chain, together with the introduction of alginate as an interpenetrated network, allowed to develop a PAA hydrogel with mechanical properties matching the ones of muscular tissue. The developed material has shown to have promising application in the minimal invasive treatment of inguinal hernia.[10] In the design of PAA hydrogels, it is however necessary to take into account that, starting from mixtures of monomers with no precautions, the step-growth of PAA generates random or quasi random networks. When amines with different reactivity are employed, it is therefore advisable to carry a two-step synthesis to ensure a fair distribution of the monomers

in the final polymer and to minimize the presence of unreacted monomers or the risk of confining the less reactive amines at the end of the chains.[2]

Compared with the aza-Michael, the thiol-Michael reaction is generally faster due to the weaker sulfur-hydrogen bonds and to the inherent electron density of the S atom which ensures the thiol reactivity.[11] The faster kinetic of this reaction allows to perform it at physiological pH without the addition of a catalyst in the preparation of hydrogels. For example Liu *et al.* used a dithiol to cross-link methacrylated dextran chains to form a cell-loaded hydrogel at physiological conditions in 4 minutes (Figure 2.2).[12] Using a similar approach, Dove an co-workers obtained a hyaluronic acid based hydrogel exploiting the thiol-yne reaction that occurred in 2 minutes.[13] The fast gelation and the possibility to obtain hydrogel at physiological conditions render the thiol-Michael reaction of particular interest for the preparation of *in situ* forming materials as it will be presented in Chapter 3.

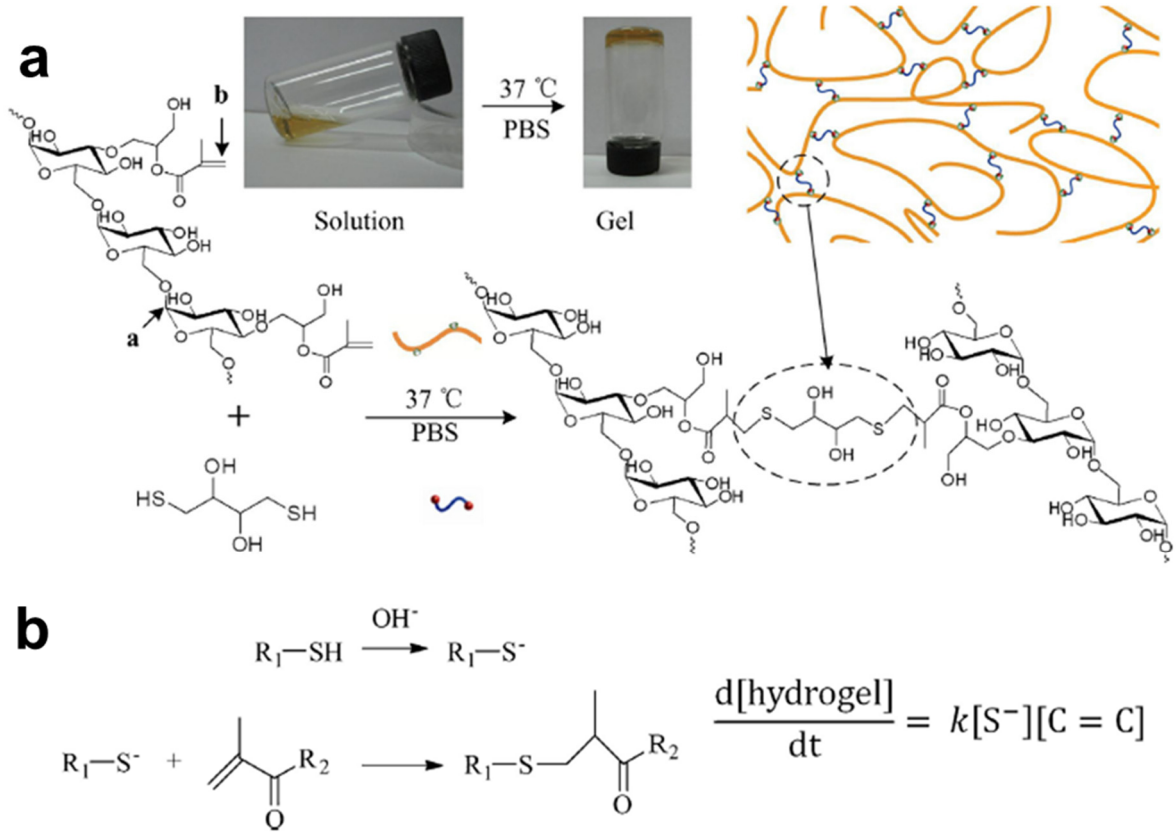

Figure 2.2: Dextran based hydrogel formation based on the thiol-Michael reaction. a) The synthesis occurs at physiological temperature and pH generating a percolated network in around 4 minutes. b) Reaction mechanism and rate equation. Reprinted with permission from: *Colloids and Surfaces B: Biointerfaces,* **2015**, 128, 140. Copyright 2015, Elsevier B.V.

2.1.2. The use of hydrogels for the minimal invasive gastric tumor resection

Endoscopic submucosal dissection (ESD) is a minimally invasive surgery procedure for the removal of early stage tumors located in the gastrointestinal tract. ESD consists in creating a cushion to separate the tumor from the muscular layer and to facilitate its removal (Figure 2.3).

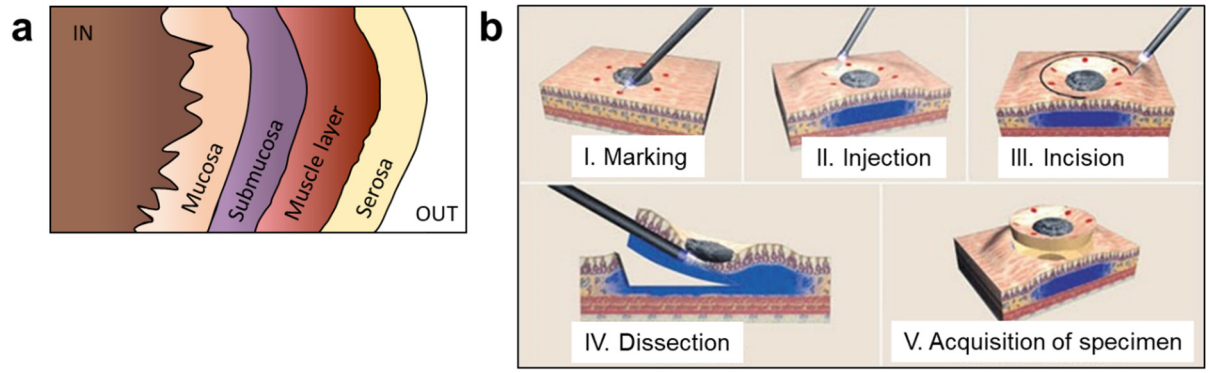

Figure 2.3: a) Stomach layers. b) Scheme of the endoscopic submucosal dissection procedure. After marking the area to be removed (I.), the lifting solution is injected (II.), the incision is made (III.) followed by the dissection (IV.) and the acquisition of the specimen (V.). Adapted from *www.ec21.com*

Saline solution is the most commonly used fluid in clinical applications, but the outcomes of the ESD are limited by the spreading of the saline solution in the tissue environment after injection, which produces a flat cushion.[14] Viscous solutions have been proposed as an alternative to saline, but their use is hampered by the difficulty of injection, the possible occurrence of inflammation[15] and, in the case of hyaluronic acid, possible tumor reoccurrence.[16] *In situ* forming hydrogels that leverage gelation processes triggered by local body temperature[17] or local application of light[18] have been proposed. Recently our group has developed a nanocomposite poly(amidoamine) hydrogel, named in this chapter as CL_PAA, that quickly forms a tissue-adhesive soft solid upon injection in the gastric tissue. It facilitates the ESD and reduces the risk of perforation compared with the use of saline solution.[19] The material is prepared starting from *N,N'*-methylenbisacrylamide (MBA) as Michael acceptor, *N,N*-dimethylethylenediamine, cystamine, and amino functionalized silica nanocapsules as Michael donors (Figure 2.4). The use of cystamine as cross-linker imparts cell-mediated degradability to the material while the nanocapsules have the function of biomolecule delivery system. When the reagents are mixed in water an inhomogeneous solution is first obtained due to the low MBA solubility (20 mg/mL); afterwards, with the formation of oligomers, a homogeneous solution is obtained in around 1 hour. At this point, if the solution is kept in a vial, a growth of

the viscosity, associated to the increase of the molecular weight of the oligomers, is observed up to the formation of a percolated network in more than 18 hours (Figure 2.5). On the contrary, if the oligomer solution is injected in the submucosal layer of the gastric tissue, it forms, in less than a minute, a tissue adherent soft solid. The fast gelation has been attributed to an interaction of the PAA oligomers with collagen chains bearing amino groups that could either be directly involved in the aza-Michael reaction or form an interpenetrated network that promotes the cross-linking process.[19]

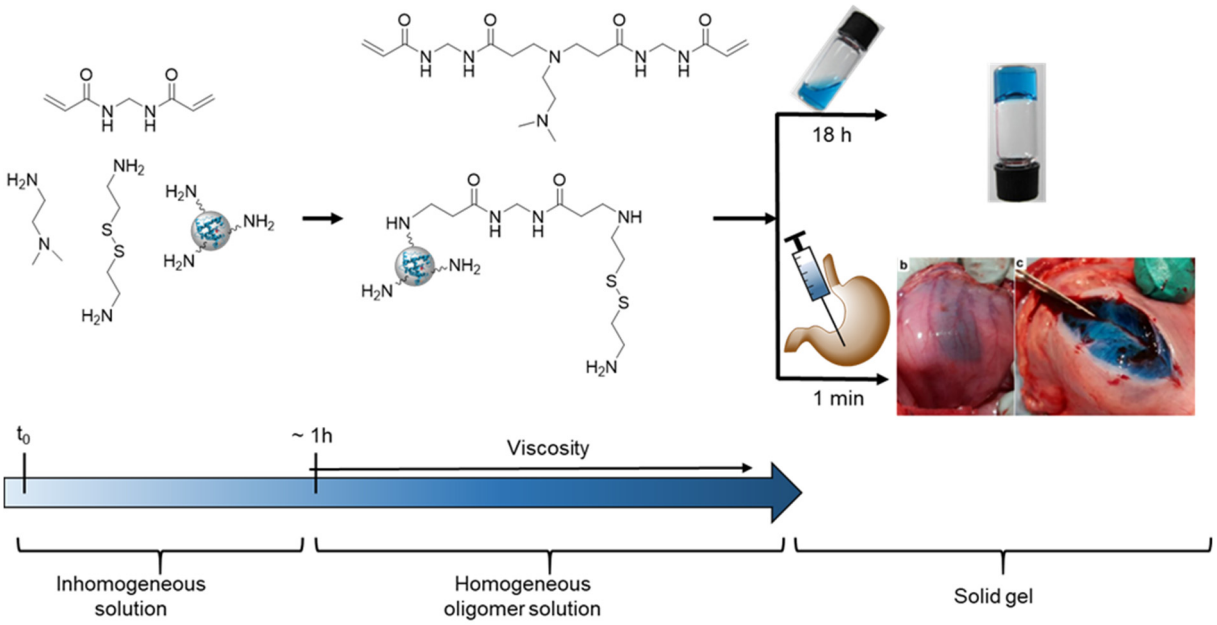

Figure 2.4: Synthesis of the cross-linked PAA hydrogel (CL_PAA) described by Alonci *et al.*[19] When the starting monomers are mixed in water, the solution is not homogeneous due to the low water solubility of MBA; with the occurring of the aza-Michael reaction, water soluble oligomers are formed and the solution is homogeneous after around 1 h at 37 °C. At this point, if the solution is injected in the submucosal layer of gastric tissue, it forms in less than a minute, a tissue adherent hydrogel. On the contrary, if the solution is kept in a vial, a gradual growth of the viscosity associated to the increase of the molecular weight of the oligomers is observed up to the sol-gel transition that occurs after more than 18 hours. The picture of the hydrogel injected in the gastric tissue has been adapted with permission from *ACS Appl. Bio Mater.* **2018**, 1, 1301. Copyright 2018, American Chemical Society.

Despite the interesting sol-gel transition triggered by the tissue and the optimal performance as lifting material in ESD application, the CL_PAA hydrogel rises concerns regarding both the toxicity of the material and its practical applicability. In fact, the injected oligomer solution has a pH around 9 and it contains unreacted acrylic and amine terminal groups that cannot be considered biocompatible. Moreover, from a practical point of view the applicability of the

hydrogel is hindered by the need of preparing the material a few hours before the injection and by the difficulty to coordinate the synthesis with the surgical preparation of the patient.

The understanding of the underlying mechanism of hydrogel formation triggered by the gastric tissue is expected to give important hints to improve the material both from the applicability and from the biocompatibility point of view.

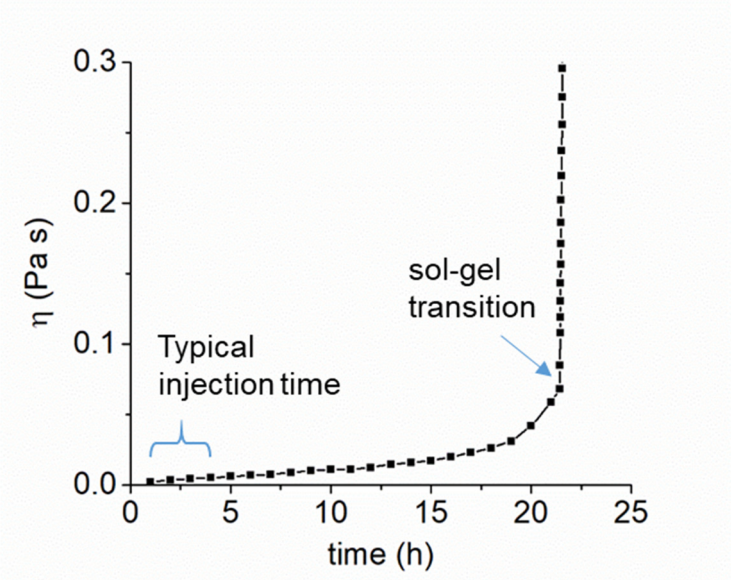

Figure 2.5: Measure over time of the viscosity of the CL_PAA oligomer solution. The measurement started after that the solution became homogeneous. The measure is done using a coaxial cylinder geometry (10 mm diameter), $\dot{\gamma}$= 10 s^{-1}, *T*= 37 °C.

2.1.3. Aim of the project

The aim of the project presented in this chapter is to investigate the mechanism underlying the gelation process triggered by the gastric tissue at the basis of the sol-gel transition of the CL_PAA and to modify the system to facilitate the applicability and optimize its biocompatibility. The hypothesis that will be investigated in detail in this chapter is that the fast *in situ* sol-gel transition is related to a supramolecular hydrogel formation triggered by the surrounding environment rather than to a catalytic aza-Michael reaction between the injected oligomers.

2.2. Results and Discussion

Starting from the observation that the CL_PAA hydrogel immediately forms upon injection in the gastric tissue while it takes hours to undergo the sol-gel transition in vial, we hypothesized that the process is independent from the *in situ* chemical cross-linking of oligomers. To study this hypothesis a linear PAA was prepared, characterized and its ability to form supramolecular hydrogels in the gastric tissue investigated.

2.2.1. Synthesis of linear poly(amidoamine)

The linear PAA is prepared reacting *N,N'*-Methylenbisacrylamide (MBA) with primary mono-amine molecules in stoichiometric ratio. The primary amines tested are 4-aminobutyrric acid (GABA) (PAA-COOH), *N,N*-dimethylethylenediamine (PAA-N(CH_3)$_2$,) or ethanolamine (PAA-OH) (Scheme 2.3). The reaction is carried at 40 °C in presence of LiOH as catalyst. The choice of a mildly warm temperature allows to speed up the reaction while preventing side reactions (retro-Michael and amide hydrolysis) that are promoted at higher temperatures.[2,3] The reaction was followed by ^{1}H-NMR until the intensity of the peak at 6.25 ppm, attributed to the unreacted double bond was no further decreasing. The reaction time was typically between 24 h and 48 h. The solutions were then neutralized to pH 7 with concentrated HCl, dialyzed and freeze dried to obtain dry polymers. The mass amount of PAA-COOH recovered was 25% of the starting materials. After the purification, the ^{1}H-NMR was repeated (Figure 2.6a) to quantify the amount of terminal double bonds and to determine the molecular weight (MW) of the obtained polymers that resulted to be 2.6 kDa for PAA-COOH, 2.8 kDa for PAA-OH and 5.8 kDa for PAA-N(CH_3)$_2$ (see experimental section). The longer polymeric chain obtained for PAA-N(CH_3)$_2$ is attributed to the presence of the tertiary amine as lateral group that may promote the Michael reaction compared with the presence of a negatively charged or neutral group. Matrix-assisted laser desorption/ionization (MALDI) analysis showed the polymer fragmentation in oligomers constituted of up to 9 repeating units (one unit is defined by the combination of one MBA molecule and one amine molecule) (Figure 2.6b).

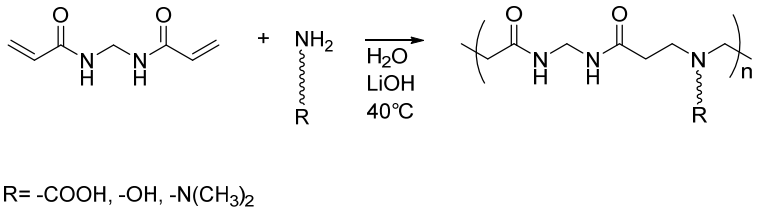

R= -COOH, -OH, -N(CH_3)$_2$

Scheme 2.3: Synthesis of the linear PAA.

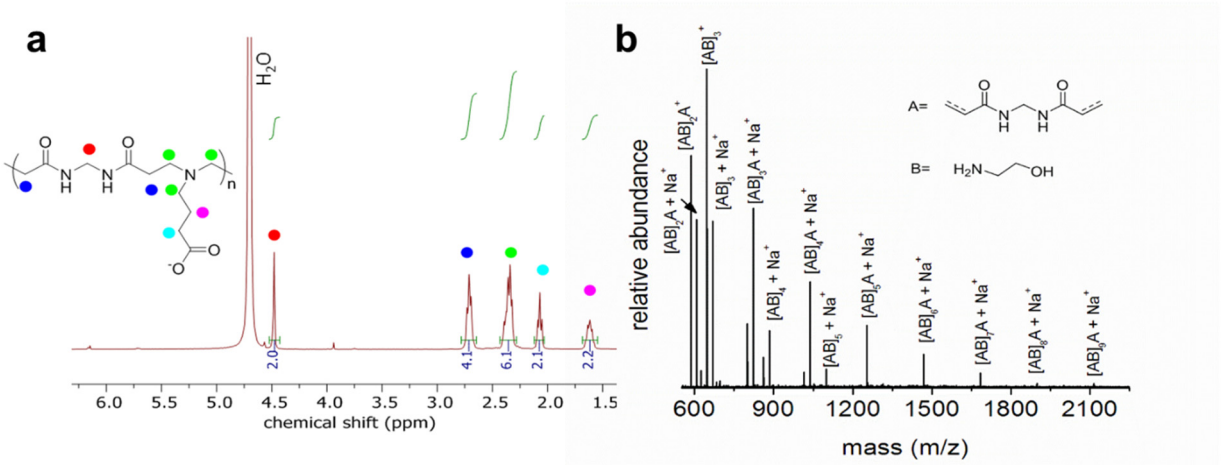

Figure 2.6: Linear PAA characterization. a) ^{1}H-NMR of PAA-COOH; the peak at 6.25 ppm is attributed to the terminal methacrylate group of the polymer. b) MALDI-TOF of PAA-OH.

The possibility to implant a fluid through an injection is determined by its rheological behavior. Endoscopic surgery, in particular, employs long needles (~1.5 m) of small diameter (23 G) that requires the fluid to be characterized by low viscosity so that it can be delivered by hand force without requiring the use of a pump. In the preparation of the PAA-COOH solution, it was considered that the CL_PAA solution has a total content of organic molecules of 223 mg/ml and that the yield of the synthesis of PAA-COOH is 25%. Taking into account that the sol-gel process is expected to rely mainly on the polymers present in solution rather than on the smaller molecules removed during the dialysis, the linear PAA-COOH solution was prepared in 55 mg/mL concentration (25% of 223 mg/mL) in PBS (0.01 M, pH 7.4). The solution behaves as a Newtonian fluid in the range of stresses tested and is characterized by low viscosity in comparison, for example, with a 2% sodium alginate solution (Figure 2.7a). The pressure necessary to flow the PAA_COOH solution through an endoscopic needle was measured using a syringe equipped with a manometer (Figure 2.7b) and compared to other fluids including water and alginate 2%. In the same figure, it is also shown the injection pressure that has been reported in literature for the delivery of a thermoresponsive material with application in the ESD, referred as Gel [a].[21] The injection of the PAA solution required a pressure of 2 atm, lower than the one necessary for Gel [a] and significantly lower than the one required for the alginate solution.

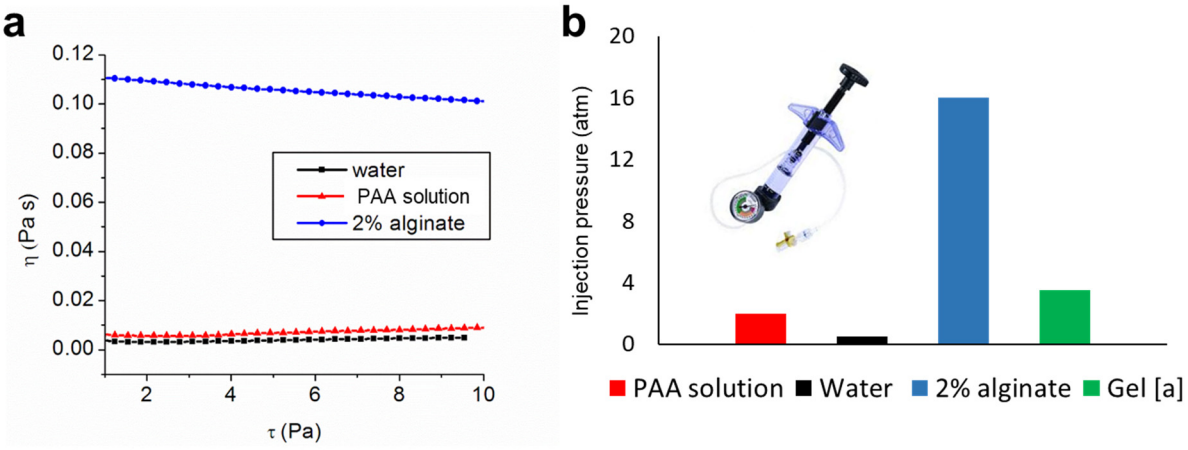

Figure 2.7: Rheological characterization of the PAA water solution. a) Viscosity measurement of water (black), PAA solution (red) and 2% alginate solution (blue); 37 °C, measuring geometry: coaxial cylinder (25 mm). b) Pressure necessary to pass different solutions through an endoscopic needle (23 G, 1.5 m); the measurements are done using a syringe equipped with a manometer. Water (black), PAA solution (red), 2% alginate solution (blue) and a gel (Gel [a]) reported in literature for endoscopic submucosal dissection application.[21]

2.2.2. The interaction of linear PAA solution with gastric tissue

A key property that made the CL_PAA an interesting material in ESD application is its ability to quickly undergo the sol-gel transition upon injection in the gastric submucosal layer forming a soft tissue-adherent hydrogel. The possibility to obtain a similar tissue-induced sol-gel transition using the linear PAA-COOH solution was studied. The solution was injected using a 23 G needle in an explanted porcine stomach through the mucosal layer (inner side of the stomach) in the submucosal layer. The solution formed in few seconds a soft solid hydrogel (Figure 2.8a, b). The hydrogel is strongly adherent to the tissue and it is not possible to remove it even with the use of tweezers. The nature of the interactions responsible of the gelation process will be discussed in detailed later in this chapter. A part of the hydrogel attached to the tissue was resected and lyophilized for SEM imaging. The hydrogel constitutes a three-dimensional porous material (Figure 2.8c). The hydrogel-tissue interface shows the optimal adhesion between the two materials (Figure 2.8d).

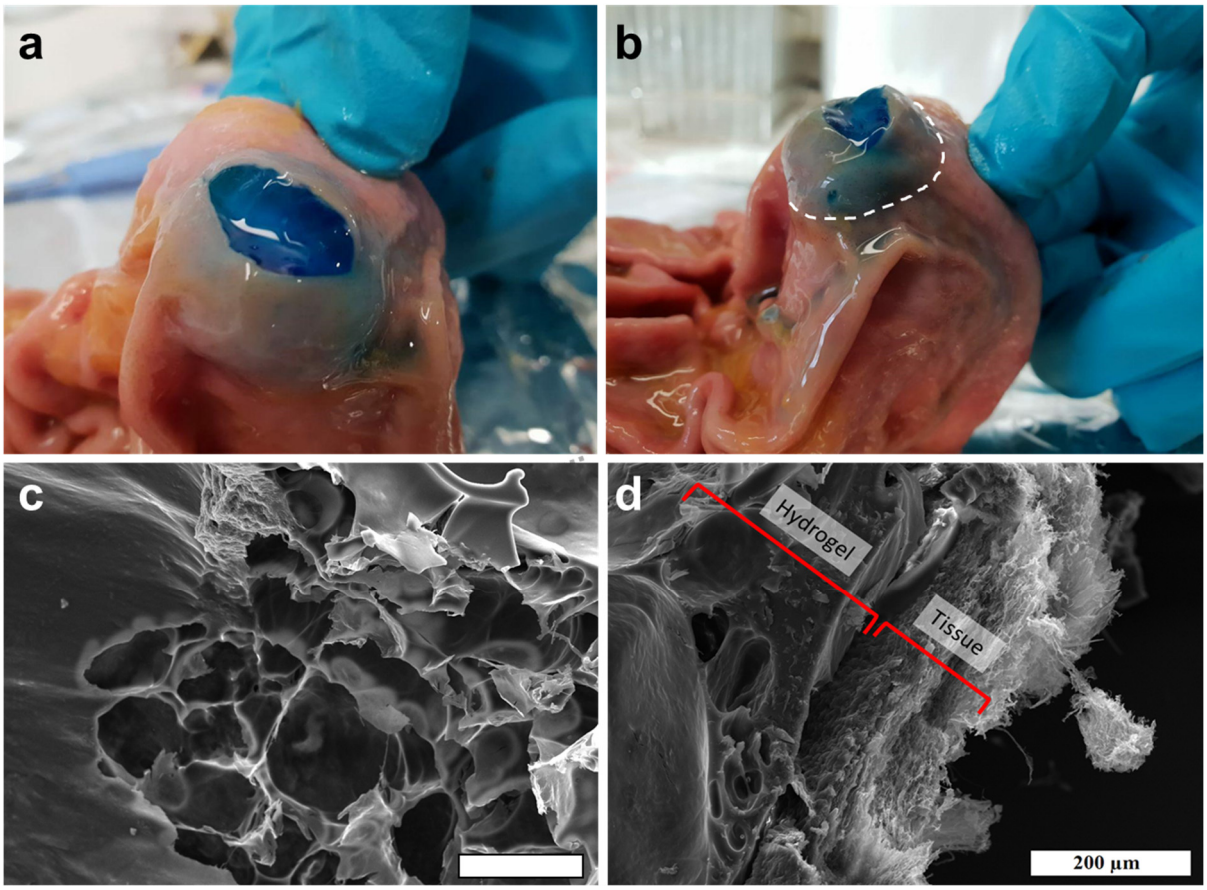

Figure 2.8: Hydrogel formation in gastric tissue after injection of a linear PAA solution. Methylene blue was added to the solution for better visualization. a) Top view of the hydrogel in the gastric tissue, b) lateral view of the hydrogel in the gastric tissue; the dashed line highlights the tissue lifting obtained with the hydrogel injection. c) SEM image of the hydrogel; d) SEM image of a portion of tissue with the adherent hydrogel. Scale bars 200µm.

The evolution of the *in situ* formed hydrogel over time was evaluated and compared with the saline (Figure 2.9). Right after injection both the PAA solution and saline gave a good tissue lifting. Saline does not undergo any transition after injection and after 20 min its diffusion is evident with the consequent decrease in the lifting; on the contrary, the PAA solution maintained an elevated lifting for the 60 minutes of observation confirming that it underwent the sol-gel transition that prevented the material spreading.

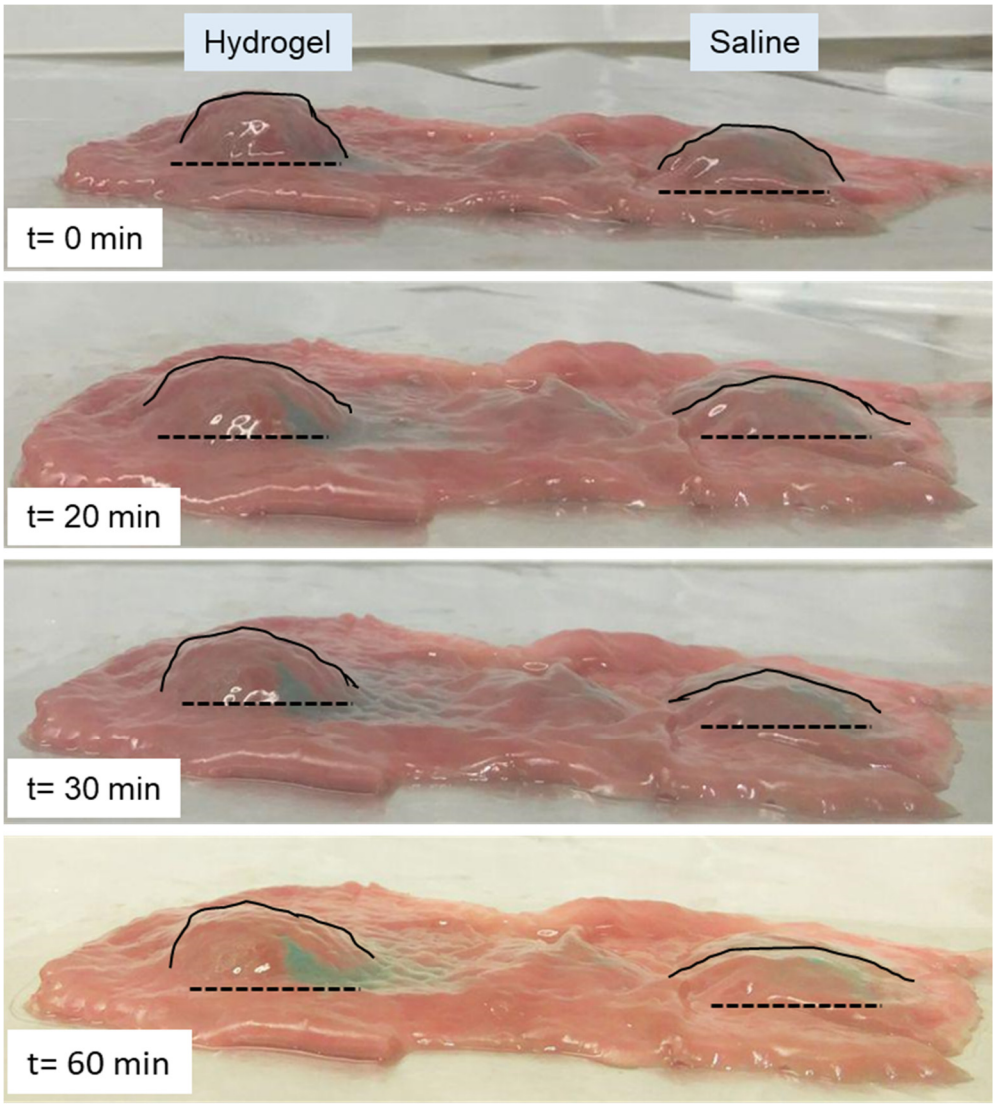

Figure 2.9: Time evolution over 1 hour of the cushion obtained from the injection of the linear PAA solution (left) and of saline solution (right) in an explanted porcine stomach. Methylene blue was added to the solutions for better visualization.

In a further experiment carried out to study the interaction between the gastric tissue and the PAA solution, after injection, a part of tissue and the hydrogel attached to it was resected and observed for one hour (Figure 2.10). Right after resection the PAA is a self-standing soft solid hydrogel while after 30 minutes it transits to the sol state and the solution starts dropping from the tissue. The observed behavior indicates that the hydrogel formed in the gastric tissue is a dynamic and reversible system and that its gel-sol transition is dependent on the presence of intact tissue around the material.

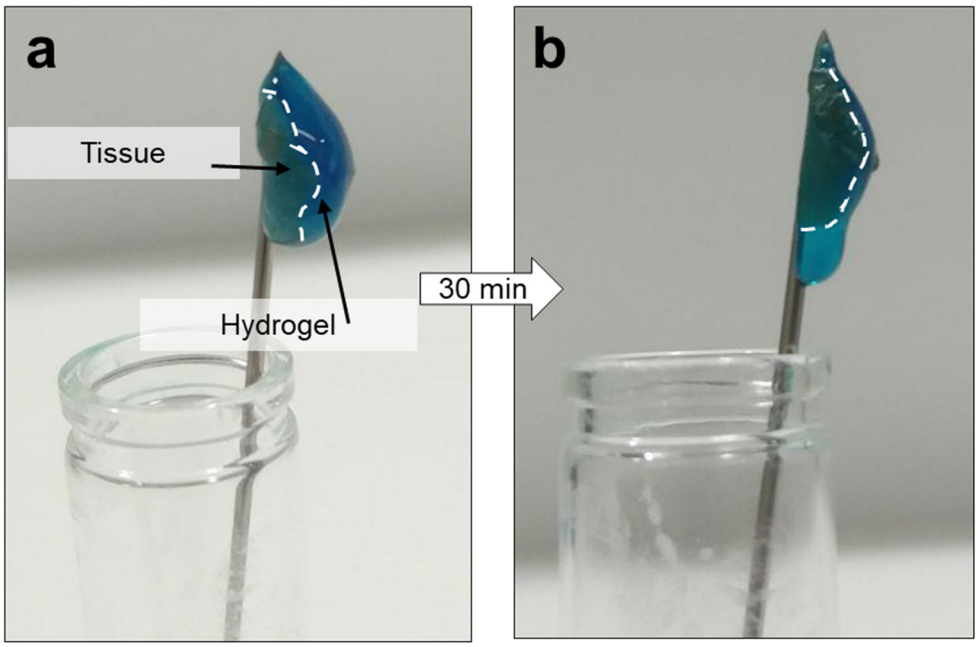

Figure 2.10: Reversible sol-gel. a) After tissue resection the hydrogel is a soft solid self-standing material; b) after about 30 min from resection the hydrogel returned to the sol state and it leaks from the tissue. Methylene blue was added to the solution for better visualization.

The mechanical properties of the supramolecular hydrogel were evaluated by oscillatory rheology (Figure 2.11). The gastric tissue can be considered, from a rheological point of view, a viscoelastic material with G'= 7800 (±2800) Pa and G''= 1900 (± 700) Pa (Figure 2.11a *i*). After the injection of the PAA solution, the elastic response of the system is halved with G' = 3800 (±400) Pa while the G'' modulus remains constant. The decrease in the G' modulus may be related to the detachment of the internal layers of the tissue that is therefore less elastic (Figure 2.11a *ii*). The absolute value of the moduli should however be considered only as an indicative value since the quantitative rheological characterization of such complex system depends on several factors such as the measuring gap and the normal force applied which are difficult to standardize. The gastric tissue was then resected with a scalpel to obtain a 8 mm disc of tissue to which the hydrogel was still strongly adherent. The rheological evaluation done on the hydrogel side (Figure 2.11a *iii*) confirmed that the material is a soft viscoelastic solid (G' > G'') with G'= 540 (±57) Pa and that the PAA solution underwent the sol-gel transition after injection. The presence of the tissue below the hydrogel may influence the measured rheological moduli. To eliminate the tissue contribute, a slice of the hydrogel was resected -it is not possible to totally remove the hydrogel from the tissue due to the strong adhesion- and its mechanical properties evaluated (Figure 2.11a *iv*). The measure confirmed that also the

implanted material alone can be defined as a gel with G'= 37 (±12) Pa. Compared with the elastic modulus measured for the gel still attached to the tissue, the gel alone has lower elastic modulus. This might indicate either, that there is a contribute of the tissue in the measurement, or that, after removing the gel from the tissue, the transition from the gel state to the sol state is promoted with the consequent decrease in the elastic modulus.

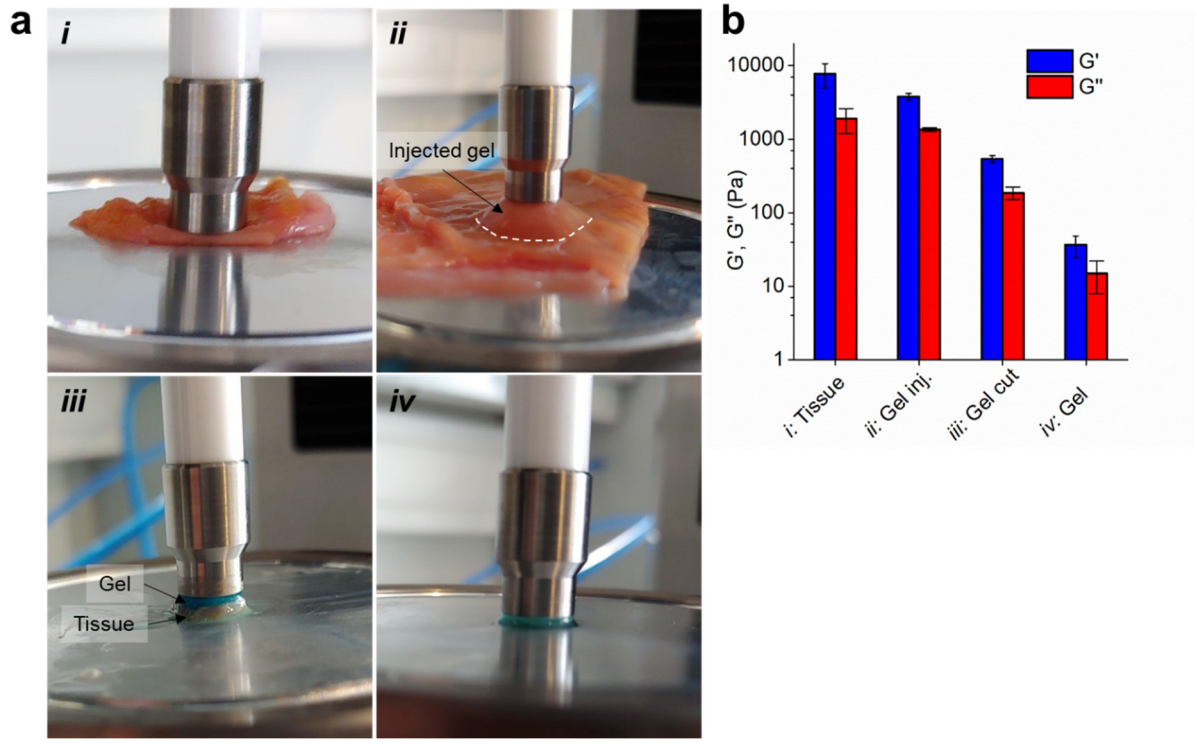

Figure 2.11: Oscillatory rheology of the tissue-hydrogel system. a) Stomach (*i*), PAA gel formed inside the tissue (*ii*), resected tissue with adherent hydrogel (*iii*) and resected hydrogel only (*iv*). b) Histogram showing the elastic modulus (G') and the viscous modulus (G'') measured for the different systems n=3. Measuring geometry: plate to plate (8 mm), γ: 5%, *f*: 1 Hz. Methylene blue was added to the solution for better visualization.

A further evaluation of the mechanical properties of the hydrogel after injection in the tissue was done by ultrasound elastography (UE). This technique evaluates the response of tissues to acoustic energy and it gives as an output their mechanical properties. In strain-based elastography, a force is exerted by the application of probe pressure which induces a deformation (strain) in the surrounding tissue dependent on their stiffness. The processing of the radiofrequency datasets obtained before and after compression gives the elastograms where a color scale indicates the tissue stiffness. The measure generally does not give an absolute value for the Young's modulus since the applied force on the tissue is usually unknown.[22] UE

was used to evaluate the mechanical properties of the PAA hydrogel formed inside the gastric tissue and to compare it with saline solution and with CL_PAA. A volume of around 3 mL of each of the fluids under study was injected in the submucosal layer of an explanted porcine stomach through the mucosal layer using a 23 G needle. UE was performed applying the probe on the internal part of the stomach in correspondence of the injection site (Figure 2.12). The analysis showed that the injected fluids are softer (red color) compared with the surrounding tissue (blue color) as already observed by oscillatory rheology (Figure 2.11). It was however not possible to observe a difference between the mechanical properties of the different implanted materials.

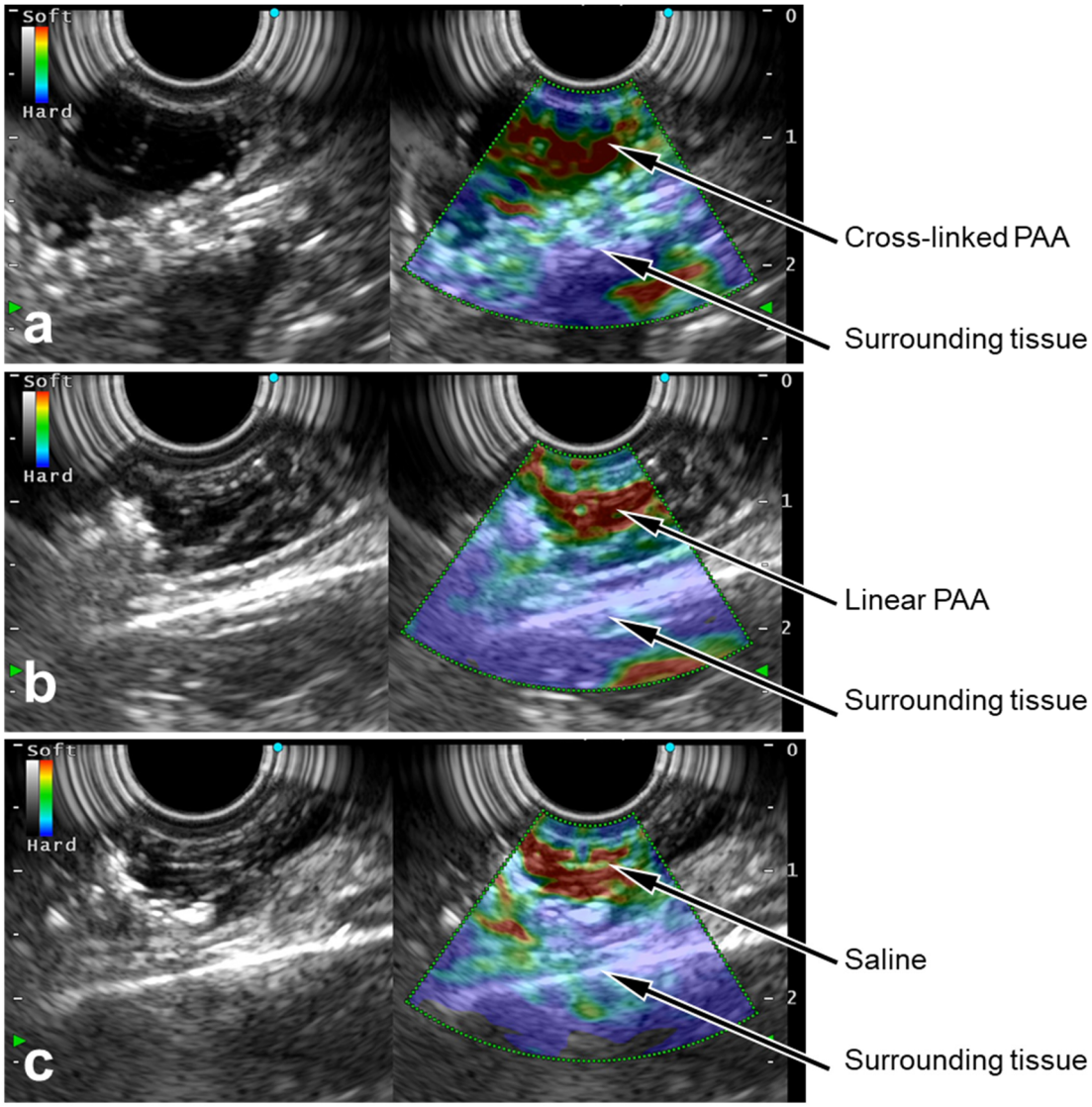

Figure 2.12: Ultrasound elastography of different solutions injected in an explanted porcine stomach. Red color represents a soft material, blue color represents a hard material. a) Cross-linked PAA used by Alonci *et al.*[19] for the endoscopic submucosal dissection; b) linear PAA hydrogel; c) saline solution.

The experiments have shown that the linear PAA solution undergoes immediate sol-gel transition after injection in the submucosal layer of the stomach forming a soft hydrogel strongly adherent to the tissue. The formed hydrogel is stable inside the integer organ (Figure 2.9) while after the resection of the tissue the material undergoes the transition from the gel state to the sol state (Figure 2.10). These observations suggest that the hydrogel formed in the submucosal layer of the stomach is a reversible supramolecular system whose sol-gel and gel-sol transitions are tissue dependent. The ability of the linear PAA to form a hydrogel upon injection suggests that also the fast sol-gel transition previously observed for the CL_PAA system should be ascribed to the formation of a supramolecular material rather than to a covalent system, based on the aza-Michael reaction, as reported by Alonci *et al*.[19] The nature of the physical cross-linking interactions underlying the hydrogel formation is investigated in the next paragraph.

2.2.3. Mechanism of hydrogel formation investigation

The supramolecular processes commonly underlying the sol-gel transition have been described in the introductive chapter of this thesis and they are: H-bonding, hydrophobic interactions, ionic/electrostatic interactions, host-guest interactions, crystallization and metal coordination. The hydrogel formation by crystallization in the system under study is excluded since it requires freeze-thawing cycles or other long processes that allow the polymer chains to organize in solution which are not compatible with the quick gelation observed herein.[23–25] Also host-guest interactions are excluded since they require a specific molecular design such as the presence of a macrocyclic host molecule (i.e. cucurbit [n]uril or cyclodextrine) that is not present in the PAA and it is not expected to be present in the tissue. Hydrophobic interactions are temperature dependent and should therefore be excluded since, when the PAA solution is injected in the explanted stomach, the material does not experience any significant temperature variation (both the solution and the tissue are at room temperature). To further investigate the possible presence of temperature dependent interactions, the gastric tissue and vials containing the PAA solutions were cooled down to 4 °C or incubated at 37 °C. Neither the cooling nor the warming of the solutions in vials induces the sol-gel transition while their injection in the gastric tissue previously cooled down to 4 °C or incubated at 37 °C generated immediately the sol-gel transition with no evident difference from the material formation observed at room temperature. The absence of temperature dependent transition was therefore confirmed. The sol-gel transition was evaluated qualitatively while a rheological quantitative comparison of the hydrogels formed in different conditions was not possible since external factors such as the

tissue variability and the injection site have an higher impact on the mechanical properties of the composite tissue-gel system compared with the temperature effect. Hydrogel formation based on H-bonding, electrostatic interactions and metal-complex formation are pH dependent and are influenced by the addition of ions to the systems. To evaluate the contribute of these interactions to the sol-gel transition of the system understudy, the pH of the PAA solution was tuned with concentrated HCl or NaOH in the range 2-14. No phase transition was observed in the vials while, when the same solutions were injected in the gastric tissue, the hydrogel formation occurred. A similar behavior was observed when $CaCl_2$ was added to the solution to evaluate the ionic effect. The solution in vial did not undergo any transition while the hydrogel was formed after injection in the tissue. The introduction of pending groups with different charges (-COOH, -OH, $-N(CH_3)_2$, Scheme 2.3) in the polymer did not influence the ability of the PAA to undergo the sol-gel transition after injection in the tissue. PAA have been reported to form complexes in presence of transition metals such as copper.[26–28] It is possible therefore, that the gelation process is triggered by metal ions or other components naturally present in the tissue. To investigate this possibility, gastric tissue was cut in ~5 mm pieces or smashed with a mixer and added to a PAA solution. Also in this case no phase transition was observed. In a further experiment, the dry PAA was dissolved in a solution of collagen type I of which the submucosa is rich; also in this case the gelation was not triggered. The PAA solution injections were repeated in other explanted porcine organs; the hydrogel formation was observed in the submucosa of the esophagus, in the submucosa of the colon while it was not observed in the liver nor in the pancreas. The results of the described experiments are summarized in Table 2.1.

Table 2.1: Effect of different stimuli on the hydrogel formation in vial or after injection in the gastric tissue.

	Condition	**Vial**	**Injection in gastric tissue**
pH	2	-	+
	7	-	+
	14	-	+
Temp.	4°C	-	+
	20°C	-	+
	37°C	-	+
Pending group	-COOH	-	+
	-OH	-	+
	$-N(CH_3)_2$	-	+
Bio stimuli	Gastric tissue	-	
	Collagen	-	

"+": The hydrogel is formed. "-": The hydrogel is not formed.

The experiments that have been carried did not give a clear explanation of the mechanism of hydrogel formation. The hypothesis is that the sol-gel transition is related not only to the supramolecular cross-linking of the PAA but it also depends on the presence of integer gastric tissue around the material that exerts a compressive force on it. When the solution is injected, it is exposed to the pressure exerted by the tissue layers, with time the tissue becomes loose and the hydrogel tends to pass to the sol state (Figure 2.9); if the tissue is resected the process is more evident with the hydrogel returning to the sol state in ~30 min (Figure 2.10). This could explain why the hydrogel formation is not observed in the liver and in the pancreas that have a spongier structure. The role of compression force was evaluated placing the PAA-COOH solution in a plastic balloon in presence of gastric tissue pieces and applying a compressive force to the balloon; no hydrogel formation was observed. We think that the mechanical force applied by the tissue on the solution triggers and promotes the formation of supramolecular interactions including H-bonding and electrostatic interactions. When the tissue is resected, in absence of compressive forces on the material, the supramolecular linking are weakened and the material undergoes the transition to the sol state with a gain in entropy (Figure 2.13).[29] It is however necessary to point out that the experimental data do not constitute a compleat proof of the proposed mechanism. Other components such as biological fluids (e.g. blood and mucucs) may have a role in the sol-gel transition.

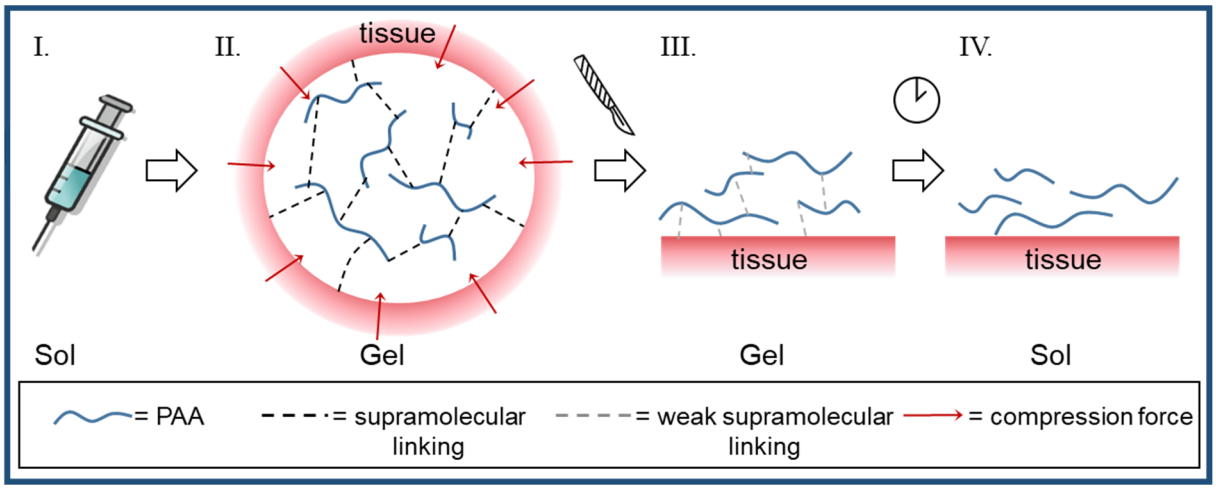

Figure 2.13: Proposed mechanism of sol-gel-sol transition of the PAA. The PAA solution in the sol state (I.) is injected in the gastric tissue where it forms a gel (II.) thanks to the presence of compression forces that promote the formation of supramolecular bonding between the tissue and the polymeric chains and inter chains. If the tissue is resected, the compression forces are removed, and the supramolecular bonding is weakened (III.) up to the disruption of the three-dimensional network and to the transition to the sol state (IV.).

Different examples of mechanical-responsive hydrogels have been reported in literature and they generally involve the formation of semi-flexible fibers, dynamic crosslinking, or the generation of nanostructures in hybrid hydrogels.[30] The effect of forces on hydrogels reported in literature can be summarized in four main categories: self-healing,[31,32] strain-stiffening,[33,34] shear-thinning[35,36] and mechano-chromic.[37,38] The behavior of the PAA system described herein does not fit in none of these categories and it might constitute a new family of stimuli-responsive materials with selectivity for certain tissues.

2.2.4. Comparison of the cytocompatibility of the linear PAA and the CL_PAA

PAA have been reported to display low cytotoxicity against many different cell lines[39,40] with improved results obtained increasing the polymer MW.[20] The cytotoxicity of the linear PAA under study and of the CL_PAA were evaluated and compared. The CL_PAA used for the ESD application has a concentration of organic molecules in water of 223 mg/mL while the linear PAA of 55 mg/mL. In order to compare the cytotoxicity of the two materials, both systems were prepared at the two concentrations in the cell culture medium as described in detail in the experimental section. The experiments were carried both on human epithelial healthy cells (MCF10 and HEK293) and on human cancer cells (Caco2). The Caco2 cell line was chosen because derived from the colon and consequently expected to better represent the gastrointestinal tissue where the material is injected. The cytotoxicity tests (Figure 2.14) showed for all the cell lines tested that the linear PAA at 55 mg/mL concentration has satisfactory cytocompatibility while, the CL_PAA is, as expected, cytotoxic even at the lowest concentration tested. The cytotoxic activity of the CL_PAA is attributed to the basic pH of the solution (~9) and to the presence of unreacted acrylic and amine terminal groups. The improved biocompatibility of the linear PAA solution described in this chapter compared with CL_PAA must therefore be attributed both to the reduction of the concentration and to the decrease of the content of reactive groups.

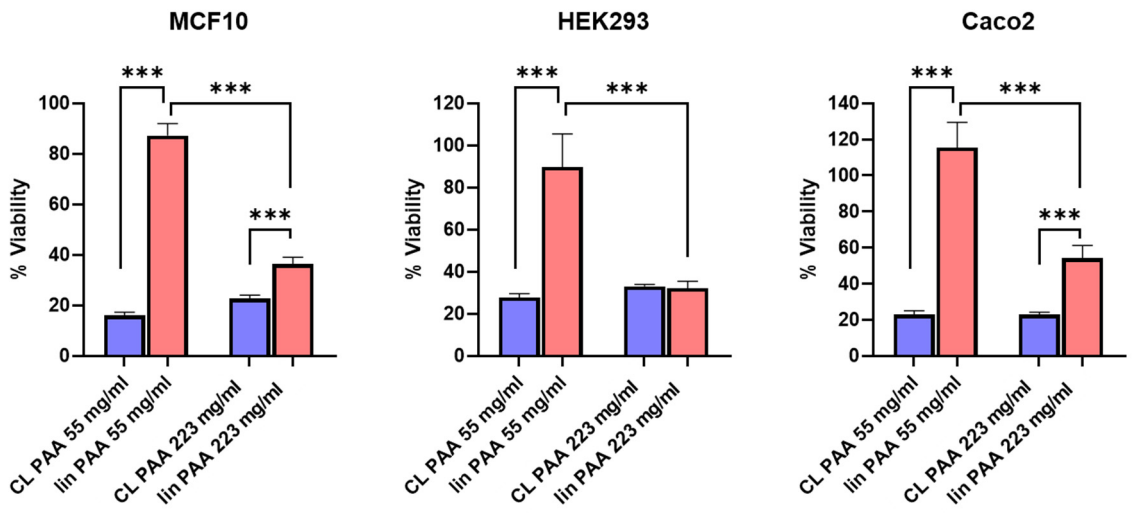

Figure 2.14: Cytotoxicity test of the CL_PAA (blue) and of the lin PAA (red) at 55 mg/mL and 223 mg/mL on MCF10, HEK293 and Caco2 cell lines. Data are normalized to control (viability =100%) and expressed as mean ± standard deviation (SD). One way ANOVA followed by Tukey´s post hoc test *** $p < 0.001$.

2.2.5. Surgical application of the linear PAA hydrogel: Endoscopic Submucosal Dissection

The experiments done in *ex vivo* have shown that the PAA solution is easily injectable and that after injection in the submucosal layer of the gastrointestinal tissue, it immediately forms a tissue adhesive soft hydrogel that gives a prolonged and high lifting of the tissue (Figure 2.9). The softness of the material (Figure 2.11) makes its resection easy. Moreover, the ability of the material to undergo the transition from the gel state to the sol state after resection (Figure 2.10) is a key characteristic since it ensures the clearance of the material from the body after the surgical procedure. All these characteristics, combined with the good cytocompatibility, make the PAA solution an ideal candidate for the endoscopic submucosal dissection and motivated us to test the material *in vivo* in a porcine model. We were particularly interested in evaluating the advantages of this solution compared with saline that is the solution currently used in clinics. The PAA-COOH was chosen for the *in vivo* experiments since its amphiphilic character is considered to impart higher biocompatibility to the system.[7] A total of 22 procedures, 10 with saline and 12 with the hydrogel under study were performed by the same experienced surgeon to evaluate the surgery time and the occurrence of perforation. Appropriate lesions of around 3 cm in diameter were set in the porcine colon and then the PAA solution or saline were injected in the submucosa. A first clear advantage that emerged from the use of linear PAA compared with CL_PAA is the ease of use. In fact, the CL_PAA previously reported[19] required the

presence of a chemist in the surgical room to prepare the material right before the injection and the feasibility of the procedure was hindered by the difficulty in the coordination of the material preparation and the medical set up of the animal. On the contrary, the linear PAA solutions described herein can be prepared in the chemistry laboratory and stored as a ready-to-use material. The linear PAA solutions can be stored at 4 °C for at least one month without evident variation in the performance. Before injection, methylene blue was added to the solutions for better visualization. The material was easily injectable with the endoscopic needle (23 G, 1.5 m long), it immediately formed a soft solid cushion after injection, and it stayed in position during the procedure time (Figure 2.15). The procedures done with saline required intra-procedural reinjection due to diffusion around the target site. The higher mucosal lifting obtained with the hydrogel improved the comfort of the surgeon. The procedure time using the hydrogel was on average almost half of the time required using the saline solution (Figure 2.16a) and the occurrence of perforation was reduced to less than one third using the hydrogel instead of the saline solution (Figure 2.16b).

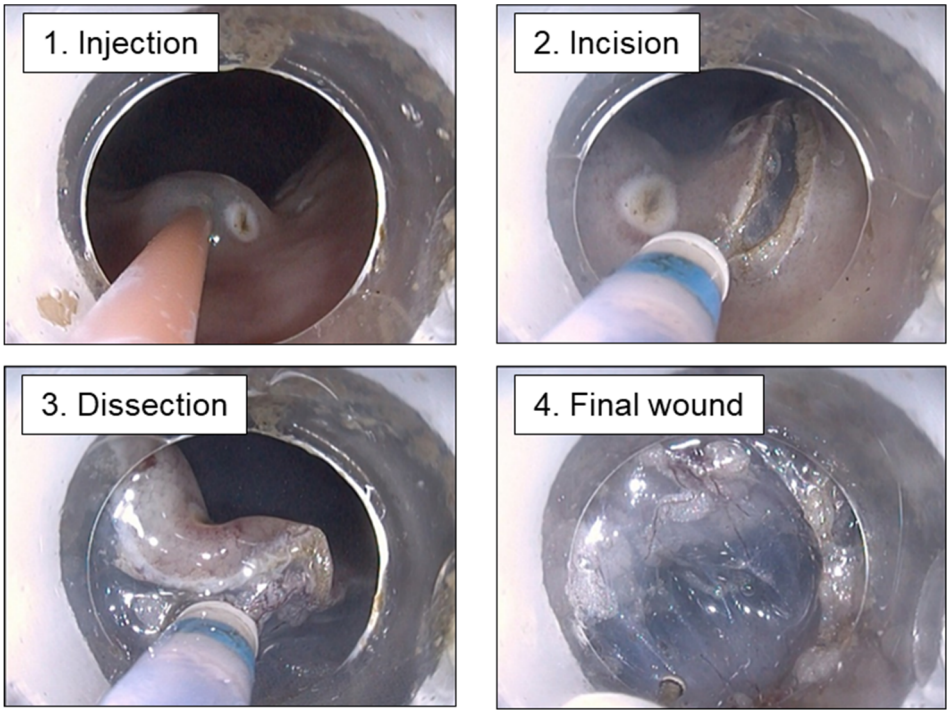

Figure 2.15: Endoscopic submucosal dissection in the colon. 1. Injection: the linear PAA solution is easily injected and it immediately forms a soft solid hydrogel. 2. Incision: the hydrogel reduces the risk of perforation. 3. Dissection: the hydrogel facilitate the in-block resection of the lesion. 4. Final wound. Methylene blue was added to the solution for better visualization.

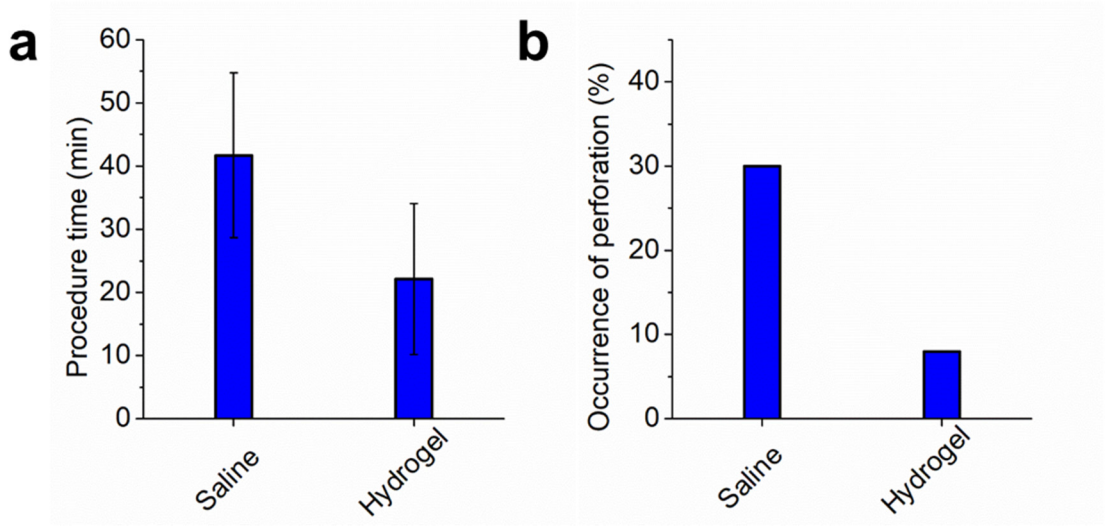

Figure 2.16: Advantages of the use of the PAA solution (hydrogel) compared with saline. a) Time of procedure reduction. b) Decrease in the occurrence of perforation.

2.3. Conclusions

In this chapter, the preparation of a linear PAA solution able to form, in the submucosal gastric layer, a tissue adhesive hydrogel was presented. The gelation process occurs instantaneously after injection and it is reversible with the sol state obtained after the resection of the tissue. The experiments done to investigate the mechanism of hydrogel formation suggested that the process is triggered by the compression force exerted by the tissue on the injected solution that promotes the formation of dynamic interactions, most likely of supramolecular nature (e.g. H-bonding, electrostatic), between the tissue and the polymer and among polymer chains. After the resection of the tissue, the mechanical forces on the hydrogel are removed, the physical interactions are weakened and the transition to the sol state is promoted by a gain in entropy. Understanding that the sol-gel transition is based on supramolecular interactions, opened the possibility to improve the CL_PAA system previously reported by our group[19] for the endoscopic submucosal dissection both from a biocompatibility point of view and from the easiness of applicability. In fact, the linear PAA solution undergoes a purification process that allows to remove unreacted monomers and to adjust the pH to neutrality before the injection, while the CL_PAA were injected at basic pH (~9) in the form of oligomers rich in reactive units. The cytotoxicity tests done on three different human cell lines confirmed the improved biocompatibility of the linear PAA system. Regarding the applicability, the PAA solution can be stored for weeks, while, on the contrary, the use of CL_PAA required the presence of a chemist in the surgical room to prepare the material right before the injection. The *in vivo*

experiments showed optimal performance of the linear PAA solution that facilitated significantly the procedure compared with saline halving the surgery time and reducing to one third the occurrence of perforation.

2.4. Acknowledgements

I would like to thank Dr. Laura Talamini for the cytocompatibility tests. The *in vivo* test were done at IRCARD (Institut de Recherche contre les Cancers de l'Appareil Digestif), Strasbourg and IHU-Institut de chirurgie guidée par l'image, Strasbourg in collaboration with Prof. Sun Gyo Lim.

2.5. Experimental Section

2.5.1. Chemicals and Materials

N,N'-Methylenbisacrylamide, 4-aminobutyrric acid, *N,N*-dimethylethylenediamine, ethanolamine, methylene blue and collagen from bovine Achilles tendon (Bornstein and Traub Type I) were purchased from Sigma Aldrich. The dialysis membrane (500-1000 D cut off, cellulose ester) were purchased from SpectrumLabs.

2.5.2. Linear PAA-COOH synthesis

In a round bottom flask containing 30 mL of distilled water are added 4.3 g of MBA (1 eq.), 2.87 g of GABA (1 eq.) and 630 mg of LiOH (1 eq.). The mixture is stirred at 40 °C and the evolution of the reaction is followed periodically by ^{1}H-NMR to evaluate its completion. The solution is then neutralized to pH 7 with 2.2 mL of HCl (37%) (1 eq.), dialyzed in a cellulose ester membrane (500-1000 D cut off) in water for three days and freeze dried.

2.5.3. Linear PAA-OH solution preparation

In a round bottom flask containing 30 mL of distilled water are added 4.3 g of MBA (1 eq.), 1.7 g of ethanolamine (1 eq.) and 224 mg of LiOH (0.3 eq.). The mixture is stirred at 40 °C and the evolution of the reaction followed periodically by ^{1}H-NMR to evaluate its completion. The solution is then neutralized to pH 7 with 0.7 mL of HCl (37%) (0.3 eq.), dialyzed in a cellulose ester membrane (500-1000 D cut off) in water for three days and freeze dried.

2.5.4. Linear PAA-N(CH_3)$_2$ solution preparation

In a round bottom flask containing 30 mL of distilled water are added 4.3 g of MBA (1 eq.) , 1.7 g of *N,N*-dimethylethilenediamine (1 eq.) and 224 mg of LiOH (0.3 eq.). The mixture is stirred at 40 °C and the evolution of the reaction followed periodically by ^{1}H-NMR to evaluate its completion. The solution is then neutralized to pH 7 with 0.7 mL of HCl (37%) (0.3 eq.), dialyzed in a cellulose ester membrane (500-1000 D cut off) in water for three days and freeze dried.

2.5.5. Molecular weight determination

The molecular weight of the polymers was calculated from the ^{1}H-NMR spectra comparing the integral of the methacrylate peaks (6.2 ppm and 5.7 ppm) with the integral of the peak at 4.5 ppm attributed to the protons bind to the carbon in α to the amide groups in the MBA unit (marked in red in Figure 2.3a). For the calculation it is assumed that each polymeric chain contains one unreacted terminal methacrylate group.

2.5.6. CL_PAA solution synthesis for ultrasound elastography measurement

The CL_PAA solution is prepared following the procedure previously reported.[19] Briefly, in a vial 2.6 mmol of MBA, 0.85 mmol of cystamine, and 1.3 mmol of *N,N*-dimethylethilenediamine are mixed in 3 mL of water. Once the solution was homogeneous it was injected in an explanted porcine stomach and used as comparison in the ultrasound elastography measurements.

2.5.7. Cell lines and culture conditions

MCF 10 (Human breast epithelial cells), HEK293 (human embryonic kidney epithelial cells) and Caco2 (human colon epithelial adenocarcinoma cells) cell lines were grown in DMEM-high glucose supplemented with 10% FBS, 1% L-glutamine (200 mM) and 100 U/mL penicillin, 0.1 mg/mL streptomycin. Cells were maintained at 37 °C in a 5% CO_2 humidified atmosphere.

2.5.8. Preparation of the CL_PAA and linear PAA solutions for cytotoxicity study

CL_PAA solution was prepared following the procedure previously reported with the difference that the amount of water used as solvent was halved.[19] Briefly, in a vial 2.6 mmol of MBA, 0.85 mmol of cystamine, and 1.3 mmol of *N,N*-dimethylethilenediamine are mixed in 1.5 mL of water and stirred at 60 °C for 1 hour. The total content of organic molecules in water is 446 mg/mL (CL_PAA 446 mg/ml). For the cytocompatibility experiments, the prepared

solution was diluted 1:1 with DMEM to obtain a final concentration of CL_PAA of 223 mg/mL, corresponding to the one employed for the *in vivo* experiments previously reported.[19] The CL_PAA 55 mg/mL solution was obtained from the dilution of the CL_PAA 446 mg/mL 1:4 with PBS followed by the dilution 1:2 with DMEM. Linear PAA was dissolved in a PBS/DMEM solution (1:1) to obtain the final concentrations of 55 mg/mL or 223 mg/mL. The control solution is PBS/DMEM solution (1:1).

2.5.9. Viability assay

The cytotoxicity tests of the materials under study were carried out on MCF 10, HEK293, Caco2 cell lines using the MTS cell viability assay (CellTiter96® Aqueous One solution Cell Proliferation Assay, Promega). The cells were seeded at 20000 cells/well into 96-well plate. 100 µL of the fresh prepared solutions (see paragraph 2.5.7) or of PBS/DMEM solution (1:1) (control) were added 24 h after the seeding. Cells were incubated with the treatment for 24 h. The CellTiter96® Aqueous reagent (20 µL/well) was then added and incubated for 2 h. At least, plates were placed in a microplate reader (TECAN) to measure the absorbance at 490 nm, and the cytotoxicity was express as % of cell viability compared to control.

2.5.10. Cytotoxicity statistical analyses

Statistical analyses were done using Prism Software (Prism 8.0; GraphPad Software, La Jolla, CA). One-way ANOVA was used for the data analyses followed by, in presence of a significant interaction among variables, Tukey's post-hoc test. For all analyses a p value < 0.001 was considered statistically significant.

2.5.11. Instruments

The rheological measurements were performed with a Thermofisher HAAKE Mars 40 rheometer equipped with a Peltier temperature module. The measuring geometry and the parameter used are specified in each experiment. SEM images were obtained from a FEI Quanta FEG 250 instrument (FEI corporate, Hillisboro, Oregon, USA) with an acceleration voltage of 10 kV. The hydrogel-tissue samples were lyophilized, attached to the SEM sample holder with carbon tape and subsequently sputtered with gold for 30 s at 60 mA. ^{1}H-NMR were recorded on a Brücker 400 MHz. The MALDI-TOF analysis was carried on a MALDI AUTOFLEX SPEED Bruker. The polymer solution was lyophilized, dissolved in methanol and drop casted on the MALDI sample holder in presence of sinapinic acid (SA) matrix. The data were recorded in positive mode with 70% laser power. Ultrasound elastography images were collected at

IRCARD (Institut de Recherche contre les Cancers de l'Appareil Digestif), Strasbourg and IHU-Institut de chirurgie guidée par l'image.

2.6. References

1. Genest, A., Portinha, D., Fleury, E. & Ganachaud, F. The aza-Michael reaction as an alternative strategy to generate advanced silicon-based (macro)molecules and materials. *Prog. Polym. Sci.* 72, 61–110 (2017).

2. Ferruti, P. Poly(amidoamine)s: Past, present, and perspectives. *J. Polym. Sci. Part Polym. Chem.* 51, 2319–2353 (2013).

3. Danusso, F. & Ferruti, P. Synthesis of tertiary amine polymers. *Polymer* 11, 88–113 (1970).

4. Lad, U. P., Kulkarni, M. A., Desai, U. V. & Wadgaonkar, P. P. Lithium tetrafluoroborate catalyzed highly efficient inter- and intramolecular aza-Michael addition with aromatic amines. *Comptes Rendus Chim.* 14, 1059–1064 (2011).

5. Sukanya, K. & Deka, D. C. Lithium hydroxide catalyzed Michael addition – An easy handling and non-toxic protocol. *Indian J. Chem.* 50B, 872–875 (2011).

6. Zintchenko, A., Aa, L. J. van der & Engbersen, J. F. J. Improved Synthesis Strategy of Poly(amidoamine)s for Biomedical Applications: Catalysis by "Green" Biocompatible Earth Alkaline Metal Salts. *Macromol. Rapid Commun.* 32, 321–325 (2011).

7. Ferruti, P., Bianchi, S., Ranucci, E., Chiellini, F. & Caruso, V. Novel Poly(amido-amine)-Based Hydrogels as Scaffolds for Tissue Engineering. *Macromol. Biosci.* 5, 613–622 (2005).

8. Karpushkin, E., Dušková-Smrčková, M., Šlouf, M. & Dušek, K. Rheology and porosity control of poly(2-hydroxyethyl methacrylate) hydrogels. *Polymer* 54, 661–672 (2013).

9. Fiorini, F., Prasetyanto, E. A., Taraballi, F., Pandolfi, L., Monroy, F., *et al.* Nanocomposite Hydrogels as Platform for Cells Growth, Proliferation, and Chemotaxis. *Small* 12, 4881–4893 (2016).

10. Giménez, M. E., Davrieux, C. F., Serra, E., Palermo, M., Houghton, E. J., *et al.* Application of a novel material in the inguinal region using a totally percutaneous approach in an animal model: a new potential technique? *Hernia* 23, 1175–1185 (2019).

11. Nair, D. P., Podgórski, M., Chatani, S., Gong, T., Xi, W., *et al.* The Thiol-Michael Addition Click Reaction: A Powerful and Widely Used Tool in Materials Chemistry. *Chem. Mater.* 26, 724–744 (2014).

12. Liu, Z. Q., Wei, Z., Zhu, X. L., Huang, G. Y., Xu, F., *et al.* Dextran-based hydrogel formed by thiol-Michael addition reaction for 3D cell encapsulation. *Colloids Surf. B Biointerfaces* 128, 140–148 (2015).

13. Pérez-Madrigal, M. M., Shaw, J. E., Arno, M. C., Hoyland, J. A., Richardson, S. M., *et al.* Robust alginate/hyaluronic acid thiol–yne click-hydrogel scaffolds with superior mechanical performance and stability for load-bearing soft tissue engineering. *Biomater. Sci.* 8, 405–412 (2020).

14. Tran, R. T., Palmer, M., Tang, S.-J., Abell, T. L. & Yang, J. Injectable Drug Eluting Elastomeric Polymer: A Novel Submucosal Injection Material. *Gastrointest. Endosc.* 75, 1092–1097 (2012).

15. Kantsevoy, S. V., Adler, D. G., Conway, J. D., Diehl, D. L., Farraye, F. A., *et al.* Endoscopic mucosal resection and endoscopic submucosal dissection. *Gastrointest. Endosc.* 68, 11–18 (2008).

16. Matsui, Y., Inomata, M., Izumi, K., Sonoda, K., Shiraishi, N., *et al.* Hyaluronic acid stimulates tumor-cell proliferation at wound sites. *Gastrointest. Endosc.* 60, 539–543 (2004).

17. Tang, B., Shan, J., Yuan, T., Xiao, Y., Liang, J., *et al.* Hydroxypropylcellulose enhanced high viscosity endoscopic mucosal dissection intraoperative chitosan thermosensitive hydrogel. *Carbohydr. Polym.* 209, 198–206 (2019).

18. Ishizuka, T., Ishihara, M., Aiko, S., Nogami, Y., Nakamura, S., *et al.* Experimental evaluation of photocrosslinkable chitosan hydrogel as injection solution for endoscopic resection. *Endoscopy* 41, 25–28 (2009).

19. Alonci, G., Fiorini, F., Riva, P., Monroy, F., López-Montero, I., *et al.* Injectable Hybrid Hydrogels, with Cell-Responsive Degradation, for Tumor Resection. *ACS Appl. Bio Mater.* 1, 1301–1310 (2018).

20. Ferruti, P., Manzoni, S., Richardson, S. C. W., Duncan, R., Pattrick, N. G., *et al.* Amphoteric Linear Poly(amido-amine)s as Endosomolytic Polymers: Correlation between Physicochemical and Biological Properties. *Macromolecules* 33, 7793–7800 (2000).

21. Cao, L., Li, Q., Zhang, C., Wu, H., Yao, L., *et al.* Safe and Efficient Colonic Endoscopic Submucosal Dissection Using an Injectable Hydrogel. *ACS Biomater. Sci. Eng.* 2, 393–402 (2016).

22. Ozturk, A., Grajo, J. R., Dhyani, M., Anthony, B. W. & Samir, A. E. Principles of Ultrasound elastography. *Abdom. Radiol. N. Y.* 43, 773–785 (2018).

23. Hassan, C. M. & Peppas, N. A. Structure and Morphology of Freeze/Thawed PVA Hydrogels. *Macromolecules* 33, 2472–2479 (2000).

24. Zhang, Y., Song, M., Diao, Y., Li, B., Shi, L., *et al.* Preparation and properties of polyacrylamide/polyvinyl alcohol physical double network hydrogel. *RSC Adv.* 6, 112468–112476 (2016).

25. Jiang, X., Xiang, N., Zhang, H., Sun, Y., Lin, Z., *et al.* Preparation and characterization of poly(vinyl alcohol)/sodium alginate hydrogel with high toughness and electric conductivity. *Carbohydr. Polym.* 186, 377–383 (2018).

26. Ferruti, P., Marchisio, M. A. & Barbucci, R. Synthesis, physico-chemical properties and biomedical applications of poly(amido- amine)s. *Polymer* 26, 1336–1348 (1985).

27. Barbucci, R., Casolaro, M., Barone, V., Ferruti, P. & Tramontini, M. Macroinorganics. 9. Enthalpies of protonation and copper(II) complex formation of some poly(amidoamines). *Macromolecules* 16, 1159–1164 (1983).

28. Barbucci, R. & Casolaro, M. Chelation of copper(ll) ion with some new poly(amido-amines). *Polymer* 23, 148–151 (1982).

29. Singha, N., Srivastava, A., Pramanik, B., Ahmed, S., Dowari, P., *et al.* Unusual confinement properties of a water insoluble small peptide hydrogel. *Chem. Sci.* 10, 5920–5928 (2019).

30. Chen, J., Peng, Q., Peng, X., Han, L., Wang, X., *et al.* Recent Advances in Mechano-Responsive Hydrogels for Biomedical Applications. *ACS Appl. Polym. Mater.* 2, 1092–1107 (2020).

31. Han, L., Lu, X., Wang, M., Gan, D., Deng, W., *et al.* A Mussel-Inspired Conductive, Self-Adhesive, and Self-Healable Tough Hydrogel as Cell Stimulators and Implantable Bioelectronics. *Small* 13, 1601916 (2017).

32. Li, L., Yan, B., Yang, J., Huang, W., Chen, L., *et al.* Injectable Self-Healing Hydrogel with Antimicrobial and Antifouling Properties. *ACS Appl. Mater. Interfaces* 9, 9221–9225 (2017).

33. Kouwer, P. H. J., Koepf, M., Le Sage, V. A. A., Jaspers, M., van Buul, A. M., *et al.* Responsive biomimetic networks from polyisocyanopeptide hydrogels. *Nature* 493, 651–655 (2013).

34. Shao, C., Meng, L., Wang, M., Cui, C., Wang, B., *et al.* Mimicking Dynamic Adhesiveness and Strain-Stiffening Behavior of Biological Tissues in Tough and Self-Healable Cellulose Nanocomposite Hydrogels. *ACS Appl. Mater. Interfaces* 11, 5885–5895 (2019).

35. Thakur, A., Jaiswal, M. K., Peak, C. W., Carrow, J. K., Gentry, J., *et al.* Injectable shear-thinning nanoengineered hydrogels for stem cell delivery. *Nanoscale* 8, 12362–12372 (2016).

36. Ding, X., Gao, J., Wang, Z., Awada, H. & Wang, Y. A shear-thinning hydrogel that extends in vivo bioactivity of FGF2. *Biomaterials* 111, 80–89 (2016).

37. Davis, D. A., Hamilton, A., Yang, J., Cremar, L. D., Van Gough, D., *et al.* Force-induced activation of covalent bonds in mechanoresponsive polymeric materials. *Nature* 459, 68–72 (2009).

38. Chen, J., Xu, L., Yang, M., Chen, X., Chen, X., *et al.* Highly Stretchable Photonic Crystal Hydrogels for a Sensitive Mechanochromic Sensor and Direct Ink Writing. *Chem. Mater.* 31, 8918–8926 (2019).

39. Richardson, S., Ferruti, P. & Duncan, R. Poly(amidoamine)s as Potential Endosomolytic Polymers: Evaluation In Vitro and Body Distribution in Normal and Tumour-Bearing Animals. *J. Drug Target.* 6, 391–404 (1999).

40. Ranucci, E., Spagnoli, G., Ferruti, P., Sgouras, D. & Duncan, R. Poly(amidoamine)s with potential as drug carriers: degradation and cellular toxicity. *J. Biomater. Sci. Polym. Ed.* 2, 303–315 (1991).

41. Lin, C., Blaauboer, C.-J., Timoneda, M. M., Lok, M. C., van Steenbergen, M., *et al.* Bioreducible poly(amido amine)s with oligoamine side chains: Synthesis, characterization, and structural effects on gene delivery. *J. Controlled Release* 126, 166–174 (2008).

Chapter 3: Injectable hydrogel for the treatment of gastrointestinal fistula

Abstract

Injectable hydrogels are of particular interest in the biomedical field because they can be implanted via minimal invasive procedures. Hyaluronic acid (HA) is a FDA approved polymer that can be functionalized in multiple positions to introduce cross-linking sites and the desired pending groups. HA solutions are characterized by shear-thinning behavior that makes them behave as a liquid during the injection and as a solid at rest. Herein we present the synthesis and characterization of a nanocomposite HA based injectable hydrogel cross-linked at physiological conditions. Mesoporous silica nanoparticles are introduced in the network opening the possibility of drug/biomolecules delivery. Such hydrogel possess a water content as high as 97% and it is characterized by a large-pore microarchitecture which is a fundamental requirement for cell proliferation. The kinetic profile of the hydrogel formation and the mechanical properties of the material are studied as a function of HA molecular weight and concentration. The optimal gel formulation was tested *in vivo* in a clinically-relevant porcine model, as a filling material to promote the healing of fistula. The hydrogel solution was easily injected and it stayed in position after injection without percolation. The animals treated with the hydrogel showed improved healing compared with the control group.

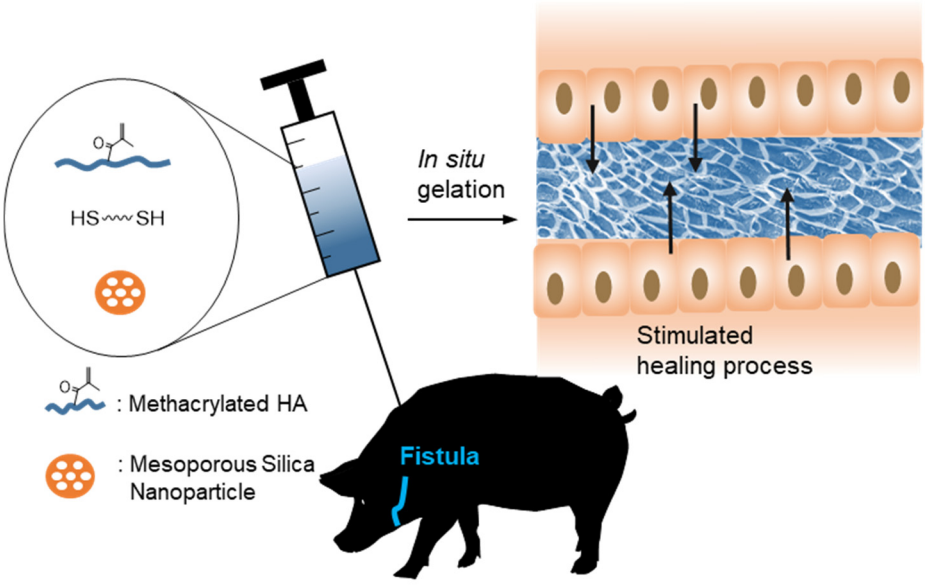

Figure 3.1: The precursors of the HA based hydrogel are easily injected through an endoscopic needle to fill the fistula where the gelation process takes place forming a matrix able to stimulate the healing process.

3.1. Introduction

3.1.1. Hyaluronic Acid based Hydrogels

Hyaluronic Acid (HA) is a glycosaminoglycan (Figure 3.2) present in the human body where its molecular weight (MW) ranges from disaccharide units up to 10^6-10^7 Da polymers.[1,2] An individual of 70 kg contains around 15 g of HA distributed for the half in the connective tissue, for a quarter in the skeleton and joints and the remaining in muscles and viscera.[1,2] High MW HA has the function of space filler in the extracellular matrix (ECM) where it lubricates and hydrates the tissue while having antiangiogenic, anti-inflammatory and immunosuppressive activity.[1,2] This latter derives in part from the ability of the space-filling polymers to interact with the cellular receptors in a polyvalent manner preventing receptor-receptor contact and inhibiting intracellular signaling pathways.[3]

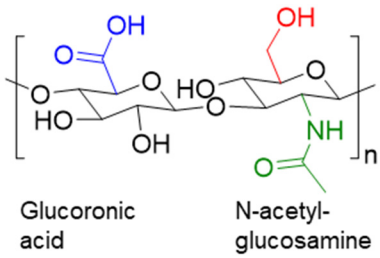

Figure 3.2: Chemical structure of HA highlighting the functional groups used to introduce modifications in the polymer: carboxylic group (blue), hydroxyl group (red) and N-acetyl group (green).

In mammals HA is degraded by the hyaluronidase enzymes with tetrasaccharides as predominant end-products. The half-time of HA depends on the tissue, in the circulation it is few minutes, in the skin it is a couple of days while in the cartilage it is extended to 1 or 2 weeks.[1] During the wound healing process, high MW HA is deposited and it binds to fibrinogen, opening up tissues spaces and allowing leukocytes to remove dead tissue, debris and bacteria.[1] The fragmentation of HA during the catabolic pathway generates products with size-specific biological activities. Fragments in the order of 20 kDa induce the synthesis of inflammatory cytokines, the angiogenesis and the endothelial recognition of the injury that stimulates fibroblast proliferation. Oligomers in the 6-20 kDa MW range interact with cell receptor in a monovalent manner allowing multi-fragment binding and stimulating cell signaling cascades that induce inflammatory gene expression in dendritic cells.[1,3] HA tetrasaccharides inhibit apoptosis and stimulate the expression of heat shock proteins.[1]

HA in solution forms an entangled 3D network where the number of entanglements depends on its MW and concentration. Low MW solutions (~100 kDa) can be considered as Newtonian fluids, while high MW solutions (~1000 kDa) present strong shear thinning behavior (i.e. their viscosity decreases under shear strain). The rheological response of the solution depends on the rate of reversible entanglement formation and disruption. In particular, the thinning of the solution is related to the predominance of the rate of disruption at higher shear.[4,5] The mechanical behavior of HA is furthermore influenced by the generation/break of H-bonds between the acetamido NH and the carboxylates on neighboring HA molecules promoted at high polymer concentration and responsible for the transition from a secondary to a tertiary structure (Figure 3.3a).[6,7]

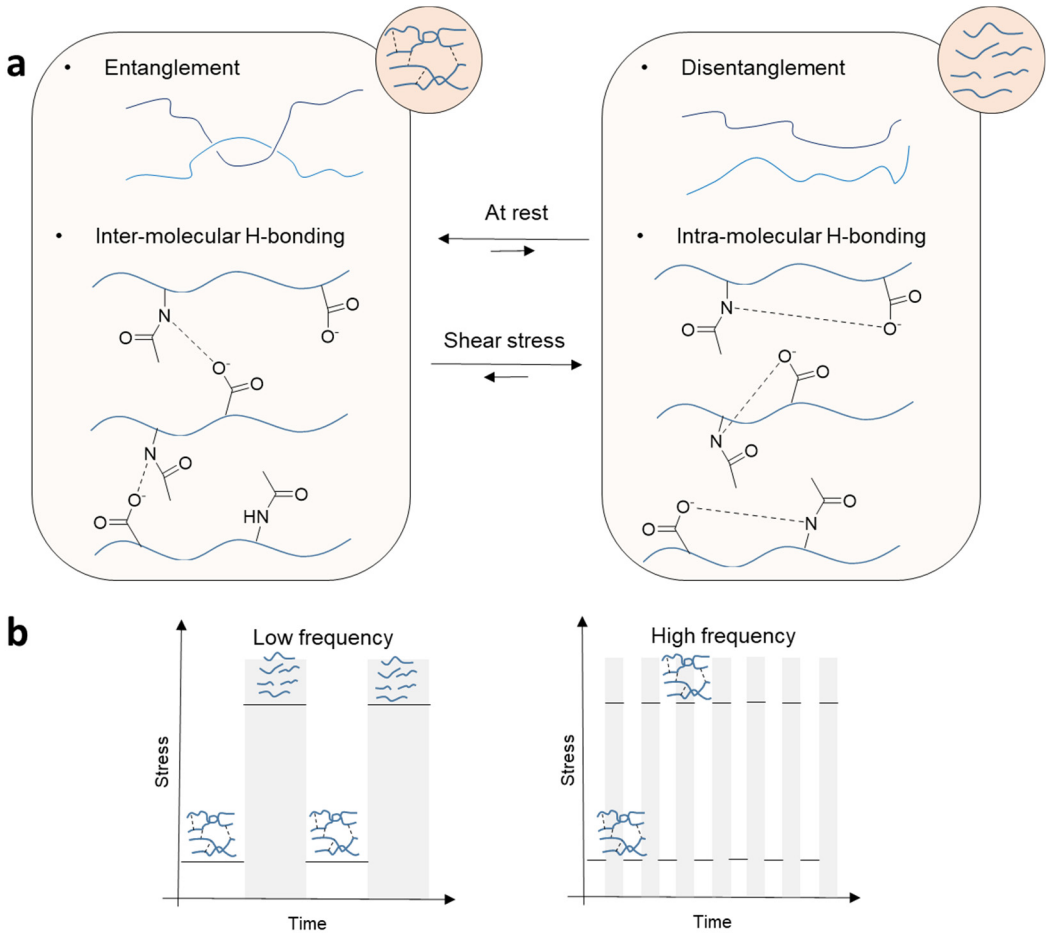

Figure 3.3: Dynamic equilibrium of formation/destruction of inter-molecular interactions in HA solutions. a) At rest inter-molecular interactions are predominant; entanglements are promoted by high MW while H-bonding is promoted by high HA concentration. When the system experiences a shear force, the inter-molecular interactions are destroyed and replaced by intra-molecular H-bonding. b) When the system is exposed to stress the equilibrium is shifted to the destruction of inter-molecular interactions: at low frequency the equilibrium is reached and the system behaves as a viscous liquid. On the contrary at high frequency the system is out of the equilibrium and it behaves as an elastic material.

The viscoelastic properties of HA solutions are correlated to the frequency of the oscillation: at low frequency, molecular chains can release stress by disentanglement, rearrange during the period of oscillation resulting into a viscous fluid; on the contrary, at higher frequency the molecules do not have the time to disentangle and the solution behaves as an elastic material (Figure 3.3b). The crossover frequency, defined as the frequency at which the solution starts to behave as an elastic material, decreases as the concentration and the MW of HA increase.[8] The frequency dependent behavior of HA is of particular importance in the synovial fluid where HA tertiary structure is at the edge of instability and it works as a lubricant at low frequency (e.g. during walking) and as an elastic "shock absorber" at higher frequencies (e.g. running).[4,6]

A large number of possible chemical modifications of HA has been reported in literature, the modification targets are the carboxylic group, the hydroxyl group or less frequently the N-acetyl group (Figure 3.2).[9,10] In the choice of the functionalization technique an important aspect to take into account is the effect of the reaction conditions on the HA hydrolysis.[11] Significant chain length damages have been reported in relation to the use of organic solvents[12], alkaline pH[13] or lyophilisation step.[14] The versatility of HA functionalization allows for the preparation of HA based hydrogels bearing covalently linked cell-adhesive biomolecules and with tunable features including mechanical properties and biodegradation.[15] Interesting biomedical applications of HA hydrogels include cartilage regeneration, cardiac tissue regeneration and cell delivery system.[7] Feng *et al.* developed a microgel made of functionalized gelatin and HA that can be injected in chondral defect and deliver mesenchymal stem cells without reducing their viability.[16] A composite hydrogel made of polydopamine nanoparticles covalently linked to a HA matrix has been tested for cardiac repair; the material was applied via injection and *in vivo* tests showed that it can improve the cardiac functions reducing the infarction size.[17] Sherman and co-workers developed HA hydrogels cross-linked via host guest interactions with application in drug delivery for glioblastoma treatment (Figure 3.4). They were able to tune the mechanical properties of the material to match the properties of the brain tissue ensuring continuous structural and shape remodeling; *ex vivo* experiments showed efficient implantation of the hydrogel and molecular release in the surrounding tissue.[18] The use of HA-based materials is already well stablished in the clinic as dermal fillers in soft tissue augmentation; examples of commercial products include: Juvéderm®, Elevess®, Prevelle Silk®, Revanesse® and Restylane®.[19]

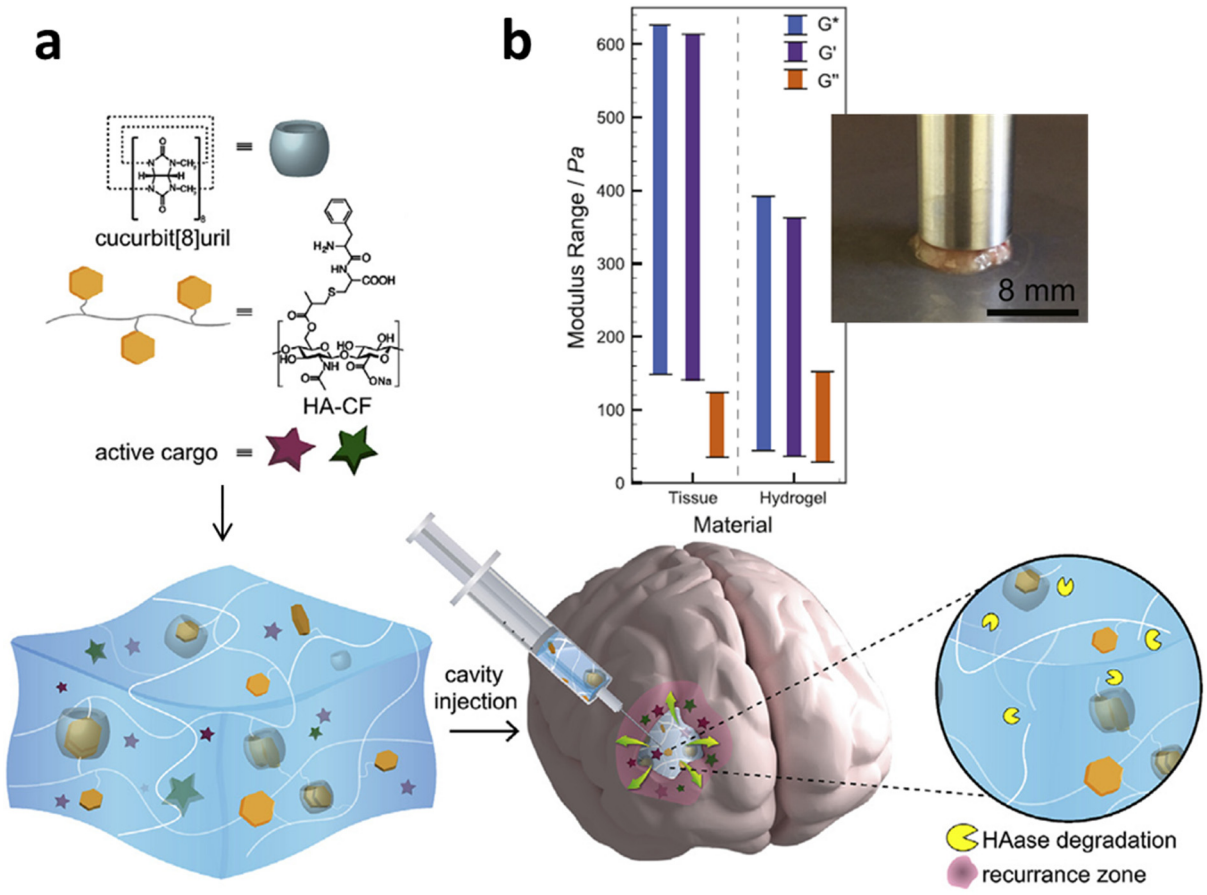

Figure 3.4: a) Use of an injectable HA hydrogel as a drug delivery system in a glioma model. b) Comparison between the mechanical properties of the material and of the brain tissue. Adapted with permission from *Biomaterials,* **2018**, 179, 199. Copyright 2018, Elsevier.

3.1.2. A clinical problem: the treatment of gastrointestinal fistulas

Gastrointestinal (GI) fistulas are defined as a pathological epithelialized communication between the GI track and the surrounding compartments and/or organs. They originate from GI inflammatory diseases, malignancies, infectious diseases, vascular failure, radiation exposure and, more frequently (up to 85% of cases), to complications related to surgical procedures.[20–22] Associated morbidity and mortality rates are substantial, especially in case of development of septic complications, nutritional deficits and concomitant comorbidities.[22–24] Medical treatment, including GI rest, parenteral nutrition and correction of electrolytes impairments is the current gold standard of treatment, with a success rate up to 70% after a mean time of 8 weeks.[22,23,25] Conversely, the surgical approach is reserved in case of no responsiveness to the conservative treatment. With the improvement of flexible endoscopic technology, new endoscopic devices and techniques have been introduced for the minimally invasive management of GI fistulas. Among them, the use of biological glues gradually increased in the

last two decades.[26–28] Their composition, made of fibrinogen and thrombin, stimulate the expression of growth factors that induce the healing of the anatomical defect, while the clot formed after injection is lately reabsorbed after a mean time of two weeks.[29,30] Although the success rate has been reported up to 86.6%[31] the use of biological glues is limited by the uniformity of the techniques described in literature, the need of multiple injections, the persistence of infection and the failure in the treatment of high-output fistulas. These weak points of such a promising technique may be mainly related to the physical properties of most biological sealants, namely, the lack of a sufficient viscosity, the absence of an antimicrobial activity and the low adhesiveness.

3.1.3. Aim of the project

The aim of the project is the development of an injectable HA based hydrogel with application in the treatment of fistula. The goal is to obtain a material that can be easily injected, behaves as a solid at rest and that undergoes the cross-linking process in a range of time compatible with the surgical procedure giving a hydrogel with suitable microarchitecture and mechanical properties to promote cell colonization. The effect of the introduction of Mesoporous Silica Nanoparticles on the mechanical properties of the system is studied. Finally the *in vivo* test to evaluate the ability of the material to promote fistula healing is presented.

3.2. Results and Discussion

3.2.1. Design, synthesis and characterization of Hyaluronic Acid derivatives

Shear thinning materials are of particular interest in the preparation of injectable hydrogels because they have the ability to flow in the needle when pressure is apply, while they behave as solid or very viscous liquid at steady state. The viscosity properties of HA solution are MW and concentration dependent. Low MW HA solution behave almost as Newtonian fluids at both the concentrations tested (1% and 10%) while high MW solutions are characterized by a strong shear-thinning behavior: the viscosity significantly drops when a shear stress is applied (Figure 3.5).

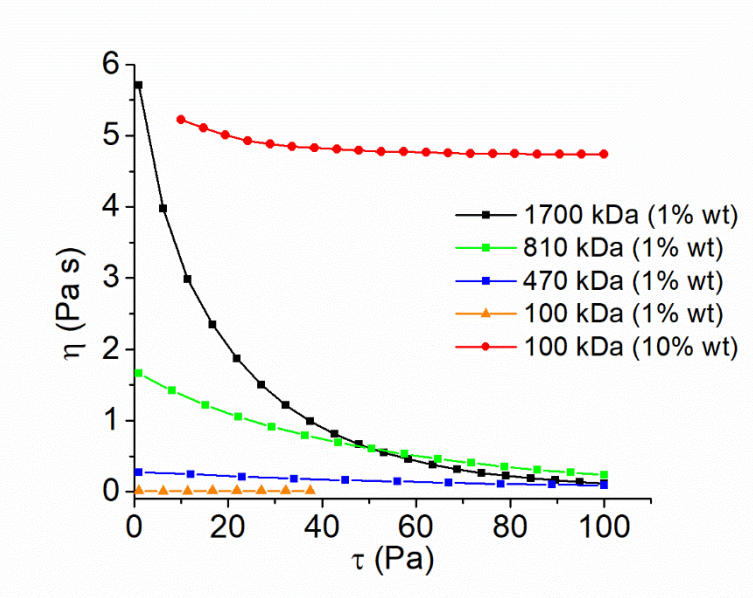

Figure 3.5: Viscosity as a function of the shear stress applied to HA solutions with different MW: 1700 kDa (black), 810 kDa (green), 470 kDa (blue), 100 kDa (orange) and 100 kDa, 10% (red). Rotational measurement done with coaxial cylinder geometry (25 mm) , *T*= 25 °C.

In the development of the hyaluronic acid based hydrogel, the process of cross-linking reaction selection involved the evaluation of the reaction kinetic, the possibility to occur at physiological conditions without the addition of an initiator and without generating any by-product. We selected the thiol-Michael addition as a suitable cross-linking reactions among the different possibility described in literature.[9] This reaction has already been widely exploited for the preparation of HA based hydrogels for biomedical applications.[32–34] The hydrogel is obtained from the reaction between dithiothreitol (DTT) and methacrylated hyaluronic acid (Me_HA) (Figure 3.6). Compared with the aza-Michael reaction exploited in the preparation of poly(amidoamine)s described in Chapter 2, the thiol-Michael reaction is generally faster and it can occur at physiological pH.[35]

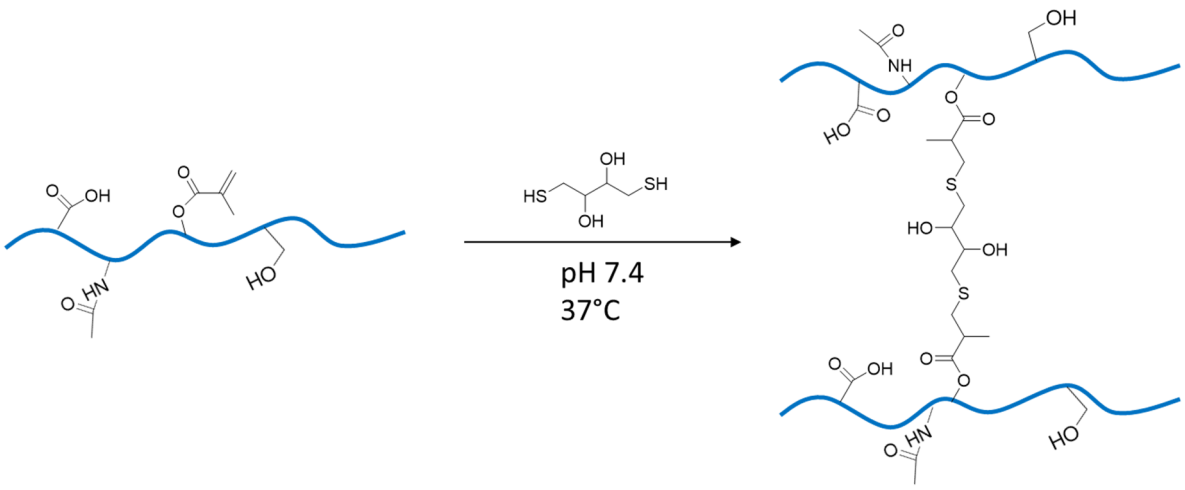

Figure 3.6: Synthesis of the HA derived hydrogel based on the thiol-Michael reaction.

The methacrylation of HA is done on the hydroxyl group while the carboxylic group is let unmodified to maintain the high hydrophilicity of the polymer and to eventually exploit it as reactive site for the introduction of desired pending groups. Methacrylated hyaluronic acid (Me_HA) was prepared according to Scheme 3.1 and as previously reported.[36,37] All the details are reported in the experimental section. The methacrylation was confirmed by ^{1}H-NMR, peaks at 5.54 ppm and 5.98 ppm (Figure 3.7a), and by ATR-FTIR, C=C peak at 1712 cm^{-1} (Figure 3.7b). The percentage of methacrylation, was calculated comparing the area of the ^{1}H-NMR peak at 5.98 ppm and the board peak in the range 3-4 ppm. The methacrylation degree for 5 kDa, 100 kDa, 470 kDa and 810 kDa HA was 100% while the methacrylation of 1700 kDa HA gave a batch to batch variability with degrees between 50% and 100%. The variability obtained from high MW HA may be ascribed to the high viscosity of the solution.

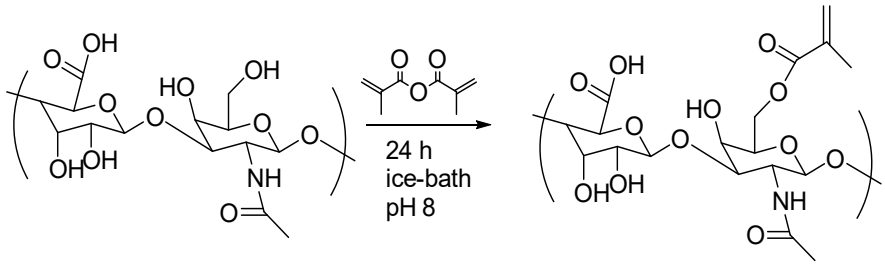

Scheme 3.1: Methacrylation of HA with methacrylic anhydride

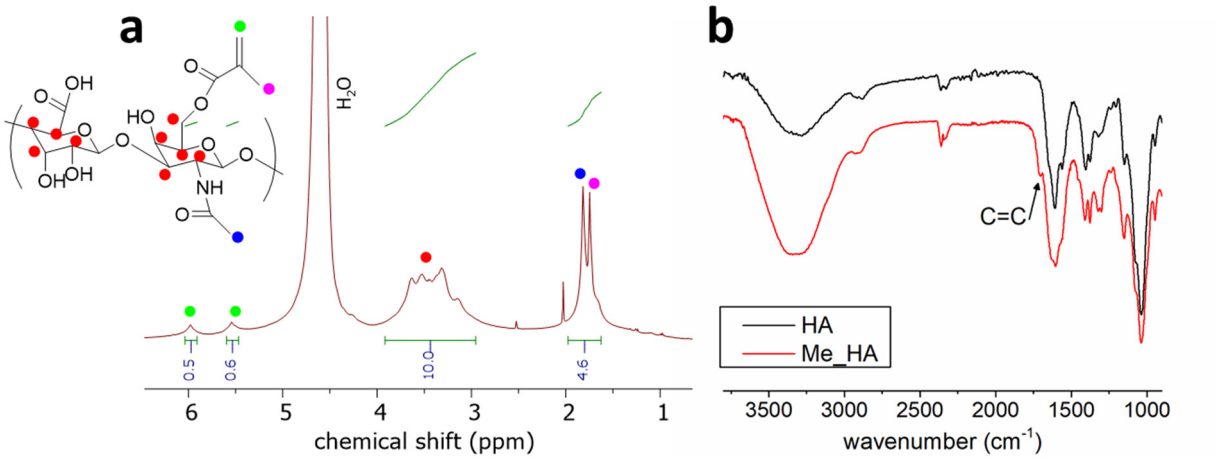

Figure 3.7: a) ^{1}H-NMR of methacrylated hyaluronic acid, 1700 kDa; b) FTIR-ATR of hyaluronic acid (black) and methacrylated hyaluronic acid (red).

The alkaline pH and the lyophilisation involved in the methacrylation of HA have been reported to reduce in some cases the polymer chain length.[11] Viscosity tests (Figure 3.8a) confirmed that the methacrylation process did not significantly reduced the length of HA chains and it did not alter the ability of the system to entangle and to form inter-molecular hydrogen bonding giving an elastic response at high frequency and low shear stress (Figure 3.8b, c).

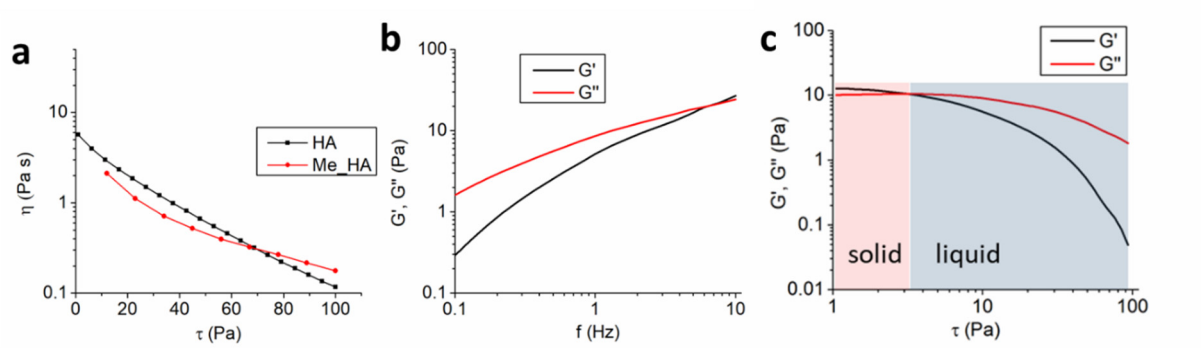

Figure 3.8: a) Shear thinning behavior of pristine HA (black) and Me_HA (red), 1700 kDa, 1% weight solutions in PBS. Plate to plate geometry (35 mm), *T*=25 °C; b) frequency sweep of Me_HA, elastic modulus (black) and loss modulus (red). Plate to plate geometry (35 mm), *T*=37 °C, τ= 10 Pa; c) Stress-sweep of Me_HA, elastic modulus (black) and loss modulus (red). Plate to plate geometry (35 mm), *T*= 37 °C, f= 1 Hz.

In order to facilitate the adhesion with the tissue, we have investigated the possibility to introduce in the Me_HA polymer the tissue-adhesive catechol groups.[38] The functionalization was done by coupling dopamine on the carboxylic group of the HA (Scheme 3.2) adapting the procedure reported in literature by Chen *et al.*[39] The white color of the product (Figure 3.9a)

indicates that the catechol groups did not undergo oxidation that would generate brownish melanin derivatives. The functionalization was confirmed by ^{1}H-NMR signal of the aromatic protons at 6.5-7 ppm (Figure 3.9b). The degree of catechol functionalization was calculated comparing the area of the ^{1}H-NMR aromatic peaks and the board peak in the range 3-4 ppm. 40% of the HA units bear a catechol group.

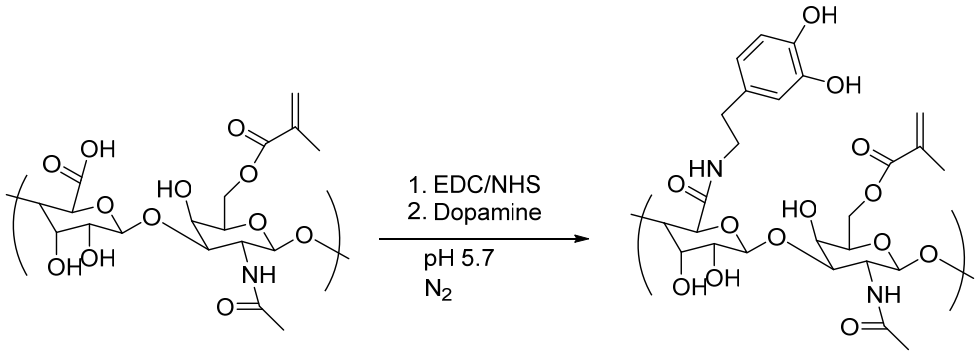

Scheme 3.2: Functionlization of methacrylated HA with dopamine.

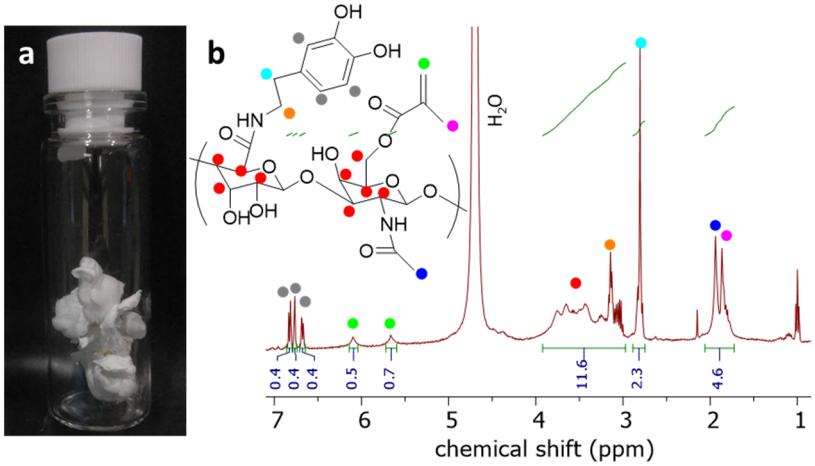

Figure 3.9: a) the obtained dopamine-functionalized HA; b) ^{1}H-NMR of dopamine functionalized HA.

3.2.2. Hydrogel preparation and characterization

The methacrylated HA is cross-linked with dithiothreitol to form a hydrogel by thiol-Michael reaction. PBS buffer (pH 7.4, 0.01 M) is used as a solvent to ensure the physiological pH of the system; the reaction occurs at 37 °C (Figure 3.6). Dithiothreitol is considered a nontoxic compound (LD oral, rat =400 mg/kg) and the eventual presence of unreacted molecules in the hydrogel is therefore expected not to affect the biocompatibility of the material. The hydrogels are obtained starting from a Me_HA solution in PBS in a typical concentration ranging from

1% to 3% by mass and adding the cross-linker molecule in stoichiometric amount (1:1 ratio between thiol and methacrylate groups). The obtained hydrogels are made of >96% of water and they are transparent (Figure 3.10a).

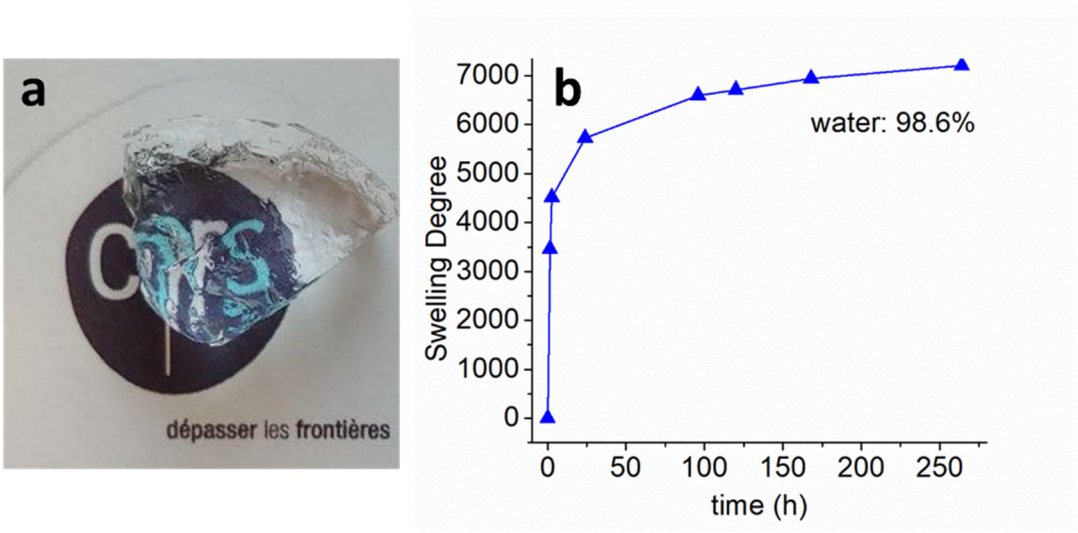

Figure 3.10: a) The obtained transparent HA based hydrogel; b) kinetic of swelling of a lyophilized hydrogel.

If the hydrogel is lyophilized and re-hydrated, it reaches the initial water content in 10 days with a swelling degree of 7300 (Figure 3.10b). The swelling degree (SD) and the water content are calculated through gravimetric measurements according to Equations 3.1 and 3.2 respectively where W_S is the weight of the swollen hydrogel and W_D is the weight of the dry material.

$$SD = \frac{W_S - W_D}{W_D} \qquad \textit{Eq. 3.1}$$

$$water\ content\ (\%) = \frac{W_S - W_D}{W_S} \cdot 100 \qquad \textit{Eq. 3.2}$$

The morphological characterization was done by cryo-SEM imaging. This technique, unlike traditional SEM that requires the lyophilisation of the sample, allows to observe the pristine structure of the material that conserves the entrapped water (Figure 3.11a, b, c, d). Figure 3.11a shows both the pristine frozen sample (bottom left) and the plane where the sample was fractured (top right). Figure 3.11b and 3.11d are enlargements of the fracture plane showing the ordered pore structure of the sample. The bottom of the pores is filled with ice so it is not possible from these images to estimate the deepness of the pores. The white dots in this pictures are probably ice crystals. Figure 3.11c shows an enlargement of the pristine frozen sample

where the pores are filled with ice. The microscopy analysis confirmed high porosity of the material with pores in the range 10-50 µm (Figure 3.11e). The presence of pores larger than cell size is of fundamental importance to allow cell proliferation in the material. In Figure 3.11f is reported a traditional SEM image on the same sample that underwent the lyophilisation process; it is evident that the pores are significantly larger than the ones present in the swollen sample.

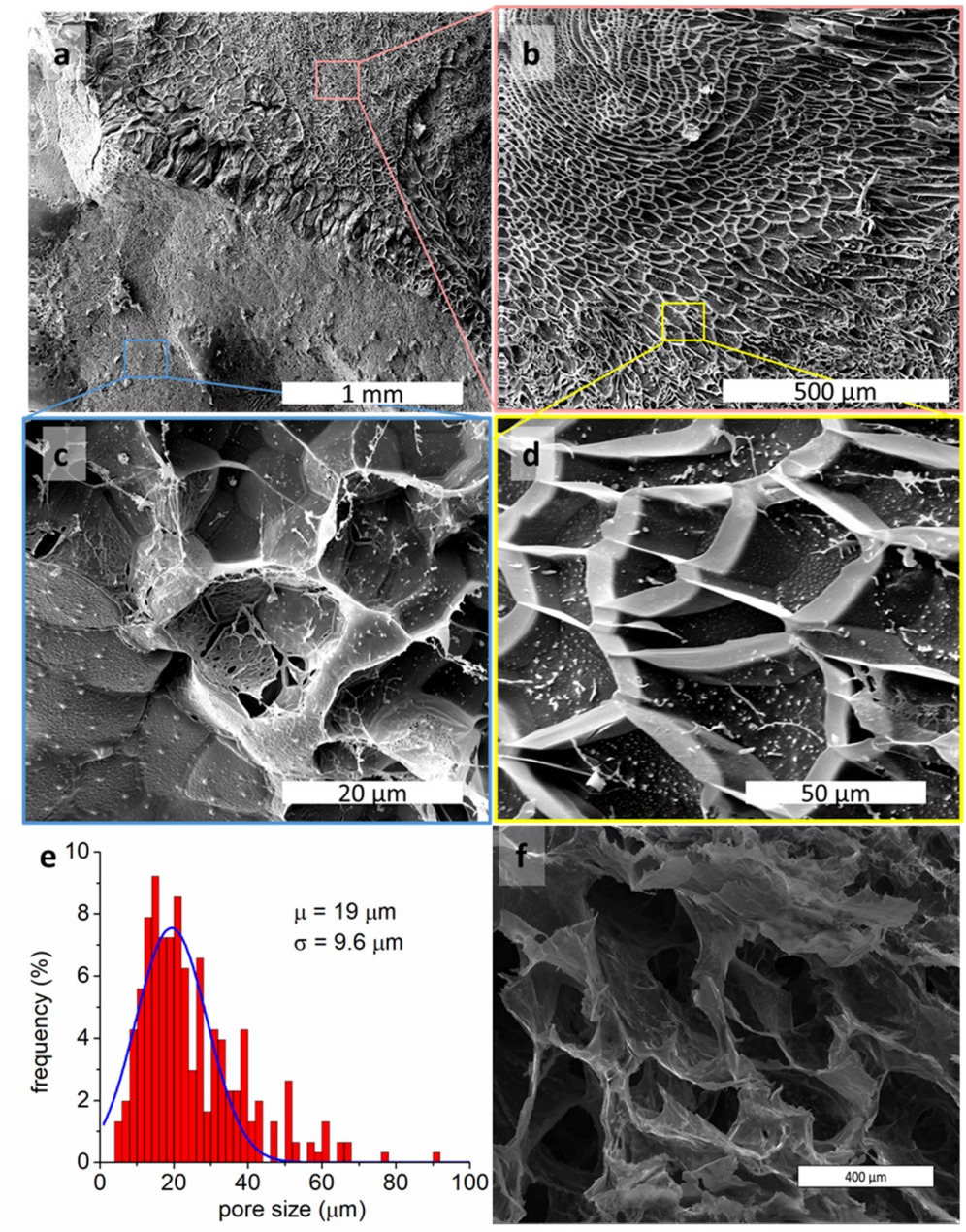

Figure 3.11: Cryo-SEM of the nanocomposite hydrogel. a) The top-right part is the fracture-plane made in the sample. The bottom-left part is the external surface of the sample. b) and d) Enlargement of the fracture-plane. c) Enlargement of the pristine outer surface of the sample. e) Pore size distribution obtained from the cryo-SEM images (software *ImageJ*). f) SEM of a lyophilized hydrogel (scale bar 400 µm).

3.2.2.1. Mechanical properties and kinetic of hydrogel formation

As discussed in Chapter 1, in the development of injectable hydrogels it is fundamental not only to consider the final mechanical properties of the material but all the kinetic profile of gel formation. Each cell type, requires a specific range of substrate stiffness to grow, the elastic modulus of the final hydrogel must therefore be within this range. Endothelial cells, involved in the cicatrisation processes for example proliferate in scaffolds with 1-2 kPa elastic modulus.[40] *In vivo* applications require furthermore the material to be deformable without getting damaged; the measure of the linear viscoelastic range (LVR) of the obtained hydrogels allows to quantify the ability of the material to sustain deformations. Literature about injectable hydrogels generally focuses on the final mechanical properties of the obtained material while the profile of hydrogel formation is neglected. Herein we present the effect of MW and concentration on the kinetic profile and on the final mechanical properties (elastic modulus, viscous modulus and linear viscoelastic range (LVR)) of HA hydrogels.

The kinetic curves obtained for HA hydrogels prepared using different MW of HA and concentration are reported in Figure 3.12.

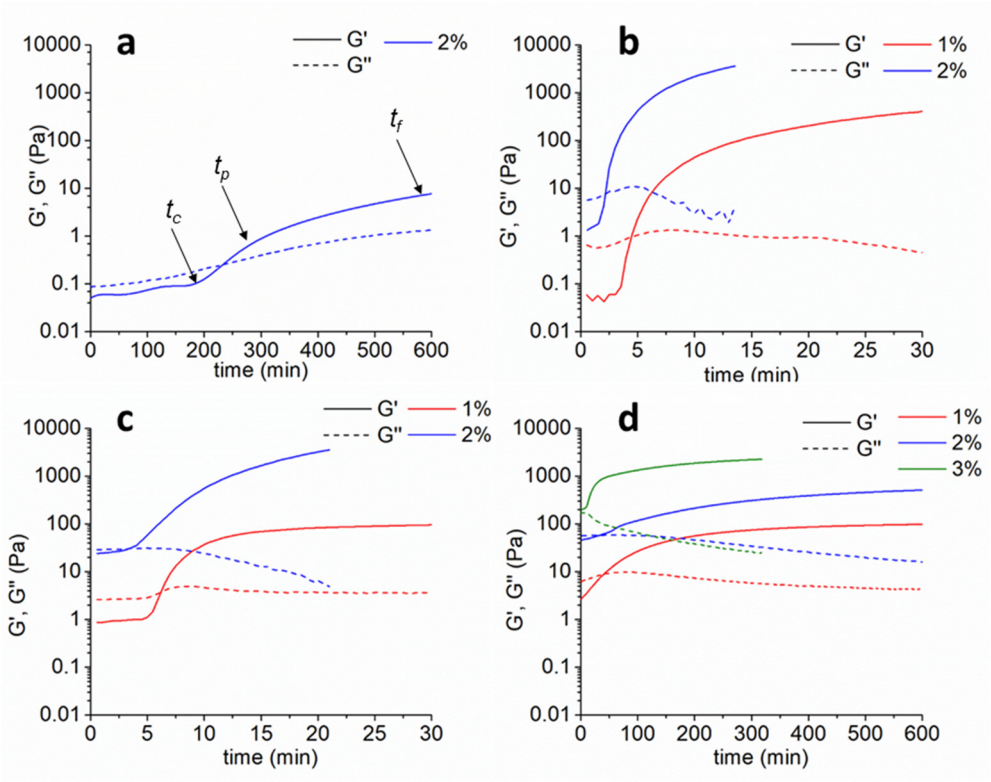

Figure 3.12: Kinetic of HA hydrogel formation. a) 100 kDa HA, b) 470 kDa HA, c) 810 kDa HA, d) 1700 kDa HA. Solid line: G', dashed line: G'', red line: concentration 1%, blue line: concentration 2%, green line: concentration 3%. 37 °C, γ= 5%, f= 1 Hz, coaxial cylinder geometry (10 mm).

The process of hydrogel formation can be divided in three phases: Phase 1: $t < t_c$, phase 2: $t_c < t < t_p$ and phase 3: $t_p < t < t_f$. Where t_c: critical time; t_p: percolation time; t_f: final time (Figure 3.12a). During phase 1, the nucleation of aggregates occurs and covalent bonds are formed at constant rate as described by the Smoluchowski model.[41] To verify if the materials under study follows the Smoluchowski model, the $log(t_c)$ of each sample was plotted as a function of $log(c)$ where c is the HA concentration. The data obtained for all the HA MW can be fitted with the equation $log(t_c) = -log(c) + k$ (Figure 3.13a) where k is a general constant confirming that the aggregate formation follows the Smoluchowski model.[41] In phase 2, all the samples show a sigmoidal growth of G', consistent with the Rouse-like percolation that describes the behavior of interconnected polymers.[41] After t_p, the hydrogel obtained from 810 kDa HA at 1% concentration reaches a plateau, indicating that the cross-linking process is completed. All the other samples, on the other side, show a G' increase between t_p and t_f indicating that a second mode of growth is occurring. This later might be ascribed to the coarsening of inter-polymer bonds.[41] The evolution of the viscous modulus, G'', over time gives information about the formation of clusters and their connection to the percolating cluster.[42] At time zero, G'' is an indicator of the viscosity of the starting system; at $t > t_0$, an increase of G'' shows either that clusters are being formed and the viscosity of the system is increasing or that ineffective structures (dangling ends and loops) are being formed. On the other side, a decrease in G'' suggests that the cluster are connecting to the network.[42] When G'' reaches a plateau, a balance of the above mentioned events is achieved. The hydrogel obtained from the 100 kDa HA (Figure 3.12a) presents a monotonic increase of G'' over the measurement time. This indicates that clusters are continuously being formed in the system. On the contrary, the hydrogel obtained from 1700 kDa HA at 3% concentration (Figure 3.12d), shows after an initial time in which G'' is constant, a monotonic decrease of the viscous modulus. This profile suggests that there are no free clusters in solution and that the system is more likely a single growing network. A third possible case is found in the hydrogel formed from the 470 kDa HA at 2% concentration (Figure 3.12b), in this sample, G'' at first increases showing the formation of clusters in solution then it decreases indicating that the clusters are getting incorporated in the network. The G'' maximum is at the percolation time. Figures 3.13b and 3.13c show the effect of MW and concentration on the time of hydrogel formation and on the final elastic modulus of the material.

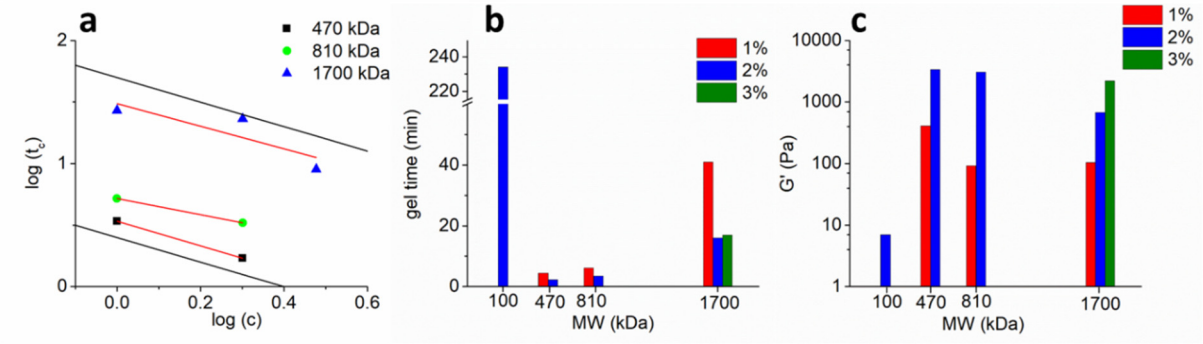

Figure 3.13: a) Scaling of $log(t_c)$ with $log(c)$ for 470 kDa (black), 810 kDa (green) and 1700 kDa (blue) gels. Red lines are the linear fitting of the experimental data. Black lines represent two functions $y= -x+k$ where k is a general constant; b) effect of MW and concentration on gel time; c) effect of MW and concentration on elastic modulus.

The effect of increasing the concentration is, in all the samples, a reduction in the time of gel formation and an increase on the G' modulus both of the starting solution and on the final hydrogel. The impact of the concentration on the gel time is particularly evident in the 1700 kDa samples when the concentration is increased from 1% to 2%. This is attributed to the effect of concentration on the reduction of ineffective intra-molecular CL reactions that are abundant in high MW polymers. The effect of the MW on the G' modulus and on the time of gel, on the contrary, is not trivial as reported also by Tabatabai *et al*. for a silk-based material.[41] The gel time is significantly decreased passing from 100 kDa HA to 470 kDa HA or 810 kDa HA but it rises again if the MW is increased to 1700 kDa. G' increases significantly passing from 100 kDa HA to 470 kDa HA or 810 kDa HA and it decreases again if the MW is increased to 1700 kDa. The polymer MW determines the viscosity of the pre-gel solution and the number of effective cross-linking reactions required to the formation of a three dimensional network and a solid hydrogel. Low MW polymers generate lower viscosity solutions in which the molecular mobility is higher and the cross-linking reactions are faster. On the other side, low MW polymers require higher number of CL reactions to obtain a hydrogel while for high MW polymers a smaller number of CL reactions are enough for the formation of the percolating cluster. It is important to underline that the cross-linking reactions can be either effective (e.g. the cross-linking occurs between two different polymeric molecules) or ineffective (intramolecular reactions that bring to the formation of loops) and only the formers contribute to the formation of the 3D network. The hydrogel formation with 100 kDa HA required a very high number of CL reactions, therefore the gelation process is slow and the final material is soft. 1700 kDa HA solutions are characterized by high viscosity that slowdown the reaction

process. We hypothesize that the reduction in G' modulus passing from 470 kDa to 1700 kDa HA is due to the higher probability in high MW polymer to have intramolecular ineffective CL reactions.

In Figure 3.14 are reported the measurement of the LVR of the obtained hydrogels. Both G' and G'' moduli were normalized to better appreciate the differences between the different samples. Figure 3.15 shows the effect of MW and concentration on the LVR. The LVR of all the materials tested mirrors the sample stiffness. The wide LVR of 1700 kDa HA hydrogels compared to 470 and 810 kDa, is ascribed to the lower CL degree and to the preservation of the intermolecular mobility. The polymer concentration reduced the LVR in all the samples.

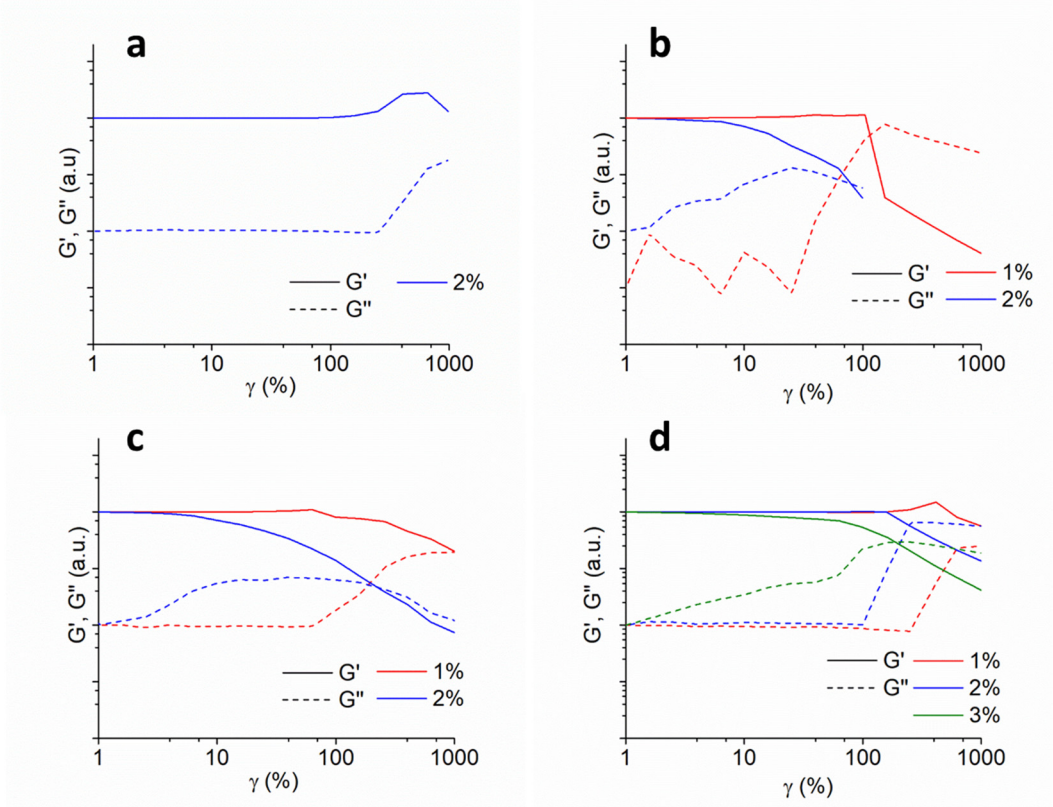

Figure 3.14: Linear Viscoelastic Range of HA hydrogels. a)100 kDa HA, b) 470 kDa HA, c) 810 kDa HA, d) 1700 kDa HA. Solid line: G', dashed line: G'', red line: concentration 1%, blue line: concentration 2%, green line: concentration 3%. 37 °C, *f*= 1 Hz, coaxial cylinder geometry (10 mm).

An injectable hydrogel for surgical application must have low viscosity during injection, high viscosity after injection, a kinetic of gel formation between 15 and 40 min and final mechanical properties that match with the substrate stiffness required by cells proliferations. 1700 kDa HA pre-gel solution at 3% concentration is characterized by strong shear thinning character that

make it behave as a low viscous fluid during injection and as a solid at rest (Figure 3.8); the hydrogel is formed in 16 min, the obtained hydrogel has a G' modulus of 2.2 kPa with a wide LVR. This hydrogel was therefore selected as the optimal candidate for the treatment of gastrointestinal fistula.

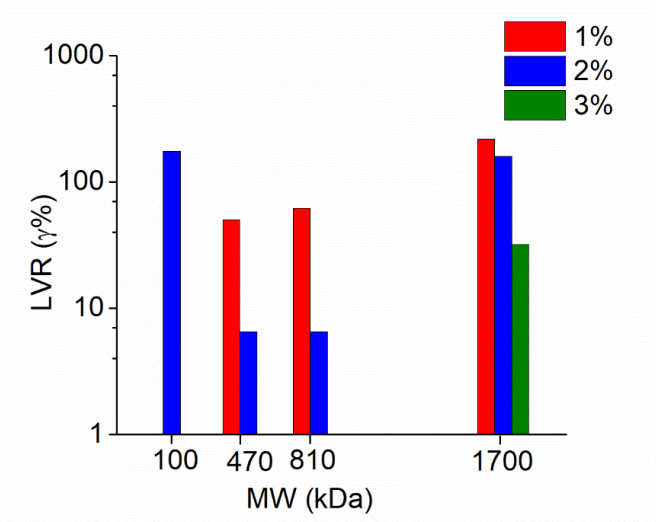

Figure 3.15: Effect of MW and concentration on the LVR.

3.2.3. The nanocomposite hydrogel: incorporation of mesoporous silica nanoparticles in the system

The introduction of nanofillers in the hydrogel network can impart to the material new properties as discussed in Chapter 1. One of the most common function of particles is the tuning of the mechanical properties of the composite material that can show changes both in stiffness and in stretch-ability.[43] The composition, the size and the shape of the nanoparticles define how the filler interact with the polymeric network and therefore the emerging properties of the hybrid system. Physical cross-linking are at the base of the G' increase in the nanoclay-keratin/Pluronic/chitosan system described by Eslahi *et al.*[44] The shape of the graphene oxide sheets, is responsible for the high elongation at break of the polyacrylamide network reported by Yu and co-workers.[45] Liu *et al.* reported that the particle size can play a significant role as well; they investigated the effect of latex particles in the size range 190-340 nm and demonstrated that smaller particles give a more effective entanglement of the polymeric chain improving the mechanical properties of the hydrogel.[46] The concentration of the filler is also a key parameter since it determines the balance between the competitive filler-polymer and polymer-polymer interactions that can result either in the stiffening or in the softening of the composite material.[47] The effect of amino functionalized silica NP on the properties of a

collagen/chitosan/hyaluronic acid hydrogel have been investigated by Nowakowska and co-workers;[48] the authors observed that at low particle concentration the elastic modulus remains unchanged while at higher filler concentration a decrees of the G' modulus is observed. This behavior is attributed to the fact that higher particle concentration brings to the formation of silica aggregates that perturb the polymeric network. Beside to tune the mechanical properties of the hydrogel, the introduction of porous nanoparticles can be exploited for the incorporation and the delivery of biomolecules. We have investigated the possibility to introduce in the system mesoporous silica nanoparticles (MSN). MSN are characterized by an extraordinary high surface area to mass ratio and have been used for the controlled delivery of cargos ranging from small molecules up to proteins.[49–51] The particles protect the payload from the surrounding environment and control its release improving the pharmacokinetics. Our group has shown that the incorporation of MSN in a poly(amidoamine) hydrogel can be exploited for the release of a chemokine able to direct the proliferation of mesenchymal stem cells in the material.[52] In the following paragraph, the synthesis and functionalization of MSN on the outer surface with thiol and/or amino groups is presented and the the possibility to link them to the polymeric network either through the formation of covalent bonds or though electrostatic interactions is investigated (Figure 3.16).

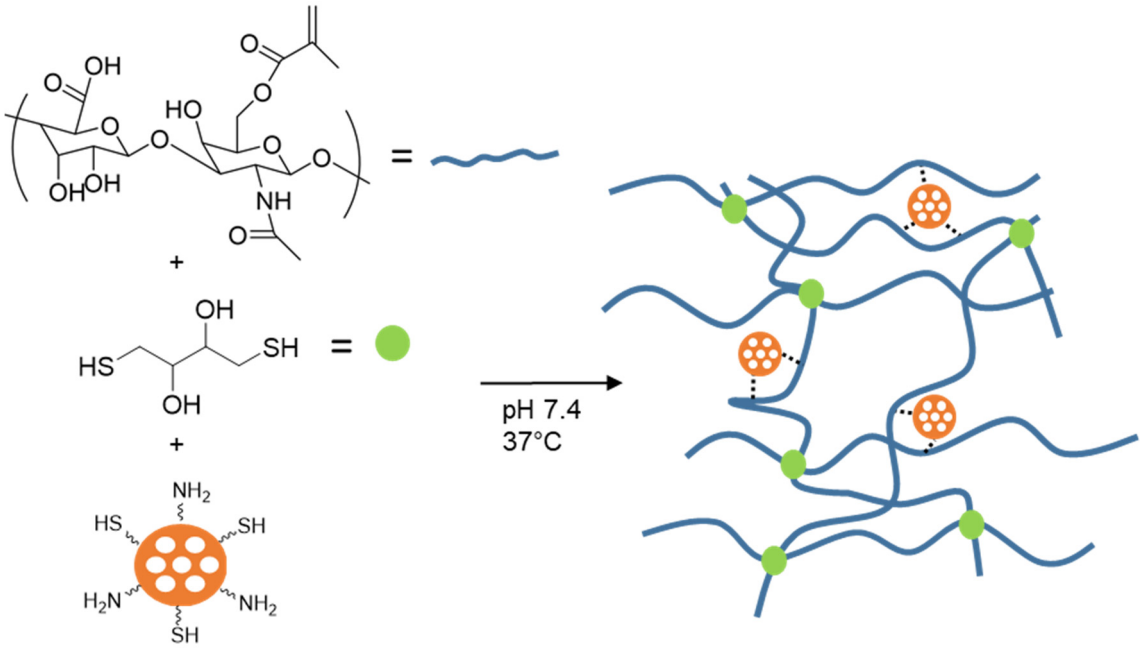

Figure 3.16: Synthesis of the nanocomposite hydrogel.

3.2.3.1. Mesoporous Silica Nanoparticles: synthesis and functionalization

50 nm spherical Mesoporous Silica Nanoparticles (MSN) were prepared following a modified Stöber process (Figure 3.17a).[53] Cetyltrimethylammonium bromide (CTAB) is used as surfactant to generate positive charged micelles that impart the porosity to the particles. The silica source is tetraethoxysilane (TEOS) that in water forms oil droplets that are adsorbed on the surface of surfactant micelles. The hydrolysis of TEOS occurs at the water-oil interface and it generates silica-surfactant micelles that, undergoing a condensation process, build the MSN. Triethanolamine (TEA) is used as base to promote the hydrolysis and the formation of nuclei and to prevent particles growth. Higher concentration of TEA generates smaller MSN. The particle growth is also promoted by high temperature and slow stirring rate.[53]

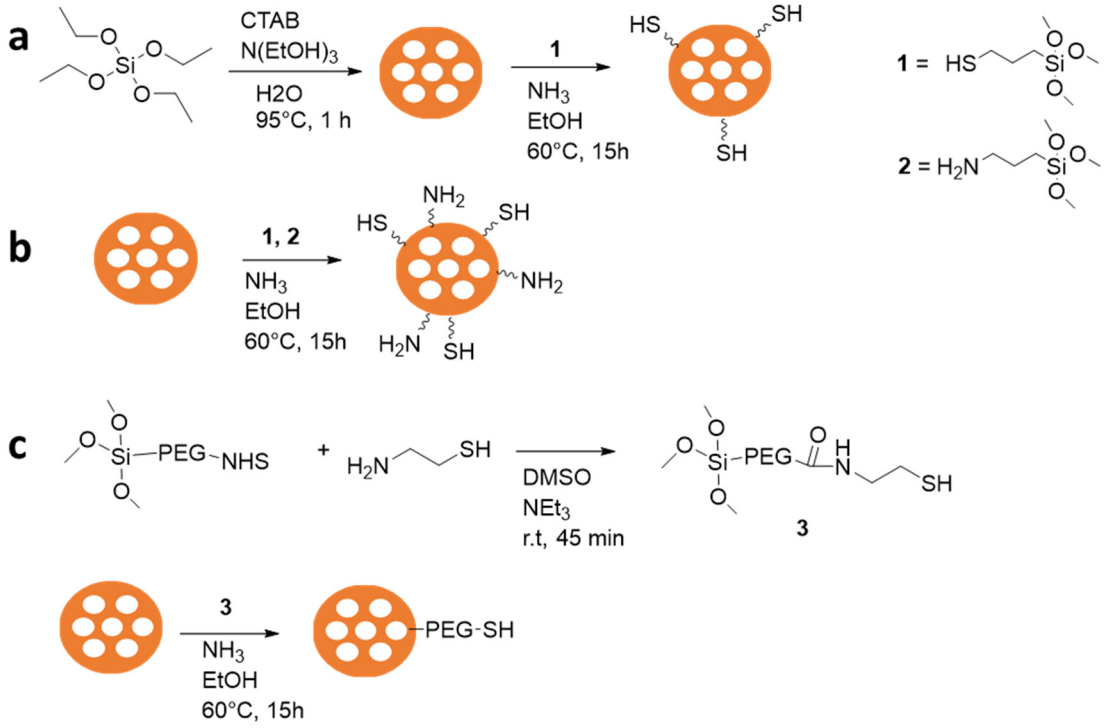

Figure 3.17: a) MSN synthesis and thiol functionalization b) MSN co-functionalization with thiol and amino groups; c) MSN functionalization with thiol-terminated PEG.

The obtained particles are spherical and uniform in size (Figure 3.18a, b) with an average diameter of 45±10 nm. TEM imaging showed the presence of pores in the MSN that are partially ordered and with wormlike structure in accordance with literature (Figure 3.18c).[53] The pore structure was further characterized by physisorption measurement (Figure 3.18d). The N_2 adsorption/desorption profile is a type IV isotherm with H1 hysteresis loop (Figure 3.18d) typical for cylindrical mesopores open at both ends.[54] The MSN surface area is 506.6 ± 1.5 m^2g^-

[1] with total pore volume of 0.5 cm^3g^{-1} and average pore size of 3.8 nm. The presence of a second pore size peak at 6 nm could indicate that the pores are slightly cone-shaped; the pore volume for pores bigger than 10 nm is attributed to the intra-particle space. The ordered structure of the MSN was characterized by small-angle x-ray scattering (SAXS) (Figure 3.18f). The pattern presents a single broad signal at the scatting value of q = 0.9 nm^{-1} attributed to the (1 0 0) Bragg peak. The absence of the additional (1 1 0) and (2 0 0) typical Bragg peaks of hexagonally arranged pores indicates the lack of long-range order.[55]

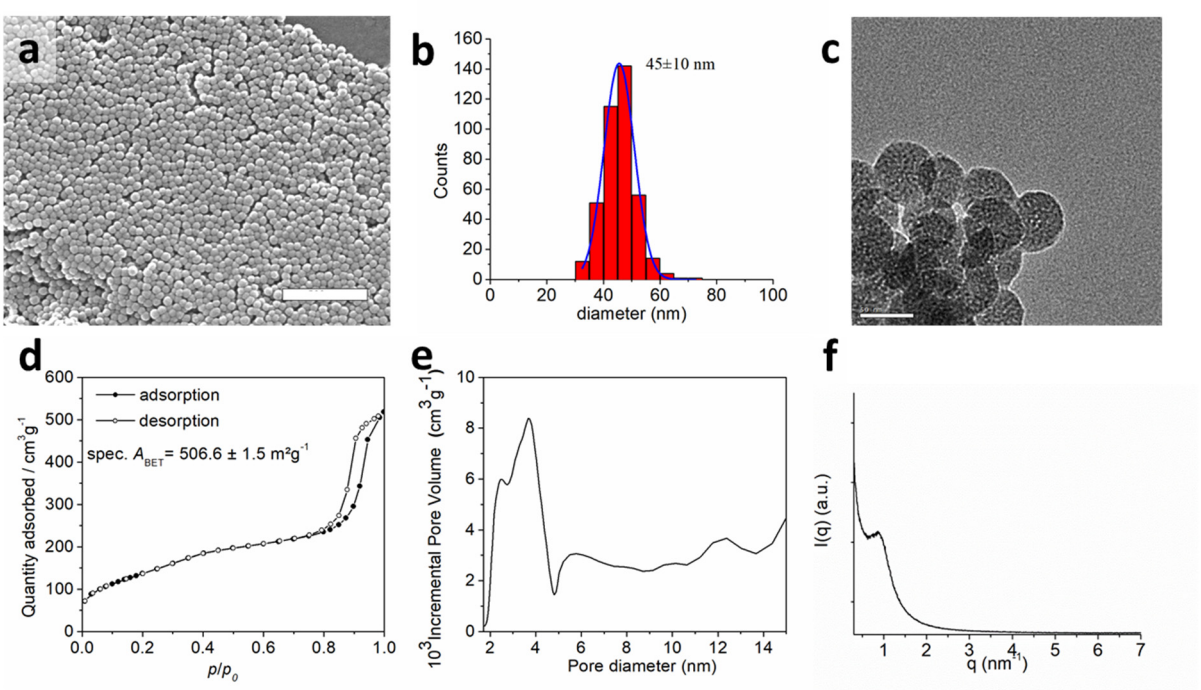

Figure 3.18: a) SEM of the MSN, scale bar: 500 nm; b) MSN size distribution obtained from the diameter measure of particles from SEM images, more than 300 particles were measured to obtain the statistic size distribution. The blue line is the Gaussian fitting of the data. The size measurement was done using the software *ImageJ*. c) TEM of the MSN, scale bar: 50 nm; d) isothermal nitrogen adsorption (black dots) and desorption (empty dots); e) pore size distribution calculated by density functional theory method on the adsorption branch. f) SAXS pattern.

In order to evaluate the interaction between MSN and the polymeric network and its effect on the mechanical properties of the nanocomposite hydrogel, three different surface functionalization have been investigated: short alkyl chain terminated with a thiol (MSN-SH) (Figure 3.17a), co-functionalization with thiols and amines (MSN-NH_2-SH) (Figure 3.17b) and use of a PEG chain as spacer between the MSN and the thiol group (MSN-PEG-SH) (Figure 3.17c). The grafting of amines increases the surface charge of the particles and it is expected to

favor the electrostatic interaction between MSN and the negatively charged HA. The use of a PEG spacer is thought to give more mobility to the thiol groups and to promote the thiol-Michael reaction with the methacrylated HA. The thiol-terminated PEG silane was obtained by the reaction of *N*-hydroxysuccinimide-terminated PEG silane with 2-Aminoethanethiol hydrochloride (Figure 3.17c). The thiol-functionalization of MSN-SH was confirmed both by XPS (Figure 3.19a, b, c) and by TGA (Figure 3.19d). The mass loss attributed to the organic functionalization is 8.5% corresponding to the presence of $1.1 \cdot 10^{-3}$ mmol of thiol groups for mg of particles and to an atomic ratio Si:S of 95:5 (the ratio obtained by XPS is 97:3). The mass loss observed in MSN-NH_2-SH is the sum of amino and thiol functionalization; assuming that the ratio between the functional groups corresponds to the stoichiometric ratio used in the preparation procedure (SH:NH_2 = 1:9), the content of thiol groups is $2.9 \cdot 10^{-4}$ mmol for mg of particles and the content of amino groups is $2.6 \cdot 10^{-3}$ mmol for mg of particles. MSN-PEG-SH lost 20.2% by mass during TGA corresponding to the presence of $4.0 \cdot 10^{-5}$ mmol of thiol groups for mg of particles. The ζ-potential measurements clearly showed the effect of the introduction of amino groups on the increase of the surface charge of the particles (Figure 3.19e). The introduction of the PEG spacer between the MSN and the thiol groups significantly increased the hydrodynamic diameter of the particles as shown by the DLS analysis (Figure 3.19f).

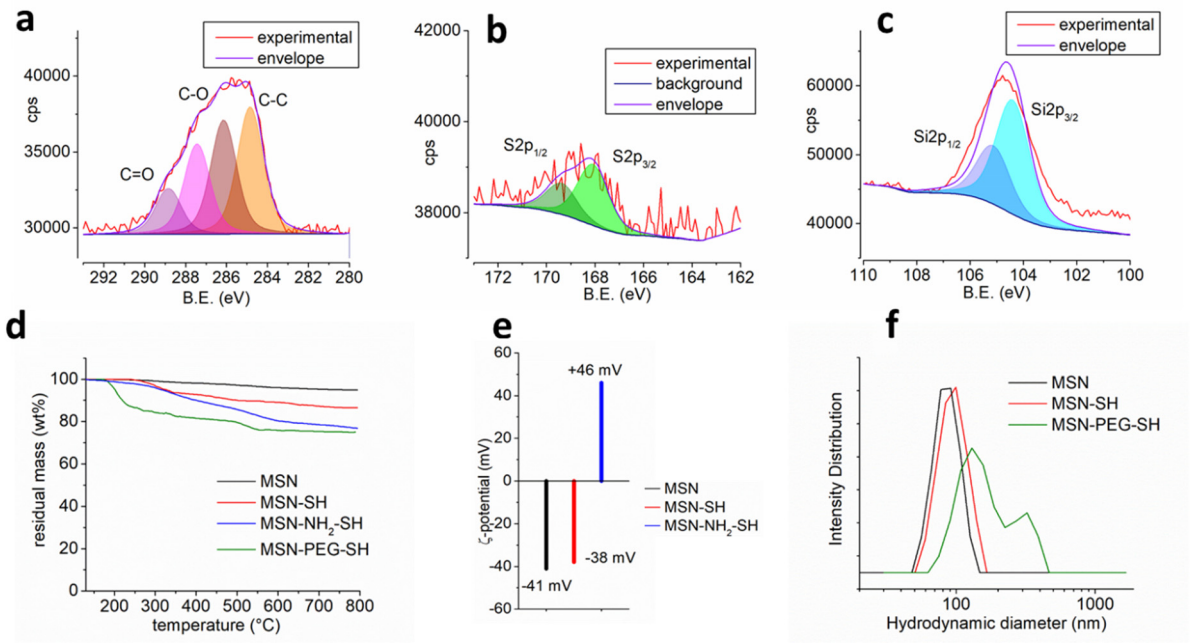

Figure 3.19: a) High resolution C 1s XPS spectrum of thio-functionalized MSN; b) high resolution S 2p XPS spectrum of thio-functionalized MSN; c) high resolution Si 2p XPS spectrum of thio-functionalized MSN. d) TGA, e) ζ-potential and f) DLS of the pristine MSN (black), thio-functionalized MSN (red), co-functionalized amino and thiol MSN (blue) and MSN functionalized with thiol-terminated PEG (green).

3.2.3.2. Interaction between the methacrylated HA and the functionalized MSN

The nature of the interactions between the MSN and the Me_HA network was investigated. In particular the possibility to form either covalent links via the thiol-Michael addition of MSN-SH or the generation of electrostatic interactions between the positively charged MSN-NH_2 and the negatively charge HA were evaluated. The addition of HA (5kDa) to a water suspension of MSN-NH_2-SH (Figure 3.20), induces an increase of the hydrodynamic diameter (Figure 3.20b) and a shift of the surface charge from positive to negative values (Figure 3.20c). In a control experiment, done using the MSN-SH, both the hydrodynamic diameter and the ζ-potential remained unchanged after the addition of HA to the suspension. The presence in the DLS analysis (Figure 3.20b) of a single distribution peak indicates that the NP are individually wrapped by the polymer. The covering of the MSN can be visualized by electronic microscopy (Figure 3.20d) where it is possible to observe both an increase of size and the presence of a blurry layer (STEM image) attributed to the lower contrast given by the polymer in comparison with the silica.

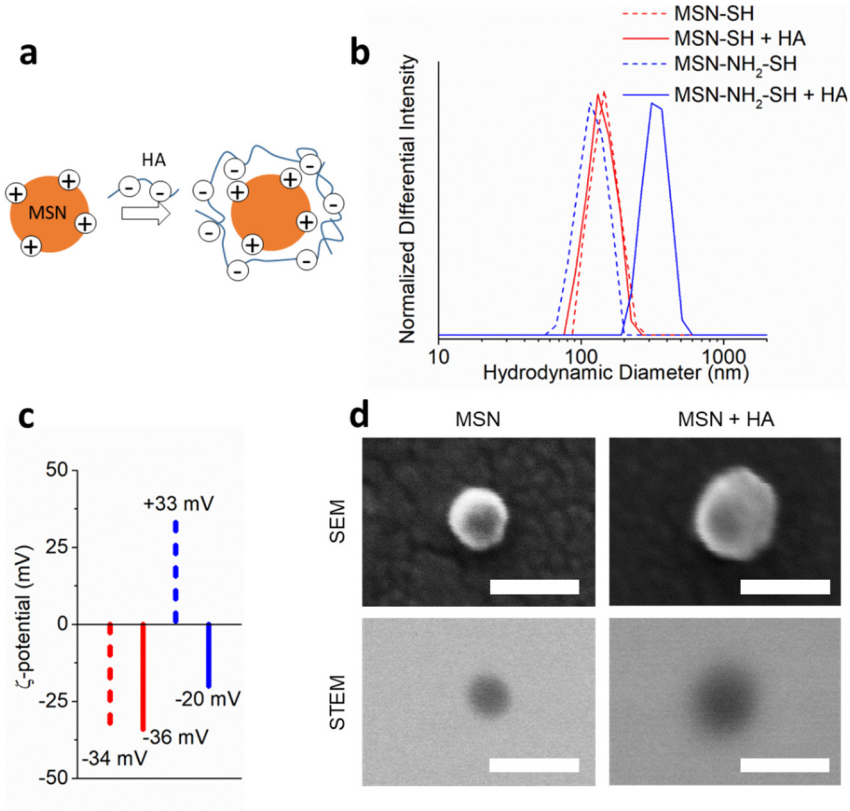

Figure 3.20: Electrostatic interaction between MSN and HA. a) Representation of the wrapping of HA around positively charged MSN. b) DLS and c) ζ-potential measurement of positively (blue) and negatively (red) charged MSN before (dashed line) and after (solid line) interaction with HA. d) SEM and STEM imaging of a positively charged MSN before and after the treatment with HA. Scale bars: 100 nm.

The ability of thiol functionalized MSN with different surface charge to covalently link to the Me_HA through the thiol-Michael addition was furthermore investigated (Figure 3.21a).

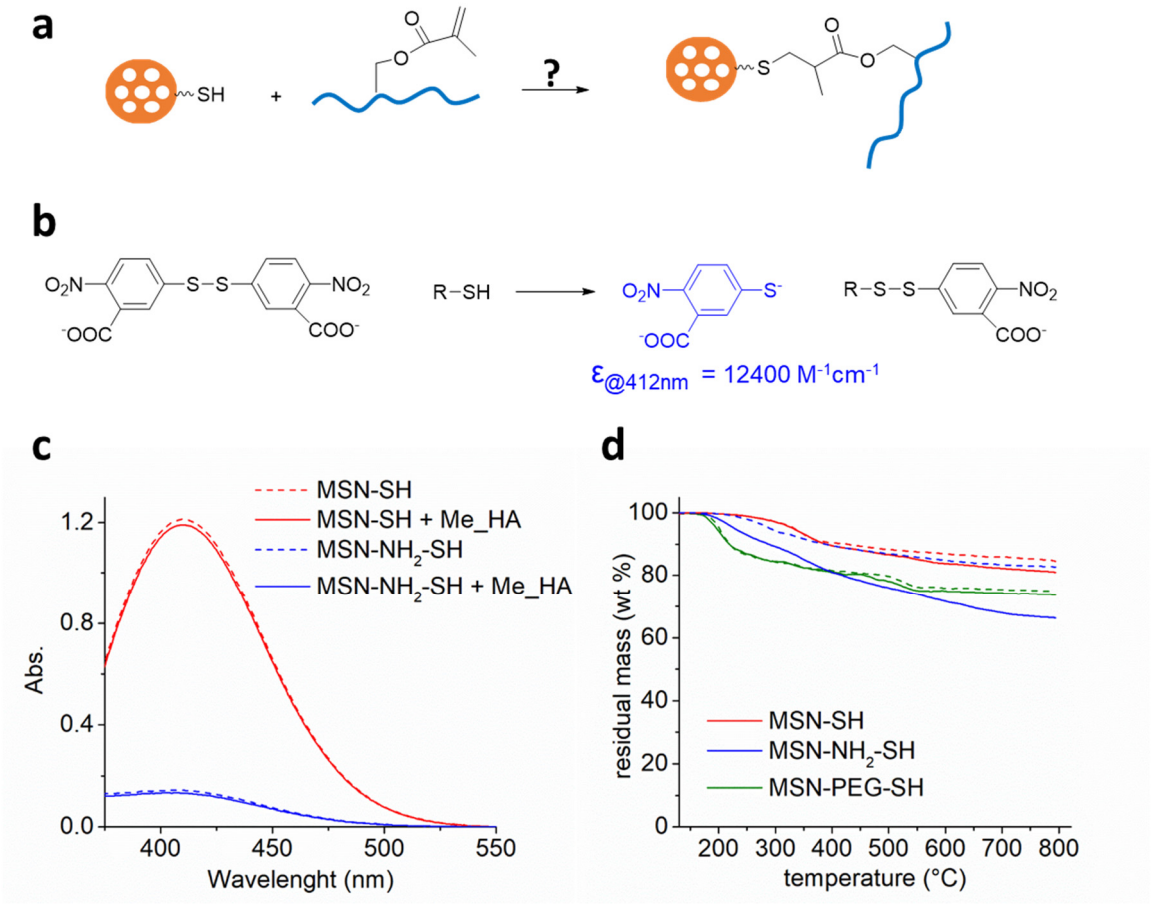

Figure 3.21: Evaluation of the formation of covalent bonds between the thiol functionalized MSN and the Me_HA. a) Scheme of the thiol-Michael reaction. b) Ellman's test for the quantification of thiols. c) Absorption spectra, after reaction with the Ellman's reagent, of MSN-SH (red) and MSN-NH_2-SH (blue) water suspension before (dashed line) and after (solid line) incubation with Me_HA. d) TGA of the MSN-SH (red), the MSN-NH_2-SH (blue) and MSN-PEG-SH (green) before (dashed line) and after (solid line) incubation with Me_HA.

The quantitative colorimetric Ellman's test (Figure 3.21b), sensitive to thiols, was used to compare the concentration of mercapto groups on the MSN before and after having been in contact with Me_HA. Both MSN with positive (MSN-NH_2-SH) and negative (MSN-SH) surface charge were involved in the test, with the latter expected to promote the approach with the Me_HA and consequently the formation of covalent bonds. The colorimetric test showed that the concentration of thiol groups in solution is unchanged after incubation with Me_HA for both the particles tested (Figure 3.21c) suggesting that the thiol-Michael reaction does not take place. In a further experiment, 5 mg of the particles under test (MSN-SH, MSN-NH_2-SH

or MSN-PEG-SH) were dispersed in 2 mL solution of Me_HA 5 kDa 5 mg/mL in PBS and stirred overnight at 37 °C. The samples were then, centrifuged, washed three times with water and vacuum dried before evaluating the presence of covalently linked polymer by TGA (Figure 3.21d). The analysis showed the absence of HA in the MSN-SH and MSN-PEG-SH samples (negative surface charge) confirming that the thiol-Michael reaction does not occur even in presence of the PEG spacer that would have been expected to improve the accessibility of the –SH groups. On the contrary, a significant mass loss, attributed to the presence of the polymer, was observed for the MSN-NH_2-SH. The HA however is probably grafted via supramolecular interactions (Figure 3.20) rather than through covalent links as indicated by the Ellman's test. The experiments carried on to study the MSN-HA interactions suggest that the positively charged MSN can act as supramolecular cross-linker in the preparation of the nanocomposite hydrogel.

The effect of the introduction of MSN, with different surface charge and in different concentrations, on the kinetic profile of gelation and on the final mechanical properties (storage modulus, loss modulus and LVR) was evaluated (Figure 3.22).

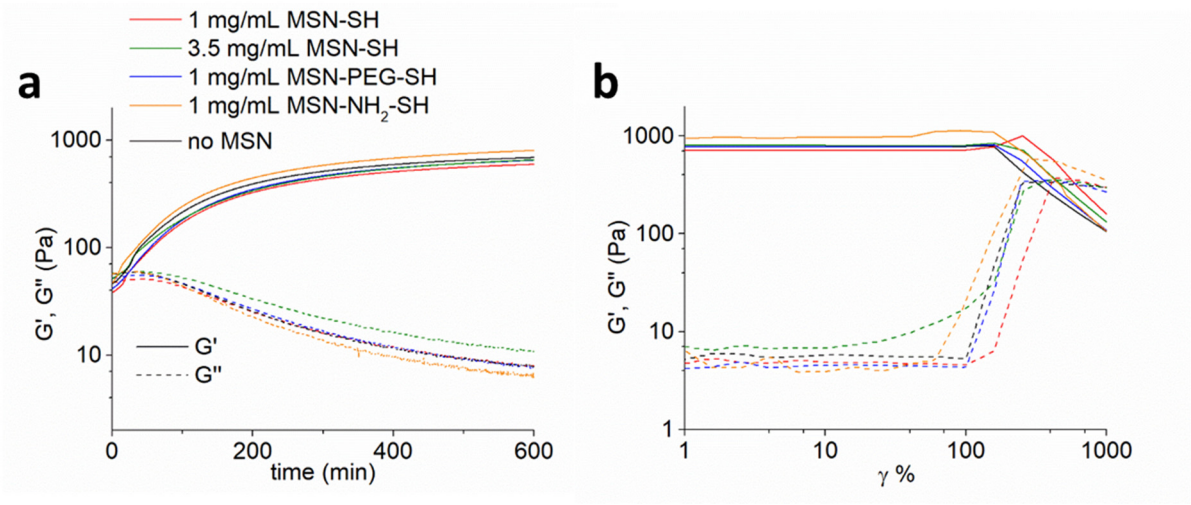

Figure 3.22: Effect of MSN on the mechanical properties of the hydrogel. a) Kinetic of hydrogel formation; b) LVR. Solid lines represent the storage modulus, dashed lines represent the loss modulus. Pristine hydrogel (black), nanocomposite hydrogels with 1 mg/mL MSN-SH (red), with 1 mg/mL MSN-PEG-SH (blue), with 1 mg/mL MSN-NH_2-SH (orange) and with 3.5 mg/mL MSN-SH (green). Coaxial cylinder geometry (diameter 10 mm), 37 °C, f= 1 Hz, γ= 1%.

The nanocomposite hydrogels are prepared starting from a 2% solution of 1700 kDa Me_HA in PBS to which the nanoparticles understudy are added and the system stirred at 37 °C for at least one hour prior to the addition of the molecular cross linker (DTT). The presence of the

MSN in all the cases studied did not alter the storage modulus of the material (Figure 3.22a). The formation of electrostatic interactions between the positively charged MSN and the negatively charged HA was also irrelevant to the rheological properties of the nanocomposite hydrogel. Comparable results have been reported in literature for a similar nanocomposite system.[48] MSN in concentration 3.5 mg/mL increased the viscous modulus of the system and reduced its LVR (Figure 3.22b), probably due to the formation of aggregates that prevent effective cross-linking reactions and reduce the deformability of the hydrogel.

3.2.4. Enzymatic degradation of the HA based hydrogel

A key aspect of implanted materials is their clearance from the body once that their function has been completed. Hyaluronic acid is naturally degraded in mammals thanks to the presence of the hyaluronidase enzymes (Hhase) that cleave the 1-4 linkage between the N-acetylglucosamine and the glucoronate unit (Figure 3.23a). The kinetic of degradation of the hydrogel under study has been studied soaking the material in solutions of Hhase at different concentrations chosen within the physiological range (0.0059 U/mL in human plasma to 38.5 U/mL in human ovaries)[56] (Figure 3.23b).

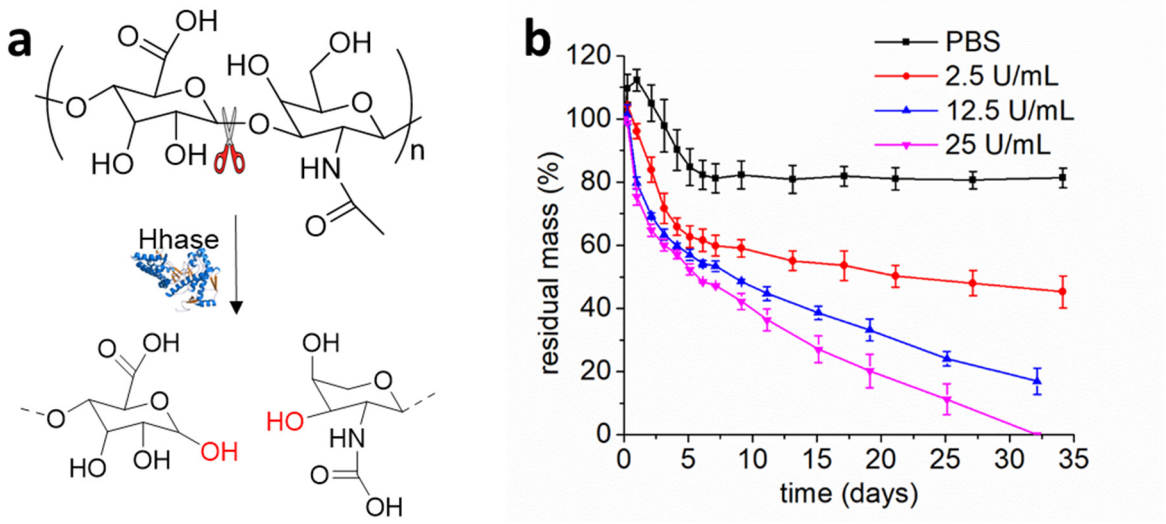

Figure 3.23: a) Enzymatic cleaving of the 1-4 linkage associated with the degradation of HA. b) Kinetic of degradation of the HA hydrogel in Hhase solutions at different concentrations: PBS control (black), 2.5 U/mL (red), 12.5 U/mL (blue) and 25 U/mL (pink) (n=3).

During the first three days a burst partial mass-loss was observed and it is attributed to the degradation of non-covalently linked HA and/or of dangling ends of the polymer. Indeed, the control experiment using only PBS, showed also a minor mass loss. The enzymatic process then continues slower with the degradation of the cross-lined polymer. In this second phase, the

kinetic is dependent on the concentration of Hhase with the highest concentration tested degrading completely the hydrogel in 32 days. The observed progressive mass loss of the HA hydrogel in presence of Hhase, suggests that the degradation of the material *in vivo* can occur in parallel with the fistula healing process creating the physical space required for the new tissue generation.

3.2.5. Evaluation of the ability of the hydrogel to adhere to the gastrointestinal tissue

One of the requirements for *in vivo* application of injectable hydrogels is the ability to stay in position without percolating outside the injection site. We evaluated the ability of the pre-hydrogel solution (1700 kDa HA, 3%) and of the cross-linked hydrogel to sustain their own weight when deposited on an explanted porcine esophagus and subject to gravity (Figure 3.24). The pre-gel solution (Figure 3.24a), thanks to its high viscosity, showed adequate tissue adhesion and the ability to sustain its own weight that was maintained after the hydrogel formation (Figure 3.24b). The results are promising for the *in vivo* application where the material is required to not flow after injection.

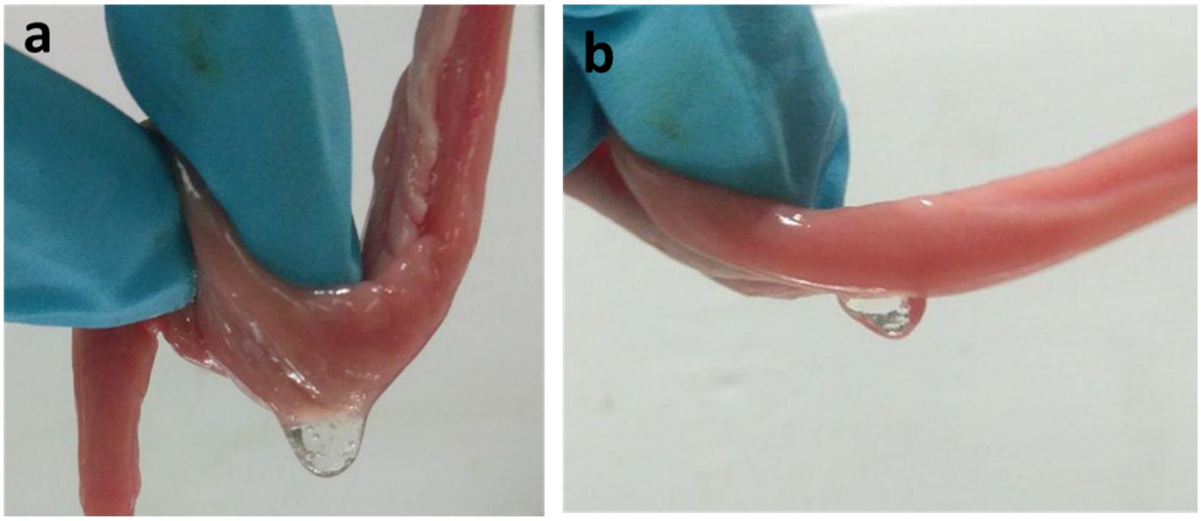

Figure 3.24: a) The methacylated hyaluronic acid pre-gel solution and b) the cross-linked hydrogel sustaining their own weight when drop casted on an explanted esophagus and exposed to gravity.

3.2.6. *In vivo* application of the nanocomposite HA based hydrogel for the treatment of fistula

The rheological study reported in Paragraph 3.2.2.1. showed that the 1700 kDa HA, 3% concentration hydrogel has suitable characteristics in term of injectability, mechanical properties of the pre-gel solution, kinetic of gelation and elastic modulus of the cross-linked

system for the application in the treatment of fistula. This material is furthermore characterized by high porosity with pores larger than cellular size (Figure 3.11) that make it a suitable scaffold for cell colonization. Since, MSN were shown to not affect the mechanical properties of the hydrogel, they were introduced in the material in 1mg/mL concentration as a proof of concept of the possibility to deliver biomolecules *in vivo*. We evaluated the therapeutic effects of the hydrogel in a clinically-relevant porcine model of esophageal-cutaneous fistula at Policlinico Agostino Gemelli IRCCS, Roma. The hydrogel precursors were mixed in the surgical room prior of material injection. A total of 4 minipigs (adults 35-40 kg) were included in the study. Two esophageal fistulas were created, as previously described,[57] for each pig for a total of 8 fistulas obtained at time 0 (post-operative day (POD) 0) (Figure 3.25). The animals were kept in the animal facility at the Catholic University of Rome, Italy and they had water and food ad libidum. The animals were fastened the day of the procedure. The procedure for obtaining a persistent and realistic fistula model last 24 days. The presence and the persistance of the internal and external orifices of the fistulas, was confirmed performimg clinical, endoscopic and radiological analysis (at POD 24).

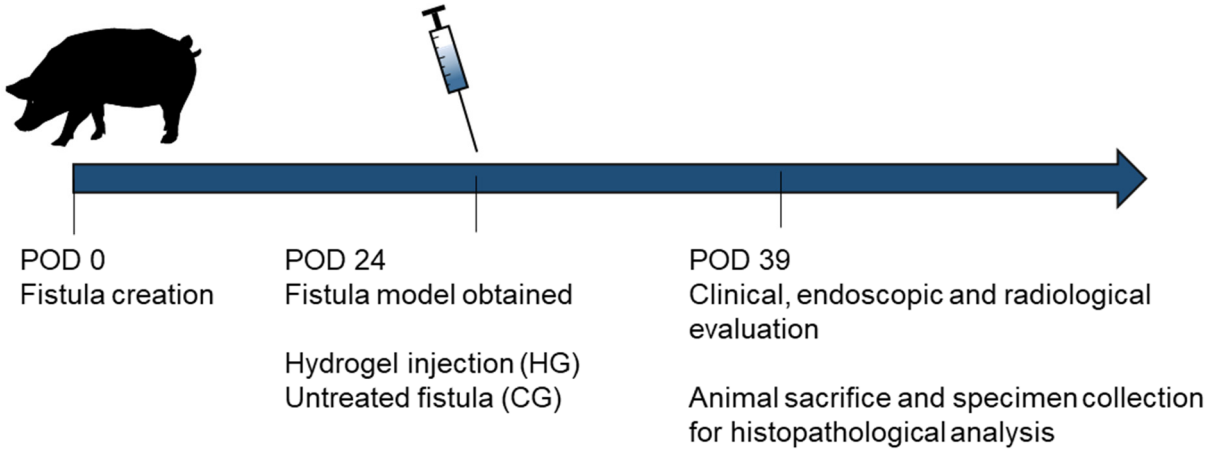

Figure 3.25. Time line of the *in vivo* experiment.

Under the clinical point of view, all the minipigs mantained a stable weight and did not present any post-procedural complication. Three of the persisting fistulas constituted the control group (CG), while the remaining fistulas (hydrogel filled) constituted the hydrogel group (HG). The CG was untreated, while in the HG a mean value of 6.7 (±3.2) mL of gel was injected in the internal fistual orfice by means of an endoscopic approach (23 gauge needle). At POD 39, corresponding to 15 days after the hydrogel injection, a further clinical, endoscopic and

radiological evaluation was performed. Macroscopically, in the CG the external fistula orifices were still persistent with a concomitant local inflammation (Figure 3.26a). Conversely, in the HG all external fistula orifices were appropriately closed in 5 out of 5 cases (Figure 3.26b).

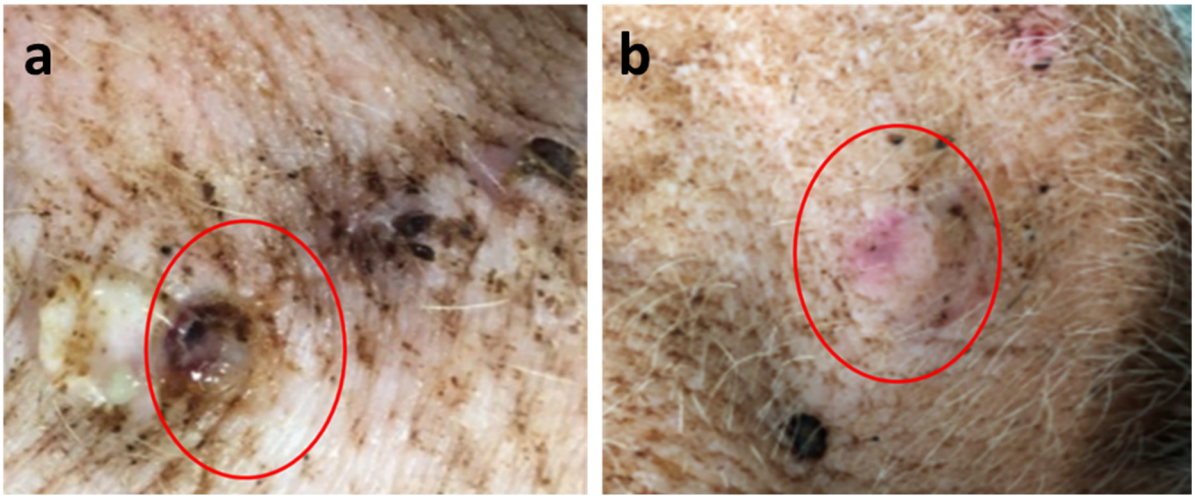

Figure 3.26: Macroscopical aspect of the external orifice of the fistulas (red circles) at POD 39: a) persistence and local inflammation in the CG, b) appropriate closure in the HG.

The endoscopic re-evaluation similarly demonstrated a persistence of the internal orifice in all the fistulas of the CG (Figure 3.27a) and an appropriate closure of the internal orifices in all the fistulas of the HG (Figure 3.27b).

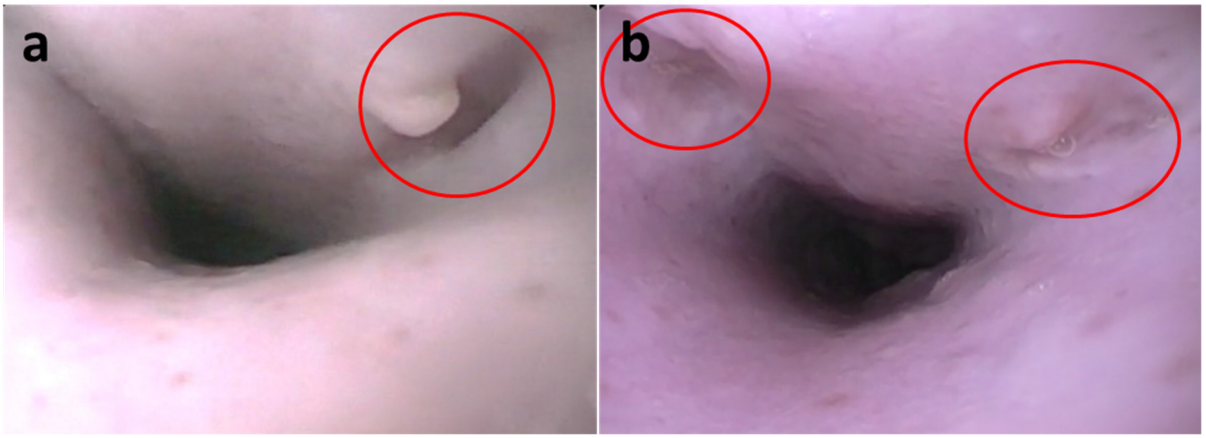

Figure 3.27: Endoscopic aspect of the internal orifice of the fistulas (red circles) at POD 39: a) persistence of the internal orifice in the CG and b) complete closure of the two fistulas in the HG.

After the clinical, endoscopic and radiological re-evaluation, all minipigs were sacrified and a specimen for each pig including esophagus, fistula tract and the corresponding muscolar,

subcutaneous and cutaneous layers were removed in order to coduct an hystopathological analysis (Figure 3.28). In this last regard, a significant inflammatory response was evidenced in the HG with a high concentration of gigantocellular elements, both in the internal and external orifices of the fistulas (Figure 3.28a and c). These microscopical aspects demonstrate an appropriate cicatrization process. Conversely, an aspecific chronic inflammatory response was documented in the CG, both in the internal and external orifices of the fistulas (Figure 3.28b and d). The absence of gigantocellular elements microscopically confirms the inappropriate tissue cicatrization process.

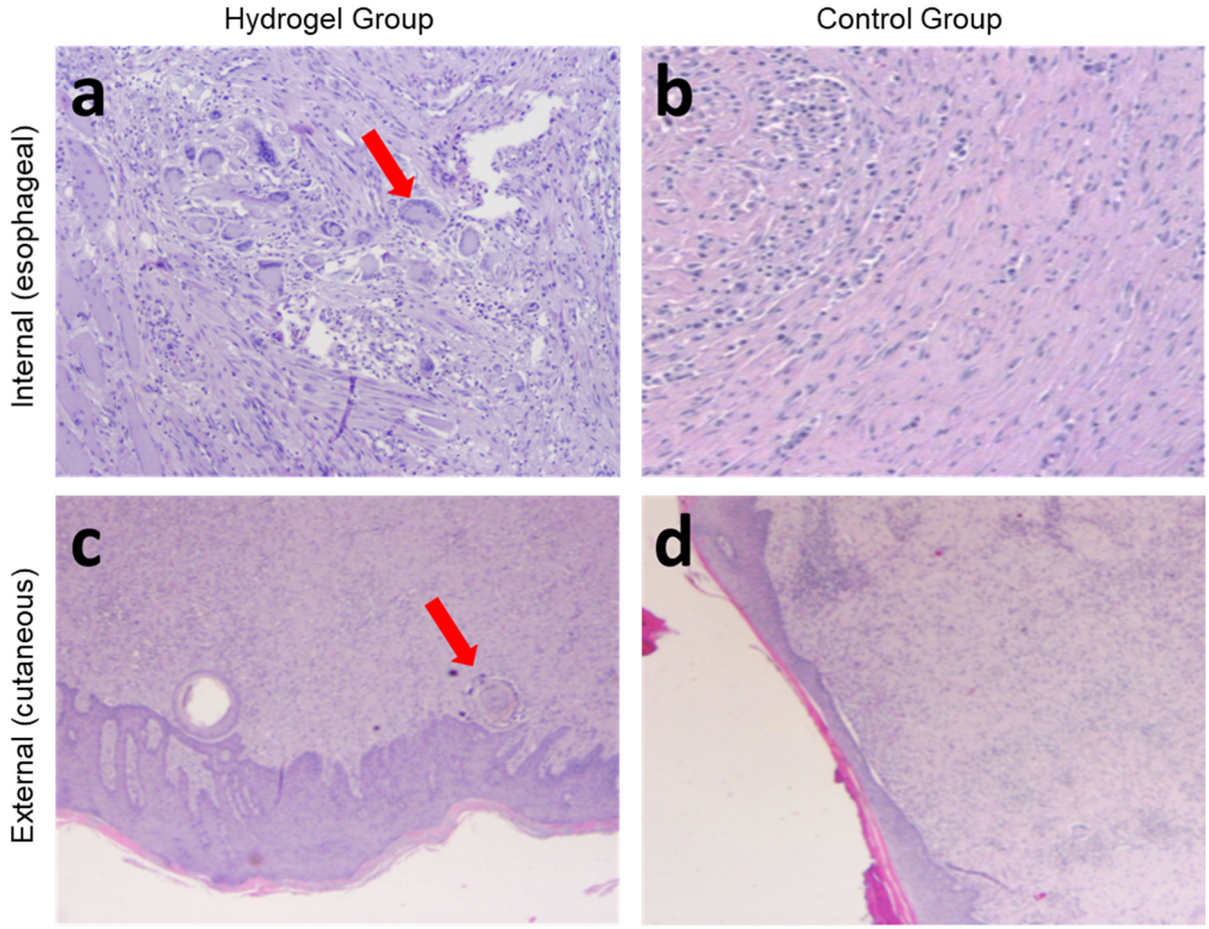

Figure 3.28: Hystopathological aspect of the a, b) internal (esophageal) and c, d)external (cutaneous) orifices at POD 39: inflammatory response with a, c) a high concentration of gigantocellular elements in the HG and b, d) aspecific chronic inflammatory response without gigantocellular elements in the CG.

Based on these macroscopical and microscopical results, we can assume that the injection of hydrogel may induce and accelerate an appropriate healing. The improved cicatrization obtained with the hydrogel suggests that epithelial cells were able to populate the hydrogel. It

is possible to hypotesize that the physiologially present hyaluronidase degraded the injected matrix generating HA oligomers and stimulating cell proliferation. The effect of the activity of hyaluronidase enzymes on the degradation of HA and, consequently, on the possibility of cells to proliferate in the material, will be presented in the Chapter 4. The highly porous structure of the material (Figure 3.11) is also tought to have played a crucial role in allowing the cell colonization of the hydrogel.

3.3. Conclusions

Hyaluronic acid is a polymer naturally present in the body where it has the function of space filler in the extracellular matrix, of lubricant in the joints and of biological activity regulator in the wound healing process. HA is characterized by a strong shear thinning behavior and it has wide versatility of functionalization that make it an interesting candidate for the preparation of injectable hydrogels with tunable properties. The hydrogels are prepared in PBS at 37°C by the cross-linking of methacrylated HA with a dithiol to give a soft material containing more than 96% of water and characterized by porous microarchitecture with pores ranging from 10 to 50 μm. The effect of HA MW and concentration on the kinetic of gelation and on the mechanical properties of the material was studied and it allowed to select the material obtained from 1700 kDa methacrylated HA in 3% concentration as the optimal candidate for the treatment of fistula. The introduction of Mesoporous Silica Nanoparticles in the system was shown to not affect the mechanical properties of the hydrogel and they were incorporated in the material as potential biomolecule delivery system. The *in vivo* experiments showed the easy injectability of the material with an endoscopic needle, the ability of the material to stay in position without percolating out of the cavity and to form *in situ* a soft solid. The animals treated with the nanocomposite hydrogel underwent better healing compared with the control group. The success of the material is attributed to the natural role of hyaluronic acid in the healing process and in the consequent stimulated cell proliferation and fistula cicatrization. The material obtained is an interesting alternative of the bio-glues that are currently used in the treatment of fistula.

3.4. Acknowledgements

I thank Pierre Picchetti (University of Strasbourg) for the N_2 adsorption, SAXS and TEM analysis, Dr. Victor Sebastian (University of Zaragoza) for the cryo-SEM imaging, Dr. Ivo

Boskoski, Giuseppe Quero, Camilla Gallo, Vincenzo Arena, Prof. Guido Costamagna (Policlinico Agostino Gemelli IRCCS, Roma) and Prof. Silvana Perretta (IHU, Strasbourg) for the *in vivo* experiments.

3.5. Experimental section

3.5.1. Chemicals and materials

5 kDa HA (4659 Da Hyaluronic acid sodium salt) was purchased from abcr GmbH, 100 kDa HA (80-100 kDa Hyaluronic acid sodium salt) was purchased from abcr GmbH, 470 kDa HA (intrinsic viscosity 1.02 m^3kg^{-1}) and 810 kDa HA (intrinsic viscosity 1.51 m^3kg^{-1}) were purchased by CONTIPRO, 1700 kDa HA was purchased from HTL Biotechnology and provided by Qventis GmbH. Dopamine hydrochloric acid (99%) was purchased form Alfa-Aesar. *N*-Hydroxysuccinimide (NHS) was purchased from ABCR. 2-Aminoethanethiol hydrochloride was purchased from Acros Organics. The silane-PEG-NHS (MW 5000 Da) was purchased from Nanocs. Dithiothreitol, methacrylic anhydride, 1-Ethyl-3-(3-dimethylaminopropyl)carbodiimide (EDC), 9,10-phenanthrenequinone, tetraethyl orthosilicate (TEOS), cetyltrimethylammonium bromide (CTAB), (3-Mercaptopropyl)trimethoxysilane, (3-Aminopropyl)trimethoxysilane and (3-Isocyanatopropyl)triethoxysilane were purchased from Sigma Aldrich.

3.5.2. HA methacrylation

To a 1% wt solution of hyaluronic acid (HA) in water, 10 equivalents of methacrylic anhydride were added under stirring in an ice-bath. The pH was adjusted to 8 with NaOH 5N. The solution is stirred for 24 hours in the ice-bath and the pH is periodically adjusted to 8 with NaOH 5N. The obtained product was precipitated pouring the solution in ethanol. The precipitate was collected and dialyzed (6-8 kDa regenerated cellulose membrane) for two days. The product was freeze-dried for two days to give a white powder.

3.5.3. Dopamine functionalization of methacrylated HA

200 mg of Me_HA were dissolved in 20 mL of PBS (0.1 M, pH 5.7) in a two necks flask. 194 mg of EDC (1 mmol) and 116 mg of NHS (1 mmol) were added and the solution was stirred for 30 min under N_2 at room temperature. 348 mg (2.5 mmol) of dopamine hydrochloric acid were then added and the solution was stirred overnight under N_2 at room temperature. The product was collected by precipitation in ethanol and it was purified by dialysis for three days

(6-8 kDa, regenerated cellulose membrane). The sample was freeze-dried for two days. The obtained product is a white solid.

3.5.4. MSN synthesis

60 mg of triethanolamine and 600 mg of CTAB were dissolved in 20 mL of H_2O and stirred at 350 rpm at 95 °C for one hour. 1.5 mL of TEOS where then added drop by drop and the mixture was kept at 95 °C for one hour. The particles were washed three times by centrifugation in ethanol. The CTAB template was removed refluxing overnight the particles in a solution of ethanol and HCl. The particles were collected by centrifugation (35 krpm, 15 min, 20 °C), washed three times in water/ethanol, and dried under vacuum.

3.5.5. MSN functionalization with (3-Mercaptopropyl)trimethoxysilane (MSN-SH)

100 mg of MSN were suspended in 40 mL of ethanol with 75 µL of NH_3 (28% aqueous solution) and 0.6 mmol of (3-Mercaptopropyl)trimethoxysilane and the mixture was stirred overnight at 60 °C. The particles were collected by centrifugation (35 krpm, 15 min, 20 °C), washed three times in ethanol, and dried under vacuum.

3.5.6. MSN co-functionalization with (3-Mercaptopropyl)trimethoxysilane and (3-Aminopropyl)trimethoxysilane (MSN-NH_2-SH)

100 mg of MSN were suspended in 40 mL of ethanol with 75 µL of NH_3 (28% aqueous solution), 0.06 mmol of (3-Mercaptopropyl)trimethoxysilane and 0.54 mmol of (3-Aminopropyl)trimethoxysilane and the mixture was stirred overnight at 60 °C. The particles were collected by centrifugation (35 krpm, 15 min, 20 °C), washed three times in ethanol, and dried under vacuum.

3.5.7. MSN functionalization with thiol-terminated PEG

0.01 mmol of *N*-hydroxysuccinimide-terminated PEG silane (MW = 5000 Da) were mixed with 0.015 mmol of 2-Aminoethanethiol hydrochloride and 0.03 mmol of triethylamine in 1 mL DMSO and stirred at room temperature for 45 min to give the thiol-terminated PEG silane. The obtained solution was added to a suspension of MSN (30 mg in 15 mL ethanol) in presence of 22 µL of NH_3 (28% aqueous solution) and stirred overnight at 60 °C. The particles were collected by centrifugation (35 krpm, 15 min, 20 °C), washed three times with ethanol and dried under vacuum.

3.5.8. Ellman's test for the quantification of thiols

To 0.5 mL of a water suspension (2 mg/mL) of the thiol functionalized MSN, were added 0.5 mL of Me_HA (1 mg/mL) (5 kDa) or water (blank) and stirred overnight at 37°C. The Ellman's test was carried adapting the procedure reported by Riener *et al.*[58] Briefly, to 600 µL of the test suspension, 1.4 mL of buffer pH 8.2, (boronic acid 100 mM, EDTA 0.2 mM, adjusted to pH 8.2 with NaOH) and 20 µL of Ellman's reagent solution (10 mM 5,5'-dithio-bis(2-nitrobenzoic acid)) were added. The mixture was then stirred for 5 min at room temperature, centrifuged (14.5 krcf, 10 min) and the supernatant collected for the UV-vis absorption measurement done against a water reference. The absorption spectrum of the blank solution (600 µL of water, 1.4 mL of buffer pH 8.2, and 20 µL of Ellman's reagent) was subtracted to the spectra of the test solutions.

3.5.9. Kinetic of hydrogel enzymatic degradation

The hyaluronidase used for the experiments contains 750-3000 U/mg; all the concentration of the enzyme reported in this chapter are therefore intervals indicated, for simplicity, as the lowest content in units: 2.5 U/mL represent 2.5-10 U/mL, 12.5 U/mL stays for 12.5-50 U/mL and 25 U/mL indicates 25-100 U/mL. A hydrogel scaffold made of 1700 kDa Me_HA (3% wt concentration) was prepared and cut in pieces of 150-300 mg each. The hydrogel pieces were weighted and incubated at 37°C in 2 mL of PBS or Hhase solution with concentration of 2.5 U/mL, 12.5 U/mL, or 25 U/mL. At each measuring time, the mass of the samples (three for each experimental condition) was measured and the solutions were replaced with fresh ones.

3.5.10. *In vivo* experiment

The study was approved by the Ethical Commetee of Università Cattolica del Sacro Cuore di Roma and the Italian Ministry of Health (number: 822/2019-PR). All the procedures were conducted according to the European Community Council directives and the Italian laws on the animal use and care.

3.5.11. Instruments

The rheological measurements were performed with a Thermofisher HAAKE Mars 40 rotational rheometer equipped with a Peltier temperature module. The measuring geometry and the parameter used are specified in each experiment. SEM images were obtained from a FEI Quanta FEG 250 instrument (FEI corporate, Hillisboro, Oregon, USA) with an acceleration voltage of 20 kV. The samples are prepared by drop-casting a suspension of NP in ethanol on a glass cover slip subsequently sputtered with gold for 30 s at 60 mA. X-ray Photoelectron

Spectroscopy (XPS) analysis was done with a K-Alpha™ X-ray photoelectron spectrometer system (Thermo Scientific). Monochromatic Al K alpha X-rays were used (15 keV, 72 W, 200 mm spot diameter). Spectra were measured using a pass energy of 200 eV for the survey spectra and of 50 eV for high resolution spectra. Binding energies were referenced to C1s peak at 284.8 eV. Thermogravimetric Analysis were done on a Perkin Elmer TGA4000 Instrument machine under N_2/O_2 flux. The samples were warmed and kept at 130°C for 20 min to remove all the adsorbed solvents then heated up to 800°C at 10°C/min rate. ^{1}H-NMR were recorded on a Brücker 400 MHz. FTIR spectra were recorded on a Shimadzu IRAffinity-1 spectrometer used in attenuated total reflectance (ATR) mode. Spectra cumulated 64 scans at a resolution of 4 cm^{-1}. UV-Vis absorption spectra were recorded on a Shimadzu UV-3600 double-beam UV-VIS-NIR spectrophotometer. TEM analysis were performed using a Jeol 2100F electron microscope operated at 200 kV. Nitrogem physiosorption isotherms were obtained with a Micrometrics ASAP-2020 physiosorption instrument. The samples were degassed at 80°C for 6 h and N_2 adsorption-desorption measurement was performed at -196°C. The surface area was calculated by Brunauer-Emmett-Teller method in the relative pressure range p/p_0 0.06-0.3. The pore size distribution and pore volume were calculated by density functional theory method on the adsorption branch. The adsorption data were analyzed by using the SAIEUS software (model used: N2@77K, cylindrical pores in oxide surface), provided by Micrometrics using a slit-based model. The total pore volume was calculated at $p/p_0 = 0.99$. DLS and ζ-potential measurements were conducted on a Delsa Nano C Particle Analyser (Beckman Coulter); operating wavelength 655 nm. The measurements were done in water at room temperature. The Contin algorithm was used to obtain the intensity distribution from DLS analysis. The small-angle X-ray scattering setup includes the SAXSess mc2 instrument from Anton Paar GmbH (Graz, Austria), containing a slit collimator system, and the PW3830 laboratory X-ray generator (40 kV, 50 mA) with a long-fine focus sealed X-ray tube (CuKα λ = 0.1542 nm) from PAN analytical. Detection was performed with the 2D imaging-plate reader Cyclone® by Perkin Elmer. Measurements were performed on powder samples for 5 min and the data collection up to scattering vector q of 7 nm^{-1} ($q=4\pi/\lambda \sin(\theta/2)$, 2θ is the scattering angle). The 2D data were converted to 1D data and back-ground corrected by using SAXSQuant software (Anton Paar GmbH).

3.6. References

1. Stern, R. Hyaluronan catabolism: a new metabolic pathway. *Eur. J. Cell Biol.* 83, 317–325 (2004).

2. Fraser, J. R. E., Laurent, T. C. & Laurent, U. B. G. Hyaluronan: its nature, distribution, functions and turnover. *J. Intern. Med.* 242, 27–33 (1997).

3. Ibrahim, S., Kang, Q. K. & Ramamurthi, A. The Impact of HA Oligomer Content on Physical, Mechanical, and Biologic Properties of Divinyl Sulfone-Crosslinked HA Hydrogels. *J. Biomed. Mater. Res. A* 94, 355–370 (2010).

4. Ambrosio, L., Borzacchiello, A., Netti, P. A. & Nicolais, L. Rheological study on hyaluronic acid and its derivative solutions. *J. Macromol. Sci. Part A* 36, 991–1000 (1999).

5. Xu, D., Liu, C.-Y. & Craig, S. L. Divergent Shear Thinning and Shear Thickening Behavior of Supramolecular Polymer Networks in Semidilute Entangled Polymer Solutions. *Macromolecules* 44, 2343–2353 (2011).

6. Scott, J. E. & Heatley, F. Biological Properties of Hyaluronan in Aqueous Solution Are Controlled and Sequestered by Reversible Tertiary Structures, Defined by NMR Spectroscopy. *Biomacromolecules* 3, 547–553 (2002).

7. Knopf-Marques, H., Pravda, M., Wolfova, L., Velebny, V., Schaaf, P., *et al.* Hyaluronic Acid and Its Derivatives in Coating and Delivery Systems: Applications in Tissue Engineering, Regenerative Medicine and Immunomodulation. *Adv. Healthc. Mater.* 5, 2841–2855 (2016).

8. Falcone, S. J., Palmeri, D. M. & Berg, R. A. Rheological and cohesive properties of hyaluronic acid. *J. Biomed. Mater. Res. A* 76A, 721–728 (2006).

9. Burdick, J. A. & Prestwich, G. D. Hyaluronic Acid Hydrogels for Biomedical Applications. *Adv. Mater.* 23, H41–H56 (2011).

10. Prestwich, G. D. Hyaluronic Acid-Based Clinical Biomaterials Derived for Cell and Molecule Delivery in Regenerative Medicine. *J. Control. Release Off. J. Control. Release Soc.* 155, 193–199 (2011).

11. Schanté, C. E., Zuber, G., Herlin, C. & Vandamme, T. F. Chemical modifications of hyaluronic acid for the synthesis of derivatives for a broad range of biomedical applications. *Carbohydr. Polym.* 85, 469–489 (2011).

12. Bergman, K., Elvingson, C., Hilborn, J., Svensk, G. & Bowden, T. Hyaluronic Acid Derivatives Prepared in Aqueous Media by Triazine-Activated Amidation. *Biomacromolecules* 8, 2190–2195 (2007).

13. Maleki, A., Kjøniksen, A.-L. & Nyström, B. Effect of pH on the Behavior of Hyaluronic Acid in Dilute and Semidilute Aqueous Solutions. *Macromol. Symp.* 274, 131–140 (2008).

14. Tokita, Y., Ohshima, K. & Okamoto, A. Degradation of hyaluronic acid during freeze drying. *Polym. Degrad. Stab.* 55, 159–164 (1997).

15. Caliari, S. R. & Burdick, J. A. A Practical Guide to Hydrogels for Cell Culture. *Nat. Methods* 13, 405–414 (2016).

16. Feng, Q., Li, Q., Wen, H., Chen, J., Liang, M., *et al.* Injection and Self-Assembly of Bioinspired Stem Cell-Laden Gelatin/Hyaluronic Acid Hybrid Microgels Promote Cartilage Repair In Vivo. *Adv. Funct. Mater.* 29, 1906690 (2019).

17. Wang, W., Chen, J., Li, M., Jia, H., Han, X., *et al.* Rebuilding Postinfarcted Cardiac Functions by Injecting TIIA@PDA Nanoparticle-Cross-linked ROS-Sensitive Hydrogels. *ACS Appl. Mater. Interfaces* 11, 2880–2890 (2019).

18. Rowland, M. J., Parkins, C. C., McAbee, J. H., Kolb, A. K., Hein, R., *et al.* An adherent tissue-inspired hydrogel delivery vehicle utilised in primary human glioma models. *Biomaterials* 179, 199–208 (2018).

19. Mandal, A., Clegg, J. R., Anselmo, A. C. & Mitragotri, S. Hydrogels in the clinic. *Bioeng. Transl. Med.* 5, 1 (2020).

20. Metcalf, C. Enterocutaneous fistulae. *J. Wound Care* 8, 141–142 (1999).

21. Berry, S. M. & Fisher, J. E. Enterocutaneous fistulas: In brief. *Curr. Probl. Surg.* 31, 474–482 (1994).

22. Evenson, A. R. & Fischer, J. E. Current management of enterocutaneous fistula. *J. Gastrointest. Surg. Off. J. Soc. Surg. Aliment. Tract* 10, 455–464 (2006).

23. McIntyre, P. B., Ritchie, J. K., Hawley, P. R., Bartram, C. I. & Lennard-Jones, J. E. Management of enterocutaneous fistulas: a review of 132 cases. *Br. J. Surg.* 71, 293–296 (1984).

24. Rubelowsky, J. & Machiedo, G. W. Reoperative versus conservative management for gastrointestinal fistulas. *Surg. Clin. North Am.* 71, 147–157 (1991).

25. Dorta, G. Role of Octreotide and Somatostatin in the Treatment of Intestinal Fistulae. *Digestion* 60, 53–56 (1999).

26. Goenka, M. K. & Goenka, U. Endotherapy of leaks and fistula. *World J. Gastrointest. Endosc.* 7, 702–713 (2015).

27. Rogalski, P., Daniluk, J., Baniukiewicz, A., Wroblewski, E. & Dabrowski, A. Endoscopic management of gastrointestinal perforations, leaks and fistulas. *World J. Gastroenterol. WJG* 21, 10542–10552 (2015).

28. Kotzampassi, K. & Eleftheriadis, E. Tissue sealants in endoscopic applications for anastomotic leakage during a 25-year period. *Surgery* 157, 79–86 (2015).

29. Becker, J. C., Beckbauer, M., Domschke, W., Herbst, H. & Pohle, T. Fibrin glue, healing of gastric mucosal injury, and expression of growth factors: results from a human in vivo study. *Gastrointest. Endosc.* 61, 560–567 (2005).

30. Mizuki, A., Tatemichi, M., Nishiya, H., Fukui, K., Hayashi, T., *et al.* Mucosal concentration of basic fibroblast growth factor in the healing process in human giant gastric ulcers. *J. Gastroenterol. Hepatol.* 19, 528–534 (2004).

31. Rábago, L. R., Ventosa, N., Castro, J. L., Marco, J., Herrera, N., *et al.* Endoscopic treatment of postoperative fistulas resistant to conservative management using biological fibrin glue. *Endoscopy* 34, 632–638 (2002).

32. Kim, J., Park, Y., Tae, G., Lee, K. B., Hwang, C. M., *et al.* Characterization of low-molecular-weight hyaluronic acid-based hydrogel and differential stem cell responses in the hydrogel microenvironments. *J. Biomed. Mater. Res. A* 88A, 967–975 (2009).

33. Li, X., Cho, B., Martin, R., Seu, M., Zhang, C., *et al.* Nanofiber-hydrogel composite–mediated angiogenesis for soft tissue reconstruction. *Sci. Transl. Med.* 11, eaau6210 (2019).

34. Pérez-Madrigal, M. M., Shaw, J. E., Arno, M. C., Hoyland, J. A., Richardson, S. M., *et al.* Robust alginate/hyaluronic acid thiol–yne click-hydrogel scaffolds with superior mechanical performance and stability for load-bearing soft tissue engineering. *Biomater. Sci.* 8, 405–412 (2020).

35. Nair, D. P., Podgórski, M., Chatani, S., Gong, T., Xi, W., *et al.* The Thiol-Michael Addition Click Reaction: A Powerful and Widely Used Tool in Materials Chemistry. *Chem. Mater.* 26, 724–744 (2014).

36. Smeds, K. A., Pfister-Serres, A., Miki, D., Dastgheib, K., Inoue, M., *et al.* Photocrosslinkable polysaccharides for in situ hydrogel formation. *J. Biomed. Mater. Res.* 55, 254–255 (2001).

37. Yeh, J., Ling, Y., Karp, J. M., Gantz, J., Chandawarkar, A., *et al.* Micromolding of shape-controlled, harvestable cell-laden hydrogels. *Biomaterials* 27, 5391–5398 (2006).

38. Hofman, A. H., van Hees, I. A., Yang, J. & Kamperman, M. Bioinspired Underwater Adhesives by Using the Supramolecular Toolbox. *Adv. Mater.* 30, 1704640 (2018).

39. Chen, T., Chen, Y., Rehman, H. U., Chen, Z., Yang, Z., *et al.* Ultratough, Self-Healing, and Tissue-Adhesive Hydrogel for Wound Dressing. *ACS Appl. Mater. Interfaces* 10, 33523–33531 (2018).

40. Butcher, D. T., Alliston, T. & Weaver, V. M. A tense situation: forcing tumour progression. *Nat. Rev. Cancer* 9, 108–122 (2009).

41. Tabatabai, A. P., Partlow, B. P., Raia, N. R., Kaplan, D. L. & Blair, D. L. Silk Molecular Weight Influences the Kinetics of Enzymatically Cross-linked Silk Hydrogel Formation. *Langmuir* 34, 15383–15387 (2018).

42. Adibnia, V. & Hill, R. J. Universal aspects of hydrogel gelation kinetics, percolation and viscoelasticity from PA-hydrogel rheology. *J. Rheol.* 60, 541–548 (2016).

43. Piantanida, E., Alonci, G., Bertucci, A. & De Cola, L. Design of Nanocomposite Injectable Hydrogels for Minimally Invasive Surgery. *Acc. Chem. Res.* 52, 2101–2112 (2019).

44. Eslahi, N., Simchi, A., Mehrjoo, M., Shokrgozar, M. A. & Bonakdar, S. Hybrid cross-linked hydrogels based on fibrous protein/block copolymers and layered silicate nanoparticles: tunable thermosensitivity, biodegradability and mechanical durability. *RSC Adv.* 6, 62944–62957 (2016).

45. Liu, R., Liang, S., Tang, X.-Z., Yan, D., Li, X., *et al.* Tough and highly stretchable graphene oxide/polyacrylamide nanocomposite hydrogels. *J. Mater. Chem.* 22, 14160–14167 (2012).

46. Liu, L., Lv, G., Ren, X., Li, X., Wang, T., *et al.* Effect of size of latex particles on the mechanical properties of hydrogels reinforced by latex particles. *RSC Adv.* 9, 14701–14707 (2019).

47. De France, K. J., Cranston, E. D. & Hoare, T. Mechanically Reinforced Injectable Hydrogels. *ACS Appl. Polym. Mater.* 2, 1016–1030 (2020).

48. Lewandowska-Łańcucka, J., Gilarska, A., Buła, A., Horak, W., Łatkiewicz, A., *et al.* Genipin crosslinked bioactive collagen/chitosan/hyaluronic acid injectable hydrogels structurally amended via covalent attachment of surface-modified silica particles. *Int. J. Biol. Macromol.* 136, 1196–1208 (2019).

49. Gao, Y., Chen, Y., Ji, X., He, X., Yin, Q., *et al.* Controlled Intracellular Release of Doxorubicin in Multidrug-Resistant Cancer Cells by Tuning the Shell-Pore Sizes of Mesoporous Silica Nanoparticles. *ACS Nano* 5, 9788–9798 (2011).

50. Slowing, I. I., Trewyn, B. G. & Lin, V. S.-Y. Mesoporous Silica Nanoparticles for Intracellular Delivery of Membrane-Impermeable Proteins. *J. Am. Chem. Soc.* 129, 8845–8849 (2007).

51. Barui, S. & Cauda, V. Multimodal Decorations of Mesoporous Silica Nanoparticles for Improved Cancer Therapy. *Pharmaceutics* 12, 527 (2020).

52. Fiorini, F., Prasetyanto, E. A., Taraballi, F., Pandolfi, L., Monroy, F., *et al.* Nanocomposite Hydrogels as Platform for Cells Growth, Proliferation, and Chemotaxis. *Small* 12, 4881–4893 (2016).

53. Lv, X., Zhang, L., Xing, F. & Lin, H. Controlled synthesis of monodispersed mesoporous silica nanoparticles: Particle size tuning and formation mechanism investigation. *Microporous Mesoporous Mater.* 225, 238–244 (2016).

54. Berlier, G., Gastaldi, L., Ugazio, E., Miletto, I., Iliade, P., *et al.* Stabilization of quercetin flavonoid in MCM-41 mesoporous silica: positive effect of surface functionalization. *J. Colloid Interface Sci.* 393, 109–118 (2013).

55. Beck, J. S., Vartuli, J. C., Roth, W. J., Leonowicz, M. E., Kresge, C. T., *et al.* A new family of mesoporous molecular sieves prepared with liquid crystal templates. *J. Am. Chem. Soc.* 114, 10834–10843 (1992).

56. Domingues, R. M. A., Silva, M., Gershovich, P., Betta, S., Babo, P., *et al.* Development of Injectable Hyaluronic Acid/Cellulose Nanocrystals Bionanocomposite Hydrogels for Tissue Engineering Applications. *Bioconjug. Chem.* 26, 1571–1581 (2015).

57. Rahmi, G., Perretta, S., Pidial, L., Vanbiervliet, G., Halvax, P., *et al.* A Newly Designed Enterocutaneous Esophageal Fistula Model in the Pig. *Surg. Innov.* 23, 221–228 (2016).

58. Riener, C. K., Kada, G. & Gruber, H. J. Quick measurement of protein sulfhydryls with Ellman's reagent and with 4,4′-dithiodipyridine. *Anal. Bioanal. Chem.* 373, 266–276 (2002).

Chapter 4: Hyaluronic acid based hydrogels with biomimetic functions for cell adhesion

Abstract

In Chapter 3, the interesting properties of hyaluronic acid (HA) with high molecular weight (MW) for the preparation of injectable hydrogels have been presented. However, a limitation to the application of materials based on HA in regenerative medicine is their inability to sustain cellular adhesion and migration into the hydrogel. Herein we present different possible approaches to control the HA-cellular receptor interactions, including functionalization of the polymer with the integrin-binding RGD peptide, the introduction in the network of gelatin to form an interpenetrated network and the combination of HA oligomers within the high MW framework. These materials were synthesized and their ability to sustain cell adhesion was evaluated by using HeLa cells as a model. The experiments showed that the functionalization of HA with the peptide sequence GCGY*RGD*SPG can induce homogeneous cell adhesion even on materials with elastic modulus lower than 100 Pa. A different successful approach consisted in the incorporation in the scaffold of HA oligomers. This result is of particular interest because it suggests that high MW HA hydrogels implanted *in vivo,* may not require any modification to be populated by cells, owing to the natural presence of the hyaluronidase enzymes that progressively degrade the polymeric network and generate oligomers.

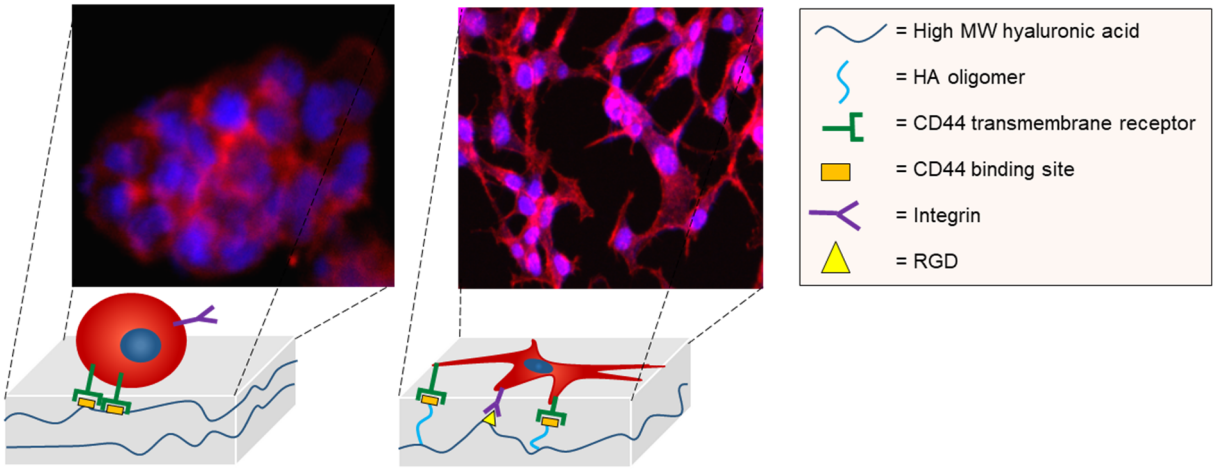

Figure 4.1: Interaction between the cell membrane receptors CD44 and integrin with the hyaluronic acid based hydrogel. High molecular weight (MW) HA induces CD44 clustering preventing the cellular adhesion. The introduction in the material of HA oligomers disrupts the CD44 clustering and promotes cell adhesion while the functionalization with RGD allows the integrin-mediated binding.

4.1. Introduction

4.1.1. Hydrogels for cell delivery

Stem cells have the extraordinary ability to regenerate the functions of a damaged tissue that could not self-heal. Stem cell therapy is a sub-type of regenerative medicine that consists in the delivery of this class of cells to the target tissue. Clinical studies have shown the potential of stem cells in the treatment of different conditions including myocardial infarction,[1] rheumatoid arthritis[2] and spinal cord injury.[3] Among stem cells, mesenchymal stem cells (MSC) are of particular interest for their ability to regulate inflammatory processes, the possibility to obtain them from abundant sources, their low immunogenicity, the absence of ethical concerns and the minimal risk of teratoma formation.[4,5] To date (September 2020), 921 clinical trials involving MSC have been registered on *ClinicalTrials.gov* and 4 of them have successfully completed phase III. Even though the clinical application of MSC on humans is not established yet, they are already used in veterinary orthopedics in equine tendinopathies and in dog cartilage degeneration.[6] The design of successful therapies based on MSC still requires the optimization of a number of key parameters including the source, the purification and the *in vitro* expansion of cells, the immune status of the recipient and the conditions of administration.[7] Bone marrow and adipose tissue are the two most commonly exploited sources of MSC, however these samplings are considered invasive and the obtained number of cells is not always sufficient. With regard to this aspect, Serteyn and co-workers have recently developed an innovative minimally-invasive technique that allows to obtain MSC in satisfactory amount by micro-biopsy of skeletal muscle from different animals including humans.[8] Concerning the *in vitro* expansion of cells, conventional culture is done in 2D, but this represents a non-physiological condition where cells have a flattened shape, experience super-physiologic stiffness and forced polarity. Culture systems that better resemble the biological environment are 3D matrix designed with optimal structural and compositional properties. In particular, hydrogels are considered the class of materials that better resembles the native extracellular matrix (Figure 4.2).[9] Conducting *in vitro* studies in an environment that closely resemble the biological milieu have been reported to be in some cases fundamental to obtain realistic data. Nguyen *et al.* for example, have evaluated the effect of a chemotherapy on cells, which were cultured on substrates with different stiffness and collagen content, and they have demonstrated that the mechanical properties of the culture system play a crucial role in the outcome of the cell viability experiments.[10] Studies about the influence of the mechanical properties of the substrate on the cell behavior have furthermore shown that cells retain memory of the past culture

environments at which they have been exposed.[11] For example, a long permanence of MSC in a soft matrix inhibits their osteogenic differentiation even when they are exposed to a stiff matrix.[12]

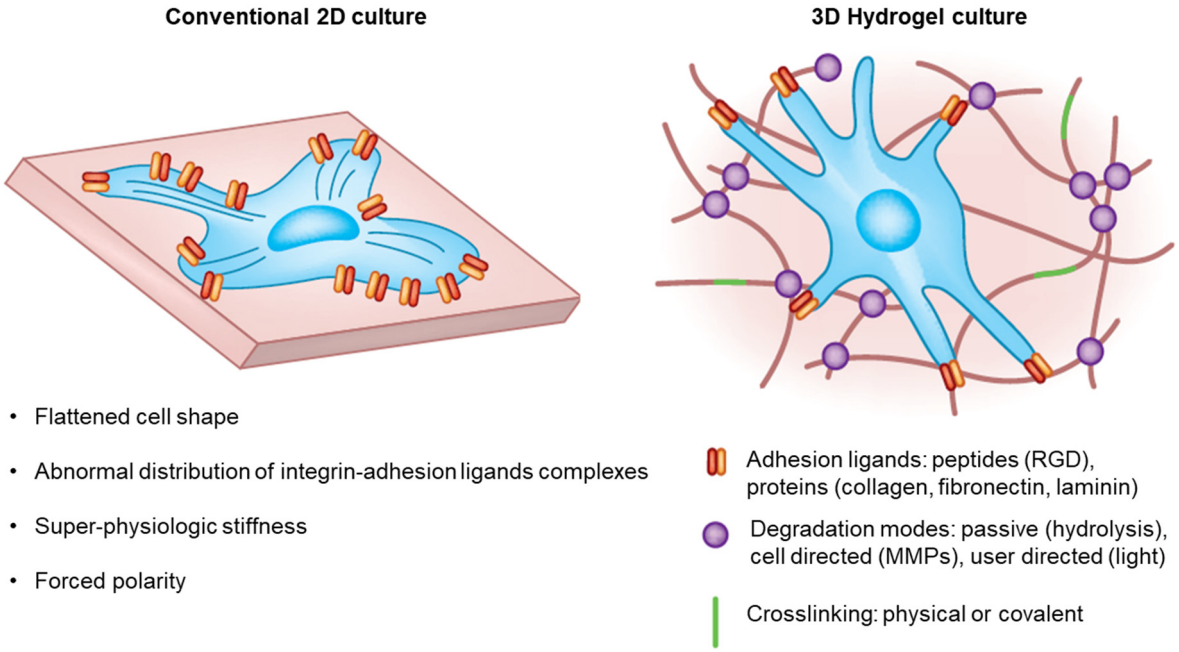

Figure 4.2: Comparison between cell culture in conventional 2D super-physiologically stiff substrate and in hydrogels engineered to provide a more realistic microenvironment. Adapted with permission from *Nat. Methods* **2016**,13**,** 405. Copyright 2016, Springer Nature.

Different kits to prepare hydrogels for cell culture are now available on the market; for example NovaMatrix® is a kit that allows to prepared alginate based hydrogels in which cells can be cultured even if they do not adhere to the scaffold; the primary advantage of this product is the easiness of matrix dissolution by cation exchange to recover the cells. The HyStem kit sold by Advanced BioMatrix is made of hyaluronic acid complemented with collagen to induce cell adhesion. Cellendes produces kits for making culture systems based on synthetic polymers that are cross-linked using cytocompatible reactions (i.e. thiol-maleimide addition) that allow to encapsulate the cells during the material synthesis. One of the most common material used in cell culture is Matrigel®, a hydrogel matrix made of native ECM proteins able to induce cell adhesion. The heterogeneous composition of Matrigel® closely mimics the native ECM but at the same time it limits the control over the cell behavior.[13] Another aspect that should be considered in the preparation of hydrogels for the growth of stem cells is the possibility to have a cell-mediated matrix degradation. Khetan *et al.* showed that in hydrogels based on hyaluronic

acid (HA), the adhesion and differentiation of MSC is dictated by the generation of degradation-mediated cellular traction rather than by the stiffness of the matrix.[14] In the regulation of cellular processes, another key role is played by growth factors which can activate the regenerative potential of resident stem cells and promote angiogenesis.[7] Their incorporation in hydrogels with application in regenerative medicine has been shown to promote the migration of autologous stem cells to the inflammation site[15] and to induce the formation of neo-cartilage.[16] In particular, the introduction in the materials of gradients of biological cues is consider to better resemble the natural ECM and has been shown to give improved cellular activity.[17] Furthermore, the use of hydrogels as cell delivery vehicles, compared with the direct administration, increases the cell survival and promote their engraftment and integration in the target tissue.[18]

In Chapter 3 we have proven the efficacy of using a hydrogel based on hyaluronic acid (HA) in the treatment of fistula where the material had the function of filler that stimulated the healing and the cicatrization process. We think that the incorporation of stem cells in the material could give not only improved fistula healing but also open new possible applications of the hydrogel in regenerative medicine. HA interacts with cells via surface receptors including the multifunctional transmembrane receptor CD44 -expressed on a variety of human cell types including MSC-, while it does not support the integrin-mediated cell adhesion.[19] The HA-CD44 interactions include both hydrophobic interactions involving the *N*-acetyl group of HA and hydrogen bonding mediated by the carboxylate group, the C6-hysroxyl group and the vicinal diols (Figure 4.3).[19,20] The chemical modification of the HA lateral groups consequently, has been reported to significantly reduce the binding affinity with the receptor.[19,20]

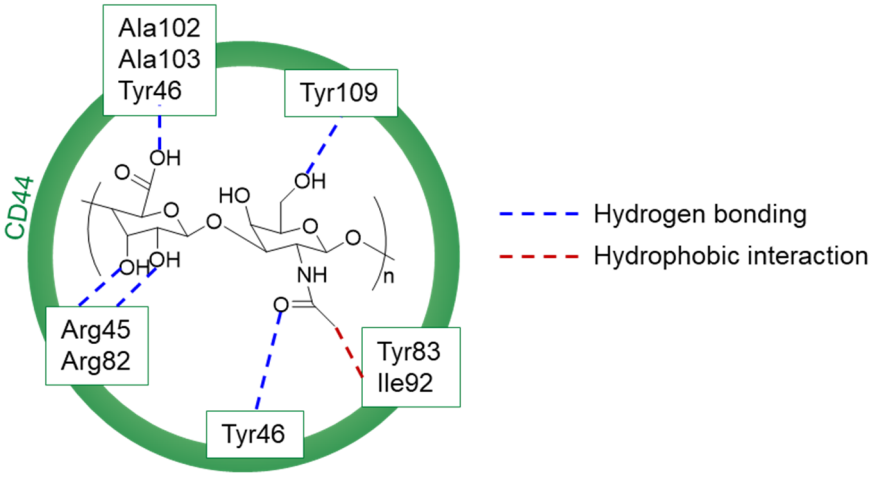

Figure 4.3: Interactions of a HA unit with the amino acids in the CD44 receptor (green). Hydrogen bonding is represented in blue while hydrophobic interactions in red.

Investigations on the role of the MW of HA on the interaction with the CD44 receptor highlighted that oligomers (oHA) (< 20 monosaccharide units) form monovalent bindings, while long chains (hHA) (> 1 MDa) give multivalent bindings that induce CD44 clustering.[21–23] The clustering of the receptor influences the physical and biochemical cellular responses, inducing opposite actions when the cells interact with HA of different MW:[24] pro- (oHA) and anti- (hHA) inflammatory activities, promotion (oHA) and inhibition (hHA) of cell migration and adhesion.[22,25,26] The ability of HA to bind to CD44 has been exploited for the selective targeting of tumors, where the receptor is overexpressed.[27]

In order to obtain cell adhesion and population in the developed injectable hydrogel made of hHA, it is therefore necessary to introduce suitable modifications in the material. Possible strategies include the introduction of HA oligomers that interact with the CD44 receptor in monovalent manner,[28,29] the generation of degradation-mediated cellular traction[14] or the incorporation in the material of biomolecules able to ligate to integrins, transmembrane receptors involved in the cell-extracellular matrix adhesion.[30] Integrins are present in all nucleated cells where they act as signaling molecules binding to different extracellular matrix molecules including fibrinogen and fibronectin.[31] Pierschbacher *et al.* identified in 1984 the RGD (arginine-glycine-aspartic acid) amino acid sequence of fibronectin to be the minimal integrin binding motif.[32] The RGD peptide ligates primarily, in presence of divalent ions, to the α_v, $\alpha_5\beta_1$ and $\alpha_{IIb}\beta_3$ integrins.[33] Moreover, the presence of specific flanking amino acids (e.g. G*RGD*SPK), significantly increases the integrin-peptide affinity.[34] However, a limit to the *in vivo* application of linear peptides is their sensitivity to enzymatic degradation. The stability of the sequence can be improved by cyclization obtaining moreover a reduction in the conformational space that can increase the biological potency.[34]

4.1.2. Aim of the project

The aim of this chapter is to evaluate possible strategies to prepare a hydrogel based on HA, able to induce cell adhesion. The investigated approaches include the incorporation of an adhesion peptide (RGD), gelatin or HA oligomers. This chapter describes the synthesis and characterization of the modified HA hydrogels as well as the *in vitro* cell adhesion tests done using HeLa cells as a model. The choice of the cell line arose from the easiness of culture and from their human origin.

4.2. Results and Discussion

4.2.1. Synthesis and characterization of RGD-functionalized Hyaluronic Acid

One of the commonly employed strategy to obtain cell adhesion is the introduction in the network of the integrin-binding RGD tripeptide. The HA functionalization with the peptide can be done either on the same functional group used for the cross-linking process or on a different group. The first approach has been used for example by Tarus *et al.* that exploited the thiol-Michael reaction to graft to the methacrylated HA (Me_HA) a peptide containing both the RGD sequence and a unit of cysteine while using a dithiol as cross-linker.[35] The main advantage of this approach is the easiness of preparation, in fact the functionalization can be done right before the cross-linking of the system without the need of a purification step. On the other side, the use of the same site for the functionalization and for the cross-linking reduces the possibility of controlling the cross-linking degree and the content of RGD, at the same time. Two different approaches have been investigated to introduce the RGD peptide in the methacrylated hyaluronic acid chain (for the methacrylation of HA, the reader is referred to Scheme 3.1 in Chapter 3). The first method consisted in the coupling of the terminal amino group of the RGD on the carboxylic group of the 100 kDa Me_HA (Scheme 4.1). The content of RGD peptide was evaluated by colorimetric test (Figure 4.4) as described in detail in the experimental section and as reported by Xu *et al.*[36] The RGD content in the polymer is $3.0 \cdot 10^{-3}$ μmol/mg of HA corresponding to 1 unit every 770 of HA bearing the peptide. The coupling reaction however could occur, not only on the terminal amine, but also, less likely, on the arginine pending group. The RGD quantification method used is selective for the arginine unit so the amount of peptide detected is coupled on the HA via the terminal amine. It is moreover possible that some RGD molecules reacted both with the terminal amine and the arginine-amine acting as a cross-linker; the obtained product was easily soluble in water suggesting that the eventual presence of cross-linked HA constitutes a neglectable percentage of the sample. When the same reaction protocol was applied for the 1700 kDa HA, the functionalization was unsuccessful probably due to the steric hindrance present in higher MW polymers.

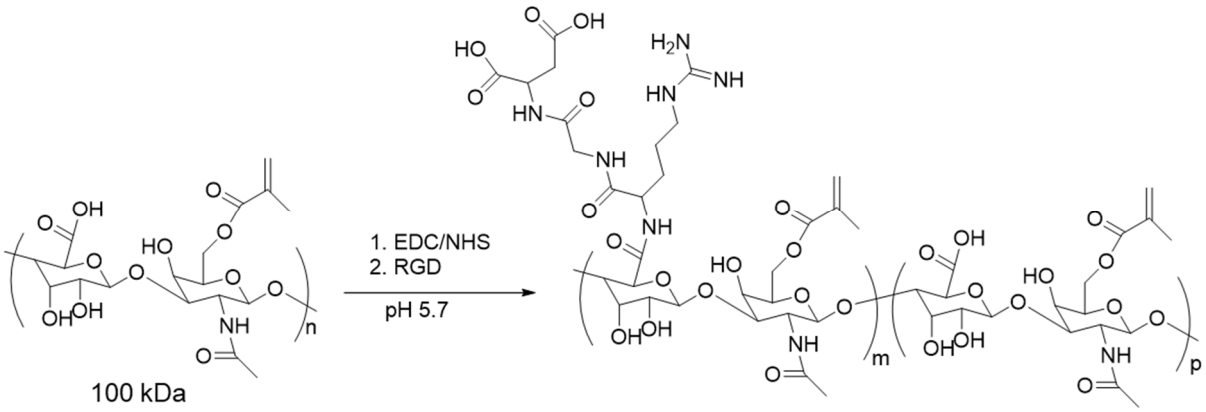

Scheme 4.1: RGD coupling on the carboxylic group of 100 kDa Me_HA.

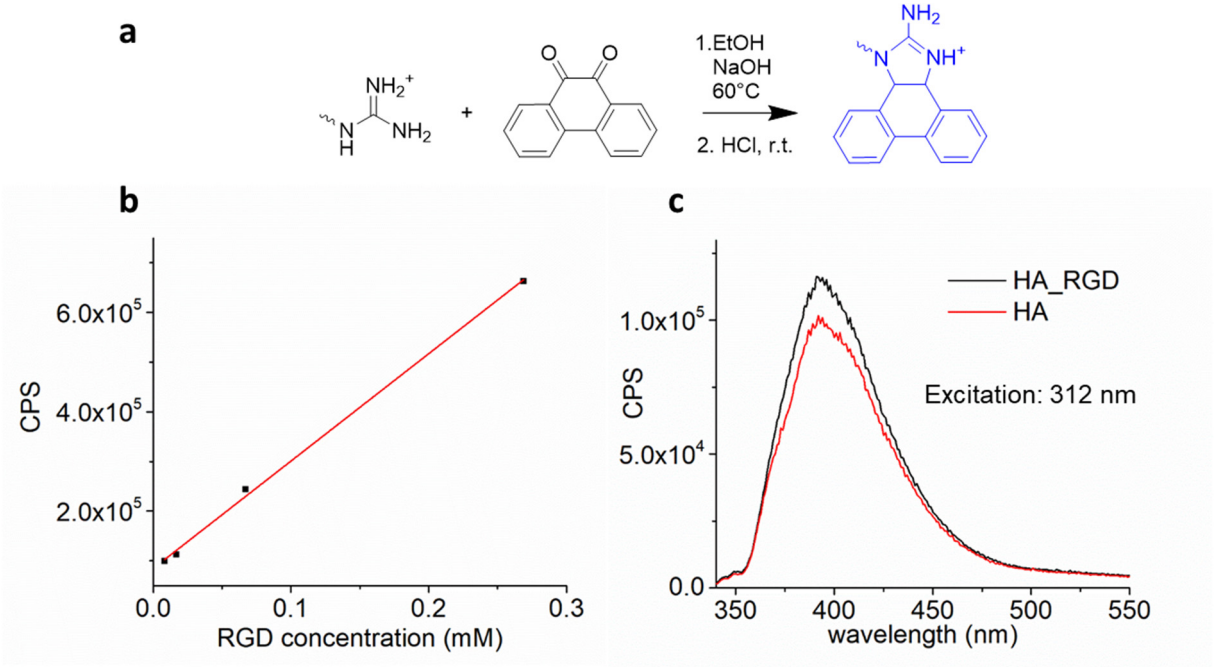

Figure 4.4: a) Reaction between the arginine lateral chain of the RGD peptide and the phenantroquinone to give the luminescent product. b) Calibration curve of the emission intensity at 392 nm of HA solutions containing different amount of RGD after reaction with the phenantroquinone. c) Emission spectra of the RGD functionalized HA (black) and bear HA (red) after reaction with the phenantroquinone. The spectra are recorded at room temperature, in water with excitation at 312 nm.

In a second approach, the peptide sequence GCGY*RGD*SPG was covalently linked to the methacrylate group of Me_HA (470 kDa or 1700 kDa) through the thiol lateral group of the cysteine unit (Figure 4.5a) following the procedure reported by Khetan *et al.*[14] The presence of flanking amino acids next to the RGD sequence, is expected to have a synergic effect on the peptide-integrin binding. The success of the functionalization was evaluated by the comparison of the concentration of free mercapto groups in solution (lateral chain of the cysteine unit)

before and after the thiol-Michael reaction with the Me_HA. 4,4'-Dithiodipyridine (DTDP) was used for the quantitative detection of thiols (Figure 4.5b, c). The use of DTDP, compared with the more common Ellman's reagent, was chosen because it has been reported to give more quantitative reactions with the substrates.[37] The 93% and the 89% of the peptide employed was covalently linked to the 1700 kDa and to the 470 kDa Me_HA respectively, corresponding to 1 unit every 24 of HA bearing the peptide. Compared to the coupling reaction on the carboxylic acid group (Figure 4.4), the thiol-Michael was found to give higher yield and to not be affected by the high MW of the HA polymer. Moreover, it was possible to use directly the functionalized polymer for the preparation of the hydrogel without the need of any purification step.

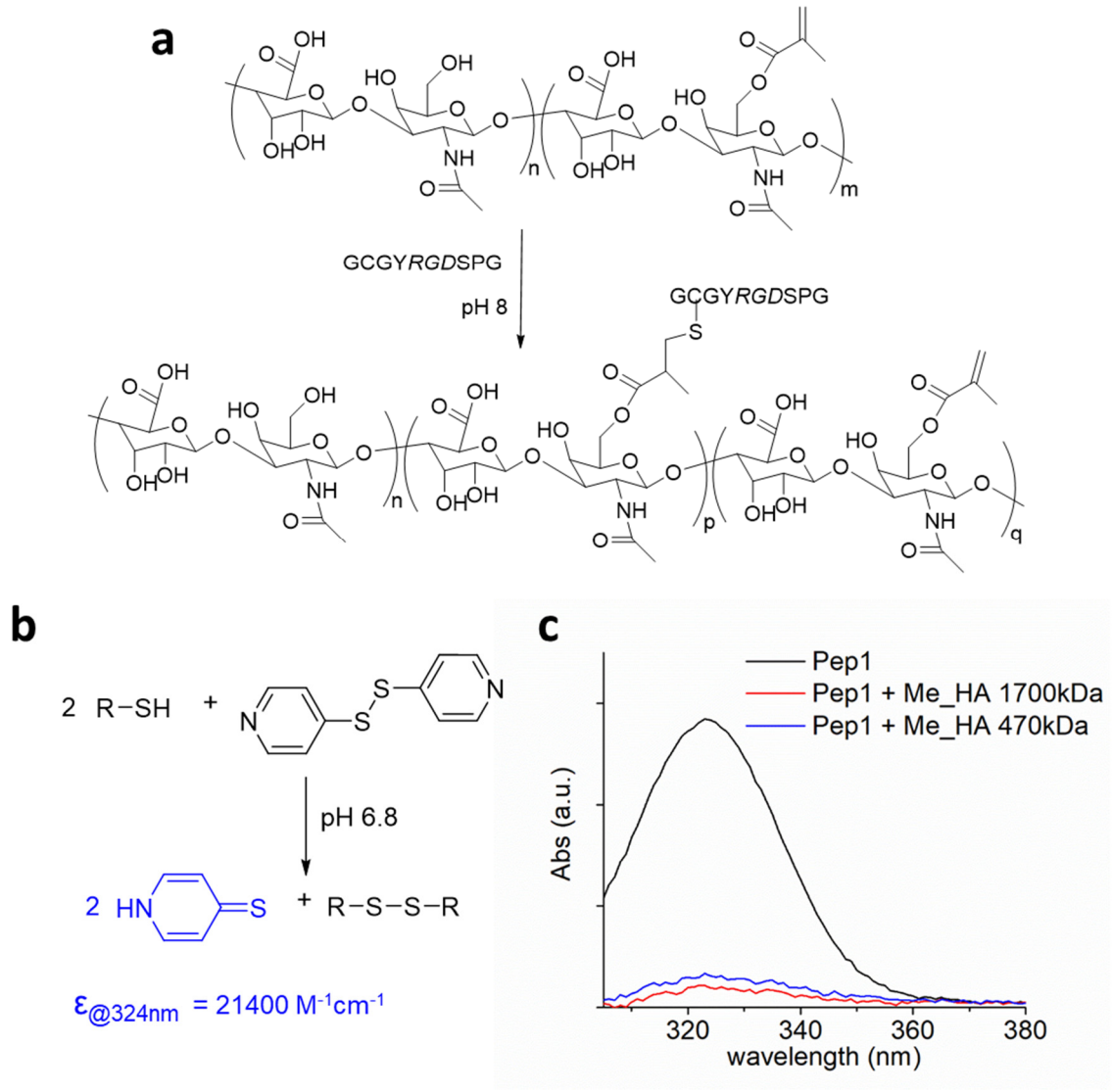

Figure 4.5: a) Thiol-Michael addition of the GCGY*RGD*SPG sequence to the methacrylate group of 470 kDa or 1700 kDa Me_HA. b) Colorimetric test for the quantification of the free thiols. c) Absorption spectra of the GCGY*RGD*SPG peptide before (black) and after reaction with the 1700 kDa (red) or the 470 kDa (blue) Me_HA.

4.2.2 Preparation of HA based hydrogels containing RGD

The RGD functionalized HA polymers were used for the preparation of the hydrogels containing RGD. The hydrogels are obtained as already described in Chapter 3 through the thiol-Michael reaction of Me_HA with dithiothreitol as cross-linker. Hydrogels prepared with 100 kDa HA are soft hydrogels (G'= 8 Pa, Figure 3.12) and they are therefore not suitable as substrates for cell culture. The 100 kDa HA functionalized with the RGD peptide was therefore mixed with 1700 kDa Me_HA in a ratio of 1:9 (the total concentration of HA in PBS is 1% by mass and the RGD concentration is 0.07 mM). The hydrogel obtained from the mixture is named as HA+HA100-RGD. The solutions of 1700 kDa and 470 kDa Me_HA functionalized with the GCGY*RGD*SPG sequence were used directly for the preparation of hydrogels by the direct addition of the dithiothreitol cross-linker. The final HA concentration is 1% by mass, the concentration of covalently linked RGD is 0.9 mM. Lei *et al.* studied the effect of the RGD concentration, in the 0.1–1.0 mM range, in HA based hydrogels. They showed that in all the concentration tested the cells had an elongated morphology; lower peptide concentrations within the range promoted the cell proliferation while higher concentrations enhanced the rate of cell migration.[38] Hydrogels based on HA (1700 kDa) containing gelatin were also prepared with the aim of evaluating the ability of the protein to induce cell adhesion to the material. Gelatin is a hydrolyzed form of collagen, characterized by good water solubility, biocompatibility and stable physical and chemical properties that make it a widely used material in tissue engineering.[39] In addition, the unfolded gelatin contains RGD strands and matrix metalloproteinase-sensitive degradation motifs in a more flexible conformation compared with the native helical form of collagen.[33,40] Gelatin, at physiological pH is positively charged, and when it is mixed with the negatively charged HA, it is expected to interact electrostatically forming an interpenetrated network (IPN). The gelatin containing hydrogel is prepared in PBS, the concentration of 1700 kDa Me_HA and gelatin are both 1% by mass. Table 4.1 summarizes the prepared hydrogels. The described hydrogels were prepared directly in the cylinder cup of the rheometer for the evaluation of the mechanical properties or in sterile well plates for the cell adhesion tests. The materials were incubated at 37 °C for 15 hours to ensure the completion of the cross-linking process before measuring the elastic (G') and viscous (G'') moduli as a function of the strain to determine the linear viscoelastic range (LVR) (Figure 4.6).

Table 4.1: Hydrogel scaffolds containing RGD for HeLa cell adhesion tests.

Sample name	HA MW (kDa)	G' (Pa)	RGD	[RGD] (mM)	RGD linking on Me_HA	MSN	Cell adhesion
HA	1700	100	-	-	-	-	-
HA+HA100-RGD	100 (10%)+ 1700 (90%)	470	RGD	0.07	-COOH	-	+-
HA-RGD	1700	95	GCGY*RGD*SPG	0.9	Me	-	+
HA470-RGD	470	800	GCGY*RGD*SPG	0.9	Me	-	+
HA+Gel	1700	360	Gelatin		IPN	-	-
HA MSN-RGD	1700	100	RGD	0.13	-	MSN-RGD	-
HA MSN-PEG-RGD	1700	100	RGD	0.07	-	MSN-PEG-RGD	-

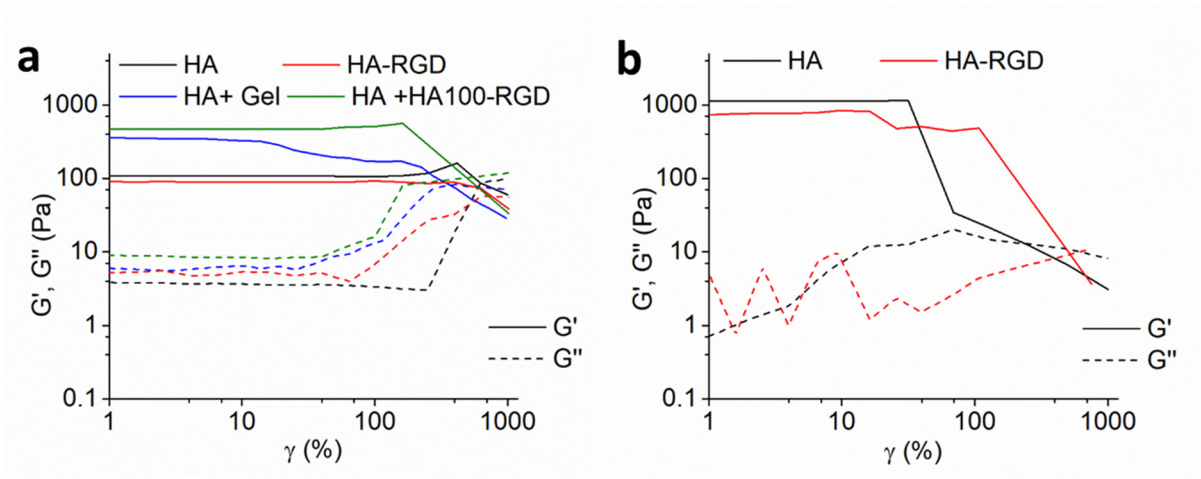

Figure 4.6: LVR of the HA based hydrogel scaffolds. a) Hydrogels obtained starting from 1700 kDa Me_HA before functionalization (black), after functionalization with GCGY*RGD*SPG (red), combined with the 100kDa HA-RGD (green) and forming an interpenetrated network with gelatin (blue). b) Hydrogels obtained starting from 470 kDa Me_HA before functionalization (black) and after functionalization with GCGY*RGD*SPG (red). Measuring geometry: coaxial cylinder (10 mm), 37 °C, *f*= 1 Hz.

The HA+HA100-RGD hydrogel is characterized by a higher G' modulus compared with the hydrogel obtained only from 1700 kDa HA (Figure 4.6a). The difference in the mechanical properties is attributed to the presence of the l00 kDa HA that is expected to have higher mobility in solution, compared with the 1700 kDa, to increase the degree of cross-linking of the system and to reduce the number of ineffective intra-molecular reactions. The introduction of the RGD peptide, through the thiol-Michael addition on the methacrylate groups, did not affect the mechanical properties of the hydrogels obtained either with the 1700 kDa (Figure 4.6a) or 470 kDa Me_HA (Figure 4.6b) (the observed difference is within the batch to batch variability).

This indicates that the functionalization of methacrylate groups with the peptide (4%) did not hindered the cross-linking process. The introduction of gelatin to form an interpenetrated network with HA gave an increase of the elastic modulus, attributed to the formation of electrostatic supramolecular bonds between the amino groups of the protein and the carboxylic groups of the glycosaminoglycan. The introduction of gelatin, however, significantly reduced the LVR of the material indicating a lower deformability of the scaffold.

In Chapter 3, the possibility to introduce mesoporous silica nanoparticles (MSN) with the function of biomolecule delivery system has been discussed. Herein we exploit the MSN for the introduction of the RGD peptide in the nanocomposite hydrogel. For the synthesis of the MSN, the reader is referred to Figure 3.17 in Chapter 3. The RGD peptide was grafted on the outer surface of MSN by RGD-silanes containing either a short alkyl chain (MSN-RGD) or a PEG chain (MSN-PEG-RGD) as spacer. In the preparation of MSN-RGD, the terminal amino group of the RGD was first reacted with (3-Isocyanatopropyl)triethoxysilane to obtain the RGD-silane (Scheme 4.2a). The obtained solution was then used to functionalize the particles to give MSN bearing the RGD groups (MSN-RGD) (Scheme 4.2b). In the preparation of MSN-PEG-RGD, the terminal amino group of the RGD was first reacted with silane-PEG-succinimide to give the RGD-PEG-silane (Scheme 4.2c). The obtained solution was used to functionalize the particles (Scheme 4.2d). The amount of RGD grafted on the surface of the particles was measured by colorimetric test, sensitive to the arginine lateral group as described in detail in the experimental section and as reported by Xu *et al.* (Figure 4.7).[36] The luminescence test indicated that the amount of RGD covalently linked on 1 mg of particles is $1.3 \cdot 10^{-4}$ mmol for the MSN-RGD and $5.0 \cdot 10^{-6}$ mmol for the MSN-PEG-RGD (Figure 4.7b).

Nanocomposite hydrogels containing the MSN-RGD or the MSN-PEG-RGD in 1 mg/mL concentration were prepared using the 1700 kDa Me_HA (1% wt/wt) as polymeric network. As already discussed in Chapter 3, the introduction of MSN in 1 mg/mL concentration in the hydrogel does not affect the mechanical properties of the material (Figure 3.22). The characteristics of the prepared RGD containing hydrogels are summarized in Table 4.1

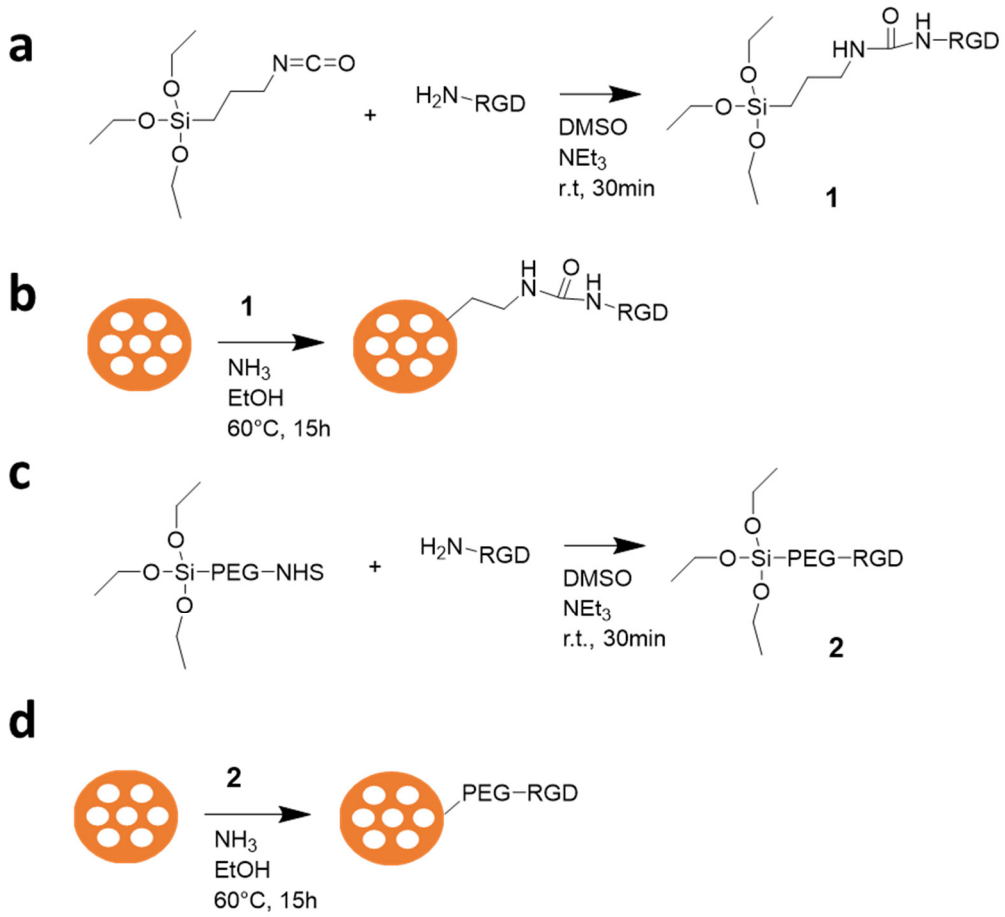

Scheme 4.2: a) Synthesis of the RGD silane containing a short alkyl chain as spacer. b) Functionalization of the MSN with RGD groups to give the MSN-RGD. c) Synthesis of the RGD silane containing a PEG chain as spacer. d) Functionalization of the MSN with RGD to give the MSN-PEG-RGD.

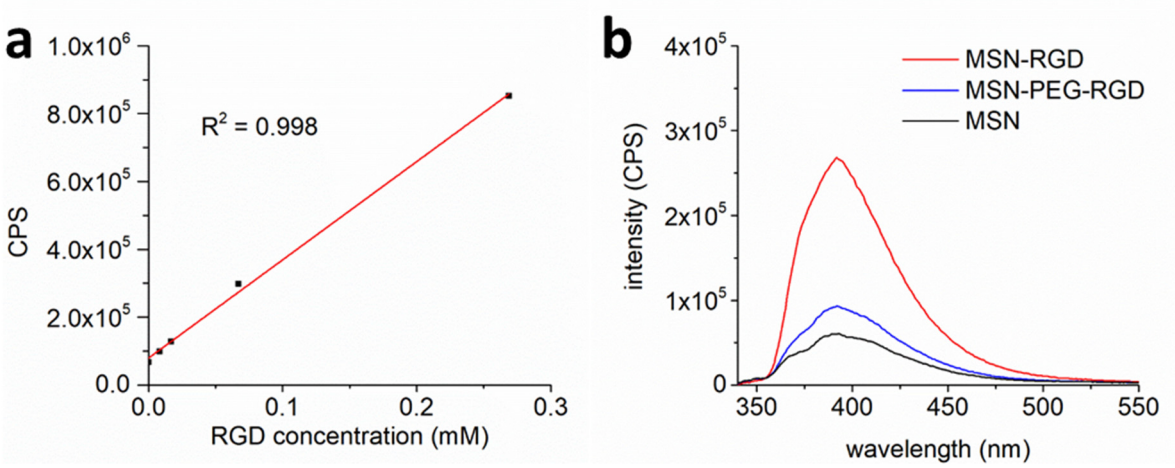

Figure 4.7: a) Calibration curve of the emission intensity at 392 nm of NaOH 2M solutions containing different amount of RGD after reaction with the phenantroquinone. b) Emission spectra of the MSN-RGD (red), the MSN-PEG-RGD (blue) and blank solution (black). The spectra are recorded at room temperature, in water with excitation at 312 nm.

4.2.3. Evaluation of the ability of the RGD containing hydrogel scaffolds to sustain cell adhesion

As previously discussed in this chapter, high MW HA interacts with cells in a multivalent manner and it hinders their adhesion to the material. In this paragraph, the effect on cell adhesion of the introduction of the integrin-binding RGD peptide or gelatin in HA hydrogels is discussed. The effect of the modification of the hydrogel on the interaction with cells is evaluated by looking at the morphology of HeLa cells, which are seeded on the surface of the material. In particular, an elongated morphology is expected when the cells interact effectively with the modified hydrogels through the integrin-RGD binding. HeLa cells were chosen as a model because they are human cells that belong to the epithelial class that plays a crucial role in wound healing.[41] Moreover, HeLa cells are characterized by the easiness of culture. After preparation, the hydrogel scaffolds were incubated overnight with Dulbecco's Modified Eagle Medium (DMEM) before seeding the cells. The ability of cells to adhere to the materials was monitored by microscopy for three days after cell seeding (Figures 4.8, 4.9, 4.10).

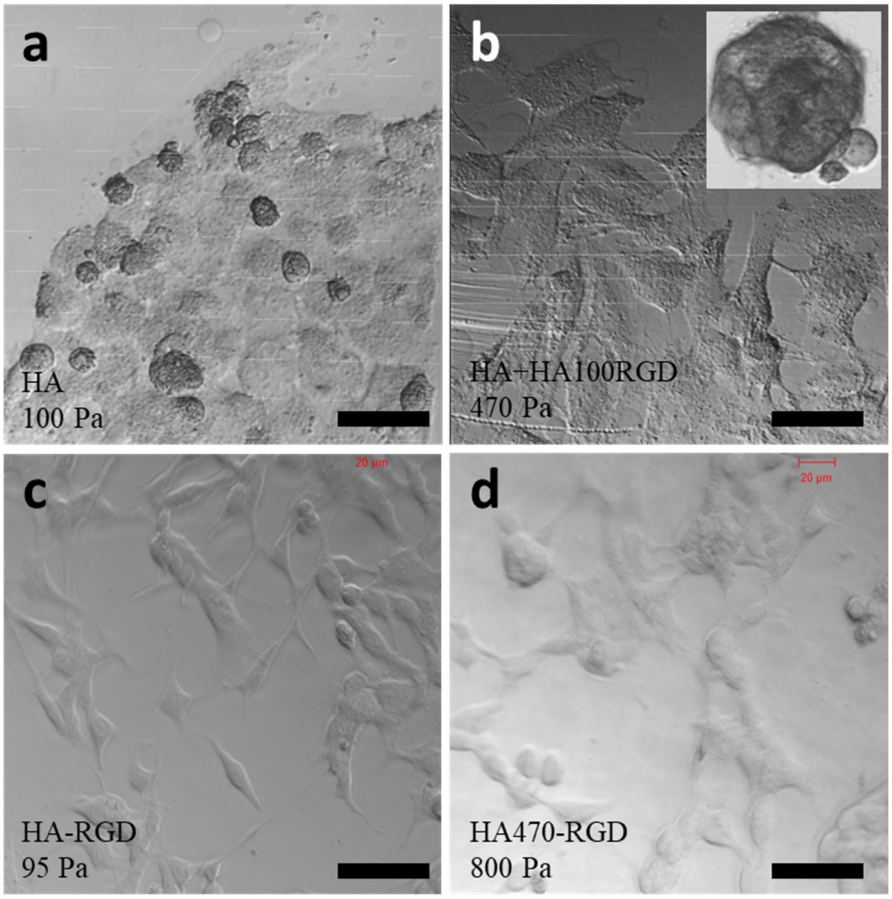

Figure 4.8: Microscopy imaging of the HeLa cells on the hydrogel scaffolds: a) HA, b) Ha+HA100-RGD, c) HA-RGD and d) HA470-RGD. The elastic moduli of the samples are reported. Scales bars: 50 µm.

In bare HA hydrogel, cells are partially attached to the material but they tend to form aggregates (Figure 4.8a). The introduction of the RGD peptide coupled on the 100 kDa Me_HA (sample HA+HA100-RGD) induced a partial cell adhesion with both elongated and round shaped cells found in the sample (Figure 4.8b). On the contrary, homogeneous cell adhesion was observed when the longer peptide sequence GCGY*RGD*SPG was linked either to the 1700 kDa Me_HA (sample HA-RGD) (Figures 4.8c and 4.9a) or to the 470 kDa Me_HA (sample HA470-RGD) (Figures 4.8d and 4.9b), despite the two scaffolds have significantly different mechanical properties ($G'_{HA\text{-}RGD}$: 95 Pa, $G'_{HA470\text{-}RGD}$: 800 Pa). The hydrogel with the RGD peptide grafted on the surface of the MSN through either the short alkyl chain or the PEG chain did not induce cell adhesion (Figure 4.10a). The IPN (gelatin 1% wt/wt) within the HA scaffold did not induce the binding of cells to the material, with the cells being round shaped (Figure 4.10b). A possible explanation of the negative result is that the introduction of gelatin in the hydrogel reduced its deformability (smaller LVR, Figure 4.6a) and consequently the possibility for cells to modulate the matrix.

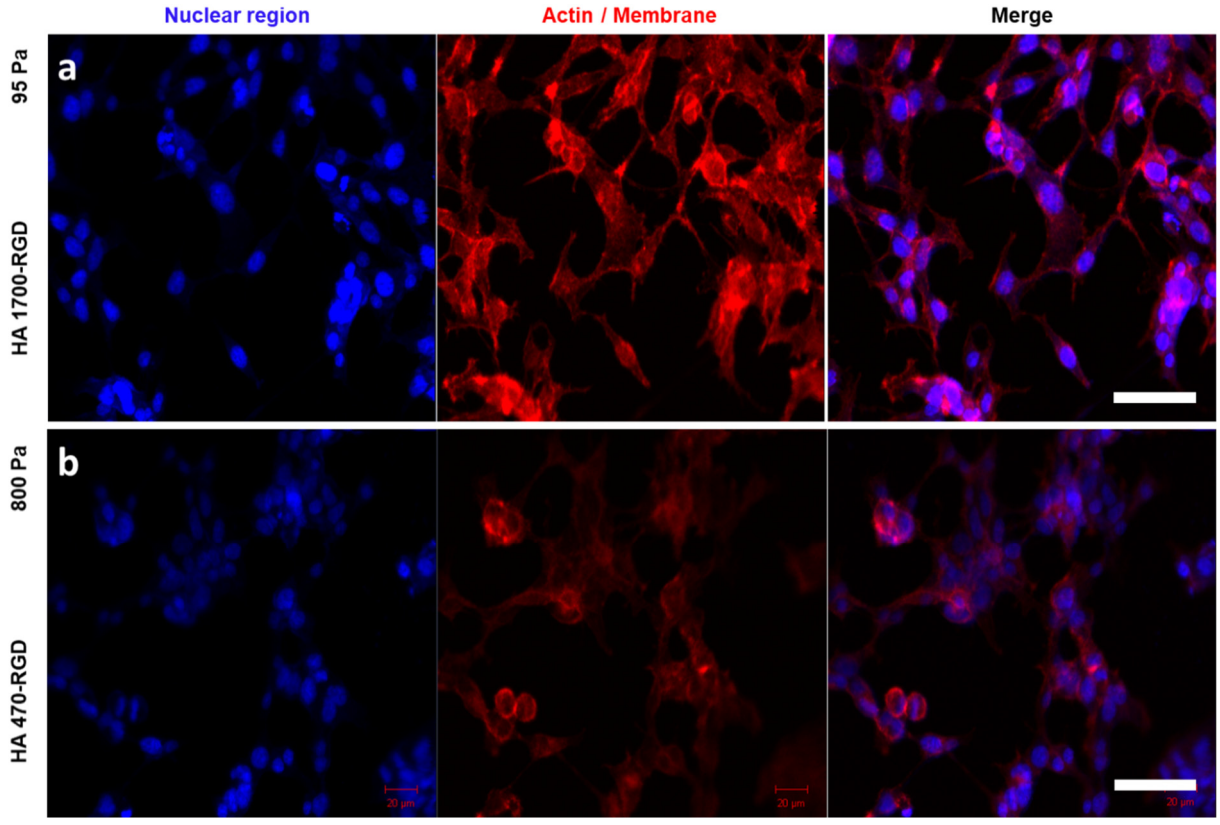

Figure 4.9: Confocal imaging of HeLa cells on the a) HA-RGD and b) HA470-RGD scaffolds. The nuclear regions are stained with 4',6-diamidino-2-phenylindole (DAPI) (blue) while the actin/membrane are stained with Phalloidin Alexa Fluor® 647 (red). The elastic moduli of the samples are reported. Scale bars: 50 μm.

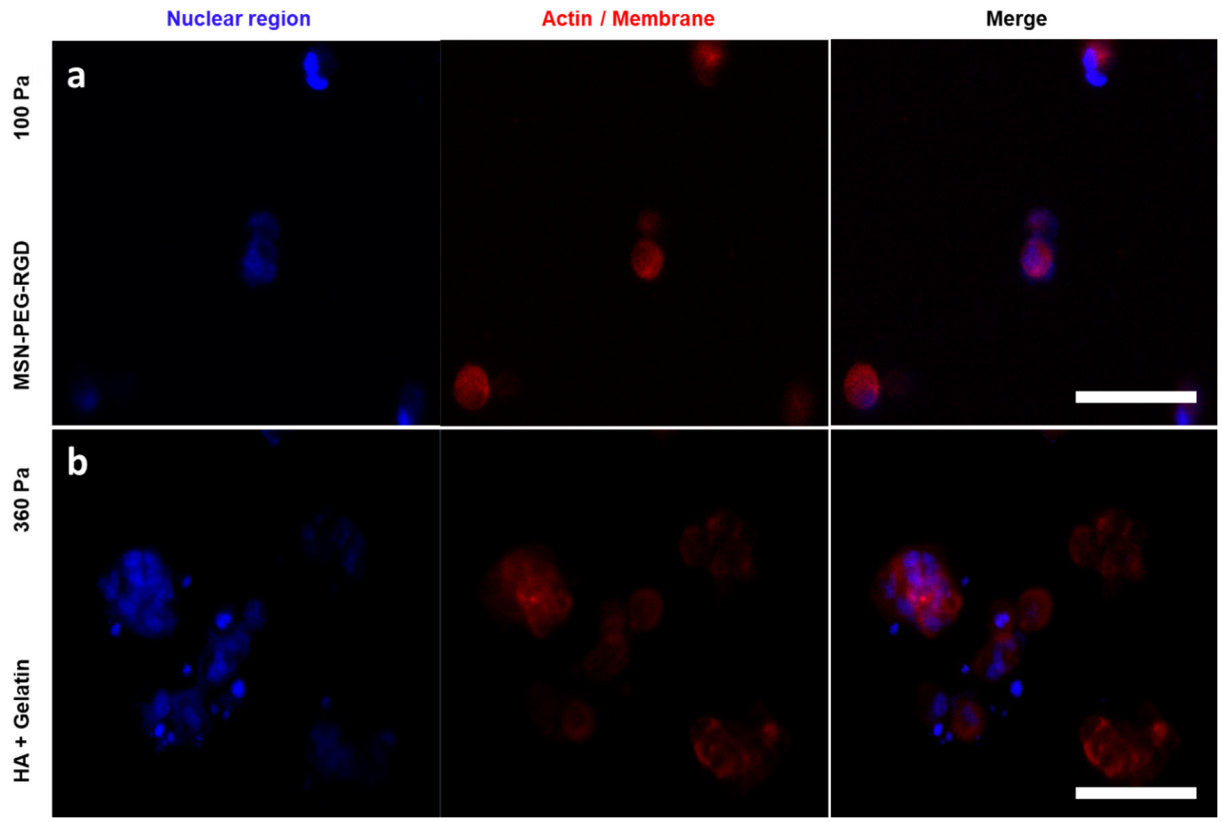

Figure 4.10: Confocal imaging of HeLa cells on the a) MSN-PEG.RGD and b) HA+Gelatin hydrogel scaffolds. The nuclear regions are stained with DAPI (blue) while the actin/membrane are stained with Phalloidin Alexa Fluor® 647 (red). Scale bars: 50 µm.

The experiments suggest that the adhesion of HeLa cells to HA hydrogels depends on the RGD-containing peptide sequence; better results are obtained in presence of RGD sequence with flanking amino acids (GCGY*RGD*SPG) as previously reported.[34] Also, the use of the GCGY*RGD*SPG, linked to the Me_HA through the thiol-Michael addition, allowed to have an higher RGD concentration in the material (Table 4.1), which probably contributed to promote the cell adhesion. In regard to the mechanical properties of the scaffolds, the G' modulus of the hydrogels under study was not a key parameter in determining the cell ability to adhere. In fact, materials with elastic modulus of 95 Pa (HA 1700-RGD) or 800 Pa (HA 470-RGD) were found to induce cell adhesion while the cells seeded on other materials with elastic modulus within this range (e.g. MSN-PEG-RGD) were round shaped. On the contrary, the deformability of the material, measured as LVR, is thought to play a role in the interaction of the material with cells. In fact, the introduction of gelatin in the scaffold reduced the LVR and hindered the cell adhesion also compared with the hydrogel made of bare HA.

4.2.4. Effect of HA oligomers on the ability of hydrogel scaffolds to sustain cell adhesion

A different approach to induce cell adhesion to the HA based hydrogel consists in the incorporation in the material of HA oligomers in the 6-20 kDa MW range that, on the contrary of high MW HA, interact with the CD44 receptor in a monovalent manner stimulating cell signaling cascades.[28,29]

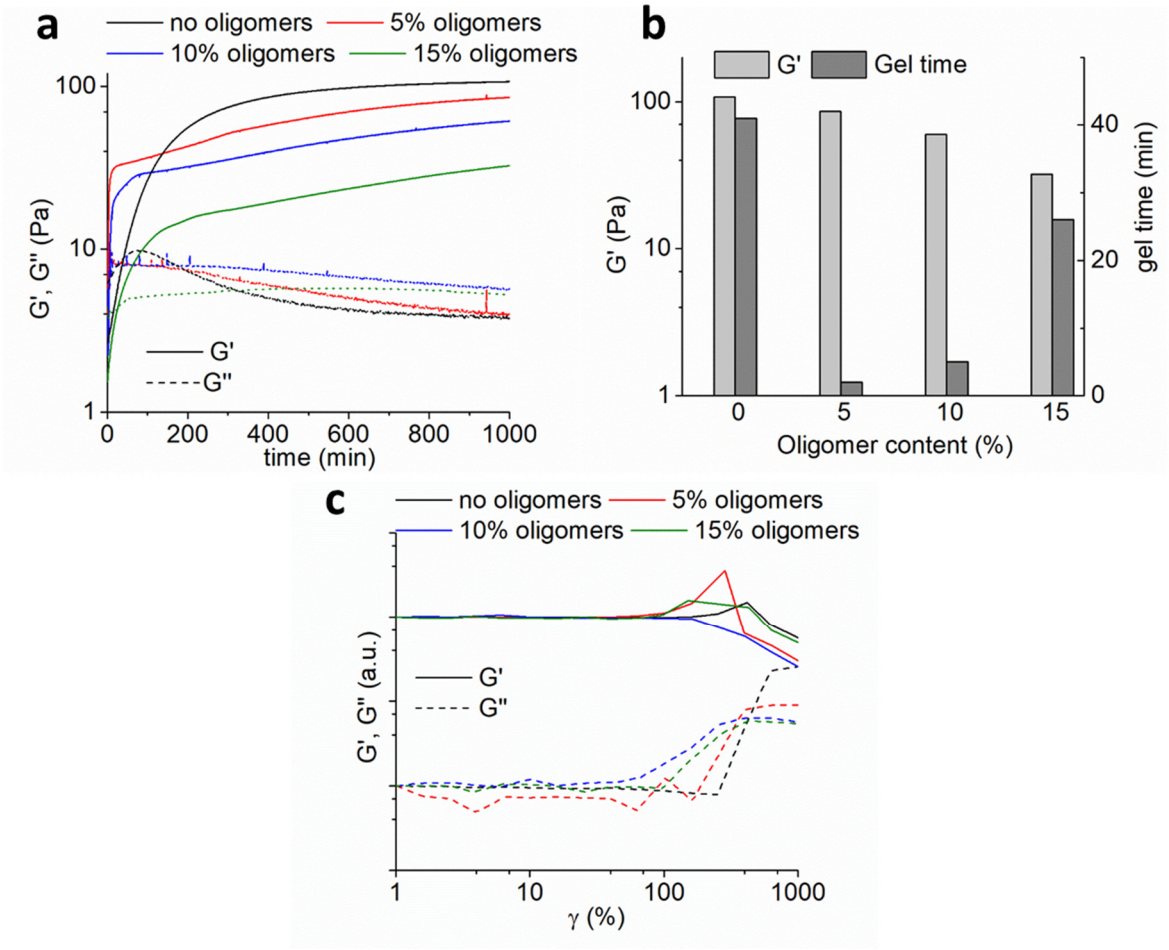

Figure 4.11: Mechanical properties of the HA based hydrogels containing different percentages of 5 kDa HA oligomers. a) Kinetic of hydrogel formation. b) Effect of the oligomers on the elastic modulus of the scaffolds and on the gelation time. c) LVR of the hydrogels. 0% oligomers (black), 5% oligomers (red), 10% oligomers (blue) and 15% oligomers (green). Measuring geometry: coaxial cylinder (10 mm diameter), T= 37 °C, f= 1 Hz, γ= 5%.

HA oligomers of 5 kDa were functionalized with methacrylate groups through the same procedure reported in Chapter 3 (Scheme 3.1) and combined with 1700 kDa Me_HA in different percentages (5%, 10% or 15%) to prepare the hydrogel scaffolds. In presence of the oligomers, the process of hydrogel formation is faster, with the 5% concentration (the lowest amount tested) giving the biggest effect (Figure 4.11a, b). This is attributed to the high mobility

of the oligomers in solution, which act as connectors between the HA polymers, promoting the inter-chain cross-linking process and reducing the occurrence of intra-molecular bonding. The increase of the oligomers concentration from 5% to 15% implied the decrease of the concentration of the 1700 kDa HA, and consequently the slower kinetic and the lower elastic modulus of the material as discussed in Chapter 3 (Figure 3.12). The LVR was not affected by the introduction of oligomers in the scaffold (Figure 4.11c).

In order to evaluate the ability of the scaffolds with different oligomer contents to sustain HeLa cell adhesion, the prepared materials were incubated with DMEM overnight before seeding the cells. After three days of incubation the cells were fixed and stained (see experimental section) for confocal microscopy imaging (Figure 4.12). The introduction of oligomers with the concentration of 5% (Figure 4.12a) induced cell adhesion with a more uniform cell spreading observed when the oligomer content was further increased to 10% (Figure 4.12b). Higher oligomer concentration (15%), on the contrary, gave the opposite effect, as the cells were round shaped and aggregated (Figure 4.12c), probably resulting from a significant decrease of the elastic modulus of the material (G': 32 Pa) (Figure 4.11b). The use of HA oligomers in the preparation of cell adhesive hydrogels is an interesting alternative to the incorporation of RGD-containing peptide sequences that are generally expensive, and that require an extra step in the preparation of the materials. Moreover, thinking about *in vivo* applications, the ability of HA oligomers to induce cell adhesion opens the possibility to employ hydrogels made of high MW HA without introducing any modification, since the naturally present hyaluronidase enzymes (Hhase) generate, by hydrolysis, progressively smaller chains of HA. The role of oligomers in the cell-scaffold interaction could explain the improved fistula cicatrization obtained with the use of the 1700 kDa HA based hydrogel reported in Chapter 3. In addition, the progressive enzymatic degradation of the implanted material creates physical space which is fundamental for the new tissue regeneration.

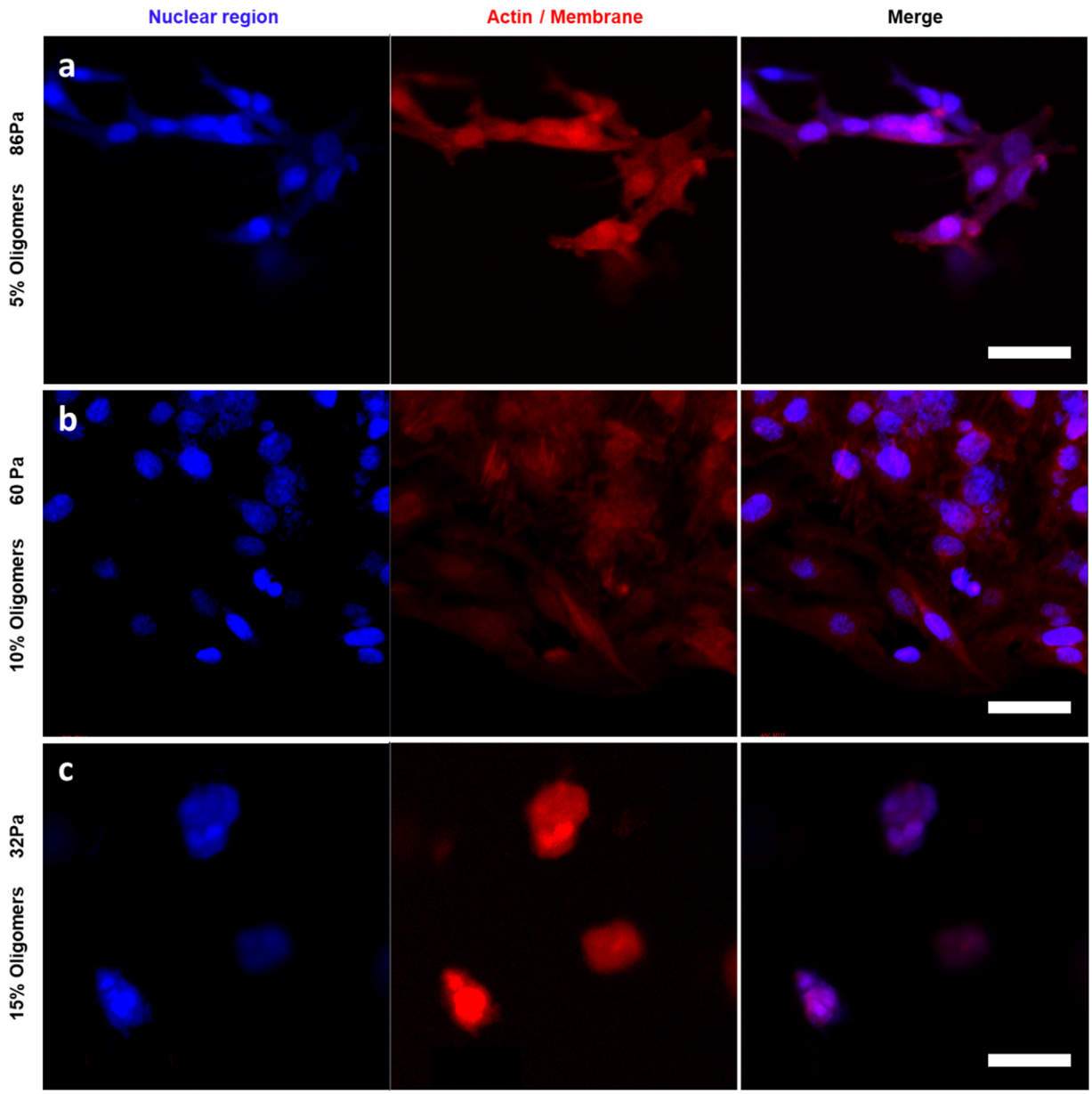

Figure 4.12: Confocal imaging of HeLa cells on the surface of HA hydrogels containing a) 5% oligomers, b) 10% oligomers, c) 15% oligomers. In blue the cellular nucleus stained with DAPI, in red the cellular membrane stained with Phalloidin Alexa Fluor™ 647. Scale bars: 50 µm.

The possibility of reproducing *in vitro* the generation of HA oligomers by the Hhase degradation of HA hydrogels to give a cell adhesive material was investigated. First, the degradation kinetic of the HA scaffold immersed in enzyme solutions was determined (Figure 4.13a, b), at concentrations within the range found at physiological conditions (0.0059 U/mL in human plasma to 38.5 U/mL in human ovaries),[42] with the aim of selecting the suitable incubation times for the cell adhesion experiments. When the scaffolds are soaked in PBS (control), a mass increase is observed due to the swelling of the material in the first two days,

followed by a reduction of the mass associated to the release of non-covalently linked molecules from the hydrogel. The presence of Hhase in 2.5 U/mL concentration brought to the total degradation of the scaffold in 3 days, while the material was completely consumed in 2 days by Hhase of 12.5 U/mL or 25 U/mL. For the cell adhesion experiments, a partial degradation of the materials was desired (Figure 4.13c); the scaffolds were therefore incubated for 24 h with 2.5 U/mL Hhase to obtain a 30% mass loss or for 8h or 24h with 12.5 U/mL or 25 U/mL (Figure 4.13b, c).

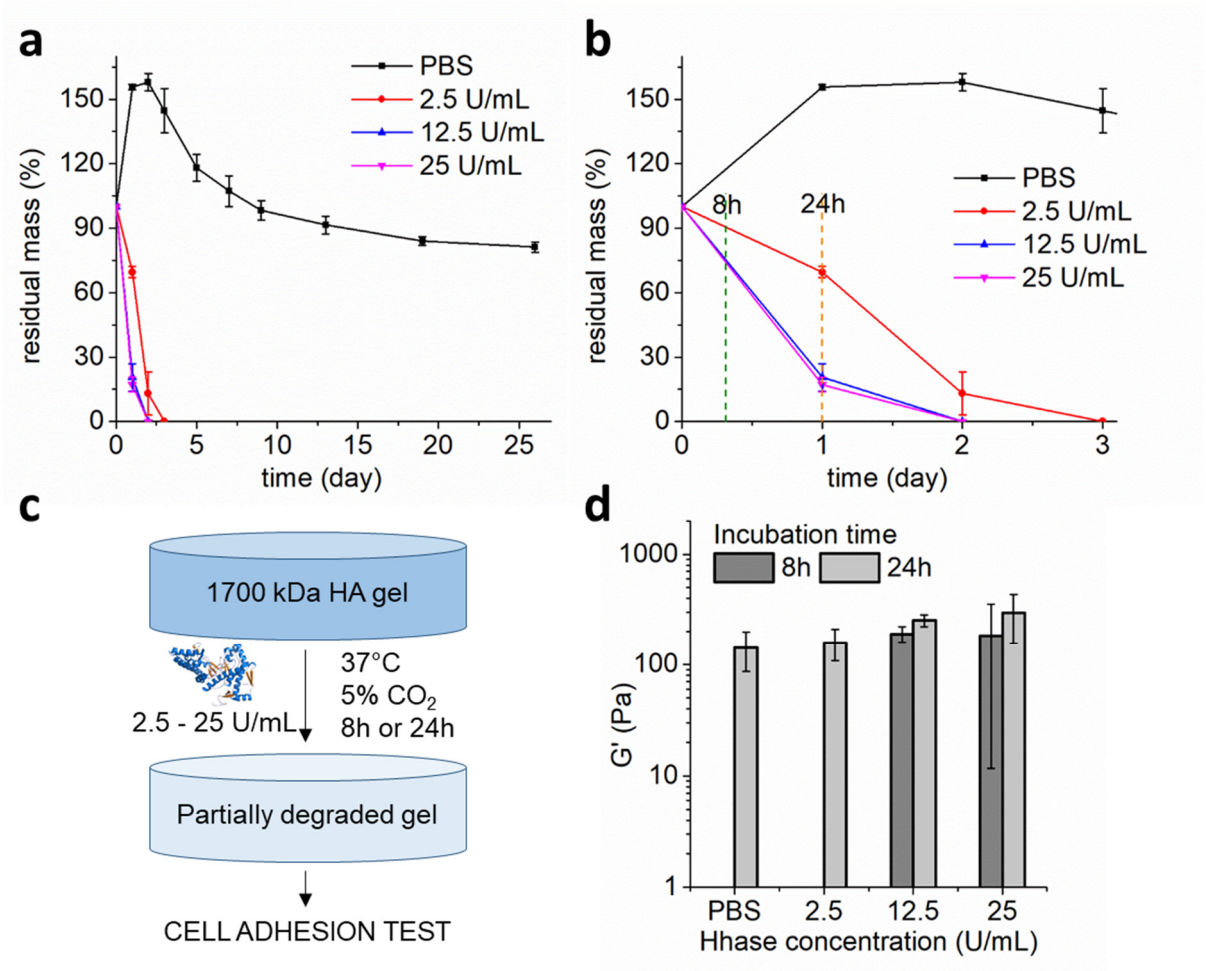

Figure 4.13: Treatment of the 1700 kDa HA based hydrogel scaffold with Hhase. a) Kinetic of degradation of the hydrogel immersed in Hhase solutions at different concentrations: PBS control (black), 2.5 U/mL (red), 12.5 U/mL (blue) and 25 U/mL (pink) (n=3). b) Enlargement between day 0 and day 3 of the kinetic profile. The dashed lines at 8 h and 24 h indicate the time points at which the cell adhesion tests were carried. c) Scheme of the enzymatic treatment on the surface of the hydrogel scaffolds prior to rheological measurements and cell adhesion tests. d) Elastic modulus of the hydrogel scaffolds after incubation with the enzyme at different concentrations for 8 h or 24 h (n=3). Measuring geometry: plate to plate (diameter 8 mm), f = 1 Hz, γ = 5%, gap = 0.5 mm.

Hydrogel scaffolds based on 1700kDa HA were prepared directly in 12- (96-) well plates and treated with the enzymatic solutions on the surface before the rheological measure (cell adhesion tests) as displayed in Figure 4.13c. It is necessary to underline that in this latter sample preparation, the Hhase solutions were dropped on the top surfaces of the hydrogels and that therefore the degradation of the material is expected to be lower compared with what observed during the kinetic experiment where the scaffolds were soaked in the enzyme solutions. The elastic modulus of the scaffolds after incubation in PBS or in the enzyme solutions were comparable to each other (Figure 4.13d) and similar to the ones of the hydrogels containing 5% or 10% of oligomers (Figure 4.11b) that induced cell adhesion (Figure 4.12a, b). After the enzymatic treatment, the samples were washed with PBS (3x) and covered with DMEM for 24 h prior to seed HeLa cells. The cells on the material were incubated for three days (37 °C, 5% CO_2) replacing the culture medium daily. HeLa cells were then fixed, stained (see experimental section) and observed at the confocal microscope (Figure 4.14). In all the observed samples the cells were round shaped and aggregated suggesting that the activity of the Hhase did not generate oligomers in suitable concentration and molecular weight to promote cell adhesion. Figure 4.14 shows selected and representative examples of the analyzed materials. This experiment constituted a trial to reproduce *in vitro* the degradation of HA based materials that occurs naturally in mammals by the activity of the Hhase enzymes. However, the several parameters involved *in vivo* make the accurate replication of the physiological environment difficult. In fact, *in vivo*, after a first degradation step that generates polymers of around 20 kDa, the hydrolysis of HA continues in the lysosomes where the fragments are internalized and transported.[26] Therefore, the negative result of this experiment should not be considered indicative of the inability of cells to proliferate *in vivo* in HA based hydrogels. For example, Liu *et al.* showed that the key parameter to obtain the population of a HA based scaffold *in vivo* is the presence of large pores in the material rather than the existence of a biochemical interaction between the polymeric network and cells.[43]

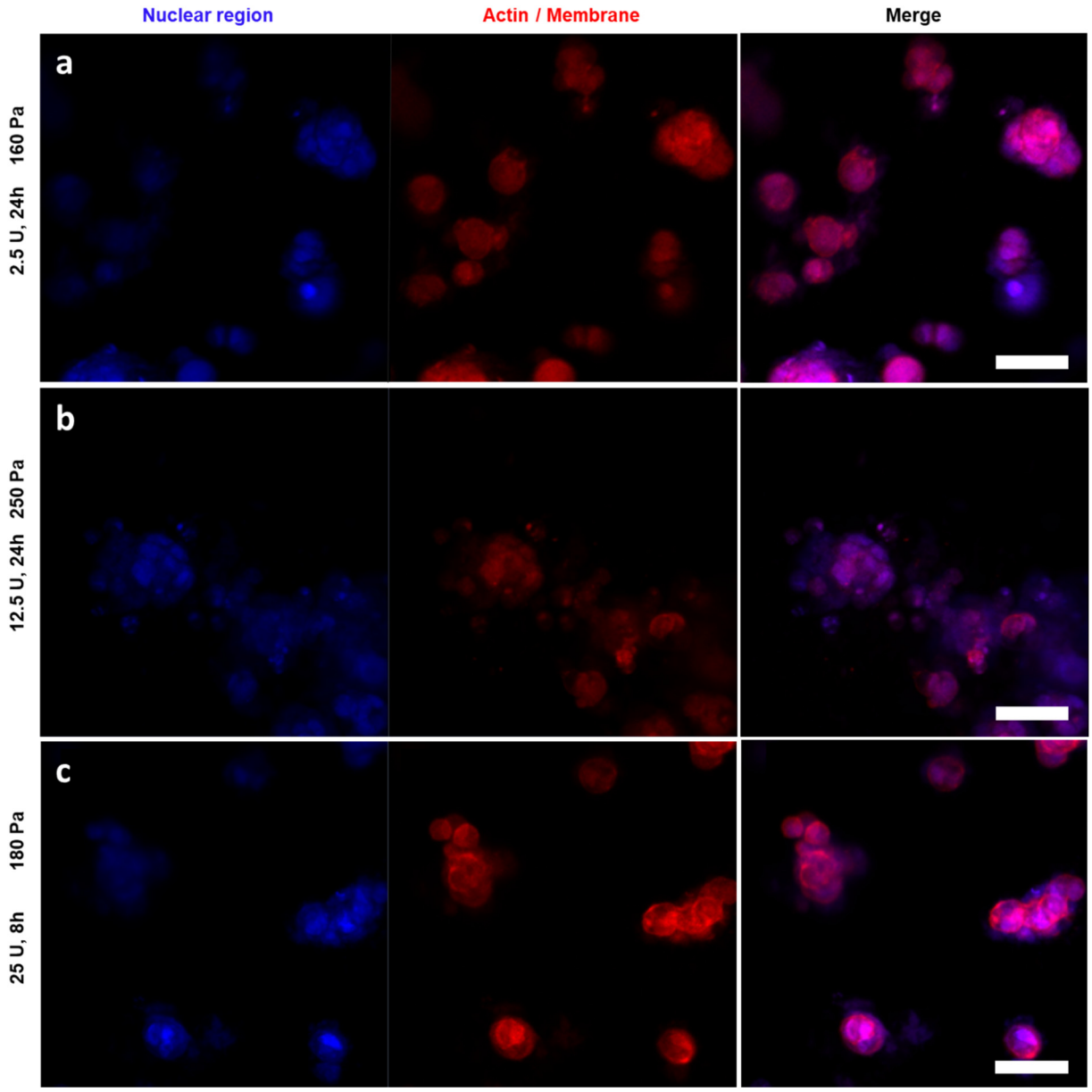

Figure 4.14: Confocal imaging of HeLa cells on the surface of HA hydrogels a) treated with 2.5 U/mL Hhase for 24 h , b) treated with 12.5 U/mL Hhase for 24 h and c) treated with 25 U/mL Hhase for 8 h. In blue the cellular nucleus stained with DAPI, in red the cellular membrane stained with Alexa Fluor™ 647. Scale bars: 50 µm.

4.3. Conclusions

The high MW HA used in the preparation of hydrogels interacts with the CD44 transmembrane receptor in a multivalent manner hindering the cellular adhesion to the material and consequently their ability to proliferate in the scaffold. In this chapter, different possible modifications of the HA based hydrogels to introduce integrin-binding molecules or induce CD44-binding have been investigated. In particular, the functionalization of the polymer with

RGD containing peptides, the incorporation of gelatin to form an interpenetrated network and the combination of HA oligomers within the high MW HA matrix have been studied. Among the different methods evaluated, the incorporation of the peptide sequence GCGY*RGD*SPG in scaffolds with elastic modulus ranging from 95 Pa up to 800 Pa gave homogeneous HeLa cell adhesion suggesting that the softness of the material under study does not affect the ability of cells to interact with the polymeric matrix. A different successful approach consisted in the incorporation of HA oligomers in the scaffold. This result is of particular interest because it suggests that high MW HA scaffolds implanted *in vivo* can be populated by cells owing to the natural presence of the hyaluronidase enzymes that progressively degrade the polymeric network generating oligomers, which can promote the colonization of the material by cells. The experiments done with HeLa cells reported in this chapter constitute preliminary results; future work will consist in the study of the ability of mesenchymal stem cells (MSC) to adhere and eventually differentiate in the hydrogel functionalized with GCGY*RGD*SPG or containing HA oligomers. We think that the successful modification of the injectable HA based hydrogels to sustain MSC proliferation would open to different interesting applications in regenerative medicine.

4.4. Acknowledgements

I would like to thank Dr. Yang Zhang and Dr. Bianca Martins Estevao for the help with the culture and staining of cells.

4.5. Experimental section

4.5.1. Chemicals and materials

5 kDa HA (4659 Da Hyaluronic acid sodium salt) was purchased from abcr GmbH, 100 kDa HA (80-100 kDa Hyaluronic acid sodium salt) was purchased from abcr GmbH, 470 kDa HA (intrinsic viscosity 1.02 m^3kg^{-1}) was purchased from CONTIPRO, 1700 kDa HA was purchased from HTL Biotechnology and provided by Qventis GmbH. *N*-Hydroxysuccinimide (NHS) was purchased from ABCR. Dithiothreitol, 1-Ethyl-3-(3-dimethylaminopropyl)carbodiimide (EDC), 9,10-phenanthrenequinone, (3-Isocyanatopropyl)triethoxysilane, 4,4'-dithiodipytidine (DTDP), ethylenediaminetetraacetic acid (EDTA), Gelatin from bovine skin type B, 4',6-diamidino-2-phenylindole (DAPI) and hyaluronidase from bovine testes (Type IV-S, 750-3000

U/mg) were purchased from Sigma Aldrich. Silane-PEG-NHS (Mn 5000 Da) was purchased from Nanocs. Dulbecco's Modified Eagle Medium (DMEM) was purchased from Life Technologies. Phalloidin Alexa Fluor® 647 was purchased from Thermo Fisher Scientific. HeLa cells were purchased from ATCC. The GCGY*RGD*SPG peptide (the italic indicates the integrin binding sequence) was kindly provided by the Mario Negri institute.

4.5.2. RGD coupling on the carboxylic group of HA

250 mg of 100 kDa Me_HA were dissolved in 20 mL of PBS (0.1 M, pH 5.7) in a round bottom flask followed by the addition of 5 mg of EDC (0.026 mmol) and 3 mg of NHS (0.026 mmol); the solution was then stirred for 30 min at room temperature. 20 mg (0.058 mmol) of RGD were then added and the solution was stirred overnight at room temperature. The product was collected by precipitation in ethanol and it was purified by dialysis in distilled water for three days (6-8 kDa, regenerated cellulose membrane). The sample was freeze-dried for two days to obtain a white solid.

4.5.3. Quantification of the coupled RGD

The RGD-HA polymer was dissolved in distilled water with a concentration of 1 mg/mL and 200 µL of the solution were mixed with 600 µL of 9,10-phenanthrenequinone (150 µM in ethanol) and 100 µL of NaOH (2 M). The mixture was stirred at 60 °C for 3 hours and then 900 µL of 1.2 M HCl were added. The solution was then kept in the dark for 1 hour before the spectroscopy measurements. The samples are excited at 312 nm and the emission is measured in the range 350-570 nm. HA solutions (1 mg/mL) containing RGD in concentration range 0.008-0.27 mM were used for the calibration curve.

4.5.4. Thiol-Michael addition of the GCGY*RGD*SPG peptide on the methacrylate group of HA

To a solution of 1% wt/wt Me_HA (1700 kDa or 470 kDa) in PBS (pH 8), the GCGY*RGD*SPG peptide was added with a final concentration of 1 mM. The solution was stirred at 37 °C for 24 hours. The functionalized polymers were used for the preparation of hydrogels without any further purification.

4.5.5. Quantification of the GCGY*RGD*SPG peptide linked to HA

20 µL of the analyte solution (GCGY*RGD*SPG functionalized HA) were added to 2 mL of the buffer solution (100 mM KH_2PO_4, 0.2 mM EDTA, adjusted to pH 6.8 with NaOH), followed by mixing with 50 µL of 4,4'-dithiodipyridine (DTDP) solution (4mM DTDP in 12 mM HCl). The solutions were stirred for 5 minutes at room temperature before recording the absorption

spectra in the range 400-300 nm (1 nm of interval), against a water reference. The blank consisted of a mixture including 20 µL of PBS (pH 8), 2mL of buffer solution and 50 µL of DTDP solution. The spectrum of the blank was subtracted to the spectra of the analyte solutions.

4.5.6. MSN functionalization with RGD groups (MSN-RGD)

RGD (0.10 mmol) and (3-Isocyanatopropyl)triethoxysilane (0.09 mmol) were dissolved in 3 mL of DMSO in presence of 0.18 mmol of triethylamine and stirred for 30 min at room temperature; the completion of the reaction was then verified by LC-MS (peak at 594 m/z (product) and peak at 797 m/z (product+2x triethylamine)). Subsequently this solution and 22 µL of NH_3 (28% aqueous solution) were added to a suspension of MSN (30 mg) in 15 mL ethanol. The mixture was stirred at 60 °C overnight. The particles were collected by centrifugation (35 krpm, 15 min, 20 °C), washed three times with ethanol and dried under vacuum.

4.5.7. MSN functionalization with PEG-RGD (MSN-PEG-RGD)

RGD (0.015 mmol) and silane-PEG-succinimide (Mn 5000 Da) (0.01 mmol) were dissolved in 1 mL of DMSO in presence of 0.02 mmol of triethylamine and stirred 1 hour at room temperature. Subsequently this solution and 30 µL of NH_3 (28% aqueous solution) were added to a suspension of MSN (30 mg) in 15 mL ethanol. The mixture was stirred at 60 °C overnight. The particles were collected by centrifugation (35 krpm, 15 min, 20 °C), washed three times with ethanol and dried under vacuum.

4.5.8. Quantification of the RGD grafted on MSN

0.5 mg of RGD functionalized MSN were dispersed in 1mL of NaOH 2M for one hour at room temperature to dissolve the particles. 200 µL of the solution were mixed with 600 µL of 9,10-phenanthrenequinone (150 µM in ethanol) and 100 µL of 2 M NaOH. The mixture was stirred at 60 °C for 3 hours and then 900 µL of 1.2 M HCl were added. The solution was then kept in the dark for 1 hour before the spectroscopy measurements. The samples are excited at 312 nm and the emission is measured in the range 350-570 nm. NaOH (2M) solution containing RGD in concentration range 0.008-0.27 mM were used for the calibration curve.

4.5.9. Hydrogel preparation

The hydrogels reported in this chapter have been prepared from a mixture of methacrylated HA (1% wt) in PBS (pH 7.4, 0.01 M) (if not differently specified) and dithiothreitol in stoichiometric amount as cross-linker. For the measurement of the kinetic of gelation and of the

linear viscoelastic range, after the addition of the cross-linker, the solutions were immediately transferred to the cup of the rheometer. The hydrogels for the cell adhesion experiments were prepared in sterile 96 well plates by using 100 µL of each precursor solution and being incubated at 37 °C for at least 18 h. Each material for the *in vitro* tests was prepared in duplicate. The scaffolds for the evaluation of the mechanical properties of the material after enzymatic degradation were prepared in triplicate in sterile 24 well plates by using 400 µL of 1700 kDa Me_HA solution (1%, wt) and being incubated at 37°C for at least 18 h. In the preparation of the nanocomposite hydrogels, MSN were added to the Me_HA solution (1 mg/mL) and stirred overnight at 37 °C prior to the addition of the molecular cross-linker.

4.5.10. Evaluation of the mechanical properties of the HA hydrogel functionalized with GCGY*RGD*SPG

The functionalization of Me_HA with GCGY*RGD*SPG through the thiol-Michael addition leaded to a partial saturation (~ 4%) of the methacrylate groups that constitute the cross-linking sites. In the evaluation of the effect of the partial saturation on the mechanical properties of the material, the GCGY*RGD*SPG peptide was replaced by the more economic cysteine (the amino acid of the peptide that is involved in the thiol-Michael addition) to obtain Me_HA with the same degree of substitution. For this purpose, a solution of Me_HA (pH 8, 1% wt) were let react with cysteine in 1 mM concentration for 24 h at 37 °C before using the functionalized polymer for the rheological characterization.

4.5.11. HeLa cell adhesion tests

The hydrogel scaffolds were covered with 100 µL of DMEM and incubated at 37 °C overnight before the seeding of 10k HeLa cells. The culture medium was replaced daily and after three days the cells were fixed on top of the hydrogel samples with 4% paraformaldehyde for 15 minutes. Samples were then washed three times with PBS and kept in Triton X-100 (0.1 % in PBS) for 10 minutes and then in 1% bovine serum albumin (BSA) in PBS for 20 min. Cells were stained with Phalloidin Alexa Fluor® 647 for actin/membrane staining for 20 min in the dark at room temperature following the manufacturer protocol, then washed three times with PBS. The nuclear region was stained with DAPI (300 nM) for 5 minutes and then the material was washed again with PBS three times. DAPI was excited at 405 nm, while with Phalloidin Alexa Fluor® 647 was excited at 650 nm during confocal imaging.

4.5.12. Kinetic of hydrogel enzymatic degradation

The hyaluronidase used for the experiments contains 750-3000 U/mg; all the concentration of enzyme reported in this chapter are intervals indicated, for simplicity, as the lowest content in units: 2.5 U/mL represent 2.5-10 U/mL, 12.5 U/mL stays for 12.5-50 U/mL and 25 U/mL indicates 25-100 U/mL. A hydrogel scaffold made of 1700 kDa Me_HA (1% wt concentration) was prepared and cut in pieces of 150-300 mg each. The hydrogel pieces were weighted and incubated at 37 °C in 2 mL of PBS or Hhase solution with concentration of 2.5 U/mL, 12.5 U/mL, or 25 U/mL. At each measuring time, the mass of the samples (three for each experimental condition) was measured and the solutions were replaced with fresh ones.

4.5.13. Instruments

The rheological measurements were performed with a Thermo Fisher HAAKE Mars 40 rheometer equipped with a Peltier temperature module. The measuring geometry and the parameter used are specified in each experiment. Thermogravimetric Analysis were done on a Perkin Elmer TGA 4000 Instrument machine under N_2/O_2 flux. The samples were warmed and kept at 130 °C for 20 min to remove all the adsorbed solvent then heated up to 800 °C at 10 °C/min rate. Confocal imaging was performed with a Zeiss LSM 710 confocal microscope system equipped with a 10x magnification, numerical aperture 0.3 of Zeiss LCI Plan-NEOFLUAR objective lens (Zeiss GmbH, Germany).

4.6. References

1. Tan, J., Wu, W., Xu, X., Liao, L., Zheng, F., *et al.* Induction Therapy With Autologous Mesenchymal Stem Cells in Living-Related Kidney Transplants: A Randomized Controlled Trial. *JAMA* 307, 1169–1177 (2012).

2. Álvaro-Gracia, J. M., Jover, J. A., García-Vicuña, R., Carreño, L., Alonso, A., *et al.* Intravenous administration of expanded allogeneic adipose-derived mesenchymal stem cells in refractory rheumatoid arthritis (Cx611): results of a multicentre, dose escalation, randomised, single-blind, placebo-controlled phase Ib/IIa clinical trial. *Ann. Rheum. Dis.* 76, 196–202 (2017).

3. Mendonça, M. V. P., Larocca, T. F., de Freitas Souza, B. S., Villarreal, C. F., Silva, L. F. M., *et al.* Safety and neurological assessments after autologous transplantation of bone marrow mesenchymal stem cells in subjects with chronic spinal cord injury. *Stem Cell Res. Ther.* 5, 126 (2014).

4. Wei, X., Yang, X., Han, Z., Qu, F., Shao, L., *et al.* Mesenchymal stem cells: a new trend for cell therapy. *Acta Pharmacol. Sin.* 34, 747–754 (2013).

5. Yang, J., Zhang, Y. S., Yue, K. & Khademhosseini, A. Cell-laden hydrogels for osteochondral and cartilage tissue engineering. *Acta Biomater.* 57, 1–25 (2017).

6. Brehm, W., Burk, J., Delling, U., Gittel, C. & Ribitsch, I. Stem cell-based tissue engineering in veterinary orthopaedics. *Cell Tissue Res.* 347, 677–688 (2012).

7. Shi, Y., Wang, Y., Li, Q., Liu, K., Hou, J., *et al.* Immunoregulatory mechanisms of mesenchymal stem and stromal cells in inflammatory diseases. *Nat. Rev. Nephrol.* 14, 493–507 (2018).

8. Ceusters, J., Lejeune, J.-P., Sandersen, C., Niesten, A., Lagneaux, L., *et al.* From skeletal muscle to stem cells: an innovative and minimally-invasive process for multiple species. *Sci. Rep.* 7, 1–9 (2017).

9. Caliari, S. R. & Burdick, J. A. A practical guide to hydrogels for cell culture. *Nat. Methods* 13, 405–414 (2016).

10. Nguyen, T. V., Sleiman, M., Moriarty, T., Herrick, W. G. & Peyton, S. R. Sorafenib resistance and JNK signaling in carcinoma during extracellular matrix stiffening. *Biomaterials* 35, 5749–5759 (2014).

11. Balestrini, J. L., Chaudhry, S., Sarrazy, V., Koehler, A. & Hinz, B. The mechanical memory of lung myofibroblasts. *Integr. Biol.* 4, 410 (2012).

12. Guvendiren, M. & Burdick, J. A. Stiffening hydrogels to probe short- and long-term cellular responses to dynamic mechanics. *Nat. Commun.* 3, 1–9 (2012).

13. Spicer, C. D. Hydrogel scaffolds for tissue engineering: the importance of polymer choice. *Polym. Chem.* 11, 184–219 (2020).

14. Khetan, S., Guvendiren, M., Legant, W. R., Cohen, D. M., Chen, C. S., *et al.* Degradation-mediated cellular traction directs stem cell fate in covalently crosslinked three-dimensional hydrogels. *Nat. Mater.* 12, 458–465 (2013).

15. Fiorini, F., Prasetyanto, E. A., Taraballi, F., Pandolfi, L., Monroy, F., *et al.* Nanocomposite Hydrogels as Platform for Cells Growth, Proliferation, and Chemotaxis. *Small* 12, 4881–4893 (2016).

16. Bian, L., Zhai, D. Y., Tous, E., Rai, R., Mauck, R. L., *et al.* Enhanced MSC chondrogenesis following delivery of TGF-β3 from alginate microspheres within hyaluronic acid hydrogels in vitro and in vivo. *Biomaterials* 32, 6425–6434 (2011).

17. Jo, H., Yoon, M., Gajendiran, M. & Kim, K. Recent Strategies in Fabrication of Gradient Hydrogels for Tissue Engineering Applications. *Macromol. Biosci.* 20, 1900300 (2020).

18. Liang, K., Bae, K. H. & Kurisawa, M. Recent advances in the design of injectable hydrogels for stem cell-based therapy. *J. Mater. Chem. B* 7, 3775–3791 (2019).

19. Kwon, M. Y., Wang, C., Galarraga, J. H., Puré, E., Han, L., *et al.* Influence of hyaluronic acid modification on CD44 binding towards the design of hydrogel biomaterials. *Biomaterials* 222, 119451 (2019).

20. Bhattacharya, D. S., Svechkarev, D., Souchek, J. J., Hill, T. K., Taylor, M. A., *et al.* Impact of structurally modifying hyaluronic acid on CD44 interaction. *J. Mater. Chem. B* 5, 8183–8192 (2017).

21. Knopf-Marques, H., Pravda, M., Wolfova, L., Velebny, V., Schaaf, P., *et al.* Hyaluronic Acid and Its Derivatives in Coating and Delivery Systems: Applications in Tissue Engineering, Regenerative Medicine and Immunomodulation. *Adv. Healthc. Mater.* 5, 2841–2855 (2016).

22. Yang, C., Cao, M., Liu, H., He, Y., Xu, J., *et al.* The High and Low Molecular Weight Forms of Hyaluronan Have Distinct Effects on CD44 Clustering. *J. Biol. Chem.* 287, 43094–43107 (2012).

23. Lesley, J., Hascall, V. C. & Tammi, M. Hyaluronan Binding by Cell Surface CD44. *Hyaluronan* 1, 341–348 (2002).

24. Caré, B. R. & Soula, H. A. Impact of receptor clustering on ligand binding. *BMC Syst. Biol.* 5, 48 (2011).

25. Fallacara, A., Baldini, E., Manfredini, S. & Vertuani, S. Hyaluronic Acid in the Third Millennium. *Polymers* 10, 1–36 (2018).

26. Cyphert, J. M., Trempus, C. S. & Garantziotis, S. Size Matters: Molecular Weight Specificity of Hyaluronan Effects in Cell Biology. *Int. J. Cell Biol.* 2015, 1–8 (2015).

27. Kelkar, S. S., Hill, T. K., Marini, F. C. & Mohs, A. M. Near infrared fluorescent nanoparticles based on hyaluronic acid: Self-assembly, optical properties, and cell interaction. *Acta Biomater.* 36, 112–121 (2016).

28. Stern, R. Hyaluronan catabolism: a new metabolic pathway. *Eur. J. Cell Biol.* 83, 317–325 (2004).

29. Ibrahim, S., Kang, Q. K. & Ramamurthi, A. The Impact of HA Oligomer Content on Physical, Mechanical, and Biologic Properties of Divinyl Sulfone-Crosslinked HA Hydrogels. *J. Biomed. Mater. Res. A* 94, 355–370 (2010).

30. Zhao, J., Santino, F., Giacomini, D. & Gentilucci, L. Integrin-Targeting Peptides for the Design of Functional Cell-Responsive Biomaterials. *Biomedicines* 8, 307 (2020).

31. Gahmberg, C. G., Fagerholm, S. C., Nurmi, S. M., Chavakis, T., Marchesan, S., *et al.* Regulation of integrin activity and signalling. *Biochim. Biophys. Acta BBA - Gen. Subj.* 1790, 431–444 (2009).

32. Pierschbacher, M. D. & Ruoslahti, E. Cell attachment activity of fibronectin can be duplicated by small synthetic fragments of the molecule. *Nature* 309, 30–33 (1984).

33. Davidenko, N., Schuster, C. F., Bax, D. V., Farndale, R. W., Hamaia, S., *et al.* Evaluation of cell binding to collagen and gelatin: a study of the effect of 2D and 3D architecture and surface chemistry. *J. Mater. Sci. Mater. Med.* 27, 1–14 (2016).

34. Kapp, T. G., Rechenmacher, F., Neubauer, S., Maltsev, O. V., Cavalcanti-Adam, E. A., *et al.* A Comprehensive Evaluation of the Activity and Selectivity Profile of Ligands for RGD-binding Integrins. *Sci. Rep.* 7, 39805 (2017).

35. Tarus, D., Hamard, L., Caraguel, F., Wion, D., Szarpak-Jankowska, A., *et al.* Design of Hyaluronic Acid Hydrogels to Promote Neurite Outgrowth in Three Dimensions. *ACS Appl. Mater. Interfaces* 8, 25051–25059 (2016).

36. Xu, Q., Zhang, Z., Xiao, C., He, C. & Chen, X. Injectable Polypeptide Hydrogel as Biomimetic Scaffolds with Tunable Bioactivity and Controllable Cell Adhesion. *Biomacromolecules* 18, 1411–1418 (2017).

37. Riener, C. K., Kada, G. & Gruber, H. J. Quick measurement of protein sulfhydryls with Ellman's reagent and with 4,4′-dithiodipyridine. *Anal. Bioanal. Chem.* 373, 266–276 (2002).

38. Lei, Y., Gojgini, S., Lam, J. & Segura, T. The spreading, migration and proliferation of mouse mesenchymal stem cells cultured inside hyaluronic acid hydrogels. *Biomaterials* 32, 39–47 (2011).

39. Qiao, Y., Liu, X., Zhou, X., Zhang, H., Zhang, W., *et al.* Gelatin Templated Polypeptide Co-Cross-Linked Hydrogel for Bone Regeneration. *Adv. Healthc. Mater.* 9, 1901239 (2020).

40. Su, J., Satchell, S. C., Wertheim, J. A. & Shah, R. N. Poly(ethylene glycol)-crosslinked gelatin hydrogel substrates with conjugated bioactive peptides influence endothelial cell behavior. *Biomaterials* 201, 99–112 (2019).

41. Stern, D. & Cui, H. Crafting Polymeric and Peptidic Hydrogels for Improved Wound Healing. *Adv. Healthc. Mater.* 8, 1900104 (2019).

42. Domingues, R. M. A., Silva, M., Gershovich, P., Betta, S., Babo, P., *et al.* Development of Injectable Hyaluronic Acid/Cellulose Nanocrystals Bionanocomposite Hydrogels for Tissue Engineering Applications. *Bioconjug. Chem.* 26, 1571–1581 (2015).

43. Liu, Y., Shu, X. Z. & Prestwich, G. D. Osteochondral Defect Repair with Autologous Bone Marrow–Derived Mesenchymal Stem Cells in an Injectable, *In Situ* , Cross-Linked Synthetic Extracellular Matrix. *Tissue Eng.* 12, 3405–3416 (2006).

Chapter 5: Hybrid scaffolds for peripheral nerve regeneration

Abstract

Porous silicon nanoparticles (pSiNP) have emerged as an interesting and promising material for bio-imaging and drug delivery applications owing to their biocompatibility, easy clearance from the body, high porosity, intrinsic luminescence and anisotropic dissolution.[1] Herein we present the development of an hybrid pSiNP/PEG hybrid hydrogel scaffold with application in peripheral nerve regeneration as an innovative alternative to autologous nerve transplantation. Stereolithograpy was used to print 3D multi-lumen hybrid scaffolds with micrometric resolution. The multi-lumen hybrid scaffolds have the function of guidance of the axons growth providing suitable microarchitecture, mechanical support and growth factors. The size and pore size of pSiP covalently linked to the polymeric network, was optimized to obtain a carrier able to protect a model protein and to control and prolong its release over a period of three weeks.

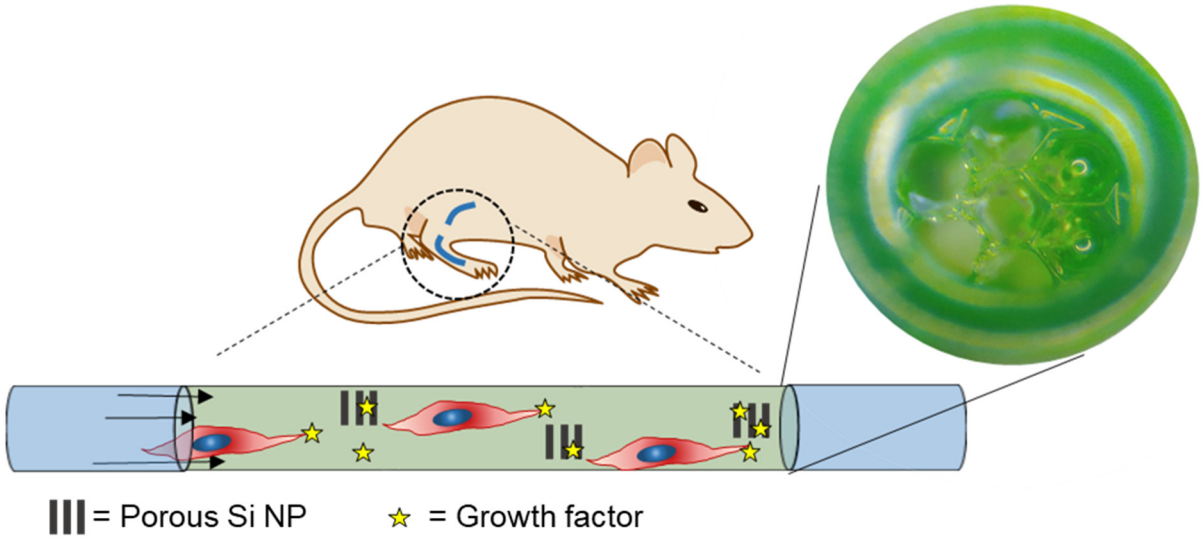

Figure 5.1: Porous silicon NP loaded with a growth factor and incorporated in a multi-channel hydrogel scaffold. The nanocoposite material as the function of guidance for the proliferation of axons.

The work described in this chapter was carried out in Prof. Michael Sailor's lab at University of California San Diego within the Nano-OligoMed H2020-MSCA-RISE project. Grant Agreement number: 778133.

5.1. Introduction

5.1.1 Porous silicon nanotechnology

The food and drug administration (FDA) requires that all the agents that are injected in the human body, be cleared completely in a reasonable amount of time.[2] Silicon is naturally introduced through the diet in the human body where it has no essential known function and where it is oxidized and hydrolyzed by the aqueous environment to generate the water soluble orthosilicic acid (Scheme 5.1) that can be excreted by the kidney. For these reasons, the introduction of silicon in the body is expected not to alter any biochemical pathway and to undergo easy clearance, that makes silicon an optimal candidate for the preparation of biocompatible nanoparticles for bio-imaging and drug delivery applications.[1]

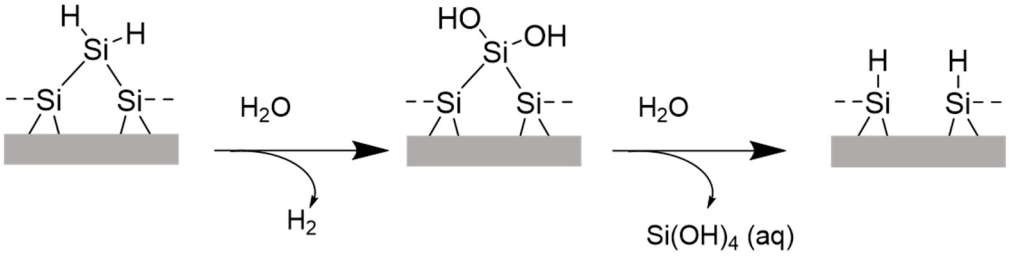

Scheme 5.1: Dissolution of silicon in aqueous environment to generate orthosilicic acid.

Porous silicon is obtained, starting from a single crystal wafer, by electrochemical etch. The silicon wafer is placed as anode and it undergoes oxidation reactions in presence of hydrofluoric acid. The electrochemical cell is represented in Figure 5.2. When the potential is applied to the cell, two competitive processes take place:

1) Porous silicon formation: $Si + 6\ HF \rightarrow 2\ e^- + SiF_6^{2-} + 4\ H^+ + H_2$

2) Electro polishing: $Si + 6\ HF \rightarrow 4\ e^- + SiF_6^{2-} + 6\ H^+$

The formation of porous silicon is a two electrons process and it is promoted by high HF concentration and low current density.[3]

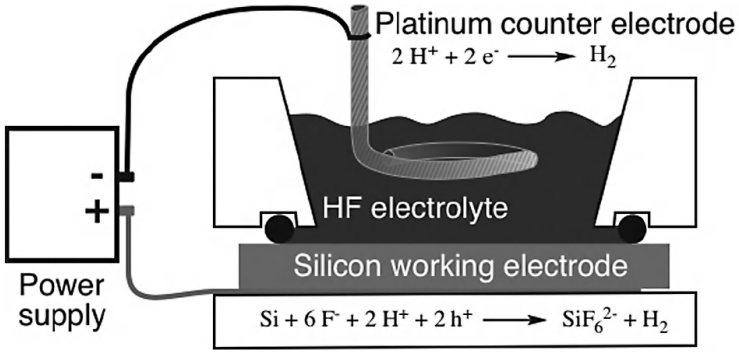

Figure 5.2: Electrochemical cell used to produce porous silicon. Adapted with permission from *Porous Silicon in Practice: Preparation, Characterization and Applications* by Sailor, M. J. Copyright 2011, Wiley.

Silicon wafers are defined by the type of dopant, its concentration and by the cutting crystallographic plane. In the design of porous silicon, the choice of the dopant type defines the pore size of the final material: p-type (e.g. boron dopant) gives micropores, n-type (e.g. phosphorus dopant) generates macropores while p^+, p^{++} and n^+ types produces mesopores.[3] In silicon, the crystallographic pores propagate in the <100> direction, the crystallographic plane of the wafer determines therefore the angle of pore propagation compared with the surface of the wafer. (100) wafers give pores perpendicular to the surface while the use of (110) generates zig-zag pores at 45°. The etching program allows to design porous silicon layers with the desired thickness, porosity and pore size. The thickness is controlled by the etch time, the porosity is defined by the HF concentration and, the pore size, beside depending on the wafer conductivity, is tuned with the current density.[3] The preparation of porous silicon films can be exploited to prepare porous silicon nanoparticles (pSiNP) with desired dimensions and pore size. pSiNP are obtained from a silicon wafer in three steps: 1) perforated etch; 2) lift-off of the film and 3) ultrasonic fracture (Figure 5.3). The perforated etch consists in applying a pulsed current density to the silicon wafer, in a high HF concentration electrolyte solution to obtain the layer of porous silicon. The etching time between pulses defines the size of the particles while the current density is correlated with the porosity of the material.[3] The use of periodic high-current density pulses generates high porous layers (cleavage planes) that allow to reduce the polydispersity index of the diameter of the final particles.[4] The lift-off of the porous film is obtained in two consecutive steps: the bottom part of the porous film is first oxidized electrochemically to SiO_2 in presence of low concentration HF; with the formation of the oxide layer the conductivity of the wafer is reduced up to the condition in which the concentration of

fluorine ions is higher than the one of electron holes ($[F^-] > [h^+]$) and the silica layer is dissolved giving the free-standing porous layer. The obtained film is then placed in an ultrasound bath where at first it is fractured along the high-porosity fracture planes, the prolonged sonication process generates then the thermodynamically more stable cubic shaped pSiNP.

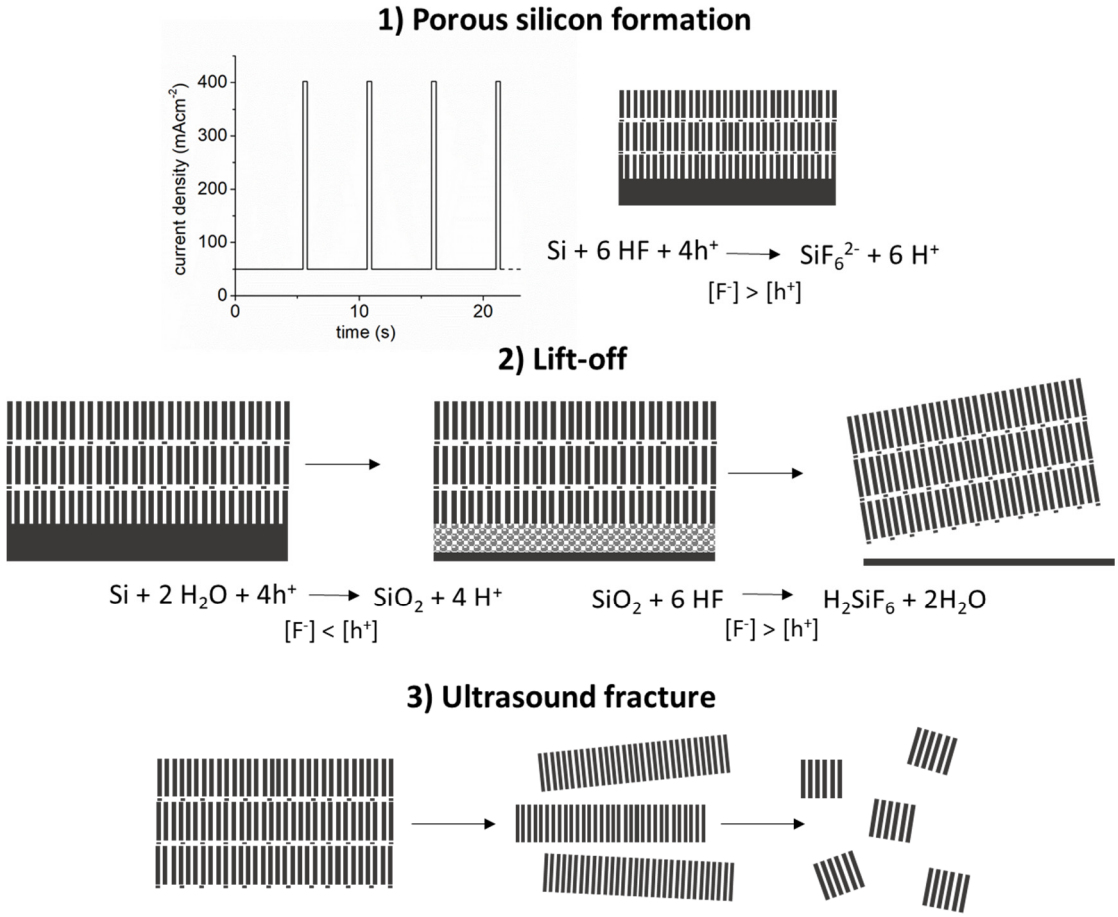

Figure 5.3: Preparation of pSiNP. 1) Perforated etch: a pulsed current density profile is applied to the silicon wafer, in a high HF concentration electrolyte solution to obtain the layer of porous silicon. 2) Lift-off: the bottom part of the porous film is first oxidized electrochemically to SiO_2 in presence of low concentration HF; the silica layer is then dissolved giving the free-standing porous layer. 3) Ultrasound fracture: the porous film is firstly fractured along the high-porosity fracture planes, the prolonged sonication process generates then the pSiNP.

In oxidative environment (e.g. aqueous solution), pSiNP are partially oxidized on the surface with the generation of a core-shell structure with luminescent quantum-confined silicon domains.[5,6] The photoluminescence lifetime of the particles is in the order of microseconds.[7] The long lasting emission allows to exploit the particles for time-gated bio-imaging suppressing the surrounding tissues signals.[8] The described pSiNP have been demonstrated to be both biocompatible and able to clear from the organism through the formation of $Si(OH)_4$ and they

are therefore of particular interest in technologically relevant biomedical applications.[1,9] The high porosity of pSiNP allows to entrap large amount of play load, which are delivered in a controlled fashion as the scaffold degrades.[10] Furthermore, pSiNP have been shown to be able to protect loaded proteins from the non-aqueous medium required during the functionalization of the particle surface.[11] The change in thickness of the silicon skeleton, that occurs during the particle degradation process, brings to a change in their photoluminescence properties, giving to pSiNP a self-reporting feature.[12] The photoluminescence is thought to be a mixture of quantum confinement and defect (interfacial oxide) emission.[3] The cubic shape of the particles is of particular interest for drug delivery applications because this shape has been reported to give a prolonged release compared with spherical particles of the same surface-to-volume ratio.[13] pSiNp are moreover expected to dissolve anisotropically with the preferential dissolution direction being parallel to the pores.[14] The particle dissolution plays a crucial role in the kinetic of drug release; in fact, an anisotropic dissolution gives a release profile that approach zero-order kinetic.[14] To better visualize the effect of anisotropic dissolution, we consider now two model particles that dissolve with a change in volume over time that is proportional to their surface area at time *t;* the first particle is cubic, with dissolution occurring only on the X-Y faces (pAC) (Eq. 5.1), while the second one is spherical and it dissolves isotropically (pIS) (Eq. 5.2). The description of how the equation were obtained is reported in the experimental section. We assume that the payload is uniformly distributed in the particle volume and that the only release mechanism is related to particle dissolution (no diffusion). The volume change of pAC is linear over time and it guarantee a constant release of drug while pIS undergoes burst volume change at the beginning of the dissolution process that brings to the decrease of the drug released over time (Figure 5.4).

$$V_{pAC} = V_i - k\ 2V_i^{2/3}t \qquad \textit{Eq. 5.1}$$

$$V_{pIS} = V_i - k\ 4\pi\left(V\frac{3\pi}{4}\right)^{2/3}t \qquad \textit{Eq. 5.2}$$

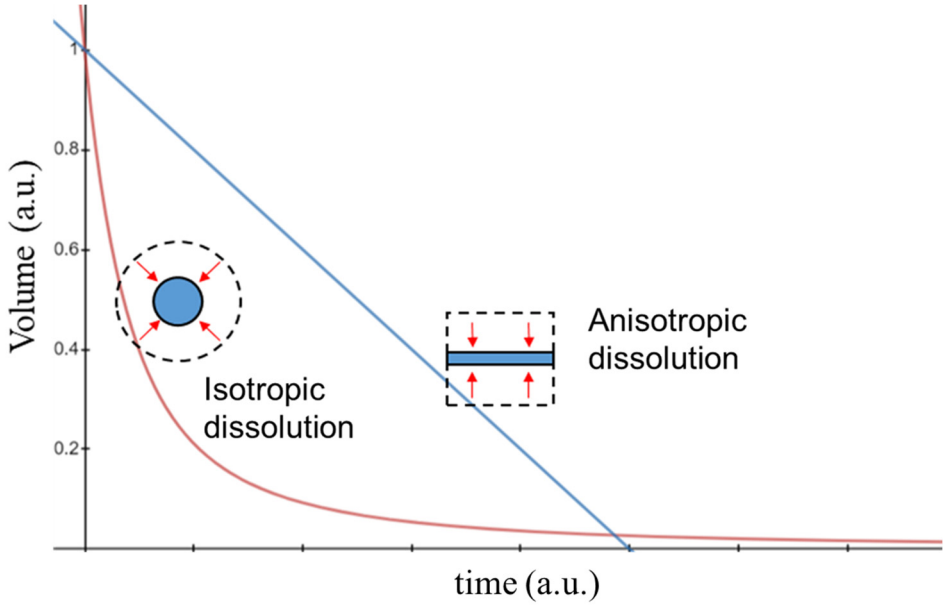

Figure 5.4: Dissolution profile of a model anisotropically dissolving cubic particle (blue) and a spherical particle dissolved isotropically (red).

5.1.2 Peripheral nerve regeneration

The current gold standard in peripheral nerve regeneration is the autologous nerve graft that is however limited by donor site morbidity, possible neuroma formation and rare full recovery.[15] A promising alternative is the implantation of bioengineered nerve conduits with the primary function of mechanical support to keep the proximal and distal nerve aligned. A suitable nerve guide should be porous to allow the diffusion of nutrients and waste removal, it is supposed to give low immunogenicity and to be biodegradable to avoid a second surgery or the occurrence of nerve compression.[16] The implant is furthermore required to have an anisotropic microarchitecture resembling the native tissue that provides instructive physical cues to guide the axons towards the target. These properties can be found in properly designed hydrogels; the structural role of the material and the need of a precise architecture hinder however the applicability of injectable hydrogels in favor of the development of pre-fabricated scaffolds. 3D printing and bio-printing have been used to prepare single lumen[17] and multi lumen[18] conduits with resolution on the micrometric scale.[19,20] The choice of multi lumen scaffolds is generally associated to better structural stability and mechanical properties.[12,21] The choice of the hydrogel polymer is based on mechanical properties, biocompatibility, biodegradability and printability of the network. Examples of both natural[22] and synthetic[17,21,23,24] polymers have been reported for the preparation of nerve guides. Examples of degradable synthetic scaffolds that are on the market are: Neurolac® (poly(D,L-lactide-*co*-ε-caprolactone), CultiGuide®

(polycaprolactone and collagen) and Neurotube® (poly(glycolic acid)).[16] Of particular interest are conductive scaffolds that are able to stimulate the regeneration of neurons via electrical signal propagation.[23,25,26] Conductive scaffolds for nerve regeneration have been prepared for example incorporating polypirrole nanoparticles in a PDLLA/PCL matrix[23] or with the inclusion of graphene in a hydrogel scaffold.[24] Proteins or other bio-molecules can be loaded in engineered tissues to guide the neural cell growth. Johnson *et al.*, for example, incorporated nerve growth factor and cell line-derived neurotrophic factor in 3D printed anatomical geometries to promote the nerve regeneration in a rat model.[27] The evolution of 3D printing technologies, the role of microarchitecture, mechanical properties and biomolecules in the preparation of scaffolds for nerve regeneration have been presented in detail in an interesting review published by Dixon *et al*.[16]

5.1.3. Aim of the project

One of the current open challenges for the preparation of suitable scaffolds is achieving a constant and prolonged release of neurotropic factors necessary to guide the regenerating axons. pSiNP have already been reported to be able to protect the payload and to control its release from polymeric fibers.[28] Herein we report the development of hybrid pSiNP/PEG-hydrogel multi-lumen scaffolds in which the pSiNP have the dual function of payload protection and drug release control. The choice of PEG hydrogel arises from its immunogenicity and antigenicity[18], its printability by stereolithography[17,18,21] and the possibility to prepare scaffolds with tailored mechanical properties changing the polymer concentration[21]. The effect of pSiNP size and pore size on the release profile is studied and the hydrogel/pSiNP system is optimized to obtain a scaffold able to sustain the neurotropic factor release up to three weeks and to guide neuronal repair in a mouse model.

5.2. Results and discussion

5.2.1 Synthesis and Characterization of porous silicon nano- and micro-particles

Porous Si nanoparticles (pSiNP) and microparticles (pSiMP) were prepared starting from a single-crystal silicon wafer by electrochemical etch followed by ultrasonication as described in detail in the experimental section. The particle size was controlled tuning the etch and the ultrasonication time while the pore size was modified changing the current density.[4] The obtained particles were soaked in deionized water at room temperature for 48 hours to partially oxidize the silicon with the aim of increasing hydrophilicity, obtaining a negatively charged

surface and reducing the pore volume. Three samples of pSiNP of different size were prepared: 300 nm with large pores (namely 300_lpNP), 250 nm with small pores (namely 250_spNP) and 400 nm with small pores (namely 400_spNP). Three samples of pSiMP with different size were prepared: 2-10μm (namely 5_MP), 5-10 μm (namely 10_MP) and 10-20 μm (namely 15_MP) all with the same porosity (Table 5.1).

Table 5.1 Particle and pore size of the samples.

Sample	**Particle size (PdI), DLS (nm)**	**Particle size (StD), TEM (nm)**	**Pore size (StD), TEM (nm)**
250_spNP	250 (0.115)	210 (74)	29 (8)
400_spNP	400 (0.064)	480 (115)	29 (8)
300_lpNP	300 (0.138)	370 (190)	50 (23)
5_MP	-	2000-10000*	29 (8)
10_MP	-	5000-15000*	29 (8)
15_MP	-	10000-20000*	29 (8)

*For the pSiMP, the particle size is reported as a range scaling from the smallest to the biggest particle observed; the number of particles observed was too small to have a statistic.

Spectroscopic liquid infiltration method (SLIM) allowed to estimate the porosity of the freshly etched particles that resulted to be 43%; the measurement was done on the porous silicon film obtained by the perforated etch, before doing the lift off. The pSiNP are cubic and with a fairly uniform size distribution as revealed by the TEM (Figure 5.5a, b, c) and DLS analyses (Figure 5.6). In contrast, pSiMP have a more irregular shape and a quite wide size distribution as shown by the TEM images (Figure 5.5d, e, f), DLS measurement was not possible due to the sedimentation of the particles. TEM imaging was in addition used to characterize the pore size of the pSiNP; for the pSiMP such evaluation was not possible due to the thickness of the particles. The pore size of pSiMP was assumed to be the same measured for the pSiNP prepared using the same etching current density and neglecting in this case the effect of the different soak time (Table 5.1).

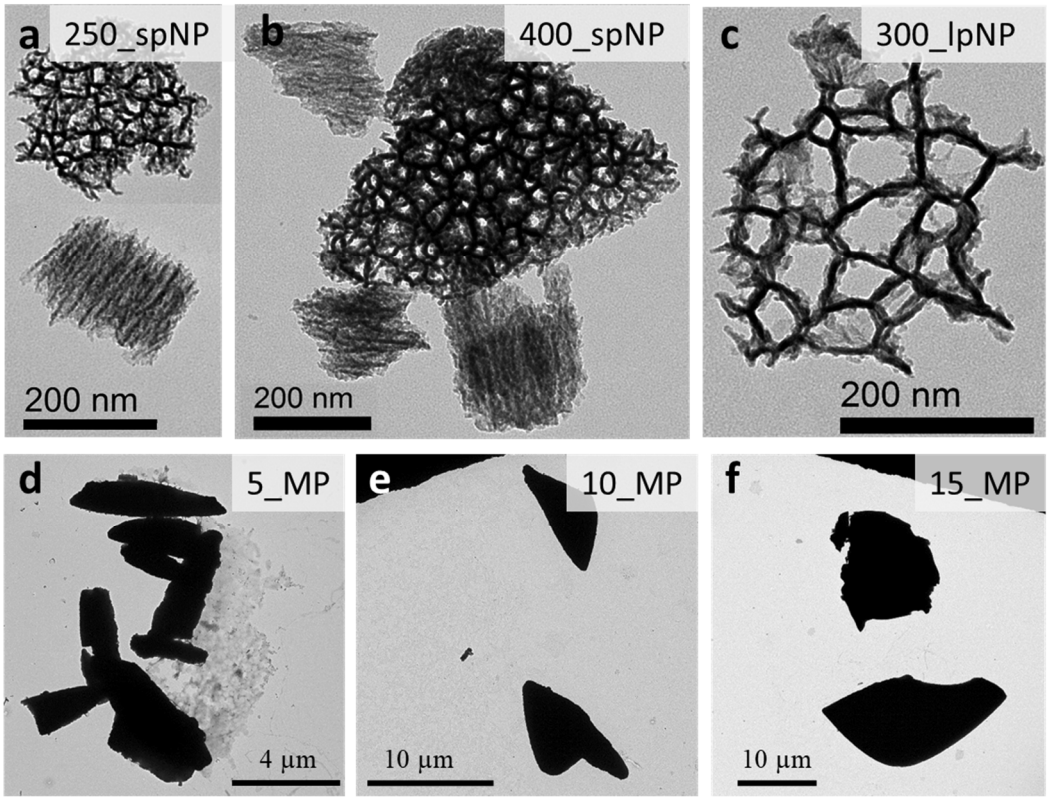

Figure 5.5: TEM imaging of pSiNP and pSiMP a) 250_spNP, b) 400spNP, c) 300_lpNP, d) 5_MP, e) 10_MP and f) 15_MP.

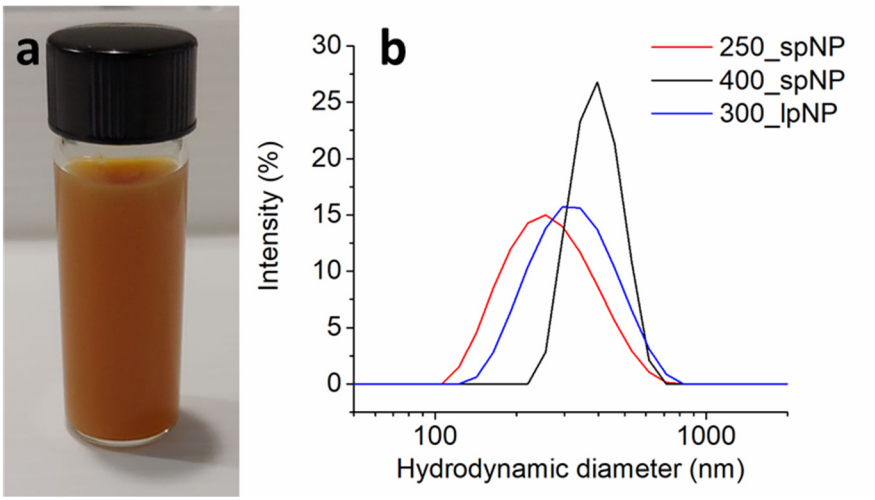

Figure 5.6: a) Ethanol suspension of 250_spNP. b) Hydrodynamic particle diameter measured by DLS. 250_spNP (red), 400_spNP (black) and 300_lpNP (blue).

5.2.2. Protein loading in the pSiNP and pSiMP

Brain derived neurotrophic factor (BDNF) plays a crucial role in supporting nerve fiber growth[16] and it was chosen as target protein to be delivered with the hybrid pSi/hydrogel

scaffolds. During the process of optimization of the system, lysozyme (Lyz) was used as a model protein to substitute the more expensive BDNF. The choice of lysozyme arises from its isoelectric point (*pI*) of 10.7,[29] similar to the one of BDNF (*pI* ~ 9-10).[30] The high *pI* makes the loading of these proteins in pSiNP possible by electrostatic interaction without the need of further treatments. The loading is done in Tris-buffered saline (TBS) that promotes the oxidation of the silicon skeleton with consequent swelling of the pore walls, as oxygen is incorporated, reduction of the pore volume and enhanced payload trapping.[31] The lysozyme loading was evaluated by assay using *Micrococcus lysodeikticus* as substrate following the provided protocol and as reported in detail in the experimental section. The Lyz loading in the particles (Table 5.2) was measured as the difference between the protein concentration in the loading solution and the protein concentration in the supernatant after loading. The pSiNP size exerts no effect on the loading while for the pSiMP a sample to sample variability was observed even if not directly related to the particle size.

Table 5.2. Lysozyme loading in the pSi particles.

Sample	**Lyz loading (StD) (µg/mg)**
250_spNP	757 (53)
400_spNP	744 (52)
300_lpNP	720 (50)
5_MP	645 (45)
10_MP	541 (38)
15_MP	805 (56)

5.2.3. Protein release from pSi particles

The ability of the pSi particles to control and sustain the release of the protein was tested. To this end, 0.5 mg of each sample of loaded pSi particles were dispersed in 1 mL of PBS and incubated at 37 °C. Periodically, the samples were centrifuged (5 min, 15 krpm), the supernatant collected for analysis and replaced with fresh PBS. The release was evaluated by assay using *Micrococcus lysodeikticus* as substrate. The replacement of the supernatant at each analysis time simulates the physiological condition of constant exchange of fluids that occurs in the body. The frequency of supernatant substitution influences the rate of protein release by diffusion. The particle size effect on the kinetic of protein release is reported in Figure 5.7.

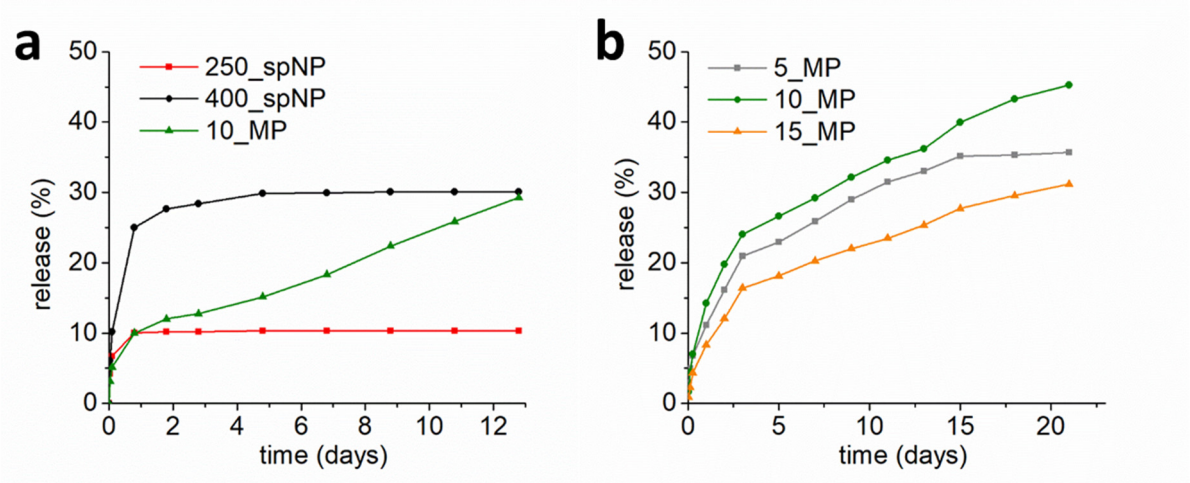

Figure 5.7: Release of active lysozyme from a) pSiNP and b) pSiMP. 250_spNP (red), 400_spNP (black), 5_MP (grey), 10_MP (green), 15_MP (orange).

The protein release occurs both by diffusion and by particle degradation. The slower particle degradation expected for bigger particles explains the constant and prolonged release. The size effect is particularly evident passing from nano- to micro-particles (Figure 5.7a). 250_spNP completed the release within one day, the process is slightly slowed down if the particle size is increased to 400 nm, still the majority of the payload was out of particles after one day and the release was completed in five days. All the micro-particle samples showed a significantly longer release time (Figure 5.7b). The kinetic of protein release from MPs was faster during the first three days followed by a slower constant release profile up to day 15 for the 5_MP sample and up to day 21 for 10_MP and 15_MP samples (Figure 5.7b). The faster release kinetic observed in the first three days may be ascribed to the higher frequency of supernatant analysis and replacement. The peripheral nerve regeneration rate has been reported to range between 1 and 2 mm/day.[32] 10_MP and 15_MP sustained the release for three weeks, long enough to ensure the regrowth of the 1 cm nerve defect under study. The particle size influences not only the kinetic but also the total amount of protein released. The total release obtained from 250_spNP and 400_spNP was respectively 10% and 30% of the payload while the MP released in three weeks between the 31% and the 45% of the protein without reaching a plateau. The lysozyme retention observed for 250_spNP may be attributed to its higher total surface area that increases the possibility of protein adsorption. The assay used to quantify the lysozyme reveals only active enzyme, this ensures that the detected protein maintained its activity. The partial protein loss may be attributed besides to the lysozyme adsorption, to a loss of enzyme activity or also to an unavoidable loss of sample during the centrifugations done at each measurement time.

5.2.4. pSiP functionalization

The scaffolds under study for nerve regeneration are made of acrylate-PEG hydrogel containing covalently linked pSi particles. In order to covalently link the particles to the 3D network of the hydrogel, the loaded particles were functionalized with a PEG-acrylate. The first functionalization step consists in the graft of amino groups that react in the next step with acrylate-PEG-succinimide to give the final acrylated particles (Scheme 5.2). Acrylate-PEG-succinimide is used in stoichiometric defect to prevent succinimide reaction with amino groups from the protein. The functionalization process is described in detail in the experimental section. The grafting process was followed by ζ-potential measurements (Figure 5.8a) and it was confirmed by thermogravimetric analysis (TGA) (Figure 5.8b). The TGA, carried under inert N_2 atmosphere, gave a mass lost, corresponding to the organic functionalization, of 21%, which corresponds to the presence of $4.2 \cdot 10^{-5}$ mmol of acrylic groups in one mg of pSiNP.

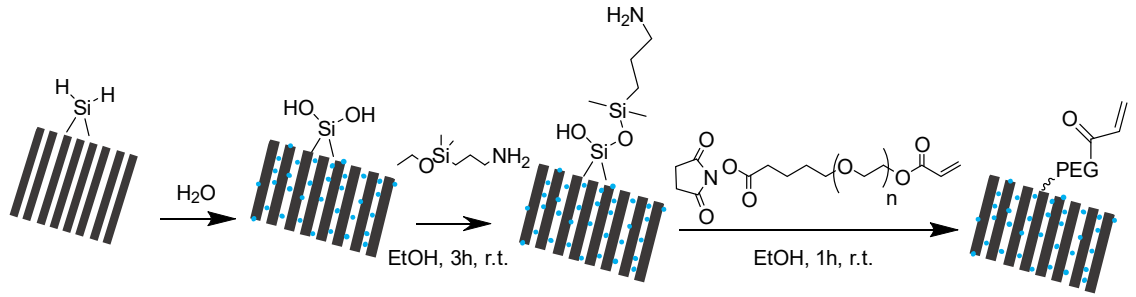

Scheme 5.2: Schematic representation of the surface modification of pSi particles.

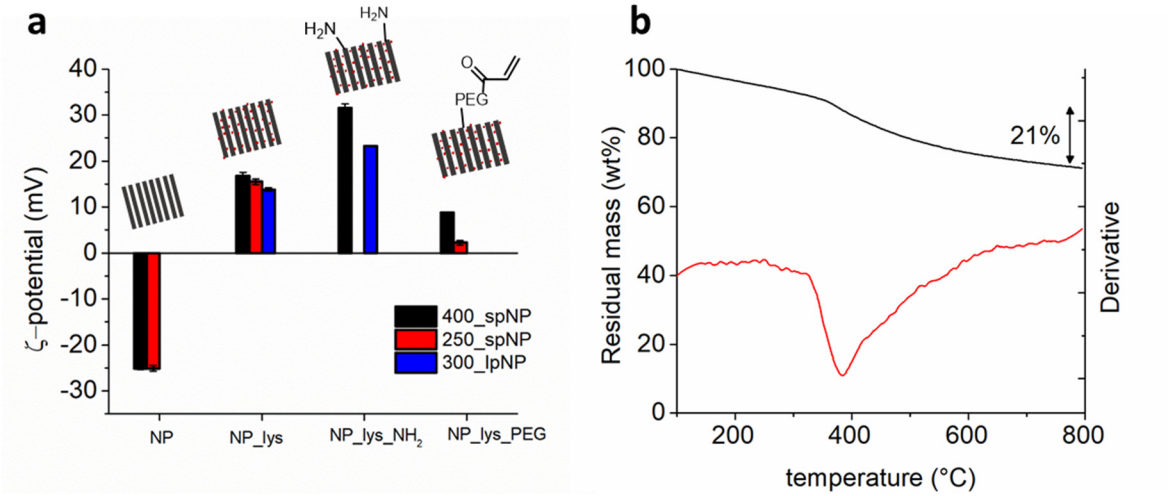

Figure 5.8: a) ζ-potential of the pristine particles (NP), the NP loaded with lysozyme (NP_lys), functionalized with amino groups (NP_lys_NH_2) and functionalized with PEG (NP_lys_PEG). b) TGA of 400_spNP functionalized with PEG-acrylate (without lysozyme loading). Residual mass (black) and derivative (red) of the residual mass as function of the temperature.

5.2.5. Printing of the hybrid pSi particles/PEG-hydrogel scaffold

The hydrogel is prepared by the photo polymerization under UV light of PEG-diacrylate (Mn 700 Da) with the PEG-acrylated pSiP in presence of lithium phenyl-2,4,6-trimethylbenzoylphosphinate as photo-initiator and yellow food color as quencher (Figure 5.9, details given in the experimental section). Scaffolds containing 250_spNP, 400_spNp, 300_lpNP or 10_MP were prepared. A control-scaffold was prepared without pSiP and the lysozyme was directly dissolved in the pre-hydrogel solution (360 µg/mL). The 3D multi-lumen scaffolds were printed by stereolitography using a 365 nm UV lamp, the setup is displayed in Figure 5.10a. The lamp is equipped with a projector connected to a computer that allows to control the motif of UV light that reaches the precursor solution and consequently to determine the cylinder cross-section (Figure 5.10b). The radical polymerization occurs only in correspondence of the UV light allowing a layer by layer printing of the cylindrical multi-lumen scaffolds. The ends of the cylinder are single lumen to facilitate the suture of the scaffold on the native nerve (Figure 5.10c). The obtained scaffolds are cylinders of 2.7 mm diameter, 1.3 cm height and they have a 13 channels cross-section that replicates the projected UV motif with micrometric resolution (Figure 5.10d). The lysozyme content in each scaffold is estimated to be around 10-20 µg.

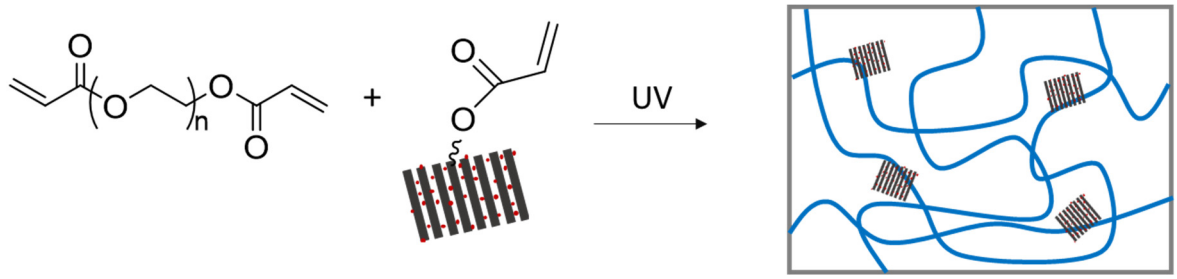

Figure 5.9: Photo polymerization of the Poly(acrylate-PEG) nanocomposite hydrogel.

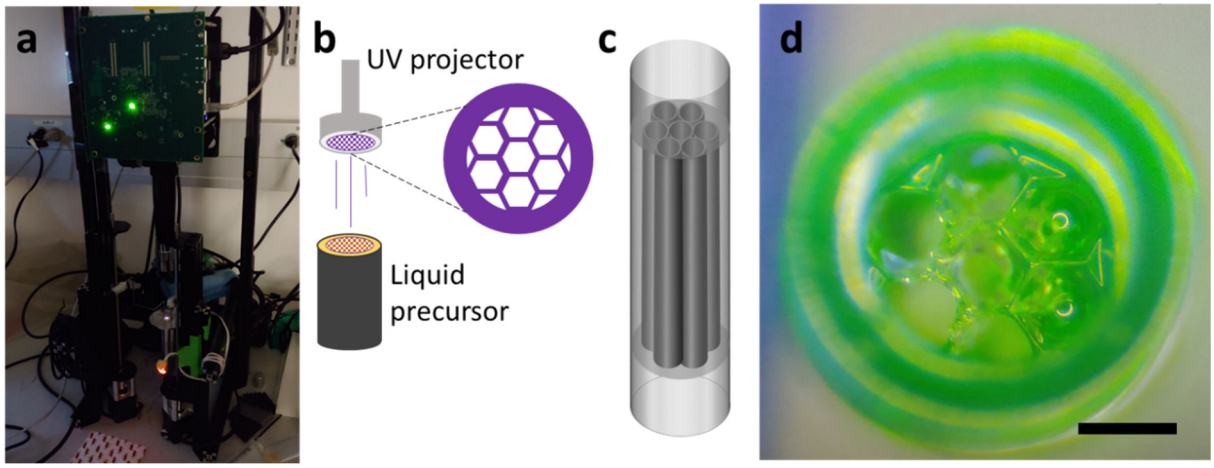

Figure 5.10: a) 3D Printing set-up. b) The UV light motif projected on top of the liquid precursors defines the cross-section of the hydrogel. c) Model of the multi-lumen scaffold with single-lumen ends. d) The 3D printed scaffold. Scale bar: 650 µm.

5.2.6. Protein release from the hybrid pSiP/PEG hydrogel scaffold

In order to study the kinetic of enzyme release from the hybrid hydrogel, each scaffold was incubated at 37 °C in 0.1 mL PBS (pH 7.4, 0.01 M). The supernatant solutions were replaced daily and the concentration of active lysozyme was evaluated until the detection limit of the assay measurement was reached. The release profiles are reported in Figure 5.11. When free lysozyme (10 µg) was directly loaded in the control-scaffold, the enzyme activity was drastically reduced highlighting the key role that pSiP play in payload protection during the 3D printing process. All the sample analyzed gave a total active lysozyme release lower than the expected 10-20 µg, indicating that a part of the protein lost its activity during the printing process, it was retained by the particles or it was trapped in the polymeric network. The ability of the protein to be released from the scaffold depends in fact both from the hydrogel-mesh/protein size ratio and from the presence of interactions with the polymer.[33] Particles with large pores (300_lpNP) released slower the payload compared with particle of similar size but with smaller pores (250_spNP); this could be explained considering that in large pore particles it is more likely that the protein is adsorbed inside the pores rather than on the outer surface. The increase of particle size had the effect of slowing the kinetic with the 10_MP giving a release prolonged over 13 days, in agreement with what observed for bare particles (Figure 5.7). On the contrary, the total amount of released payload decreased with the increase of the particle size, in contrast with what observed for bare particles (Figure 5.7). The lower lysozyme release observed for scaffolds containing bigger particles may be attributed to a minor total protein

content in the hydrogel rather than to a direct size effect. In fact, during the 3D printing process, big particles are more likely to sediment in the precursor solution hindering their incorporation, and consequently the one of the protein, in the scaffold. A possibility to overcome this limit and to obtain a high and prolonged protein release from the scaffolds could be the combination of particles of different size.

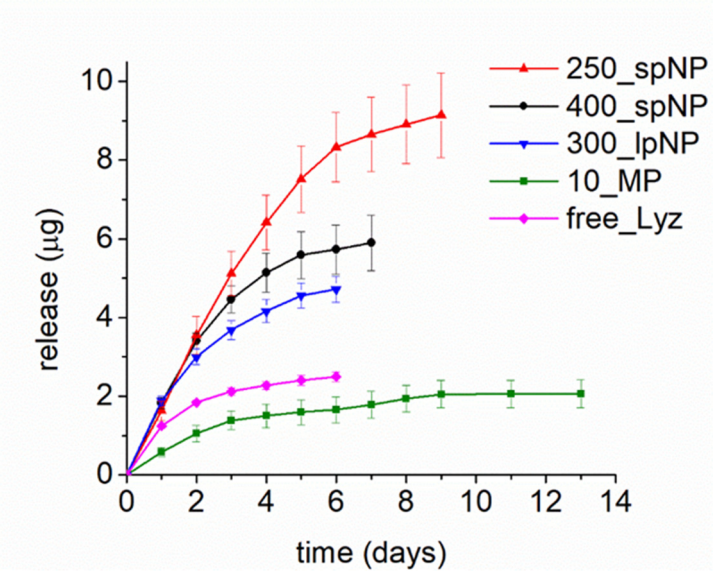

Figure 5.11: Cumulative Lysozyme release from hydrogel scaffolds containing particles of different size. 250_spNP (red), 400_spNP (black), 300_lpNP (blue), 10_MP (green) and free lysozyme (pink).

5.3. Conclusions

Silicon is naturally introduced in the human body with the diet, it is not involved in any known biochemical pathway and it is excreted by the kidney as soluble orthosilicic acid. The absence of interactions of silicon with the body, make it a suitable candidate for drug delivery and bioimaging applications. pSiNP are thought to dissolve anisotropically in physiological environment ensuring the prolong and constant payload release fundamental in drug delivery applications. pSi particles of different size (ranging from 250 nm to 15 µm) and pore size (30 nm and 50 nm) were prepared by perforated electrochemical etch of a single crystal silicon wafer. Lysozyme was chosen as a model protein for BDNF and it was loaded in the different particles giving satisfactory and fairly homogeneous loading without showing particle size or pore size effect among the samples. The release experiment from bare particles showed that increasing the particle size it is possible to slow the kinetic and to increase the percentage of released payload. 10_MP and 15_MP gave a sustained and constant protein release for three

weeks. The pSiP functionalization strategy exploited in this work allows the incorporation of the particles in the PEG-based hydrogel that can be used to generate multi-lumen scaffolds with micrometric resolution by 3D printing. The study of the enzyme release profile from the scaffolds highlighted the fundamental role that pSiP play in the protection of the payload during the 3D printing process. Scaffolds containing bigger particles release slower the protein and gave overall a lower cumulative release. This is attributed to the possible sedimentation of bigger particles during the printing process that may reduce the total amount of particles and consequently of payload in the scaffold. This problem may be overcame by the combination of particles with different size to prevent sedimentation, ensure homogeneity in the hydrogels and prolong the protein release. The project is still ongoing and it will be carried on by Dr. Jonathan Zuidema at UC San Diego; the next steps include further optimization of the system and *in vivo* studies to evaluate the ability of the loaded hybrid scaffolds to guide and promote the nerve growth in the sciatic nerve in a mouse model.

5.4. Experimental section

5.4.1. Chemicals and materials

The silicon wafers were purchased from Virginia Semiconductor Inc., the Acrylate-PEG-Succinimide (5 kDa) was purchased from Laysan Bio. 3-(Ethoxydimethylsilyl)propylamine, lysozyme from chicken egg white, *Micrococcus Lysodeikticus*, lithium phenyl-2,4,6-trimethylbenzoyl phosphinate and PEG diacrylate (Mn 700 Da) were purchased from Sigma Aldrich.

5.4.2. Anisotropic and Isotropic particle dissolution: mathematical model

The dissolution of two model particles is consider to occur with a change in volume over time that is proportional to their surface area at time t (Eq. 5.3). Where V is the particle volume at time t, V_i is the initial volume of the particle, k is the dissolution constant expressed in length over time, A is the particle surface area affected by dissolution and t is the time. The two model particles under study are a cubic particle that dissolves only on the X-Y faces (pAC) and a spherical particle that dissolves isotropically (pIS). For pAC, the surface area affected by dissolution stays constant over time and it corresponds to two times the area of the X-Y face (Eq. 5.4). Where l_i is the initial edge of the particle. Substituting Eq. 5.4 in Eq. 5.3 it is possible to obtain the volumetric profile of pAC over time (Eq. 5.5). The surface area of pIS affected by dissolution decreases with time and it can be expressed as a function of the volume V at time t

(Eq. 5.6). Where r is the radius of the particle at time t. Substituting Eq. 5.5 in Eq. 5.3 it is possible to obtain the volumetric profile of pIS over time (Eq. 5.7).

$$V = V_i - \Delta V = V_i - k\,A\,t \qquad \textit{Eq. 5.3}$$

$$A = 2\,l_i^2 = 2\,V_i^{2/3} \qquad \textit{Eq. 5.4}$$

$$V_{pAC} = V_i - k\,2\,V_i^{2/3}\,t \qquad \textit{Eq. 5.5}$$

$$A = 4\pi r^2 = 4\pi\left(\frac{3V}{4\pi}\right)^{2/3} \qquad \textit{Eq. 5.6}$$

$$V_{pIS} = V_i - k\,4\pi\left(\frac{3V}{4\pi}\right)^{2/3}\,t \qquad \textit{Eq. 5.7}$$

5.4.3. Synthesis of porous silicon nanoparticles

The particles were obtained starting from a p^{++}-type (100) single crystal silicon wafer with a resistivity of 1.1 mΩcm following a method already reported in literature.[1] The etching was carried out in a Teflon etch cell that exposed 8.6 cm^2 of the polished silicon wafer surface, using a platinum coil counter electrode. The silicon wafer was contacted on the backside with a strip of aluminum foil. A typical etching waveform consisted of a square wave in which a lower value of current density of 50 $mAcm^{-2}$ was applied for 1.818 s for 140 cycles (200 nm NP) or for 5.454 s for 47 cycles (400 nm NP), followed by an upper value of current density of 400 mA cm^{-2} applied for 0.363 s. A higher current density (60 $mAcm^{-2}$) was used to prepare large pore NP. The waveform was repeated for several cycles generating a porous film with alternating layers of high and low porosity. The layered porous nanostructure was removed from the crystalline silicon substrate by application of a current pulse of 12.5 $mAcm^{-2}$ for 150 s in an electrolyte consisting of 1:30 vol/vol of 48% aqueous HF : absolute ethanol. The freestanding pSi films were then fractured by ultrasonication in ethanol for 22 hours (200 nm NP) or for 15 hours (400 nm NP). The obtained suspension was let set for one hour, the precipitate was removed and the NP in the supernatant washed three times by centrifugation in ethanol at 15 krpm for 5 min. The obtained particles were soaked in deionized water at room temperature for 48 hours to partially oxidize silicon with the aim of increasing hydrophilicity, obtaining a negatively charged surface and reducing the pore volume.

5.4.4. Synthesis of porous silicon micro-particles

The particles were obtained starting from a p^{++}-type (100) single crystal silicon wafer with a resistivity of 1.1 mΩcm following a method already reported in literature.[1] The etching was

carried out in a Teflon etch cell that exposed 8.6 cm^2 of the polished silicon wafer surface, using a platinum coil counter electrode. The silicon wafer was contacted on the backside with a strip of aluminum foil. A typical etching waveform consisted of a square wave in which a lower value of current density of 50 $mAcm^{-2}$ was applied for 9.090 s (5_MP), 18.180 s (10_ MP), 27.270 s (15_ MP) or 36.360 s (20_MP), followed by an upper value of current density of 400 $mAcm^{-2}$ applied for 0.363 s. The waveform was repeated for several cycles generating a porous film with alternating layers of high and low porosity. The layered porous nanostructure was removed from the crystalline silicon substrate by application of a current pulse of 12.5 $mAcm^{-2}$ for 150 s in an electrolyte consisting of 1:30 vol/vol of 48% aqueous HF : absolute ethanol. The freestanding pSi films were then fractured by ultrasonication in ethanol. After 1 hour of sonication the suspension was let sediment for 1 hour followed by the collection of the precipitate that was suspended in ethanol and fractured by ultrasonication for further 3 hours. The suspension was again let sediment for one hour, the precipitate collected, re-suspended in ethanol, sonicated for 18 hours, let sediment for 1 hour and the micro-particle precipitate was finally collected. This process allowed to fracture the pSi film and at the same time to eliminate the small nanoparticles that are formed in the process. The obtained particles were soaked in deionized water at room temperature for 48 hours to partially oxidize silicon with the aim of increasing hydrophilicity, obtaining a negatively charged surface and reducing the pore volume.

5.4.5. Lysozyme loading in pSiNP and pSiMP

The ethanol suspensions of NP or MP are centrifuged and the particles washed in Tris-buffered saline (TBS) (3 x 5 min. 15 krpm). The loading is done in TBS at 1 mg/mL of pSiNP or pSiMP and 1 mg/mL of lysozyme at room temperature overnight. After loading the particles are washed once in water, once in H_2O/EtOH (30/70 vol/vol) and once in EtOH.

5.4.6. pSi particle functionalization

Amino Functionalization: To 8 mL of suspension of 1 mg/mL of pSiP in EtOH, 96 µL (86.4 mg, 510 mmol) of 3-(Ethoxydimethylsilyl)propylamine are added and the mixture is mixed at r.t. for 3 hours. The Particles are washed by centrifugation in EtOH three times (20 °C, 5 min, 15 krpm).

Acrylate-PEG-functionalization: To 6.4 mL of suspension of 1 mg/mL of amino functionalized pSiP in EtOH, 1.6 mL of an ethanol solution 2.5 mg/mL of Acrylate-PEG-Succinimide (5 kDa) are added and the mixture is mixed at r.t. for 1 hour. The Particles are washed by centrifugation in EtOH two times (20 °C, 5 min, 15 krpm).

5.4.7. Lysozyme quantification

The lysozyme concentration was measured mixing 30 µL of analyte solution with 70 µL of *Micrococcus lysodeikticus* lyophilized cells (1 mg/mL) at room temperature in a 96-well plate and measuring the rate of absorbance decrease at 450 nm over a period of 5 min with a plate reader. The rate of absorbance reduction is directly related to the enzyme concentration. In Figure 5.12 is reported the calibration curve used for the evaluation of the Lyz concentration.

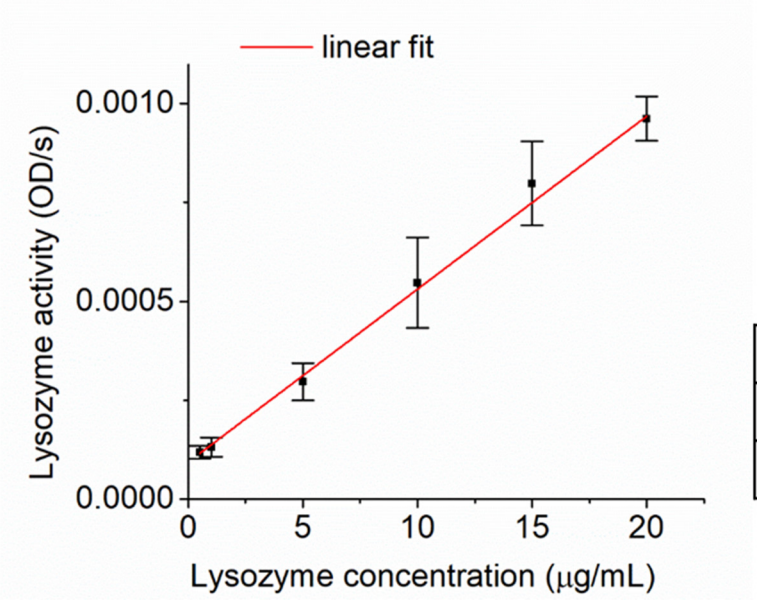

Slope	4.38 (0.089) · 10^{-5}
Intercept	9.28 (0.46) · 10^{-5}
R^2	0.998

Figure 5.12: Lysozyme concentration calibration curve

5.4.8. Printing of the hybrid pSi particles/PEG-hydrogel scaffold

The pre-gel solution is prepared adding to 16 mL of 25% (v/v) PEG diacrylate (Mn 700 Da) PBS solution, 8 mg of PEG functionalized pSiNP, lithium phenyl-2,4,6-trimethylbenzoyl phosphinate as photo-initiator and 30 µL of yellow food color as quencher.

5.4.9. Instruments

Etching waveforms were generated in a computer program written in Labview (National Instruments, Inc.) and the etch was driven by a Keithley 2651A SourceMeter power supply interfaced to the Labview program. Particles were ultrasonicated in a 50T Ultrasonic Bath, VWR, Inc. Transmission electron microscopy (TEM) images were obtained with a JEOL-1200 EX II instrument. The hydrodynamic size and ζ-potential were measured using dynamic light scattering, Zetasizer ZS90, Malvern Instrument. TGA was carried out using an STA 6000 Simultaneous Thermal Analyzer (PerkinElmer) in a nitrogen ambient. The porosity of the pSi

films were determined by optical means, using the spectroscopic liquid infiltration method (SLIM).[34] Lysozyme quantification was done with an absorbance plate reader Molecular Devices Spectramax 340Pc384.

5.5. References

1. Park, J.-H., Gu, L., von Maltzahn, G., Ruoslahti, E., Bhatia, S. N., *et al.* Biodegradable luminescent porous silicon nanoparticles for *in vivo* applications. *Nat. Mater.* 8, 331–336 (2009).

2. Soo Choi, H., Liu, W., Misra, P., Tanaka, E., Zimmer, J. P., *et al.* Renal clearance of quantum dots. *Nat. Biotechnol.* 25, 1165–1170 (2007).

3. Sailor, M. J. *Porous Silicon in Practice: Preparation, Characterization and Applications*. (Wiley VCH, 2011).

4. Qin, Z., Joo, J., Gu, L. & Sailor, M. J. Size Control of Porous Silicon Nanoparticles by Electrochemical Perforation Etching. *Part. Part. Syst. Charact.* 31, 252–256 (2014).

5. Joo, J., Cruz, J. F., Vijayakumar, S., Grondek, J. & Sailor, M. J. Photoluminescent Porous Si/SiO_2 Core/Shell Nanoparticles Prepared by Borate Oxidation. *Adv. Funct. Mater.* 24, 5688–5694 (2014).

6. Heinrich, J. L., Curtis, C. L., Credo, G. M., Sailor, M. J. & Kavanagh, K. L. Luminescent Colloidal Silicon Suspensions from Porous Silicon. *Science* 255, 66–68 (1992).

7. Ko, M. C. & Meyer, G. J. Dynamic Quenching of Porous Silicon Excited States. *Chem. Mater.* 8, 2686–2692 (1996).

8. Joo, J., Liu, X., Kotamraju, V. R., Ruoslahti, E., Nam, Y., *et al.* Gated Luminescence Imaging of Silicon Nanoparticles. *ACS Nano* 9, 6233–6241 (2015).

9. Godin, B., Gu, J., Serda, R. E., Bhavane, R., Tasciotti, E., *et al.* Tailoring the degradation kinetics of mesoporous silicon structures through PEGylation. *J. Biomed. Mater. Res. A* 94A, 1236–1243 (2010).

10. Kaasalainen, M., Rytkönen, J., Mäkilä, E., Närvänen, A. & Salonen, J. Electrostatic Interaction on Loading of Therapeutic Peptide GLP-1 into Porous Silicon Nanoparticles. *Langmuir* 31, 1722–1729 (2015).

11. Kim, D., Zuidema, J. M., Kang, J., Pan, Y., Wu, L., *et al.* Facile Surface Modification of Hydroxylated Silicon Nanostructures Using Heterocyclic Silanes. *J. Am. Chem. Soc.* 138, 15106–15109 (2016).

12. Lee, B.-J., Cho, B., Koh, M., Sohn, H. & Ko, Y. C. Fabrication and optical characterization of a porous silicon distributed Bragg reflector. *J. Korean Phys. Soc.* 62, 132–135 (2013).

13. Nejati, S., Mohseni Vadeghani, E., Khorshidi, S. & Karkhaneh, A. Role of particle shape on efficient and organ-based drug delivery. *Eur. Polym. J.* 122, 109353 (2020).

14. Hollett, G. I. PhD thesis: Selective Sensing and Sustained Release: Biomedical Applications of Porous Silicon. (University of California San Diego, 2019).

15. Panagopoulos, G. N., Megaloikonomos, P. D. & Mavrogenis, A. F. The Present and Future for Peripheral Nerve Regeneration. *Orthopedics* 40, e141–e156 (2017).

16. Dixon, A. R., Jariwala, S. H., Bilis, Z., Loverde, J. R., Pasquina, P. F., *et al.* Bridging the gap in peripheral nerve repair with 3D printed and bioprinted conduits. *Biomaterials* 186, 44–63 (2018).

17. Pateman, C. J., Harding, A. J., Glen, A., Taylor, C. S., Christmas, C. R., *et al.* Nerve guides manufactured from photocurable polymers to aid peripheral nerve repair. *Biomaterials* 49, 77–89 (2015).

18. Evangelista, M., Perez, M., Salibian, A., Hassan, J., Darcy, S., *et al.* Single-Lumen and Multi-Lumen Poly(Ethylene Glycol) Nerve Conduits Fabricated by Stereolithography for Peripheral Nerve Regeneration In Vivo. *J. Reconstr. Microsurg.* 31, 327–335 (2015).

19. Ji, S. & Guvendiren, M. Recent Advances in Bioink Design for 3D Bioprinting of Tissues and Organs. *Front. Bioeng. Biotechnol.* 5, (2017).

20. Xie, R., Zheng, W., Guan, L., Ai, Y. & Liang, Q. Engineering of Hydrogel Materials with Perfusable Microchannels for Building Vascularized Tissues. *Small* 16, 1902838 (2020).

21. Arcaute, K., Mann, B. K. & Wicker, R. B. Fabrication of Off-the-Shelf Multilumen Poly(Ethylene Glycol) Nerve Guidance Conduits Using Stereolithography. *Tissue Eng. Part C Methods* 17, 27–38 (2011).

22. Gong, H., Fei, H., Xu, Q., Gou, M. & Chen, H. H. 3D-engineered GelMA conduit filled with ECM promotes regeneration of peripheral nerve. *J. Biomed. Mater. Res. A* 108, 805–813 (2020).

23. Zhang, Z., Rouabhia, M., Wang, Z., Roberge, C., Shi, G., *et al.* Electrically Conductive Biodegradable Polymer Composite for Nerve Regeneration: Electricity-Stimulated Neurite Outgrowth and Axon Regeneration. *Artif. Organs* 31, 13–22 (2007).

24. Jakus, A. E., Secor, E. B., Rutz, A. L., Jordan, S. W., Hersam, M. C., *et al.* Three-Dimensional Printing of High-Content Graphene Scaffolds for Electronic and Biomedical Applications. *ACS Nano* 9, 4636–4648 (2015).

25. Wu, C., Liu, A., Chen, S., Zhang, X., Chen, L., *et al.* Cell-Laden Electroconductive Hydrogel Simulating Nerve Matrix To Deliver Electrical Cues and Promote Neurogenesis. *ACS Appl. Mater. Interfaces* 11, 22152–22163 (2019).

26. Marchesan, S., Ballerini, L. & Prato, M. Nanomaterials for stimulating nerve growth. *Science* 356, 1010–1011 (2017).

27. Johnson, B. N., Lancaster, K. Z., Zhen, G., He, J., Gupta, M. K., *et al.* 3D Printed Anatomical Nerve Regeneration Pathways. *Adv. Funct. Mater.* 25, 6205–6217 (2015).

28. Zuidema, J. M., Kumeria, T., Kim, D., Kang, J., Wang, J., *et al.* Oriented Nanofibrous Polymer Scaffolds Containing Protein-Loaded Porous Silicon Generated by Spray Nebulization. *Adv. Mater.* 30, 1706785 (2018).

29. Abeyrathne, E. D. N. S., Lee, H. Y. & Ahn, D. U. Sequential separation of lysozyme, ovomucin, ovotransferrin, and ovalbumin from egg white. *Poult. Sci.* 93, 1001–1009 (2014).

30. Hempstead, B. L. Brain-Derived Neurotrophic Factor: Three Ligands, Many Actions. *Trans. Am. Clin. Climatol. Assoc.* 126, 9–19 (2015).

31. Kang, J., Joo, J., Kwon, E. E., Skalak, M., Hussain, S., *et al.* Self-Sealing Porous Silicon-Calcium Silicate Core-Shell Nanoparticles for Targeted siRNA Delivery to the Injured Brain. *Adv. Mater. Deerfield Beach Fla* 28, 7962–7969 (2016).

32. Fisher, J., Mikos, A. & Bronzino, J. *Tissue Engineering*. (Taylor & Francis Group, 2007).

33. Li, J. & Mooney, D. J. Designing hydrogels for controlled drug delivery. *Nat. Rev. Mater.* 1, 16071 (2016).

34. Segal, E., Perelman, L. A., Cunin, F., Di Renzo, F., Devoisselle, J.-M., *et al.* Confinement of Thermoresponsive Hydrogels in Nanostructured Porous Silicon Dioxide Templates. *Adv. Funct. Mater.* 17, 1153–1162 (2007).

General Summary and Perspectives

Hydrogels are three dimensional polymeric hydrophilic networks able to entrap a large amount of water in their structure, they are characterized by a porous structure that makes them permeable to oxygen and metabolites.[1] Both from a structural and from a mechanical point of view, hydrogels are considered the artificial material that better resembles the extracellular matrix in the human body. Hydrogels with tailored properties are obtained from the selection of the constituent polymer, the cross-linking mechanism and with the introduction of specific pending groups. The incorporation of micro and nanofillers has emerged moreover as a strategy for generating hydrogel systems equipped with sets of advanced characteristics such as stretchability,[2] anisotropy[3] and adhesiveness[4].[5,6] The integration of nanomaterials into the structural network can furthermore be exploited for the preparation of biomolecule-delivery systems that allow to control the payload release. Injectable hydrogels are administrated in the form of liquid precursors to the target site where they undergo the sol-gel transition. This class of materials have the dual advantage of being implantable with a minimally invasive approach and of adapting their shape to the target cavity. At the moment (October 2020), there are 28 clinically approved injectable hydrogels with application as dermal filler (e.g. Juréderm®), in tissue regeneration (e.g. Infuse®) and cancer treatment (e.g. Vantas®).[7]

The open challenge in the development of new hydrogels consists in being able to control and tune the desired properties all at once. The aim of the thesis is to develop and exploit nanocomposite and injectable hydrogels for specific biomedical applications.

In particular, Chapter 2 presents an injectable hydrogel obtained from a linear Poly(amidoamine) (PAA) solution. The injection of the solution in the submucosal layer of the gastrointestinal apparatus selectively triggers the formation of dynamic interactions between the tissue and the polymer and among the polymeric chains and it consequently brings to the formation of a tissue-adhesive hydrogel. The dynamic nature of the linking at the base of the hydrogel formation makes the process reversible with the gel to sol transition observed after the resection of the tissue. The injectable hydrogel was exploited *in vivo* as a lifting fluid for the endoscopic resection of gastrointestinal tumors. Compared to saline, the hydrogel halved the time necessary for the procedure and it reduced to one third the occurrence of perforation.

The PAA hydrogel, showed interesting performance in the specific application; its tissue-selectivity however limited the expansion of its use. In Chapter 3 of the thesis is presented a more versatile hydrogel based on hyaluronic acid (HA). HA was chosen as the building block since it is FDA approved, it is characterized by a strong shear thinning behavior in water solution and its chemical structure presents different lateral functional groups that can be exploited to introduce the desired pending groups and cross-linking units. The methacrylate form of HA was used for the preparation of the injectable hydrogel through the thiol-Michael reaction. This strategy allowed to obtain the cross-linked system at physiological temperature and pH without releasing any byproduct. The obtained material is constituted for more than 96% by water and it is characterized by the large-pore morphology necessary to allow the cellular proliferation. The kinetic of hydrogel formation and the mechanical properties of the resultant material can be tuned and adapted to the specific application changing the molecular weight and the concentration of the HA used. Mesoporous silica nanoparticles are introduced in the network opening the possibility of drug/biomolecules delivery. The rheological study allowed us to choose the optimal material to be used as a filler to stimulate the healing of a gastrointestinal fistula (i.e. strong shear thinning behavior, gelation time compatible with the surgery, final mechanical properties adequate for the cell proliferation). The *in vivo* experiments, done in a porcine relevant model, showed the ability of the hydrogel to induce a faster and more homogeneous cicatrisation compared to the control group.

The high MW HA used in the preparation of the hydrogel used in the fistula treatment is known to hinder cell adhesion due to its space filler function in the extracellular matrix that prevents inter cellular signaling.[8] The possibility to introduce suitable modifications in the material to induce cell adhesion is studied in Chapter 4 with the aim of opening new possible applications of the hydrogel in the field of regenerative medicine. The introduction of the integrin-binding RGD sequence induced the homogeneous adhesion of HeLa cells on HA based hydrogels with elastic moduli ranging from 95 Pa up to 800 Pa. A second successful approach to promote the cell proliferation in the material, consisted in the incorporation in the scaffold of HA oligomers that, on the contrary of high MW HA, interact with cell receptor in a monovalent manner allowing multi-fragment binding and stimulating cell signaling cascades.[8,9] This result is of particular interest because it suggests that high MW HA scaffolds implanted *in vivo,* owing to the natural presence of the hyaluronidase enzymes that progressively degrade the polymeric network generating oligomers, can be colonized by cells.

Finally Chapter 5 presents the development of a nanocomposite hydrogel scaffold for peripheral nerve regeneration. The material is 3D printed with a multi-channel architecture to provide cells with structural guidance, while porous silicon nanoparticles (pSiNP) are linked to the polymeric network with the function of controlling the delivery of a growth factor during the process of tissue regeneration. In particular, the focus of the Chapter, is on the study of the effect of the size of pSiNP on the kinetic of protein release. The release experiment from bare particles showed that increasing the particle size it is possible to obtain a constant release for up to three weeks. The study of the enzyme release profile from the scaffolds highlighted the fundamental role that pSiP play in the protection of the payload during the 3D printing process. Future work will include a further optimization of the system and *in vivo* studies to evaluate the ability of the loaded hybrid scaffolds to guide and promote the sciatic nerve regeneration in a mouse model.

In this thesis it has been shown that from the selection of the suitable polymer and cross-linking strategy it is possible to control and tune the kinetic of hydrogel formation and its final mechanical properties. Moreover, with the introduction in the network of specific pending groups (e.g. the peptide sequence RGD) it is possible to impart to the material emerging characteristics such as cellular adhesion. In addition, the introduction in the hydrogels of nanoparticles has been presented as an interesting approach to control and prolong the delivery of biomolecules. The structural, mechanical and chemical properties of the described materials were adapted to specific biomedical applications; the *in vivo* experiments showed that the hydrogels were able to facilitate surgical procedures and to improve the tissue regeneration processes.

We think that further studies will give the possibility of using the hydrogels as delivery vehicle for stem cells opening to different innovative applications in regenerative medicine.

References

1. Liu, J., Tan, C. S. Y., Yu, Z., Lan, Y., Abell, C., et al. Biomimetic Supramolecular Polymer Networks Exhibiting both Toughness and Self-Recovery. Advanced Materials 29, 1604951 (2017).

2. Liu, R., Liang, S., Tang, X.-Z., Yan, D., Li, X., et al. Tough and highly stretchable graphene oxide/polyacrylamide nanocomposite hydrogels. J. Mater. Chem. 22, 14160–14167 (2012).

3. Liu, M., Ishida, Y., Ebina, Y., Sasaki, T., Hikima, T., et al. An anisotropic hydrogel with electrostatic repulsion between cofacially aligned nanosheets. Nature 517, 68–72 (2015).

4. Rose, S., Prevoteau, A., Elzière, P., Hourdet, D., Marcellan, A., et al. Nanoparticle solutions as adhesives for gels and biological tissues. Nature 505, 382–385 (2014).

5. Gaharwar, A. K., Peppas, N. A. & Khademhosseini, A. Nanocomposite hydrogels for biomedical applications. Biotechnol. Bioeng. 111, 441–453 (2014).

6. Zhao, H., Liu, M., Zhang, Y., Yin, J. & Pei, R. Nanocomposite hydrogels for tissue engineering applications. Nanoscale 12, 14976–14995 (2020).

7. Mandal, A., Clegg, J. R., Anselmo, A. C. & Mitragotri, S. Hydrogels in the clinic. Bioengineering & Translational Medicine 5, 1 (2020).

8. Stern, R. Hyaluronan catabolism: a new metabolic pathway. European Journal of Cell Biology 83, 317–325 (2004).

9. Ibrahim, S., Kang, Q. K. & Ramamurthi, A. The Impact of HA Oligomer Content on Physical, Mechanical, and Biologic Properties of Divinyl Sulfone-Crosslinked HA Hydrogels. J Biomed Mater Res A 94, 355–370 (2010).

Acknowledgments

Firstly, I'd like to thank Prof. Luisa De Cola who gave me the possibility of being part of the Lab de Chimie et des Biomatériaux Supramoléculaires. I'm really grateful for the opportunity of working on different stimulating and interdisciplinary projects. I got through numerous challenges that made me grow both from a scientific and from a personal point of view.

I would also like to thank Prof. Michael J. Sailor who welcomed me in his lab at the University of California San Diego for three months. Your passion for research and for teaching has been inspiring. Thank you as well to Dr. Jonathan Zuidema who guided me through the project.

A sincere acknowledgement to the surgeon teams for the fruitful collaborations. In particular Prof. Silvana Perretta, Prof. Mariano Gimenez, Prof. Sun Gyo Lim, Dr. Ludovica Guerrero and Dr. Alain Garcia at the Research Institute against Digestive Cancer in Strasbourg and Dr. Ivo Boskoski at Policlinico Gemelli in Rome.

I'm thankful to all the members of the jury committee of my defence, Prof. Silvia Marchesan, Prof. Valentina Cauda and Dr. Jean-François Lutz who kindly accepted to judge this thesis.

I thank Solvay for founding my PhD and, in particular, Dr. Patrick Maestro for his interest in my work and for the fruitful discussions.

My gratitude goes to Alessandro, Guillermo, Mike and Yang who read the draft of this thesis giving me precious advices to improve it.

A big "thank you!" to Mariel and Pierre, my PhD-adventure mates. I'm sincerely grateful for your constant presence in the last three years; you helped me to face the toughest moments and to appreciate the success.

I would like to thank all the past and present colleagues. I'm really glad for the friendly environment that there has always been in the lab. Compleating the PhD would have been much more harder without your daily help, the Okidoki team, the climbing sessions, the "Bang!" games and all the extracurricular activities. I'm happy to have sheared this important part of my life with all of you.

I wish to warmly thank my family for the support throughout these years in which I've been far from home.

A final and special thanks to Carlo for being by my side, always ready to listen and encourage me.

Curriculum Vitae

Etienne Piantanida

Strasbourg (France)
(+39) 320 64 53 582
piantanida@unistra.fr etienne.piantanida@gmail.com
Date of birth: 08-04-1992 Nationality: Italian

EDUCATION AND TRAINING

Sep. 2017-Oct. 2020 **PhD student in Chemistry**
Solvay PhD fellowship, Institut de Science et d'Ingénierie Supramoléculaires, University of Strasbourg (France)
Supervisor: Prof. Luisa De Cola
Title of the thesis: Development of Hydrogels for Biomedical Applications

Jul.-Sep. 2019 **Visiting Graduate Student**
Nano-Oligomed project participant in the framework of the Marie Curie-RISE 2017 H2020 Project
University of California San Diego (USA)
Supervisor: Prof. Michael J. Sailor

Oct. 2014-Oct. 2016 **Master's degree in Industrial Chemistry**
University of Padova (Italy)
Supervisor: Prof. Armando Gennaro
Title of the thesis: Nitrogen and Sulfur doped carbon based nanomaterials for the selective electroreduction of CO_2 to CO in aqueous solution
Final grade: 110/110 cum laude

Feb.-Jul. 2016 **Master Internship**
University of Aarhus (Denmark)
Supervisor: Prof. Kim Daasbjerg

Oct. 2011-Sep. 2014 **Bachelor's degree in Industrial Chemistry**
University of Padova (Italy)
Supervisor: Prof. Valerio Di Marco
Title of the thesis: ICP-MS analysis: recovery efficiency and digestion procedure
Final grade: 110/110 cum laude

WORK EXPERIENCE

Feb. 2017-Jul. 2017 **R&D Material Development**
Eldor corporation, Orsenigo (Italy)
Quality evaluation of plastic materials in the automotive field

Nov. 2016-Feb. 2017 **Primary School Teacher**
Istituto comprensivo Carminati, Lonate Pozzolo (Italy)

Oct. 2015-Jan 2016 **Student Tutor**
University of Padova (Italy)

LANGUAGES

	Listening	Reading	Speaking	Writing
Italian	Mother tongue			
English	C1	C1	C1	C1
French	C1*	C1*	B2	B1

Common European Framework of Reference for Languages
**TFI* test certificate

SCIENTIFIC PUBLICATIONS AND AWARDS

Publications

E. Piantanida , G. Alonci, A. Bertucci, L. De Cola "Design of Nanocomposite Injectable Hydrogels for Minimally Invasive Surgery" *Acc. Chem. Res.* 2019, 52, 2101

M. E. Gimenéz, C. F. Davrieux, E. Serra, M. Palermo, E. J. Houghton, G. Alonci, E. Piantanida, A. Garcia Vazquez, V. Lindner, B. Dallemagne, M. Diana, J. Marescaux, L. De Cola "Application of a novel material in the inguinal region using a totally percutaneous approach in an animal model: a new potential technique?" *Hernia* 2019, 23, 1175

E. Piantanida, I. Boskoski, G. Quero, C. Gallo, Y. Zhang, V. Arena, G. Costamagna, S. Perretta, L. De Cola "Nanocomposite Hyaluronic Acid based Injectable Hydrogel for the Treatment of Gastrointestinal Fistula" *ACS Nano* 2020, *submitted.*

L. De Cola, S. Perretta, G. Alonci, P. Riva, E. Piantanida, L. Guerriero "Injectable hybrid alginate hydrogels and uses thereof" WO/2019/053269, 2019

Awards

"Best group presentation" at the Summer School in Silicon Nanotechnology, 2019 San Diego (USA)

"Best poster prize" Forum BioChem, 2018 Strasbourg (France)

"Best presentation prize" European Winter School on Physical Organic Chemistry, 2018 Bressanone (Italy)

Université de Strasbourg
Excellence University

Etienne PIANTANIDA

EDSC
École Doctorale des Sciences Chimiques

Development of hydrogels for biomedical applications

Résumé

Le travail de recherche présenté dans cette thèse se concentre sur le développement et la caractérisation d'hydrogels aux propriétés adaptées à différentes applications biomédicales. En particulier, un matériau injectable à base de poly(amidoamine) qui subit sélectivement la transition sol-gel dans le tissu gastrique a été conçu et exploité pour minimiser l'invasion et faciliter la résection des tumeurs gastriques. En outre, un hydrogel à base d'acide hyaluronique contenant des nanoparticules de silice poreuse comme système de délivrance de biomolécules a été conçu. Sa capacité à induire la guérison stimulée des fistules gastro-intestinales a été testée *in vivo*. La possibilité de modifier l'hydrogel développé par l'introduction de bio-stimuli dans le but d'induire la croissance et éventuellement la différenciation cellulaire dans la matrice est également discutée. Enfin, la préparation d'un hydrogel à base de PEG contenant des nanoparticules de silicium poreux et conçu pour soutenir la libération prolongée d'une protéine est discutée en relation avec son application comme support pour la régénération des nerfs périphériques.

Mots-clés : Hydrogels injectables, nanocomposite, gélification in situ, chirurgie mini-invasive

Résumé en anglais

The research work presented in this thesis focuses on the development and characterization of hydrogels with tailored properties for different biomedical applications. In particular, an injectable poly(amidoamine) based material that selectively undergoes the sol-gel transition in the gastric tissue has been conceived and exploited as a tool for the facilitate and minimally invasive resection of gastric tumors. Moreover, a shear-thinning hydrogel based on hyaluronic acid and containing mesoporous silica nanoparticles as biomolecule-delivery system has been designed. Its ability to induce the stimulated healing of gastrointestinal fistulas was tested *in vivo*. The possibility to modify the developed hydrogel by the introduction of bio-stimuli with the aim of inducing cellular growth and eventually differentiation in the matrix is furthermore discussed. Finally, the preparation of a PEG based hydrogel containing porous silicon nanoparticles and designed to sustain the prolonged release of a protein is discussed in relation to its application as scaffold for the peripheral nerve regeneration.

Keywords: Injectable hydrogels, nanocomposite, *in situ* gelation, minimally invasive surgery